REPORT NO.
UCB/SEMM-90/01

STRUCTURAL ENGINEERING
MECHANICS AND MATERIALS

IMPLICATIONS OF STRONG MOTION DATA FOR DESIGN OF REINFORCED CONCRETE BEARING WALL BUILDINGS

BY

JACK P. MOEHLE

JOHN W. WALLACE

JOSE MARTINEZ-CRUZADO

Final Report To
California Strong Motion Instrumentation Program
State of California

JUNE 1990

DEPARTMENT OF CIVIL ENGINEERING
UNIVERSITY OF CALIFORNIA
BERKELEY, CALIFORNIA

IMPLICATIONS OF STRONG MOTION DATA FOR DESIGN OF REINFORCED CONCRETE BEARING WALL BUILDINGS

Final Report

to

California Strong Motion Instrumentation Program
Division of Mines and Geology
State of California

by

Jack P. Moehle
Associate Professor of Civil Engineering
University of California at Berkeley

John W. Wallace
Assistant Professor of Civil Engineering
Clarkson University

Jose Martinez-Cruzado
Research Assistant
University of California at Berkeley

1 June 1990

IMPLICATIONS OF STRONG MOTION DATA FOR DESIGN OF REINFORCED CONCRETE BEARING WALL BUILDINGS

ABSTRACT

A study is made of the performance of two reinforced concrete bearing wall buildings subjected to recent California earthquakes. The buildings are analyzed to verify modeling techniques. The verification of modeling techniques provides a springboard for an analytical evaluation of the relation between proportions of wall buildings and demands for structural details. The evaluation suggests that confined boundary elements are not required for a broad class of bearing wall buildings. This hypothesis is supported by observations of the performance of buildings in Chile that were subjected to the 1985 Chile earthquake.

Note: The report is presented in three parts. The first part is a summary paper describing the scope of the work and the main findings. The second two parts (Appendices A and B) describe in detail the investigation made on each of the two buildings that were the main focus of this project. Each of the three parts is written so as to be complete unto itself.

IMPLICATIONS OF STRONG MOTION DATA FOR DESIGN OF REINFORCED CONCRETE BEARING WALL BUILDINGS

by

Jack P. Moehle
Associate Professor of Civil Engineering
University of California at Berkeley

John W. Wallace
Assistant Professor of Civil Engineering
Clarkson University

Jose Martinez-Cruzado
Research Assistant
University of California at Berkeley

1 June 1990

INTRODUCTION

Observations of building performances following previous earthquakes have revealed comparatively good performances for reinforced concrete shear wall buildings. These observations extend not only to the combined frame-wall system that has been a popular form of construction in recent years, but also to the bearing wall system in which the walls act as both the vertical and lateral load resisting system. Despite the good performance record of reinforced concrete shear wall buildings, current codes [eg., the Uniform Building Code (UBC) (1)] effectively penalize such buildings in design. A study of the performance of bearing wall buildings during recent earthquakes and of their inherent response characteristics has been undertaken so that more consistent recommendations can be developed.

The study is founded largely on the measured responses and observed performances of shear wall buildings during recent

earthquakes. The measured responses have been obtained from two multistory bearing wall buildings located in California that were subjected to low to moderate intensity ground motions. The measured data are used to calibrate analytical models of bearing wall buildings. Having developed confidence in the modeling procedure, responses of bearing wall buildings with a variety of configurations are studied analytically, and the requirements for ductile details are evaluated. From the analysis and a comparison with similar buildings that were subjected to the 1985 Chile earthquake, it is concluded that there exists a broad class of bearing wall buildings for which ductile details are not necessary.

BEHAVIOR OF TWO BEARING WALL BUILDINGS DURING RECENT CALIFORNIA EARTHQUAKES

Description of the Buildings

The two buildings under study are designated in this paper as Building 1 and Building 2. (These are identified in the California Strong Motion Instrumentation Program [CSMIP] as CSMIP Building SN 356 and CSMIP Building SN 385, respectively.) The buildings are each ten stories tall. Plan views of the two buildings are in Fig. 1. The vertical and lateral force resisting system for both buildings consists of reinforced concrete bearing walls coupled by thin slabs. The walls in Building 2 are precast with hollow mandrels into which concrete and reinforcement are cast in the field, apparently achieving an effectively monolithic construction. Slabs in Building 1 are post-tensioned and in Building 2 are precast panels with topping. All walls are continuous over height except

within Building 1 for which the two interior corridor walls are discontinued at the sixth floor.

Building 1 was constructed in 1971/72. Building 2 was constructed in 1974. Details appear to be consistent with those in common practice at the time of construction. Materials in Building 1 are: 3000-psi NWC in the walls; 4000-psi LWC in the slabs; Grade 60 reinforcement for all bars larger than No 5, otherwise, Grade 40 reinforcement. Materials in Building 2 are: 5000-psi precast walls with 4000-psi mandrels (4600 psi assumed average); LWC slabs; Grade 60 reinforcement throughout.

The total weight of Building 1 was calculated to be 24,000 kips. The total weight of Building 2 was calculated to be 23,000 kips.

Computed Building Strengths

Base shear strengths of the two buildings were calculated in each of two principal directions considering (a) flexural mechanisms extending over the height, and (b) wall shear strength computed according to the UBC. For Building 2, rectangular precast wall panels had been joined to form T- and U-Shaped wall cross sections. Available information on structural details along the joint was incomplete, but suggested that fully composite action of the orthogonal wall panels was unlikely. Thus, for Building 2, flexural strengths for fully noncomposite and fully composite walls are presented.

Dynamic Analytical Model

Analysis of building response records and comparison with calculated strengths suggested that responses of the two buildings during the earthquakes being studied were in the linear range. Therefore, linear-elastic properties of the buildings were modeled using conventional computer software. Effects of soil-structure interaction were investigated.

Given the near symmetry in the floor plan of Building 1, a simple 2-dimensional model was prepared for each direction. The model of the transverse direction considered contributions only of walls aligned in that direction. The model in the longitudinal direction considered two frames (one to model the exterior column lines and another to model the corridor walls). In both models, gross-section properties (or a fraction thereof) were assumed for all elements. Fully composite action was assumed between orthogonal panels of T- and L-shaped walls. Effective widths of coupling slabs were computed using the results of Qadeer, et al. [2] (the resulting slab width was typically equal to wall width plus six slab depths). A rigid floor diaphragm was assumed. Responses of the 2-D models were computed using the program SAP-80.

Because Building 2 had some asymmetry in plan, a complete 3-D model was prepared using the program ETABS. Member modeling assumptions were essentially the same as those assumed for Building 1.

Although not observed following the earthquakes, some cracking should generally be anticipated in reinforced concrete elements with

light axial loads because of effects of temperature, shrinkage, foundation settlements, and lateral loads. At the present time, techniques are not available by which to estimate the degree of stiffness reduction due to these effects. If lateral load were the only source of cracking, it is likely that widely-accepted formulations for stiffness reduction as a function of loading would be roughly applicable [7]. However, as noted above, lateral load is not the only source of concrete cracking. For the reinforced concrete walls considered in the present study, the fully-cracked section stiffness is approximately one-third of the gross-section stiffness. Because complete cracking is not anticipated for these buildings, a stiffness reduction less than the fully-cracked value would be appropriate. In some of the analyses presented here, an effective stiffness equal to half the gross-section stiffness is therefore considered.

In some of the analyses, soil-structure interaction effects were modeled using springs at the bases of the structures. Soil mechanical properties were not available. As an approximation, mechanical properties were approximated as; unit density = 115 pcf, Poisson's ratio = 0.35, and static shear modulus = 3300 ksf. With these assumed mechanical properties, translational and rotational properties of springs at the base of the structure were calculated with the foundation considered as a rigid mat [6]

Measured and calculated periods for the models are in Table 2. The fundamental periods are approximately N/20, where N is the number of stories in the building. For comparison with the values

in Table 2, Eq. 12-3 of the UBC gives a fundamental period of 0.58 sec for each building.

Ground Motions at Building Sites

Response records for Building 1 were obtained for the Morgan Hill and Mt. Lewis earthquakes. Only the former is considered here. Response records for Building 2 were obtained for the Whittier-Narrows earthquake and aftershocks. Only the former is considered in this paper. Instrument and processing details can be obtained from the CSMIP. Ground acceleration histories (obtained from instruments in the ground floor of the buildings) are plotted in Fig. 2.

Measured and Computed Responses

Responses to the measured horizontal ground accelerations were computed for each of the buildings using the analytical models described previously. For the 3-D model of Building 2, the two horizontal components were considered to act simultaneously. Viscous damping equal to five percent of critical was assumed for all calculations.

Computed and measured roof relative displacements are compared in Fig. 3 (gross-section, fixed base), Fig. 4 (gross-section, with soil-structure interaction), and Fig. 5 (half gross-section, soil-structure interaction). In those figures, measured relative roof displacement is computed as the difference between measured absolute displacements at the roof and the base. The measured absolute displacements were obtained by integration and correction of the

acceleration records. (For relative transverse displacements of Building 1, the error margin is estimated to be one-third of the measured displacement. Thus, because it is not possible to accurately gage responses for the transverse direction for this building, no transverse displacement plots are shown.)

From the data in Table 2 and Fig. 3, it is apparent that the computed gross-section, fixed base building periods are too short. As calculated (Table 2 and Fig. 4), soil-structure interaction results in an increase in period of approximately ten-percent of the gross-section value. With this increase, the calculated period is still short in comparison with the measured values.

A comparison of the calculated wall moments (from the gross-section analysis) and nominal cracking strengths indicates that the walls in both buildings should have been cracked due to lateral load alone. Including effects of temperature, shrinkage, settlement, and other loadings during the life of the buildings, a significant stiffness reduction would be expected for the buildings. As described previously, lacking an established technique for estimating stiffness reduction, a stiffness equal to half the gross-section value was assumed for some of the analyses.

Table 2 and Fig. 5 present results obtained using the half gross-section model including soil-structure interaction. For Building 1, which had the lower intensity ground motion of the two buildings being studied, the half gross-section model is too flexible, resulting in an overestimation of the periods and displacement responses. For Building 2, the reduced stiffness model

greatly improves the correlation with measured results.

For Building 2, it is noted that the computed and measured periods in Fig. 5 compare reasonably throughout the entire duration of response. The implication is that, cracking aside, the response of the building during these earthquakes was basically elastic. This conclusion is supported by comparison between the measured base shears and the calculated base-shear strengths (Table 1). Measured base shears developed at the base of the buildings were estimated as the sum of the products of calculated floor masses and floor accelerations. Floor accelerations were measured at the base, roof, and two intermediate floors of each building. Accelerations at other floors were estimated by linear interpolation. Base shears obtained by this procedure are compared with calculated strengths in Table 1. Calculated base-shear strengths consistently exceed the measured values.

Responses of the buildings to stronger ground motions cannot be gaged directly from the measured responses to the lower intensity ground motions. Although projections of expected response of these two buildings to assumed strong ground motion are possible using nonlinear computer models, results from such projections are fraught with uncertainties that arise from uncertainties in modeling. Such results are not pursued in this study. Rather, a generalized study of the likely demands during strong ground motions is made in the balance of this paper.

AN EVALUATION OF THE NEED FOR CONFINED BOUNDARY ELEMENTS IN BEARING WALL BUILDINGS

To understand the requirements for wall boundary element confinement of bearing wall buildings a study of the likely response characteristics and capacities was carried. The study includes determination of fundamental period, expected roof drift, and expected roof drift capacity for walls without special boundary element confinement.

Fundamental Period

A relatively simple procedure can be used to estimate the fundamental period of a building in which flexural behavior of structural walls dominates the lateral load response. The procedure was described by Sozen [8]. For a uniform cantilever, the effective stiffness and mass can be estimated as

$$K = 3EI/h^3 \tag{1}$$

$$M = mh_w/3 \tag{2}$$

in which E = modulus of elasticity, I = moment of inertia, h_w = wall height, and m = mass per unit length of wall including the tributary gravity weight. Equation (1) is lateral stiffness of a cantilever subjected to a point load at the free end. Equation (2) is based on the assumption of a linear mode shape (this is inconsistent with the shape function used to determine the effective stiffness, but does not affect results significantly). Based on these two equations, the fundamental period of the building can be expressed as

$$T = 6.28\sqrt{M/K} \quad (3)$$

Equations (1) through (3) can be used to estimate the period of a building as a function of the wall area to the floor area if the building height h_w and wall aspect ratio h_w/l_w are specified, and if a mass distribution of the building is assumed. In this study a mass distribution of 175 psf is assumed. In addition, the thickness of walls is assumed to be constant over height, and for buildings with multiple walls, walls of uniform height and length are assumed.

Figure 6 presents the period estimate based on the aforementioned assumptions as a function of wall area to floor area ratio for wall aspect ratios of 3, 5, and 7. In calculating the ratio, only wall webs parallel to a single principal axis of the building are considered, rather than the full cross-sectional area of all walls in the floor plan. For a building with wall area to floor area ratio of 0.01 and wall aspect ratio of 5, a period of approximately one second is estimated.

The validity of the period estimate of Fig. 6 is demonstrated by comparison with measured building periods in Fig. 7. The selected buildings include the two study buildings from California (described in detail previously) and several similarly configured buildings in Chile for which aftershock vibratory data are available [4]. The procedure used to estimate fundamental period provides a reasonably accurate measure of actual building period.

Roof Drift

Linearly elastic displacement response spectra can be used readily to estimate inelastic roof drift for multistory buildings if it is assumed that drift of a building in the inelastic range of response is approximately equal to the elastic drift calculated for the initial period of the building. Several previous studies have demonstrated that this approximation is reasonable if the initial period exceeds the characteristic ground period [10,11]. Appropriate displacement response spectra could be developed for a particular building site, or generalized spectra could be used (eg., ATC-3 spectra, Fig. 8. A simplified spectrum is used for this study (Fig. 8). The spectrum is representative of U.S. spectra for strong ground motion on firm soil. Five percent damping is assumed.

To obtain a high estimate of drift, the stiffness of a typical building was assumed to be equal to half the gross-section value, rather than the gross-section value as given in Fig. 6. Given this relation, the spectral displacement for a building of a given number of stories and a given wall area to floor area ratio can be estimated. Roof displacement is approximated as 1.5 times the modal spectral displacement. Finally, a roof drift as a percent of height can be calculated assuming a typical story height of 10 ft.

Figure 9 plots calculated roof drift ratios versus the wall area to floor area ratio. The curves plotted in that figure represent quantities calculated directly from the simplified spectrum (Fig. 8). The drift ratio is independent of building height due to the assumed linear displacement spectrum and

assumptions used to estimate the fundamental period. At low ratios of wall to floor area, increasing the wall area ratio results in a substantial reduction in roof drift. At higher ratios, an increase in the wall area ratio has little effect.

For buildings with wall aspect ratios of five or less and wall area ratios of 1.5% or greater, calculated roof drifts of 0.01 or less are expected. Roof drift of this magnitude would be expected to cause some nonstructural damage, but perhaps tolerable structural damage. An evaluation of the expected structural damage follows.

Required Details

The need for confined boundary elements in bearing wall buildings can be estimated almost directly from calculated drift demands for such buildings (Fig. 9). The evaluation procedure has been described previously in relation to a study for Chilean buildings [9].

The procedure for relating building drifts to local inelastic demands is based on the model of Fig. 10. The model assumes that elastic curvatures are distributed uniformly over the wall height. For inelastic response, the maximum elastic curvature is equal to the yield curvature, which is defined as the curvature at first yield of the wall boundary steel. Inelastic curvatures up to the maximum available curvature accumulate near the base of the wall along a height l_p. For an unconfined concrete wall section, the ultimate curvature can be estimated using conventional flexural theory for reinforced concrete with a maximum usable concrete compression strain of 0.004. The length l_p typically ranges between

$0.5l_w$ and $1.0l_w$. In this study, the value $0.5l_w$ is used so as to ensure conservative results.

Given the model of Fig. 10, and the analytical relations presented therein, the ultimate curvature ϕ_u required to achieve a given drift can be solved. The result is expressed in dimensionless form as $\phi_u l_w$ in Eq. 4, and plotted in Fig. 11.

$$\phi_u l_w = 0.0025(1-0.66h_w/l_w) + 2d_u/h_w \quad (4)$$

in which d_u = the expected maximum roof displacement. Figure 11 enables the required ultimate curvature to be estimated as a function of building roof drift ratio and wall aspect ratio. For example, a building having wall aspect ratio of 5 and drift demand equal to 0.01 will require an ultimate curvature equal to $0.015/l_w$.

Figure 12 plots calculated moment-curvature relations for walls of rectangular cross section having length of 20 ft and width of 12 inches. Reinforcement consists of uniformly distributed steel (providing steel ratio equal to 0.0025) plus boundary reinforcement. The uniform reinforcement plus boundary reinforcement provide total reinforcement ratios ranging from 0.0025 to 0.02 as indicated in the figure. Reinforcement has yield stress of 60 ksi and typical strain hardening for Grade 60 reinforcement. Concrete has compressive strength of 4 ksi with stress-strain relation based on typical unconfined properties. Axial load produces an average compressive stress of $0.1f'_c$. An ultimate concrete compressive strain equal to 0.004 is assumed.

The moment-curvature relations of Fig. 12 indicate that a

curvature in excess of 0.0009/ft is available for the walls under consideration. Because the wall has length l_w = 20 ft, the available ultimate curvature is $0.018/l_w$. In a ten story building, the value h_w/l_w is approximately 5 for a wall length of 20 ft. Using the relation plotted in Fig. 11, it is concluded that this wall section would perform satisfactorily for roof drifts beyond 0.01H. As indicated in Fig. 9, a building having wall area ratio equal to or exceeding approximately 0.01 would meet this drift requirement and therefore not require boundary element confinement for the sake of achieving flexural ductility requirements.

The argument of the preceding paragraph is bounded by the geometric constraints of the idealized problem for which it was devised. As indicated by the plan view of Building 2 (Fig. 1) it is common practice in bearing wall construction for orthogonal walls to be monolithically interconnected, forming T-, L- and U-shaped walls. If rectangular walls having proportions described above are interconnected to form these more complex wall cross sections, the calculated drifts and moment-curvature relations change markedly. When the stem of T-shaped walls is in tension, the available ultimate curvature capacity without confinement is very large (Fig. 13). However, for the stem in compression the ultimate curvature is reduced. The reduction occurs because the relatively narrow compression zone (the stem) must develop the tensile capacity of the entire flange. For this reason, T-, L-, and U-shaped walls tend to have lower deformation capacity than the individual rectangular elements that compose the wall.

In the interest of developing a general design guideline, a simple wall cross section was investigated (Fig. 14). The wall has uniformly distributed steel ($0.0025t_w l_w$) plus boundary reinforcement. The quantity of boundary steel at either end of the wall can be varied independently. Thus, although the wall cross section section shown is rectangular, T-, L-, and U-shaped walls can be approximately represented by including in the boundary steel all reinforcement in the wall flanges. For the present analysis, concrete compressive strength is 4 ksi. Steel has nominal yield stress of 60 ksi, but develops a stress equal to $1.25f_y$ in the boundary elements. Axial load is centered on the wall. Using the rectangular stress block to represent concrete action in the compression zone [7], with ultimate compressive strain of 0.004, relations between geometry, axial load, and ultimate curvature can be developed. These are plotted in Fig. 15.

The results of Fig. 15 (available deformation capacity) can be compared with those of Fig. 9 and 11 (required deformation capacity) to determine the need for special confinement reinforcement in boundary elements. Considering a typical bearing wall building to be one in which (a) wall axial stresses do not exceed $0.1f'_c$ and (b) the ratio of wall to floor area for walls aligned in one direction exceeds 0.01, it is indicated from these relations that walls having rectangular cross section do not require special transverse reinforcement to confine the compression zones. In walls having T-, L-, or U-shaped cross sections, the stem of the wall should be confined.

Given the frequency of strong earthquakes, the Chileans have developed a formula for building design that is markedly different from that in the US. Whereas in the U.S. it is common to rely on frames and combined frame wall systems to resist lateral loads in multistory buildings, in Chile the almost universally used system is the reinforced concrete bearing wall building. The Chilean structures are designed for lateral forces similar to those prescribed in the U.S. However, in sharp contrast with U.S. practice, special transverse reinforcement to confine the boundary elements is not required and typically not used.

The success of the Chilean "formula" for design was apparent following the 1985 Chile earthquake [3]. The city of Vina del Mar, with over 400 reinforced concrete buildings over 5 stories, was subjected to a ground motion having peak acceleration of 0.36 g and duration of strong shaking in excess of one minute. The success of the Chilean construction is apparent in the cost of repair, which averaged only 35 cents per square foot.

An analysis of the Chilean buildings has been reported elsewhere [4,9]. The analysis suggests that the typical building has strength and stiffness characteristics similar to those of U.S. bearing wall construction on the West Coast. The relations for evaluating the need for special boundary element confinement (Fig. 9, 11, and 15) apply to the Chilean buildings and indicate that special reinforcement to confine the boundary elements is not required. The 1985 Chile earthquake provides a physical

demonstration that such reinforcement is indeed not a fundamental requirement for this type of building.

CONCLUSIONS

Based on a study of California bearing wall buildings and of similar buildings in Chile, the following have been observed:

1. Periods and responses of reinforced concrete bearing wall buildings cannot be adequately gaged on the basis of uncracked section properties, even when the earthquake loading is not severe, and even when cracks are not visible in the concrete sections.

2. By reducing the stiffness of the walls in the two study buildings, ostensibly to account for effects of concrete cracking, good correlation with measured behavior could be obtained. The degree of stiffness reduction is likely to depend in part on the loading intensity. As a simple approximation to estimating maximum drift, a stiffness reduction to half the gross-section stiffness was recommended.

3. An evaluation of the need for special transverse reinforcement to confine the boundaries of walls in bearing wall buildings indicates that such reinforcement is not required in walls of rectangular cross section. Such reinforcement is required in the stem of T-, L-, and U-shaped walls.

4. Similarities in characteristics of U.S. and Chilean bearing wall construction were noted. The Chilean construction is similar in most regards, except special transverse reinforcement to confine

boundary elements is generally not used. Low damage levels were observed following the 1985 Chilean earthquake. This large-scale test of bearing wall construction lends credibility to the contention that special boundary element confinement is not generally required in typical bearing wall construction.

ACKNOWLEDGEMENT

The work described in this report was supported with funds from the California Strong Motion Instrumentation Program. Tony Shakal, Mo Huang, and Carlos Ventura of the CSMIP are thanked for assistance in obtaining and interpreting building records. Statements made in this paper are the responsibility of the authors, and do not necessarily represent the views of the CSMIP or individuals working with that organization.

REFERENCES

1. Uniform Building Code, International Conference of Building Officials, Whittier, California, 1988.

2. Qadeer, Aslam, and Smith, "The Bending Stiffness of Slabs Connecting Shear Walls," ACI Journal, June 1969, pp. 464-473.

3. "The 1985 Chile Earthquake," EERI Spectra, February, 1986.

4. Wallace, J. W., and Moehle, J. P., "The 3 March 1985 Chile Earthquake: Structural Requirements for Bearing Wall Buildings," EERC Report No. UCB/EERC-89/ , Earthquake Engineering Research Center, University of California at Berkeley, July 1989.

5. T. Paulay, "The Design of Ductile Reinforced Concrete Structural Walls for Earthquake Resistance," EERI Spectra, October 1986.

6. Applied Technology Council, "Tentative Provisions for the Development of Seismic Regulations for Buildings," ATC 3-06, U. S. Government Printing Office, Washington, 1978.

7. ACI Committee 318, "Building Code Requirements for Reinforced Concrete (ACI 318-89)," American Concrete Institute, Detroit, 1989.

8. Sozen, M. A., Proceedings, 5th Chilean Conference on Earthquake Engineering, Santiago, Chile, August 1989.

9. Moehle, J. P., and Wallace, J. W., "Ductility and Detailing Requirements of Shear Wall Buildings," Proceedings, 5th Chilean Conference on Earthquake Engineering, Santiago, Chile, August 1989.

10. Newmark, N. M., and Hall, W. J., Earthquake Spectra and Designn, Engineering Monographs on Earthquake Criteria, Structural Design, and Strong Motion Records, Earthquake Engineering Research Institute, 1982.

11. Sozen, M. A., "A Frame of Reference," Peck Symposium, University of Illinois, Urbana, June 1987.

Table 1 - Computed Base Shear Strengths and "Measured" Base Shears

Building 1

	Shear Strength	Flexural Strength Composite	Flexural Strength Non-Composite	Maximum Measured
Transverse	0.47W	0.32W	-	0.10W
Longitudinal	0.20W	0.22W		0.10W

Building 2

	Shear Strength	Flexural Strength Composite	Flexural Strength Non-Composite	Maximum Measured
Transverse	0.62W	0.71W	0.32W	0.17W
Longitudinal	0.56W	0.59W	0.29W	0.24W

Note: W = 24,000 kips for Building 1.
W = 23,000 kips for Building 2.

Table 2 - Computed and Measured Periods, sec

Building 1

	Measured	Calculated			
		Model 1	Model 2	Model 3	Model 4
Transverse	0.45	0.32	0.38	-	0.50
Longitudinal	0.65	0.49	0.59	-	0.74

Building 2

	Measured	Calculated			
		Model 1	Model 2	Model 3	Model 4
Transverse	0.51	0.32	0.38	0.45	0.50
Longitudinal	0.57	0.35	0.41	0.50	0.55
Torsional	0.56	0.28	0.35	0.40	0.45

Note: Model 1 is gross-section model without soil-structure interaction.
Model 2 is gross-section model with soil-structure interaction.
Model 3 is half gross-section model without soil-structure interaction.
Model 4 is half gross-section model with soil structure interaction.

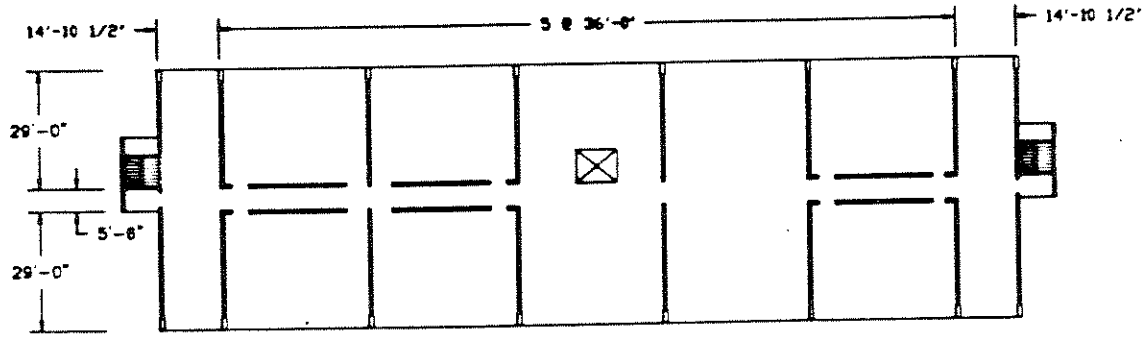

(a) Building 1

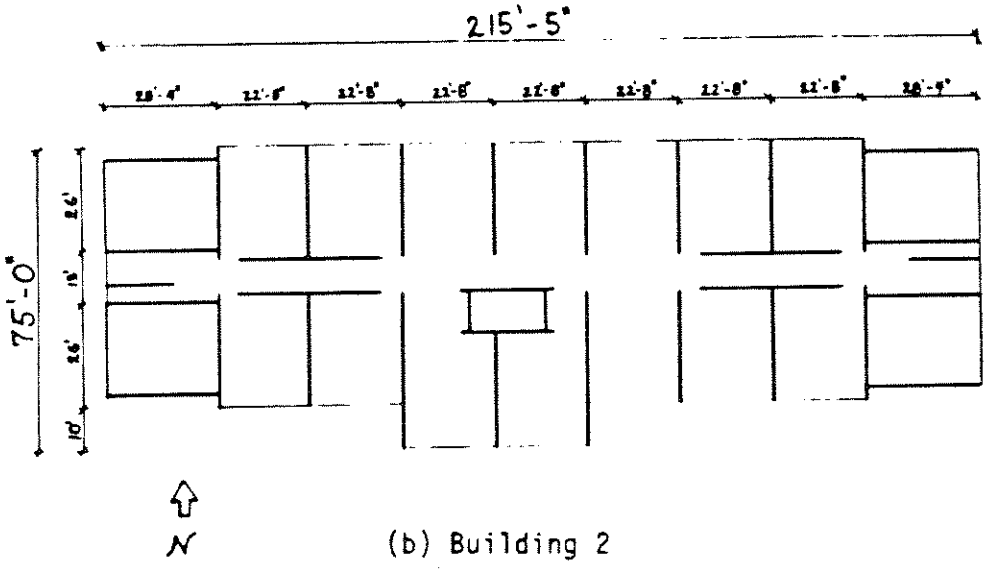

N

(b) Building 2

Fig. 1 Building Plans

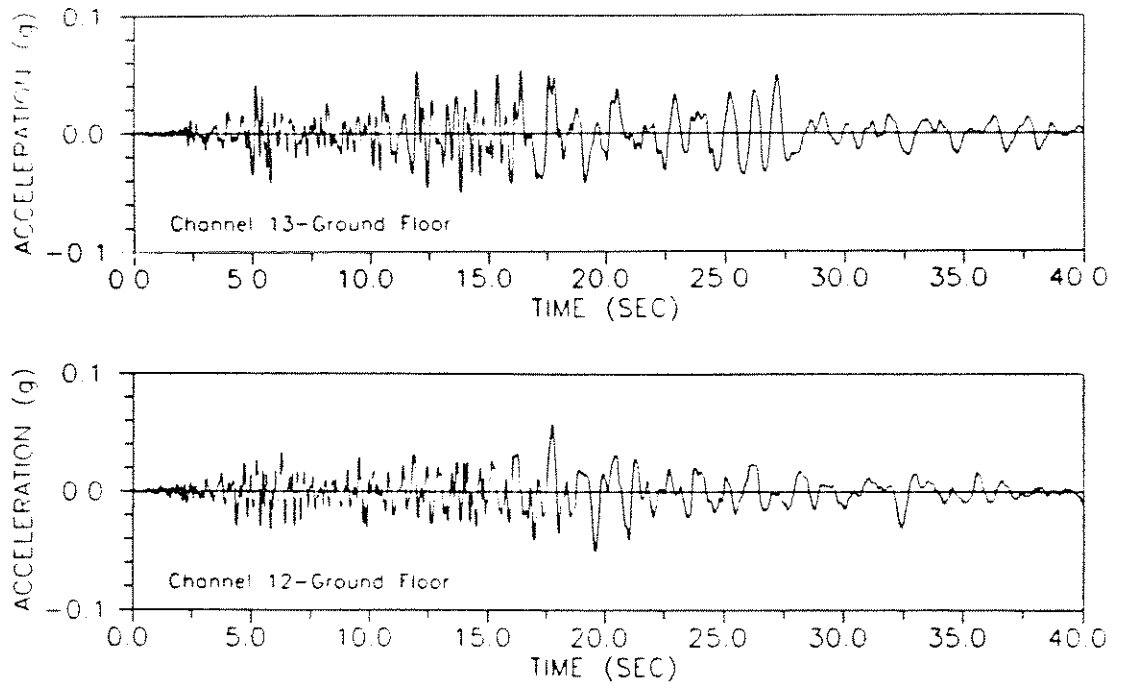

(a) Building 1

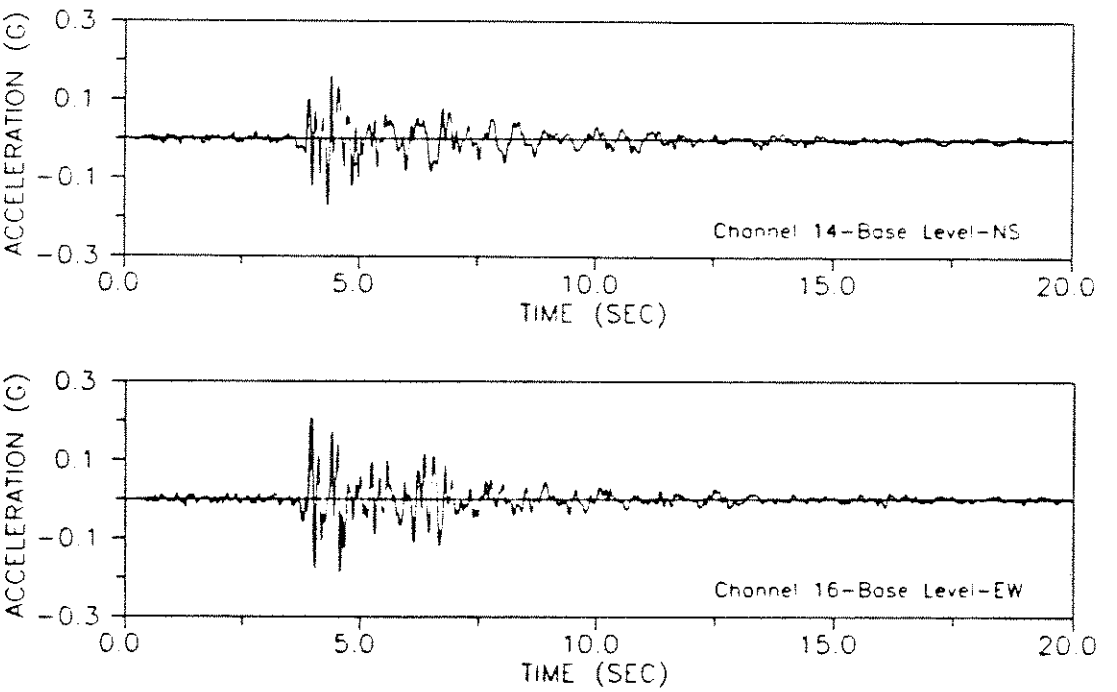

(b) Building 2

Fig. 2 Measured Base Accelerations

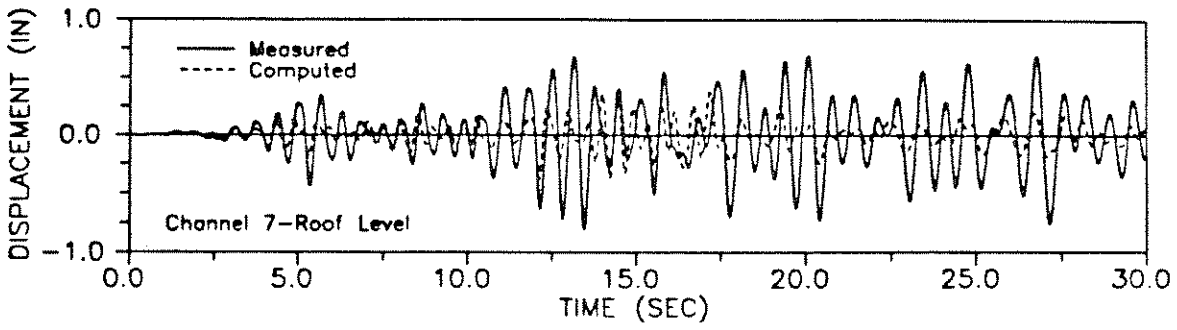

(a) Building 1, Longitudinal

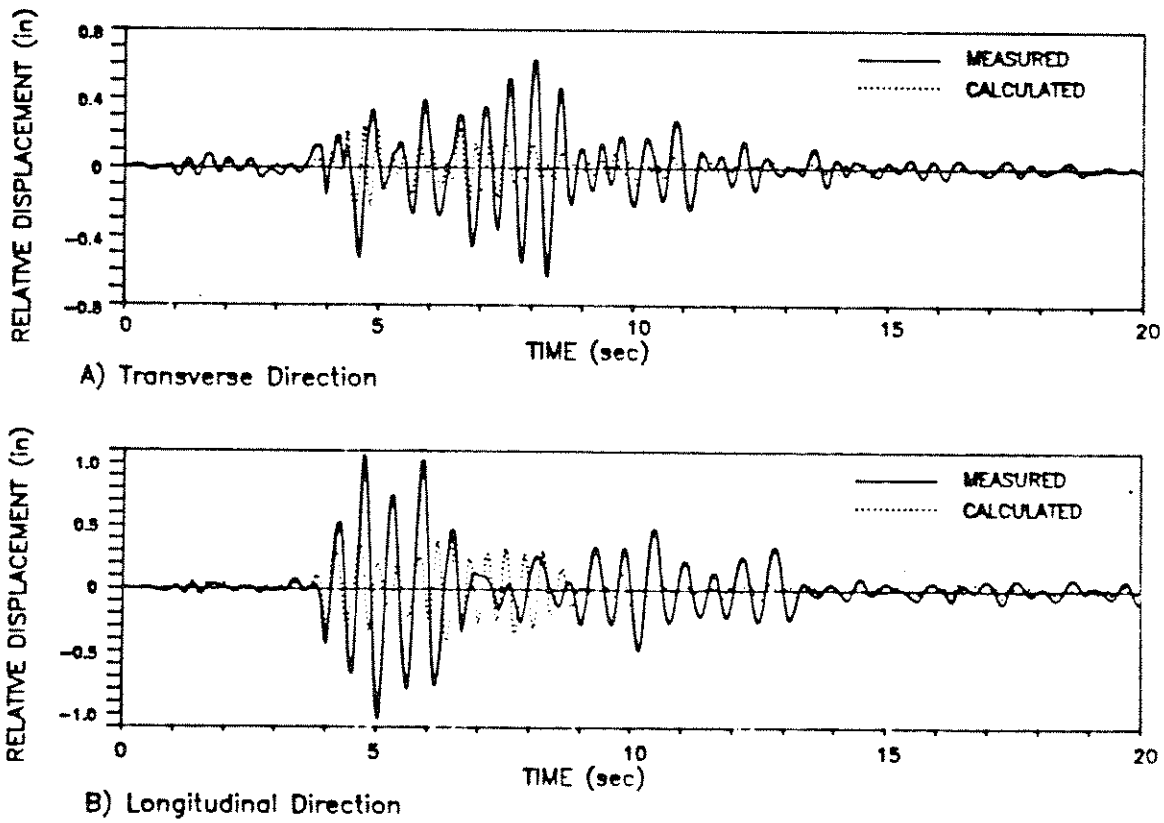

(b) Building 2

Fig. 3 Measured and Calculated Roof Displacement Responses, Gross-Section Model with Fixed Base

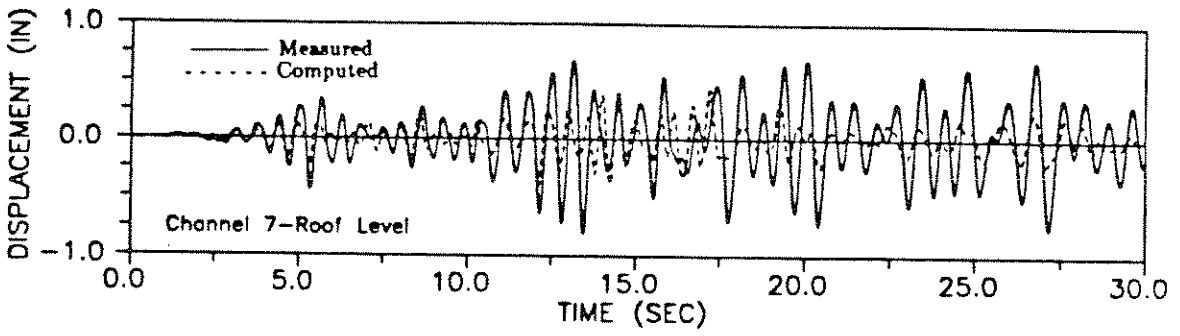

(a) Building 1, Longitudinal

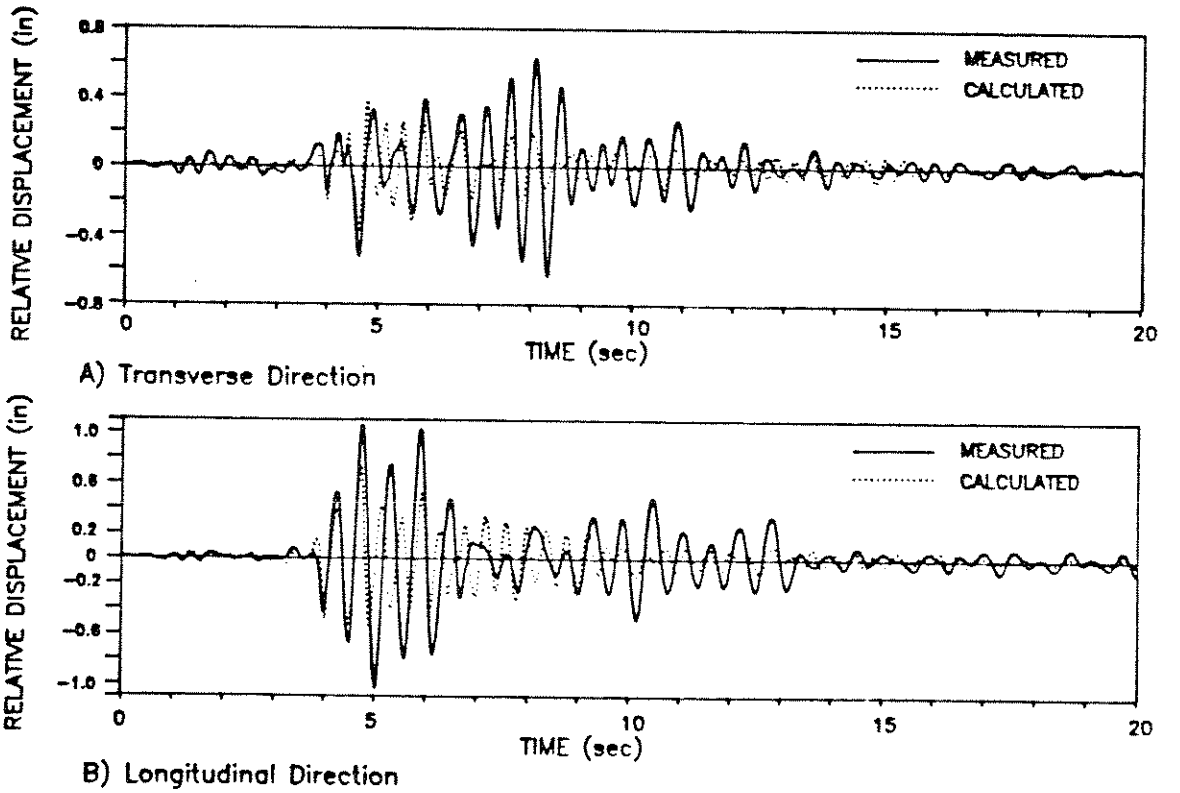

(b) Building 2

Fig. 4 Measured and Calculated Roof Displacement Responses, Gross-Section Model including Soil-Structure Interaction

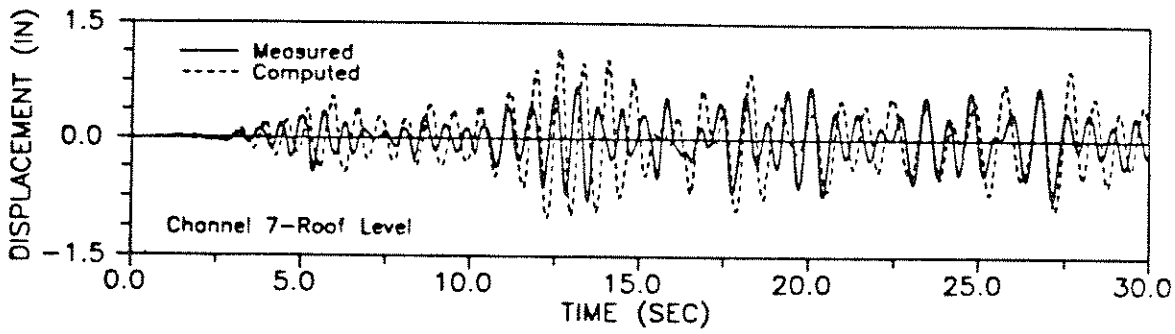

(a) Building 1, Longitudinal

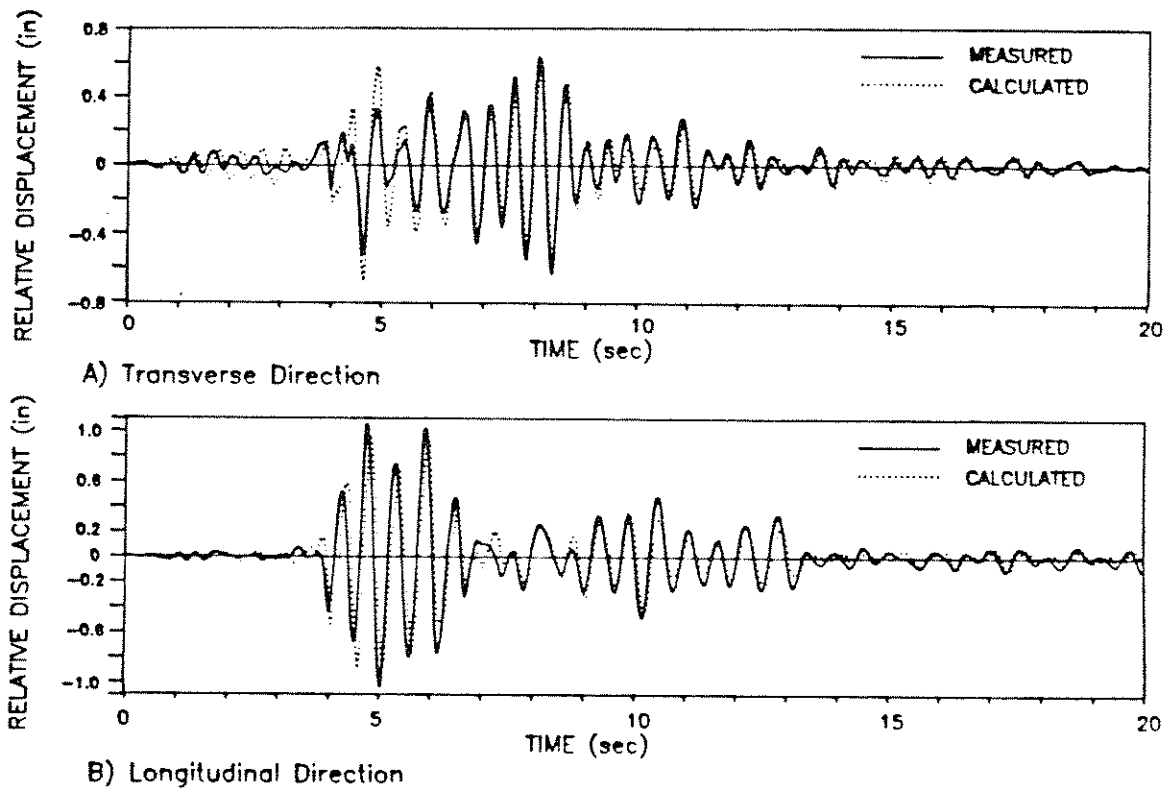

(b) Building 2

Fig. 5 Measured and Calculated Roof Displacement Responses, Half Gross-Section Model including Soil-Structure Interaction

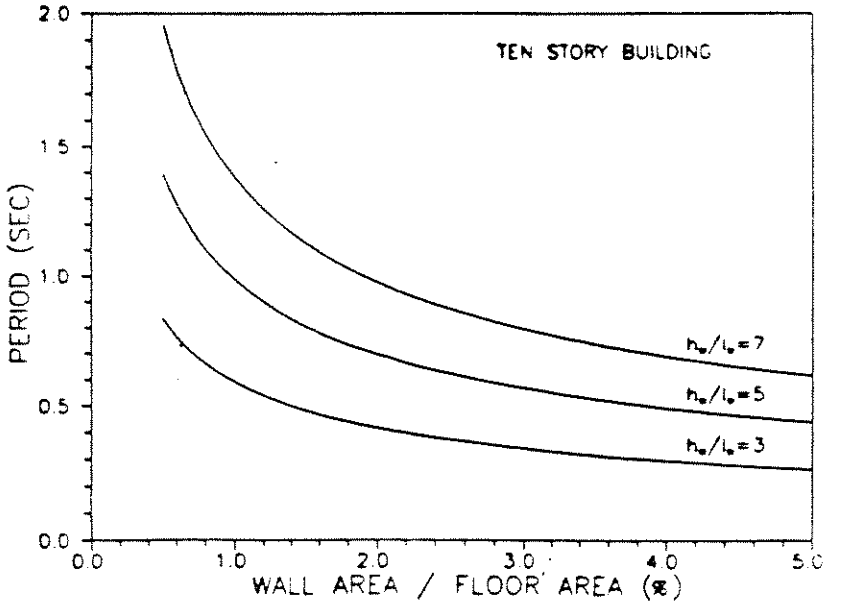

Fig. 6 Calculated Periods for Uniform Bearing Wall Buildings

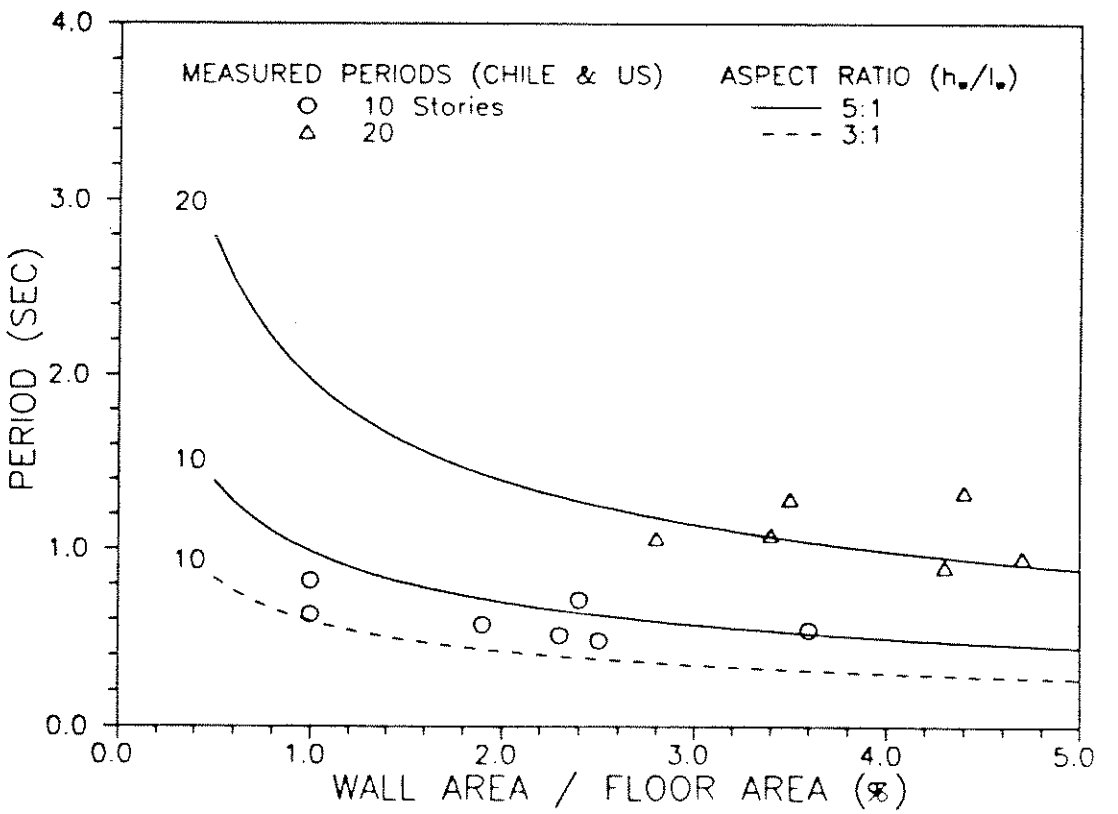

Fig. 7 Comparison of Measured and Calculated Periods

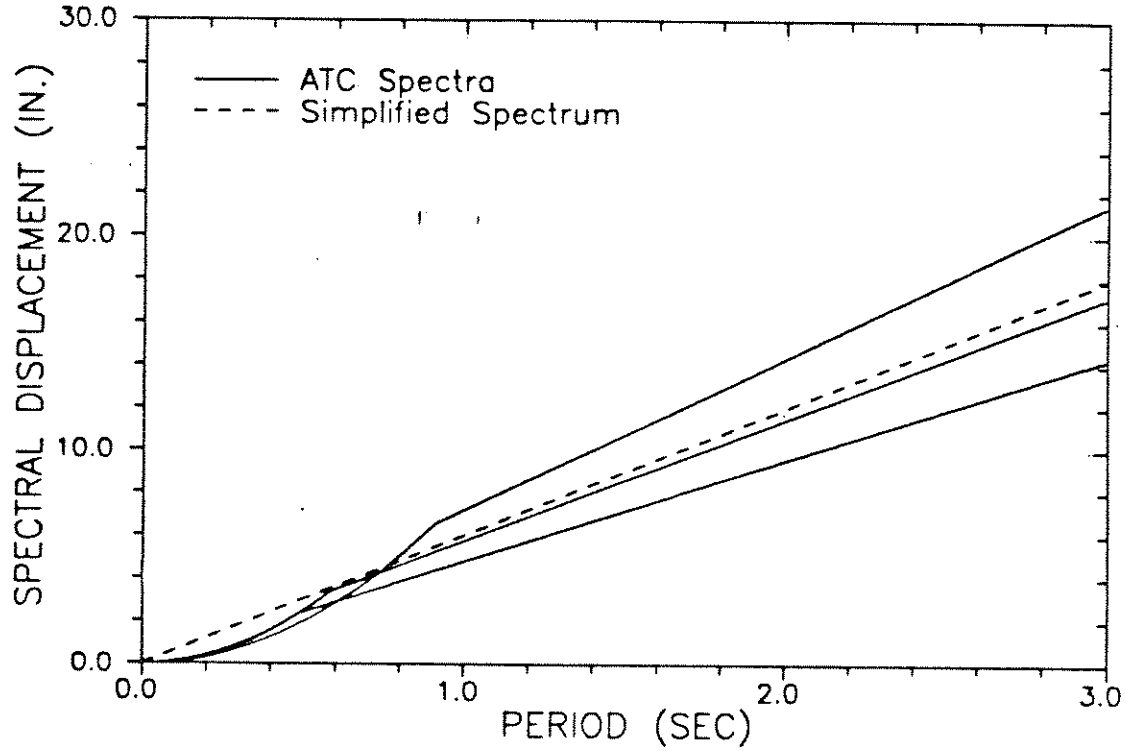

Fig. 8 ATC and Simplified Displacement Response Spectra, 5% Damping

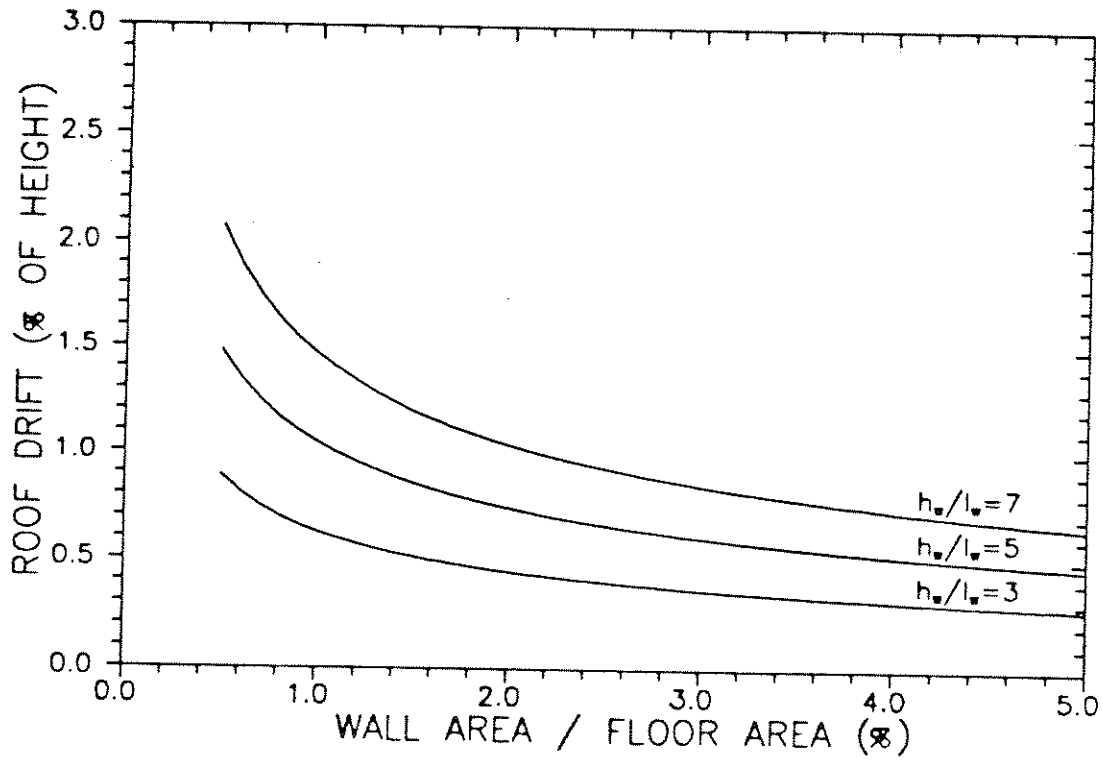

Fig. 9 Calculated Roof Drift as a Function of Building Configuration

$$\delta_u = \delta_y + \theta_p h_w$$

$$\delta_u = \frac{\phi_y h_w^2}{3} + (\phi_u - \phi_y)\frac{h_w l_w}{2}$$

$$\phi_y = \frac{0.0025}{l_w}$$

$$\varphi_u l_w = 0.0025\left[1 - \frac{2h_w}{3l_w}\right] + \frac{2\delta_u}{h_w}$$

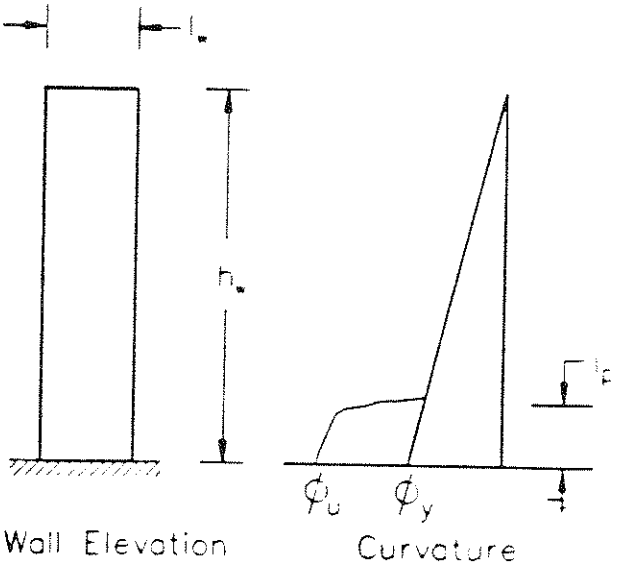

Fig. 10 Model for Estimation of Ultimate Curvature Demands

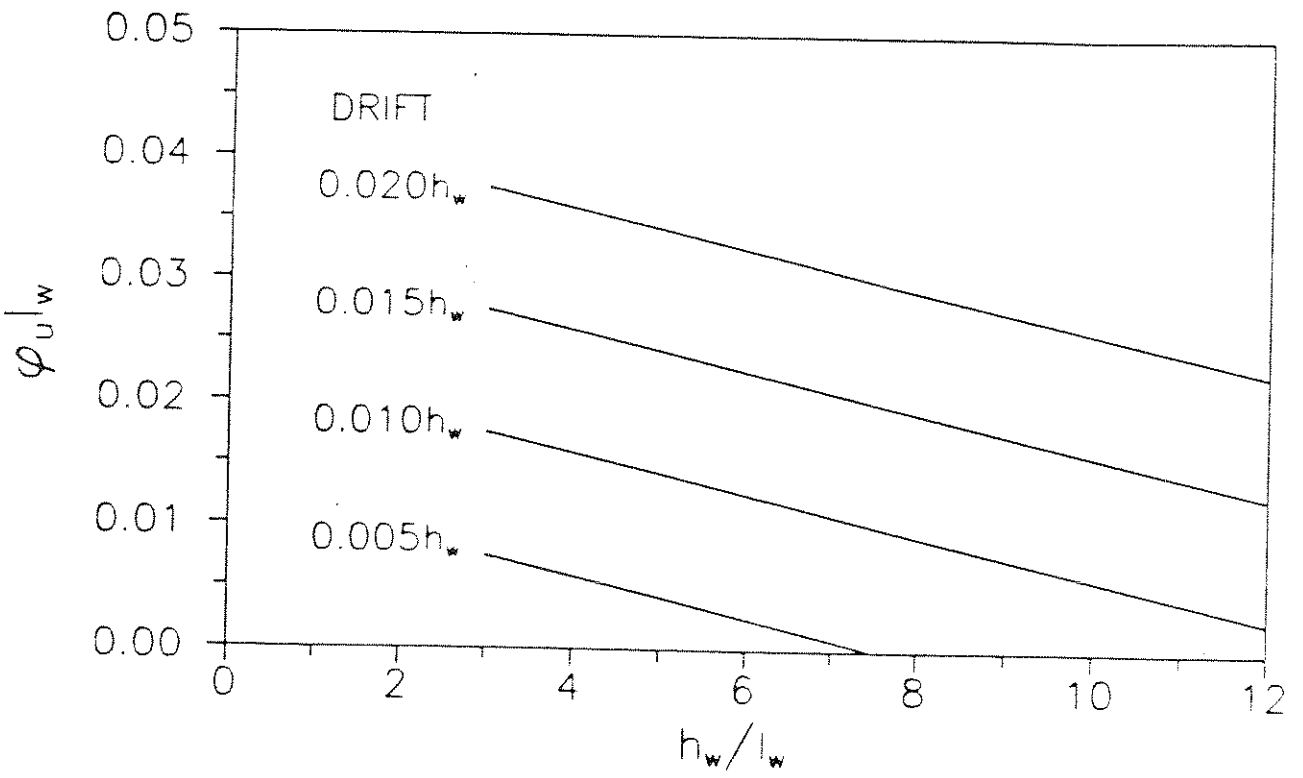

Fig. 11 Relation Between Ultimate Curvature and Building Drift

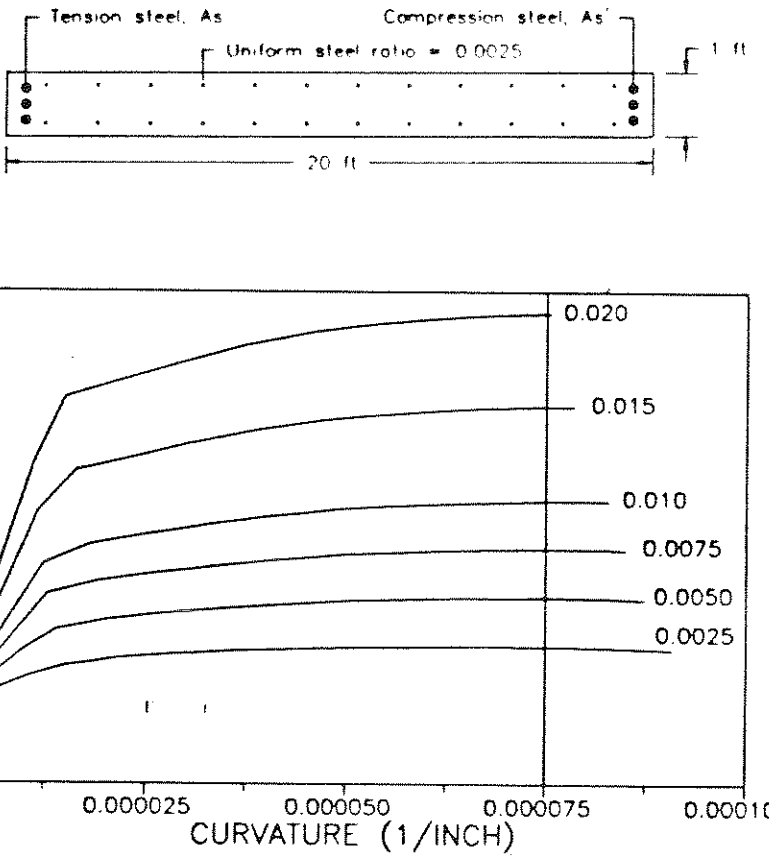

Fig. 12 Calculated Moment-Curvature Relations for Unconfined Walls Having Rectangular Cross Section

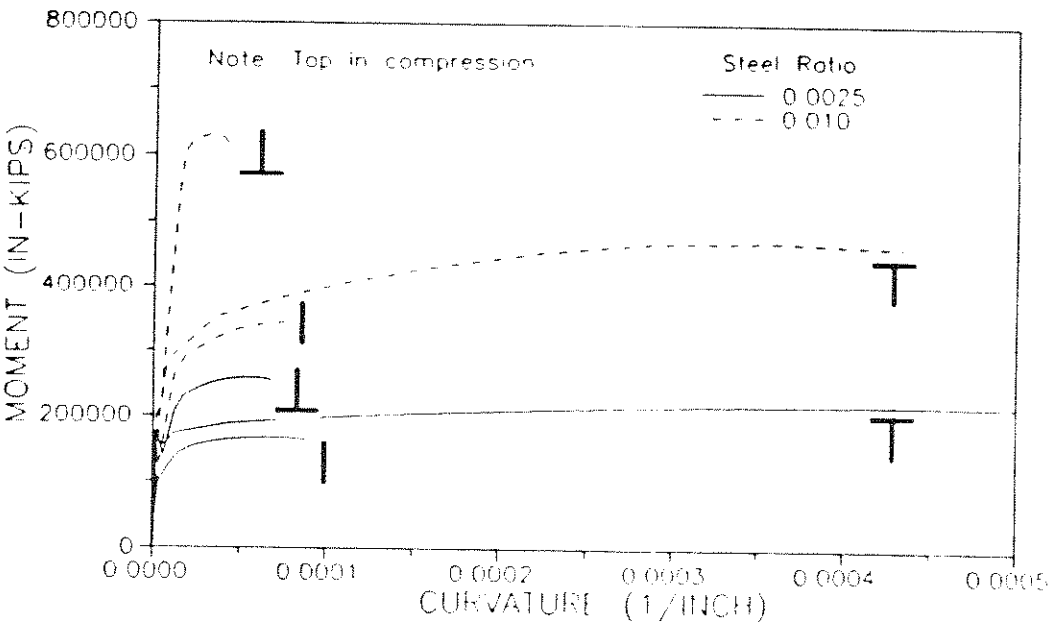

Fig. 13 Calculated Moment-Curvature Relations for Unconfined Walls Having Tee Shaped Cross Section

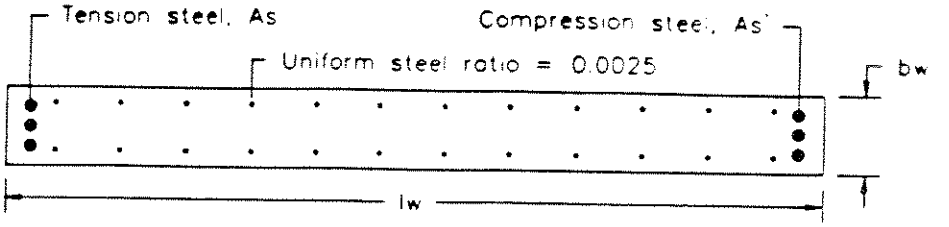

$$\phi_u l_w = \frac{[0.85^2 \epsilon_{cu} f_c'/f_y + 2\epsilon_{cu}\rho'']}{(\rho - \rho') + \rho'' + P/bt_w f_y}$$

Fig. 14 Idealized Wall Cross Section

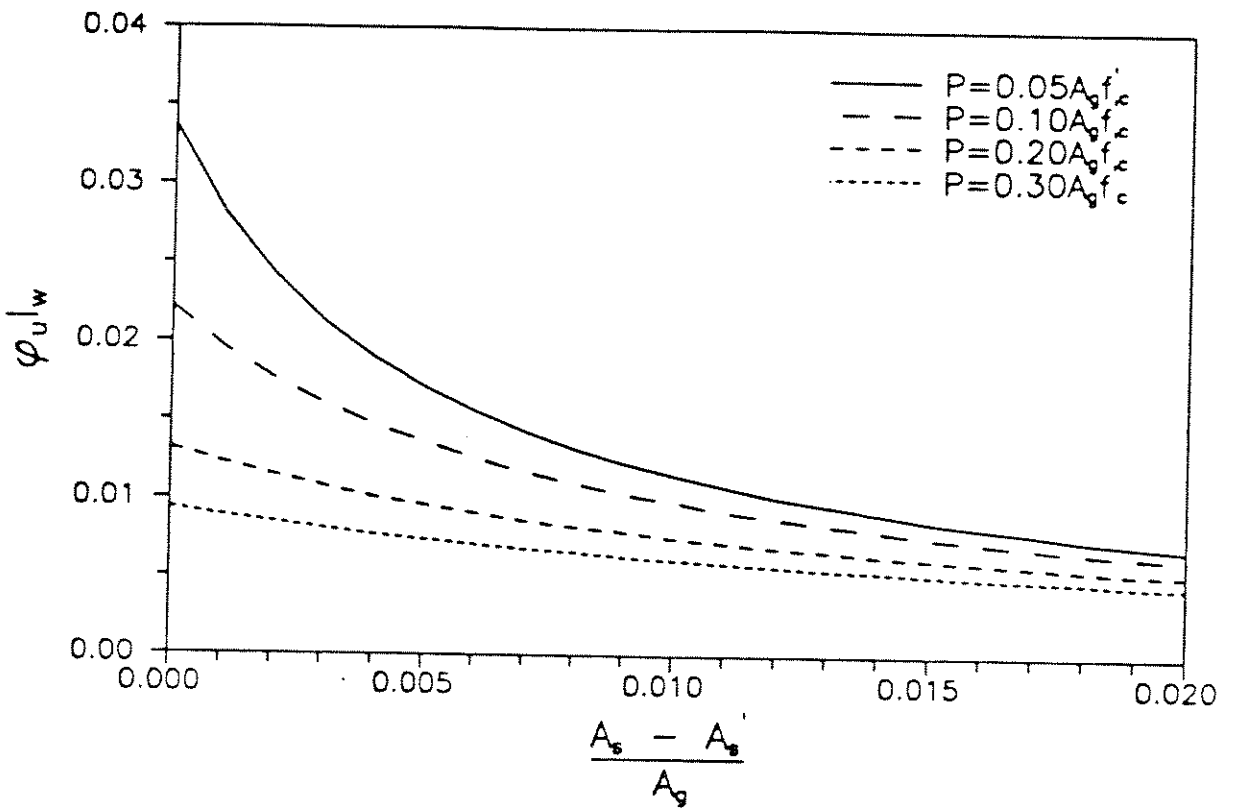

Fig. 15 Calculated Ultimate Curvature Capacity for Unconfined Walls

APPENDIX A

DETAILED EVALUATION OF CSMIP BUILDING SN-356

Prepared by

John W. Wallace

ABSTRACT

A 10-story building subjected to moderate ground motions during the 1984 Morgan Hill Earthquake is investigated. The bearing wall building, designed in 1970 according to UBC requirements, did not experience any apparent damage from the earthquake ground motions. The building is one of approximately 100 buildings in California to be instrumented by the CDMG Strong Motion Instrumentation program. Thirteen strong-motion instruments located throughout the building measured building responses resulting from the Morgan Hill Earthquake.

The measured acceleration responses are presented and analysed. Fundamental periods in the transverse and longitudinal directions are computed from the measured displacement responses and are compared with those assumed during design of the building. Damping ratios for the structure in both the principal directions are estimated using the measured acceleration response. Base-shear and base-overturning moment responses are also derived from measured accelerations. Response spectra for an elastic system and displacement ductility spectra for the inelastic system are computed for the horizontal components of ground motions to investigate the behavior of the structure.

Two and three dimensional analytical models are developed for the building to investigate modeling techniques for bearing wall buildings. Various elastic analyses on the building are carried out using these analytical models to address the importance of soil-structure interaction, damping and structural element stiffness typically assumed.

TABLE OF CONTENTS

LIST OF FIGURES

LIST OF TABLES

LIST OF SYMBOLS

f'_c	concrete strength
γ	unit weight of soil
V	total base-shear
C	coefficient based on fundamental period
K	horizontal force coefficient
T	fundamental period
H	height of the building
D	plan dimension of the building parallel to the direction of applied load
W	weight of the building
N	number of stories
C_y	base shear yield strengh
h_w	height of wall
l_w	length of wall
V_n	shear strength
A_{cv}	shear area
ρ_n	steel reinforcing ratio
f_y	steel yield stress
$\tilde{T}$	effective natural period of modified system
K_x	translational stiffness of the foundation
K_θ	rocking stiffness of the foundation
K	lateral stiffness of the structure
h	height from the base of the structure to the centroid of the inertia forces
G	shear modulus of the soil
ν	poisson's ratio
v_s	shear wave velocity
g	acceleration due to gravity
r	radius of foundation
A_0	effective area of contact between the foundation and soil
I_0	static moment of inertia of the foundation
$\tilde{\beta}$	damping factor of the elastically supported structure
β	damping factor of the fixed base structure
β_0	foundation damping ratio
f_{min}	minimum point in the real portion of frequency response function
f_{max}	maximum point in the real portion of frequency response function
ζ	damping ratio

Chapter - 1

INTRODUCTION

Current code requirements for earthquake resistant design of buildings are based on the philosophy of limiting damage in moderate earthquakes and providing life safety in major earthquakes. However, recent earthquakes in California have pointed out that this philosophy may not be appropriate for all buildings. In particular, for buildings with important functions or valuable contents, more stringent guidelines may be needed.

To obtain improved building performance in both moderate and major earthquakes requires a reliable distribution of strength and stiffness throughout a structure, and the control of lateral drift. For buildings of moderate height (5 to 20 stories), an ideal system to obtain reliable performance is a bearing wall system. Bearing wall systems provide a reliable level of strength to the building, and also limit lateral deformations. Although a bearing wall system appears to be an ideal building system to meet a particular set of design objectives, current code requirements typified by the Uniform Building Code (1988) penalize the use of such systems by requiring susbtantially higher design forces compared with ductile moment frame systems. In addition, ductile detailing requirements and inspection to the same degree as for moement resisting frame system. Recent research [Wallace and Moehle (1989)] has revealed the possibility of alleviating construction inspection and expensive ductile detailing practices without loss in performance reliability. However, these conclusions cannot be stated definitively at present due to the lack of information to verify analytical models available for bearing wall buildings.

In this report the behavior of a ten-story bearing wall building subjected to moderately intense ground motions is studied. Structural walls are used to provide the vertical and

lateral load resisting systems of the building. No apparent damage to the structural or non-structural components of the building was reported following the earthquake. The structure is studied using the measured responses of thirteen strong-motion accelerographs that were installed in the building. The measured responses are correlated with computed responses using analytical models developed using computer program SAP-90 [Wilson (1989)]. Based on the results of the analyses, recommendations are presented.

1.1 The 24 April 1984 Morgan Hill Earthquake

On Tuesday, 24 April 1984, at 7:00 a.m., a moderate earthquake occurred in the San Francisco Bay area of California [EERI (1985)]. The epicenter of the earthquake was located in the town of Morgan Hill, approximately 10 miles southeast of San Jose, California (Fig. 1), and approximately 40 miles south of the city of San Francisco. The estimated focal depth of the earthquake was 5 miles. The earthquake affected the entire San Francisco Bay area, and was felt as far away as Reno, Neveda and Santa Barbara, California, approximately 200 miles from the epicenter. The earthquake had a surface magnitude, $M_s = 6.4$, and a P-wave magnitude, $M_b = 6.9$. Modified Mercalli Intensities were VII to VIII in the epicentral regions. Several aftershocks were recorded [EERI (1985)].

The earthquake resulted in moderate damage in Morgan Hill. Less than 1% of the residential structures suffered major damage, and approximately 8% suffered varied degrees of damages in the epicentral region. A majority of the damage was the result of wood-framed houses sliding off their foundation. No significant damage was reported in the city of San Jose. No deaths resulted from the earthquake, and only minor injuries were reported.

1.2 Building Description

CSMIP Building SN-356, hereinafter known as Building SN-356, is located in San Jose, California. The 10-story building is rectangular in plan (Fig. 2), and is almost symmetrical.

The building was constructed in 1971-72, and would be classified as a bearing wall building by current code (UBC-1988) classifications.

Elevation views of the building are presented in Fig. 3. All stories have a height of 9 ft except the first, which is 15 ft, for a total superstructure height of 96 ft. The transverse wall thickness varies from 9 in. at the base to 6 in. at the roof (Fig. 3.a). The longitudinal wall thickness varies from 11 in. at the base to 7 in. at the roof (Fig. 3.b). The transverse walls are supported on 2 ft deep footings (2'-6"and 4'-4" wide), whereas the longitudinal walls are supported on 5 ft deep footings that span the central corridor (8'-0" wide) (Fig. 4). The footings are supported on precast concrete or steel pipe with cast in place concrete piles.

Structural walls coupled by a 10-inch floor slab predominate the lateral and vertical loads resisting systems of the structure. The sixteen transverse walls are continuous over the height of the building (Fig. 3.a), except at the first floor where several openings exist in the transverse walls to accomodate door openings. The longitudinal walls are continuous over the height of the building except between axes 4 and 6, where the two interior walls terminate at the sixth floor (Fig. 3.b). Typical reinforcing details at the base of the transverse and longitudinal walls are shown in Fig. 3.a and 3.b, respectively. No wall boundary elements are used except at the exterior of the building of the transverse walls, where 36 x 14 inches columns exist. The roof slab is 8.5 inches thick. Both the floor slab and roof slab are post-tensioned, and were designed to carry loads in only one direction.

Building SN-356 was designed in 1970-71, and constructed in 1971-72. Details appear to be consistent with those in common practice at the time of construction (no specially detailed boundary elements for the walls). Typical material properties were used for the building. Lightweight concrete (f'_c = 4000 psi, γ = 110 pcf) was used for the slabs, and normal weight concrete (f'_c = 3000 psi) was used for the walls. Grade 60 reinforcement was used for all bars greater than Number 5; otherwise, Grade 40 reinforcement was used.

The building was designed using Uniform Building Code equation V = KCW, where

K=1.33, $C = \frac{0.05}{\sqrt[3]{T}}$, $T = \frac{0.05H}{\sqrt{D}}$, W is the building weight, H is the height of the building, and D is the plan dimension of the building parallel to the direction of the applied load. The relation for the period results in estimates of 0.59 sec and 0.32 sec for the transverse and longitudinal directions, respectively. The resulting design base shear coefficients are 0.079W for the transverse direction and 0.097W for the longitudinal direction.

The floor area of the building is approximately 13650 ft^2 (63.5' x 210'). A mass distribution of 175 psf was computed for the building (Table 1.1), yielding a total building weight of 24000 kips (excluding the foundation). The ratio of the cross-sectional area of the structural walls at the base of the building to the total floor area are 2.8% and 1.0% in the transverse and longitudinal directions, respectively. All of the walls in the building are appoximately the same size (wall length times thickness: 29' x 9" transverse, 24' x 11" longitudinal); therefore, the building is substantially stiffer in the transverse direction compared with the longitudinal direction.

Chapter - 2

MEASURED RESPONSES

As part of the California Strong-Motion Instrumentation Program (CSMIP) thirteen analog accelerometers were installed in Building SN-356. The layout of the sensors is shown in Fig. 5. Three vertical and three horizontal (two transverse and one longitudinal) accelerometers were attached at the base of the building, three horizontal (two transverse and one longitudinal) accelerometers were attached at the sixth floor, and four horizontal (three transverse and one longitudinal) accelerometers were attached at the roof. The measured responses [CDMG (1984)] are presented, analysed, and discussed in the following subsections.

2.1 Acceleration Responses

Figure 6 plots the recorded acceleration for the thirteen instruments. The peak ground acceleration recorded [CDMG (1984)] at the base of the building was 0.062g and 0.058g for Channels 11 and 12, respectively (transverse direction), and 0.054g for channel 13 (longitudinal direction). The plots for the transverse motions at the base (channels 11 and 12), the sixth floor (channels 8 and 9), and the roof (channels 4, 5, and 6) are very similar, indicating no significant torsional response of the building or in-plane flexibility of the floor diaphragm as a result of the earthquake induced forces. The maximum vertical acceleration recorded at the base of the building was 0.044g at channel 1 (Fig. 6.a). The maximum recorded acceleration at the roof was 0.14g (Fig. 6.d) and 0.21g (Fig. 6.g) in the transverse and longitudinal directions, respectively. This represents an acceleration response amplification of approximately 2.3 and 3.9 in the transverse and longitudinal directions, respectively.

2.2 Displacement Responses

The recorded displacements for the thirteen instruments are also plotted in Figure 6. For the instruments located at the sixth and roof levels, the relative displacement of that level with respect to the base is plotted. The maximum ground displacement recorded at the base of the building was 0.86 inches in the transverse direction (Fig. 6.l), and 1.11 inches in the longitudinal direction (Fig. 6.m). The maximum recorded roof relative displacement was 0.23 in. (0.02% of the building height) and 0.81 in. (0.07% of the building height) in the transverse and longitudinal directions, respectively.

The displacement response over the height of the building is plotted in Fig. 7 and Fig. 8 for the transverse and longitudinal directions, respectively. The measured displacements are plotted between t = 17.50 sec to 17.80 sec in the transverse direction, and for t = 13.14 sec to 13.48 sec in the longitudinal direction, when maximum roof displacement occurred. Linear interpolation is used between the measured displacement response at the roof, 6th floor, and the base of the building. The maximum displacement response indicates that first mode response was dominant for both the transverse and longitudinal directions.

2.3 Estimates of Fundamental Periods

Estimates for the fundamental period in the transverse and longitudinal directions were obtained from the measured relative displacement response by averaging the duration between several cycles of response near the maximum response. The resulting estimates of fundamental period are 0.45 sec (N/22), and 0.65 sec (N/15) in the transverse and longitudinal directions, respectively, where N is number of stories. These periods differ significantly from those assumed during design of the building (0.59 sec in transverse and 0.32 sec in longitudinal direction). The difference is due primarily to the UBC equation which does not account for the distribution of stiffness in each of the principal directions of the building (i.e., number of walls).

2.4 Damping Ratios

Damping ratios for the structure were estimated using the measured acceleration response using a procedure described by Farrar and Bennet (1988). The calculated transverse and longitudinal damping ratios are assumed independent, and are obtained by using a frequency response function. The frequency response function is defined as the Fourier transform of the absolute acceleration response at the roof level divided by the Fourier transform of the acceleration input at base of the building. In general, the function is complex; however, only the real portion of the frequency response function is used to estimate the damping characteristics of the structure. The damping ratio can be determined from the following expression

$$\zeta = \frac{1}{2}\left[\frac{(f_{min}/f_{max})^2 + 1}{(f_{min}/f_{max})^2 - 1}\right] \tag{2.1}$$

where ζ is damping ratio, f_{min} and f_{max} are minimum and maximum points in the real portion of frequency response function.

For the transverse direction of the building, the damping ratio is estimated using the measured acceleration response at channels 4 and 11 (Fig. 6.d, 6.k). For the longitudinal direction, the damping ratio is computed using measured acceleration response at channels 7 and 13 (Fig. 6.g, 6.m). The estimated frequency response functions are plotted in Fig. 9 and Fig. 10 for the transverse and the longitudinal directions, respectively. The damping ratios calculated using the recommended procedure are 4.9% and 11.5% in longitudinal and transverse directions, respectively. The damping ratio of approximately 5% for the longitudinal direction is consistent with that expected for a R.C. building subjected to moderate response levels [Gulkan and Sozen (1974)]. The damping ratio for the transverse direction appears high. However, the effects of soil-structure interaction, which are likely to be more significant for the transverse direction due to the geometry and structural layout of the building, have not been considered. Mahin (1989) calculated damping ratios of 5% and

14% for Building SN-356 using the measured acceleration responses. The damping ratios calculated by Mahin (1989) are similar to those computed using the frequency response function approach. The difference in the damping ratios computed for the transverse direction (11% vs 14%) may be due to processing errors which are significant for the transverse direction response (see Section 4.3, Analysis - 1).

2.5 Base-Shear and Base-Overturning Moment Responses

Base-shear and base-overturning moment response for the transverse and longitudinal directions of the building are estimated using the measured acceleration response records. Because acceleration response was not measured at every floor, accelerations at intermediate floor levels were determined using linear interpolation from measured accelerations at base, sixth, and roof levels. Base shear was computed by summing the product of the estimated mass and measured acceleration response at each floor level. Base-overturning moment was computed as the sum of the product of the story mass, acceleration, and height. Computed base-shear and base-overturning moment responses are plotted in Fig. 11.

For the transverse direction, channels 4, 8, and 11 were used to compute base-shear and base-overturning moment. The maximum calculated base shear for the building is 2415 kips and the maximum calculated base-overturning moment is 1593600 in-kips at 17.80 seconds. Assuming the base-shear and base-overturning moment are equally distributed to the sixteen walls in the transverse direction, the maximum calculated base-shear and base-overturning moment per wall are 151 kips ($0.9\sqrt{f'_c}$)and 99600 in-kips, respectively.

For the longitudinal direction, base shear and base moment were computed at the top of the first story due to the very high flexural stiffness of the first story (Fig. 3b). Acceleration responses at channels 7, 10, and 13 were used to compute base shear and moment response. The base-shear and base-overturning moment responses are shown in Fig. 12. The maximum calculated base-shear for the building (at the top of the first story) is 2450 kips and overturning moment is 1530000 in-kips at 17.78 seconds. Assuming the

shear and overturning moment are equally distributed to the six walls in the longitudinal direction, the maximum calculated shear and overturning moment per wall are 410 kips ($2.9\sqrt{f'_c}$) and 255000 in-kips, respectively.

2.6 Base Rotation

During an earthquake a building supported on flexible foundation materials may rotate at its base. This base rotation may significantly affect the response of the building. To gage the importance of this rocking motion, the measured base responses were used to compute the base rotation during the earthquake. The base rotaion is computed using the recorded vertical displacements at the building base and the geometry of the building. The displacements in vertical direction were recorded at three locations (channels 1, 2, and 3) during the earthquake (Fig. 5). From these recorded displacements, the rotation of the base of the building in the transverse direction is computed. The base rotation is computed by two methods to evaluate the reliability of the results. In the first method, rotation (θ_1) is calculated as the relative displacement between channel-2 and channel-3 divided by the distance between the channels (approximately 336 in). Similarly, rotation (θ_2) is calculated as the relative displacement between channel-1 and channel-3 divided by the distance between the channels (approximately 672 in). The calculated base rotations for the transverse direction are plotted in Fig. 13. An examination of Fig. 13 reveals that the two estimates follow a similar pattern; therefore, it is reasonable to assume that the results can be used to compare with analytically obtained results, and that the footings at the base of building behave essentially as a rigid plate (for transverse direction responses).

The base rotation cannot be computed in the longitudinal direction because no instruments were used to record vertical movements along this axis of the building.

Chapter - 3

RESPONSE SPECTRA

Response spectra for an elastic system and displacement ductility spectra for an inelastic system were computed for the horizontal components of ground motion. Numerical integration employing Newmark's Beta Method [Newmark (1959)] for constant acceleration was used to compute the maximum response quantities. A maximum time step of 0.01 seconds was used.

3.1 Elastic Response Spectra

Elastic response spectra for viscous damping of five percent of critical were computed. Figure 14 presents the calculated spectral displacement and spectral pseudo-acceleration for the horizontal components at the base of the building.

The spectral shapes for the transverse acceleration (Channels 11 and 12) are nearly identical (Figs. 14.a), indicating that the motion at the base of the building did not vary significantly with distance along the longitudinal axis of the building. The peak ordinates of spectral acceleration are 0.18g and 0.24g for the transverse and longitudinal directions, respectively. The peak spectral ordinates occur between periods of approximately 0.5 to 0.8 seconds and 1.2 to 1.4 seconds for the transverse direction, and 0.2 to 0.4 seconds and 0.8 to 1.2 seconds for the longitudinal direction.

The ordinates of spectral displacement are relatively small for periods less than 0.2 seconds, then increase moderately to a value of approximately 0.80 inches at a period of 0.80 seconds. The ordinates increase abruptly to approximately 3 inches for periods greater

than approximately 0.80 seconds. For buildings with periods less than 0.80 sec., roof drift would be relatively small. For example, roof drift for a ten-story wall building with a period 0.80 sec would be approximately 0.10% (roof drift calculated as 1.4 times the spectrum drift, and 9 ft story heights are assumed).

3.2 Inelastic Displacement Ductility Spectra

Inelastic displacement ductility spectra for the transverse and longitudinal horizontal base motions were computed for base shear yield strengths (C_y) of 10, 20, and 30 percent of building weight. Viscous damping was taken as five percent of critical for the elastic structure. Perfectly plastic yielding was assumed for post-yield behavior. The displacement ductility spectra are presented in Fig. 15.

The spectra reveal that significant inelastic responses would not be expected to result from the earthquake ground motions. For a building with a base shear strength of 0.10W, displacement ductility demands are two or less for all periods. However, the minimum code strength of a typical ten story building with structural walls (aspect ratio for the wall, h_w/l_w, of 3:1) would be expected to be approximately 0.20W [Wallace and Moehle (1989)]; therefore, essentially elastic response is expected for both transverse and longitudinal building response for all periods.

Chapter - 4

ANALYTICAL MODELING AND RESPONSE CORRELATION

Several analyses were conducted to understand the behavior of building SN-356 during the 1984 Morgan Hill earthquake. The analytical modeling techniques used and the analysis results are presented and discussed in this chapter.

4.1 Modeling Techniques

Analytical modeling techniques for the elastic analysis of the building are described. Emphasis was placed on the modeling techniques that could be used readily in the design-office practice. Flexural and shear deformations were included for all members whereas axial deformations were included only in the column and wall elements. Element lengths were defined by centerline-to-centerline dimensions. Stiffness calculations were based on concrete gross sections for the initial calculations, and joint regions were assumed to be infinitely rigid.

Effective widths of coupling slabs were computed using the results of Qadeer et al (1969). The resulting slab width is typically equal to the wall width plus six slab depths. Effective slab widths were varied to determine their influence on computed responses. The results of these analyses indicated that the effective slab width did not significantly influence computed responses.

The column analogy was used to model the structural walls (Fig. 16). The moment of inertia and area of the column were taken equal to that of the wall. Rigid beams extending to

the wall boundary were used at each story level to maintain the kinematics of the structural system. This analogy is reasonable for walls where flexural behavior dominates the response. The aspect ratios (h_w/l_w) of the walls for Building SN-356 are 3.3:1 (transverse) and 4:1 (longitudinal). These ratios are in a range where flexural behavior dominates wall behavior; therefore, it was reasonable to use the column analogy.

4.2 Computed Strength

Base shear strength of Building SN-356 was calculated in each of the principal directions considering (1) flexural mechanisms extending over the height, and (2) wall shear strength computed according to the Uniform Building Code (1989).

Calculations of element flexural strengths to compute base shear strength of the building were based on the same element cross–sections and material properties used for the elastic analysis. A larger effective slab width may be appropriate; however, the strength contribution of the slab is insignificant compared with the strength contribution of the walls. Typical wall reinforcement is shown in Fig. 3.a and 3.b for the transverse and longitudinal walls, respectively.

The flexural strength of Building SN-356 was computed for a triangular loading distribution over the building height (Fig. 17). The controlling mechanism consisted of yielding at the base of the walls and in the coupling beams over the height of the building (Fig. 17). Uplifting of the walls due to rocking was neglected; therefore, the work required to uplift wall tributary gravity loads was not considered. The distribution of strength over the height of the wall was checked to ensure that wall yielding did not occur at other levels. The flexural strength of the slabs and walls were computed including the effects of steel strain hardening. Unconfined concrete was assumed because the detailing provided in the walls would not significantly increase the flexural strength. The flexural strength of the walls was calculated based on tributary gravity loads using the computer program BIAX [Wallace and Moehle (1989)].

The shear strength of the walls was computed to compare with the flexural capacity. Wall shear strength was computed using UBC(1988) Equation (25–6).

$$V_n = A_{cv}\left[2\sqrt{f_c'} + \rho_n f_y\right] \tag{4.1}$$

where, A_{cv} is the shear area of the wall in square inches, ρ_n is the steel ratio for the wall web, and f_y is the yield stress for the web steel in ksi. Concrete strength is based on specified design values (f_c' = 3000 psi). Specified yield stress is used for the steel (f_y = 60 ksi or 40 ksi for number 3 bars or smaller).

Table 4.1 presents the computed base shear and flexural strengths of the building. The computed flexural strengths of the building are 0.32W and 0.22W in the transverse and longitudinal directions, respectively. The computed flexural strengths are similar to those reported for bearing wall buildings in Chile [Wallace and Moehle (1989)], and are consistent with minimum flexural strengths expected for bearing wall buildings [Wallace and Moehle (1989)]. The computed shear strengths of the building are 0.47W and 0.20W in the transverse and longitudinal directions, respectively. The strength of the building is limited by the flexural strength of the walls in the transverse direction; however, flexural and shear strengths are approximately equal in the longitudinal direction. The computed strengths in the transverse direction are greater than those in the longitudinal direction because 16 walls resist loads in the transverse direction, whereas only 6 walls resist loads in the longitudinal direction.

Based on the computed flexural strengths and the inelastic displacement ductility spectra presented in Section 3.2, inelastic response demands can be estimated for the building. For the measured transverse period of approximately 0.45 sec (Section 2.3) and the computed flexural strength of 0.32W, displacement ductility demand is approximately 0.40. For the measured longitudinal period of approximately 0.62 sec (Section 2.3) and a computed flexural strength of 0.22W, displacement ductility demand is approximately 0.70. It is noted that for the computed building strengths that the displacement ductility demand is one or

less for all periods. A displacement ductility of one or less represents elastic response; therefore, essentially no inelastic deformations are expected for response of the building to the recorded ground motions in either of the principal directions. However, larger responses are expected for the longitudinal direction which could lead to more load induced cracking of the walls aligned in this direction.

4.3 Dynamic Response Analysis

Linear elastic response history analyses were conducted using conventional software programs (the SAP–89 program was used). The analyses had the objectives of calculating periods and response quantities that could be compared with those recorded during the earthquake, and establishing appropriate analytical models for the buildings.

Given the symmetry of the floor plan of Building SN-356, relatively simple two-dimensional models were prepared for the transverse and longitudinal directions. The model for the transverse direction considered contributions of only the walls aligned in that direction (Fig. 2). The model for the longitudinal direction considered two frames, one to model the transverse walls (and exterior columns) and one to model the corridor walls. Effective coupling slabs were based on the procedures outlined in Section 4.1. A 3D model was also prepared to investigate the effects of coupling between walls aligned in the transverse and longitudinal directions.

Several analyses were conducted for each of the building models discussed in the preceding paragraph. The analyses addressed uncertainties in the building stiffness and the influence of soil flexibility on building responses. Responses to the measured horizontal ground accelerations were computed for each of the models. For the 2D models, a single component of transverse ground acceleration (Channel 12) was used, whereas two components of horizontal ground acceleration (channel 12 and 13) were used for the 3D model. Viscous damping equal to five percent of critical was assumed for all analyses unless noted. Each of the analyses are described in the following subsections.

Analysis 1: Concrete Gross–Sections – Fixed Base Model

The first analysis assumed concrete-gross sections and a fixed base foundation to represent building stiffness. These assumptions are consistent with those commonly used in design office practice for typical buildings.

Computed periods for the building model are presented in Table 4.2. For comparison, periods estimated from the measured displacement response (Fig. 6), UBC-1985 Eq. $T = \frac{0.05h}{\sqrt{D}}$, and UBC-1988 Eq. $T = C(h)^{\frac{3}{4}}$ are also given in Table 4.2. The computed periods of 0.32 and 0.59 sec for the transverse and longitudinal models, respectively, are substantially less than the 0.45 and 0.65 sec estimated from the measured displacement response. The computed periods are also significantly different from those estimated using UBC equations.

Computed and measured roof and sixth floor relative displacement responses are plotted in Fig. 18. The measured roof relative displacement is computed as the difference between measured absolute displacement of the roof and the base of the building. Estimated processing errors for the displacements are 0.04 inches [CDMG (1985)]; therefore, errors of 0.08 in. are possible for the relative roof displacment. The maximum computed roof relative displacements are 0.163 in. and 0.372 in. for the transverse and longitudinal directions, respectively; therefore, processing errors are expected to be significant, especially in the transverse direction. From the data in Fig. 18, it is apparent that the computed building periods are too short. Sources of error include processing errors and the estimated values for the mass, viscous damping ratio, and stiffness (concrete gross–sections and fixed base).

The calculated mass is likely to be within 10 to 20% of the actual mass distribution. The period of the building is related to the square root of the mass distribution; therefore, changes in mass distribution are not likely to significantly affect building response. Changes in damping ratios have an insignificant effect on building period; however, they do affect amplitude of response. The assumed stiffness values for the building may have a significant impact on the period and responses of the building. Therefore, more detailed representations

of the building stiffness are studied in the following subsections, as analyses 2 and 3.

Analysis 2: Concrete Gross-Section – Flexible Base Model

Some of the error in Analysis 1 is likely to arise because effects of soil-structure interaction (SSI) have not been considered. For typical buildings, SSI effects typically result in increases of fundamental period of approximately ten percent. However, for relatively slender builidngs with numerous structural walls, more significant changes in fundamental period may result. The following paragraphs incorporate SSI effects into the model used for Analysis 1 to gage there importance on building behavior.

Simplified approaches to the soil–structure interaction problem generally focus on two factors that are primarily responsible for the difference in response of a rigidly and flexibly supported structure. First, the elastically supported structure can translate and rotate about its base; therefore, it has different dynamic characteristics than the rigidly supported structure. Second, a substantial part of the vibrational energy of the elastically supported structure may be dissipated into the supporting medium by radiation and by hysteric action in the soil.

Two different approaches may be used to assess the effects of soil structure interaction. The first approach involves modifying the prescribed free-field design ground motion and evaluating the response of the structure to the modified ground motion. The second approach involves modifying the dynamic properties of the structure and evaluating the response of the modified structure to the prescribed free–field gound motion. Either approach can be used to yield satisfactory results [Veletsos (1977)].

The simplified procedures discussed in the following subsections are based on linear elastic methods. The first procedure presents a method that simplifies the modeling of the soil, whereas the second procedure is recommended in ATC–3–06 (1978). Both methods assume that the structure and the underlying soil remain bonded throughout the duration of motion and that there are no soil instabilities or large foundation settlements.

(a) Elastic Halfspace

If the foundation of the building can be considered a rigid disk supported on a deep, relatively uniform soil medium, an elastic halfspace model can be used [Clough and Penzien (1975)]. The three rotational and three translational degrees of freedom at the base of the structure can be modeled using springs. Approriate spring constants can be evaluated for the elastic halfspace by methods of continuum mechanics. In general, the stiffness, mass, and damping associated with the soil are frequency dependent. However, for most building systems, sufficient accuracy can be obtained by using frequency independent soil parameters [Newmark and Rosenbleuth (1971)].

(b) ATC-3-06 Procedure

The ATC-3-06 (1978) procedures for soil-structure interaction are based on methods that modifying the dynamic characteristics of the structure. It has been shown that the interaction effects may be expressed by an increase in the fundamental period of vibration of the structure, and by a change (usually an increase) in the effective damping. The increase in the fundamental period is a result of the flexibility of the foundation soil, whereas the change in damping is mainly a result of the energy dissipation in the soil due to radiation and material damping.

The foundation system is considered to be a rigid circular plate of negligible thickness which is bonded to the supporting medium. Both the foundation weight and the weight of the structure are assumed to be uniformly distributed over foundation-soil contact area. The effective natural period $\tilde{T}$ of the modified system is given by,

$$\tilde{T} = T\sqrt{1 + \frac{k}{k_x}\left[1 + \frac{k_x h^2}{k_\theta}\right]} \tag{4.2}$$

where T is the natural period of the fixed base structure; k_x is the horizontal translational stiffness of the foundation defined as the horizontal force at the level of the foundation

necessary to produce a unit deflection at that level; k_θ is the rocking stiffness of the foundation defined as the moment necessary to produce a unit rotation of the foundation; and k is the lateral stiffness of the structure (for the mode of interest); and h is the height from the base of the structure to the centroid of the inertia forces (for the mode of interest).

The stiffness values k_x and k_θ depend on the geometry of the foundation-soil contact area, the properties of soil beneath the foundation; and the intensity of the ground motion. For a rigid circular foundation mat, the translational stiffness is given by

$$k_x = \frac{8}{(2-\nu)} Gr \tag{4.3}$$

and the rocking stiffness is given by

$$k_\theta = \frac{8}{3(1-\nu)} Gr^3 \tag{4.4}$$

where r is the radius of the foundation; G is the shear modulus of the soil; and ν is Poisson's ratio.

The shear modulus, G, is related to the shear wave velocity, v_s, by the equation,

$$G = \frac{v_s^2 \gamma}{g} \tag{4.5}$$

where γ is the unit weight of the soil and g is acceleration due to gravity.

For mat foundations of arbitrary shape, the soil stiffnesses defined by equations 4.3 and 4.4 are modified. The radius, r in Eq. (4.3) is specified as

$$r_a = \sqrt{\frac{A_0}{\pi}} \tag{4.6a}$$

and the radius in Eq. (4.4) is specified by

$$r_m = \sqrt[4]{\frac{4I_0}{\pi}} \tag{4.6b}$$

where A_0 is the effective area of contact between the foundation and the soil, and I_0 is the static moment of inertia of the area about the centroidal axis in the direction in which the response is being evaluated.

The damping factor of the elastically supported structure, $\tilde{\beta}$, may be expressed in the form,

$$\tilde{\beta} = \beta_0 + \frac{\beta}{(\tilde{T}/T)^3} \tag{4.7}$$

where β represents the damping factor of the fixed-base structure and β_0 represents the contribution of the foundation damping. The damping ratio, $\tilde{\beta}$ depends primarily on three parameters: (1) the ratio of natural periods of the elastically supported and fixed base structure, $\tilde{T}/T$; (2) the ratio of the height of the structure to the radius of the foundation h/r; and (3) the damping capacity of the soil. The variation of β_0 with $\tilde{T}/T$ and h/r is shown in Fig. 19 [Veletsos (1977)] for two intensities of ground acceleration.

The effect of soil-structure interaction in the ATC-3-06 (1978) procedures always results in a reduction in the lateral forces, base shear, and overturning moment [Veletsos (1977)]. Because of the rocking and translation of the foundation, the displacements relative to the base may be larger than those for the fixed-base structure.

(c) Incorporation of SSI Effects

To incorporate SSI effects into the building analysis, information on the foundation and soil systems is required. The foundation for Building SN-356 consists of rectangular footings beneath the walls supported on piles. Dimensions of the footings for the transverse walls are: 2'-0" deep and 2'-6" wide at axes 1, 2, 12, and 13; 2'-0" deep and 4'-4" wide at

the remaining walls (Fig. 4). The footings for the transverse walls are connected to the footings for the longitudinal walls, which are 5'-0" deep and 8'-0" wide and are centered on the central corridor of the building. The transverse footings are supported on 12-3/4 in. diameter piles. No specific information is available for the soils at the building site; therefore, typcical soil properites were assumed based on values reported for the San Francisco Bay Area [Celibi (1987)]. A shear wave velocity of 2000 ft/sec was assumed to be representative for the soil.

Due to uncertainties in soil properties and superstructure-foundation-pile-soil interaction, a relatively simple model was used to investigate the importance of soil-structure interaction for the building. The model is based on the assumption that the footings are rigid disks supported on a soil that can be represented as an elastic half space (Eq. 4.3 to 4.6). The responses of the mathmatical model of the building to earthquake motions can be evaluated by modal analysis if the damping ratio of the soil is assumed to be the same as that for the building. Viscous damping of 5% of critical was assumed for both the building and the soil.

The computed values of K_x, K_θ, and K_z are shown in Table 4.4 for both the transverse and longitudinal directions. In the transverse direction, three springs were used at the center of the building to model soil-structure interaction effects. In the longitudinal direction, the foundation is not continuous but consists of two independent footings; therefore, more detailed models may be needed to incorporate soil-structure interaction effects. Two models were used to investigate the effects of SSI in the longitudinal direction. The first model considered two independent footings. Each of the footings was assumed to act as a rigid disk. The second foundation model assumed that the entire foundation acted as a rigid disk (a simplified approach). For each of the models an additional story was used to model SSI effects (Fig. 19). the stiffness values of the columns (located under each wall and fixed at one end and attached to very rigid beams representing the foundation) in the additional story were selected such that

$$K_x = n\left[\frac{12EI}{L^3}\right] \tag{4.8}$$

$$K_\theta = \left[\frac{AE}{L}\right]\sum_{i=1}^{n} x_i^2 \tag{4.9}$$

where n is the number of columns, E is the modulus of elasticity, I is the column moment of inertia, and A is the column area, L is the column length, and and x_i is the horizontal distance of each column from the center of footing. The moment of inertia and the area of the columns were computed by assuming arbitrary values for the modulus of elasticity and column length.

Computed fundamental periods for the combined structure–foundation system did not vary significantly for the two models. Based on this result, and because of uncertainties in the values for the soil properties and the foundation-pile-soil interaction, the foundation was modeled as one continuous disk (model 2).

Periods were computed for the 2–D models of the building, and are presented in Table 4.2. For the 2–D model in the transverse direction, the fundamental period increased to 0.36 sec, or approximately an 12.5% increase compared with the fixed base period (a similar result is obtained for the 3-D model). For the 2-D model for the longitudinal direction, the fundamental period increased by 6.25% to 0.51 seconds. The computed periods are still less than those estimated from the displacement response (0.45 sec transverse, and 0.65 sec longitudinal).

Computed and measured roof and sixth floor relative displacement responses are plotted in Fig. 20. Improved correlation is obtained for the displacements in both the transverse and longitudinal directions (compared with analysis 1). The correlation is good early in the response, but gets progressively worse. It appears that the computed periods for both the transverse and longitudinal directions are still too short.

Shear response at the base of the transverse walls is calculated for the flexible base model. The maximum base shear is 2475 kips ($1.0\sqrt{f'_c}$) at 17.70 seconds (33% of wall shear strength). The maximum computed shear stress of $1.0\sqrt{f'_c}$ is approximately one-half the shear stress that can be resisted by the concrete alone (according to ACI 318-89 provisions). It is evident that the shear forces experienced by the wall under the earthquake motions are considerable less than the available strength of the wall; therefore, no significant damage is expected in the wall.

In the longitudinal direction, the shear force is computed at the top of the first story level due to the abrupt change in the wall cross section at this level (the base level is very rigid). The maximum computed shear is 2460 kips ($2.4f'_c$) at 17.22 sec (50% of wall shear strength). The plot reveals that the computed shear stress is less than the computed shear strength ($4.6\sqrt{f'_c}$; therefore, no significant damage is expected in the wall. The maximum calculated shear stress of $3.0\sqrt{f'_c}$, is more than the shear stress that can be resisted by the concrete alone (according to ACI 319-89 provisions).

Incorporting the effects of SSI resulted in improved correlation between measured and computed responses for both principal directions of the building. Given the assumptions inherent in the model used to incorporate SSI effects (especially for the shear wave velocity of the underlying soils), the results give only a rough indicatation of the influence of SSI. The analysis results indicate that SSI is an important consideration for modeling the response of the building in both the directions.

Analysis 3: Cracked–Section – Flexible Base Model

The consideration of SSI improved response correlation; however, the periods for both the transverse and longitudinal directions are less than those estimated from the measured displacement response. Another likely source of error lies in the assumption that the element stiffnesses can be based on gross-section quantities. In the absence of lateral load, some initial cracking can be expected due to shrinkage and temperature effects, and dead load

stresses. A modest reduction in stiffness would be expected due to these effects. Under moderate to high lateral loads, load-induced cracking will result in more significant reduction of stiffness. Currently no well-established technique exists by which to gage the degree of cracking that occurs in a structure over time. Moment-curvature analyses for the walls in Building SN-356 (Fig. 21 and 22) indicate a fully-cracked stiffness on the order of 40 percent of the gross-section stiffness. Results of Analysis 2 revealed response levels of approximately 33% and 50% of the computed moment capacity for the transverse and longitudinal directions, respectively. Therefore, the effective stiffness for both directions is expected to fall in the cracked range of the moment-curvature response. Although no well-defined method exists by which to select effective stiffness values; based on response levels, an effective stiffness of 80% and 70% in the transverse and longitudinal direction appears reasonable.

Computed periods for the 2-D models incorporating the effects of SSI and cracking are given in Table 4.2. The fundamental period for the transverse direction is 0.40 sec for the 2-D model. The fundamental period for the longitudinal direction is 0.62 sec for the 2-D model. The fundamental periods for both models are within the range of periods estimated by using the displacement response (Fig. 6.d, 6.g).

Computed and measured roof and sixth floor displacement response are plotted in Fig. 23. Good correlation is achieved for both principal directions based on the assumed values for crack-section stiffness (and the assumed values for the soil stiffness calculations). The maximum computed roof relative displacement is 0.28 in. (0.025%) in the transverse direction and 0.80 in. (0.07%) in the longitudinal direction.

It is noted that the computed and measured periods in Fig. 23 compare reasonable well throughout the duration of response. The implication is that, initial cracking aside, the response of the building during the earthquake was essentially elastic. This conclusion is consistent with the relativley high base shear strength of the building compared with the response levels.

Analysis 4: Concrete Half-Gross Section – Flexible Base Model

The consideration of soil-structure interaction and the reduced stiffness due to cracking in Analysis–3 resulted in good correlation between computed and measured responses. From the results of Analysis–3, it is evident that for moderate earthquake ground motions, a moderate stiffness reduction for load induced cracking can be expected. However, for more intense ground motions, the building will be expected to experience a more substantial reduction in stiffness due to load induced cracking.

A simplified model was used to model a building subjected to a greater level of elastic response. The simplified model assumes that the stiffness of the walls can be represented by using an effective stiffness equal to one-half the gross-section stiffness to estimate lateral displacement response. The model is based on typical cracked section stiffness values for walls with low levels of axial stress and moderate reinforcing ratios.

Computed periods for the 2-D models incorporating the effects of soil-structure interaction and section cracking are given in Table 4.2. The fundamental period for the transverse direction is 0.5 sec. and for the longitudinal direction is 0.74 sec. for 2-D models. The period increases by approximately 11% and 14% of the period calculated from the measured responses in the transverse and longitudinal directions, respectively.

The relative displacements at sixth floor level and roof level are computed using these assumptions and they are plotted in Fig. 24 (it is noted that the measured ground motion may not be representative of more intense ground motions; however, the results are plotted to gage the effect of load-induced cracking). The maximum computed roof relative displacement is 0.60 in. (0.053 %) in the transverse direction and 0.95 in. (0.084%) in the longitudinal direction. The drift in transverse direction increases to almost double of the elastic Analysis-3 whereas in longitudinal direction, it increases insignificantly. It is noted that, depending on the building geometry, it may not be necessary to include the effects of SSI in the simplified analysis. If the effects of SSI are expected to be insignificant, then they could be neglected. The ATC–3 procedures may be useful in determining the effects

of SSI and the need to consider these effects in a more detailed analysis.

Chapter - 5

SUMMARY AND CONCLUSIONS

A 10-story reinforced concrete bearing wall structure subjected to moderately intense ground motions during 1984 Morgan Hill Earthquake in California is presented. The building is one of approximately 100 buildings instrumented by CDMG Strong Motion Instrumentation Program in California. Thirteen strong-motion instruments measured responses resulting from the Morgan Hill Earthquake. The structure did not experience any apparent damage during the earthquake.

The structure was designed in 1970 according to UBC requirements. The lateral-force resisting system consists of shear walls coupled by thin floor slabs in both the transverse and longitudinal directions. Lightweight concrete (f'_c = 4000 psi and γ = 110pcf) was used for the floor slabs, and normal weight concrete (f'_c = 3000 psi) was used for the walls. Elastic analyses were conducted to investigate the performance of the building. Based on the studies conducted on the structure, the following conclusions can be made:

(i) Damping ratios of 4.9% and 11.5% were computed in the longitudinal and transverse directions, respectively using the recorded acceleration responses. The damping ratio of 5% for the longitudinal direction is consistent with that expected for a R.C. building subjected to moderate ground motions, whereas the relatively high damping ratio for transverse direction is likely due to the effects of soil-structure interaction. The studies suggest that even for moderately intense ground motions, damping ratios are likely to be 5% or greater for bearing wall buildings. In addition, the effects of soil-structure interaction may significantly affect damping ratios.

(ii)The maximum displacement response over the height of the building indicates that the first mode response is dominant for both the transverse and longitudinal directions. Maximum roof relative displacements of 0.23 in. (0.02% of the building height) and 0.81 in. (0.07% of the building height) were measured in the transverse and longitudinal directions, respectively. The measured roof drifts are less than 15% of the UBC allowable interstory drift. By limiting drift, damage to non-structural elements will be avoided.

(iii) The periods computed from the measured displacement responses differ significantly from those estimated during design (using $T = 0.05h/\sqrt{D}$). UBC(1988) Equation (12.3) provides improved estimates of period because the equation accounts for the distribution of stiffness in each principal direction. However, in general, UBC Equation (12.3) may not provide reasonable period estimates because it does not account for the mass distribution (per wall) in a building.

(iv) The maximum base-shear and base-overturning moment calculated using measured responses indicate that the building responded in the essentially elastic range for the moderately intense ground motions.

(v) Fundamental periods computed using concrete gross-sections and a fixed base model (typical design practice) are not realistic, and at best, represent a lower bound of actual values. The consideration of the effects of soil-structure interaction improved correlation: however, soil-structure interaction is apparantly not the main reason for the discrepancy between the periods computed from the gross section model and the actual periods.

(vi) Good correlation between the computed and measured responses was obtained by using a cracked section stiffness and soil-structure interaction. The computed periods for the models are within the range of periods estimated by using displacement response. Therefore, it is concluded that the soil-structure interaction and section cracking effects are important modeling parameters for bearing wall buildingsand in particular, the effects of section cracking are significant.

(vii) For buildings with walls subjected to low levels of axial stress and typical reinforcing ratios, a simplified model model assuming a cracked section stiffness equal to one-half the gross-section stiffness can be used. This simplified model reduces cumbersome calculations and provides a good estimate to measured displacement responses.

The effects of soil-structure interaction may or may not be included depending on the expected influence of soil-structure interaction. This influence can be gaged by using simplified procedures, such as those recommended by ATC-3.

REFERENCES

ACI-318(1983),"Building Code Requirements for Reinforced Concrete," *American Concrete Institute*, Detroit, Michigan, 1983.

ACI-318(1989),"Building Code Requirements for Reinforced Concrete," *American Concrete Institute*, Detroit, Michigan, 1989.

Allen,F. and Darvill,P.(1977),"Lateral Load Equivalent Frame," *ACI Journal*, July 1977, pp 294-299.

Applied Technology Council (1978),"ATC-03-06: Tentative Provisions for the Development of Seismic Regulations for Buildings," *Applied Technology Council*, Palo Alto, California, 1978.

CDMG Strong-Motions Records, Morgan Hill, California Earthquake of 24 April 1984.

Celebi, M., Bongiovanni, G., and Safak, E. (1987),"Siesmic Rocking Response of a Triangular Building Founded on Sand," *Earthquake Spectra* Vol. 3, No. 4, November 1987.

Colough,R.W. and Penzien,J.(1975),"Dynamics of Structures," *McGraw-Hill, Inc.*, 1975.

Coull,A. and Hag,A.A.E.(1975),"Effective Coupling of Shearwalls by Floor Slabs," *ACI Journal*, Aug. 1975, pp 429-431.

EERI(1985), *Earthquake Spectra* Vol. 1, No. 3, May 1985.

Farrar,C.R. and Bennet,J.G.(1988),"Experimental Assessment of Damping in Low Aspect Ratio, Reinforced Concrete Shear Wall Structure," *U.S. Nuclear Regulatory Commission*, Washington, D.C., August 1988.

Gulkan,P. and Sozen,M.A.(1974),"Inelastic Response of Reinforced Concrete Structures to Earthquake Motions," *ACI Journal*, Vol. 71, No. 12, Dec. 74, pp 604-610.

Mahin (1989),"Presentation at SMIP-89 Seminar," Sacramento, California, May 1989.

Newmark, N.M.(1959),"A Method of Computation for Structural Dynamics," *Journal of the Engineering Mechanics Division*, ASCE, Vol. 85, EM3, July 1959, pp 69-86.

Newmark,N.M. and Rosenbleuth,E.(1971),"Fundamentals of Earthquake Engineering," *Prenticel-Hall*, 1971.

Paulay,T. and Taylor, R.G.(1981),"Slab Coupling of Earthquake- Resisting Shearwalls," *ACI Journal*, March-April 1981, pp 130-140.

Pecknold,A.(1975),"Slab Effective Width for equivalent Frame Analysis," *ACI Journal*, April 1975, pp 429-431.

Qadar,A. and Smith(1969),"The Bending Stiffness of Slabs Connecting Shear Walls," *ACI Journal*, June 1969, pp 464-473.

Veletsos,A.S. (1977),"Dynamics of Structure - Foundation Systems," *Structural and Geotechnical Mechanics*, A Volume Honoring N.M. Newmark (W.J. Hall, Editor), Prentice Hall, Inc. Englewood, N.J., 1977.

Wallace,J.W.(1989),"BIAX: A Computer Program for the Analysis of Reinforced Concrete Sections," *University of California, Berkeley*, Report No. UCB/SEMM-89/12, 1989.

Wallace,J.W. and Moehle,J.P.(1989),"The 1985 Chile Earthquake. An Evaluation of Structural Requirements for Bearing Wall Buildings." *University of California, Berkeley*, Report No. UCB/EERC-89/05, July 1989.

Wilson, E.L.(1989),"SAP-89: A Series of Computer Programs for the Static and Dynamic Finite Element Analysis of Structures," 1989.

Table 1.1 Mass Distribution

(1)	Slab (10 in. LWC) @ 110 lb/ft^3	85 psf
(2)	Miscellaneous (floor/ceiling)	20 psf
(3)	Walls - R.C./Partition	50 psf
(4)	Live load 25% X 40 psf	10 psf
Total mass		175 psf

Table 4.1 Computed Base Shear and Flexural Strength

Shear strength		Flexural strength	
Trans.	Long.	Trans.	Long.
0.47W	0.20W	0.32W	0.22W
Note: W = 24.000 kips for the Building			

Table 4.2 Computed Periods

Analysis	Trans.	Long.
Calculated from Measured Response	0.45	0.65
Using UBC(1985) Equation	0.59	0.32
Using UBC(1988) Equation	0.29	0.52
Gross-Section–Fixed Base 3-D Model	0.31	0.48
Gross-Section–Fixed Base 2-D Model	0.32	0.48
Gross-Section–Flexible Base 2-D Model	0.36	0.51
Cracked-Section–Flexible Base 2-D Model	0.40	0.62
Half Gross-Section–Flexible Base 2-D Model	0.50	0.74

Table 4.3 Computed Soil Stiffness Values

Direction	Tanslational K_x kip/in	Rocking K_θ kip.in/rad.	Vertical K_z kip/in
Transverse	82.36×10^3	5.44×10^9	104.53×10^3
Longitudinal	292.63×10^3	3.3×10^{11}	371.4×10^3

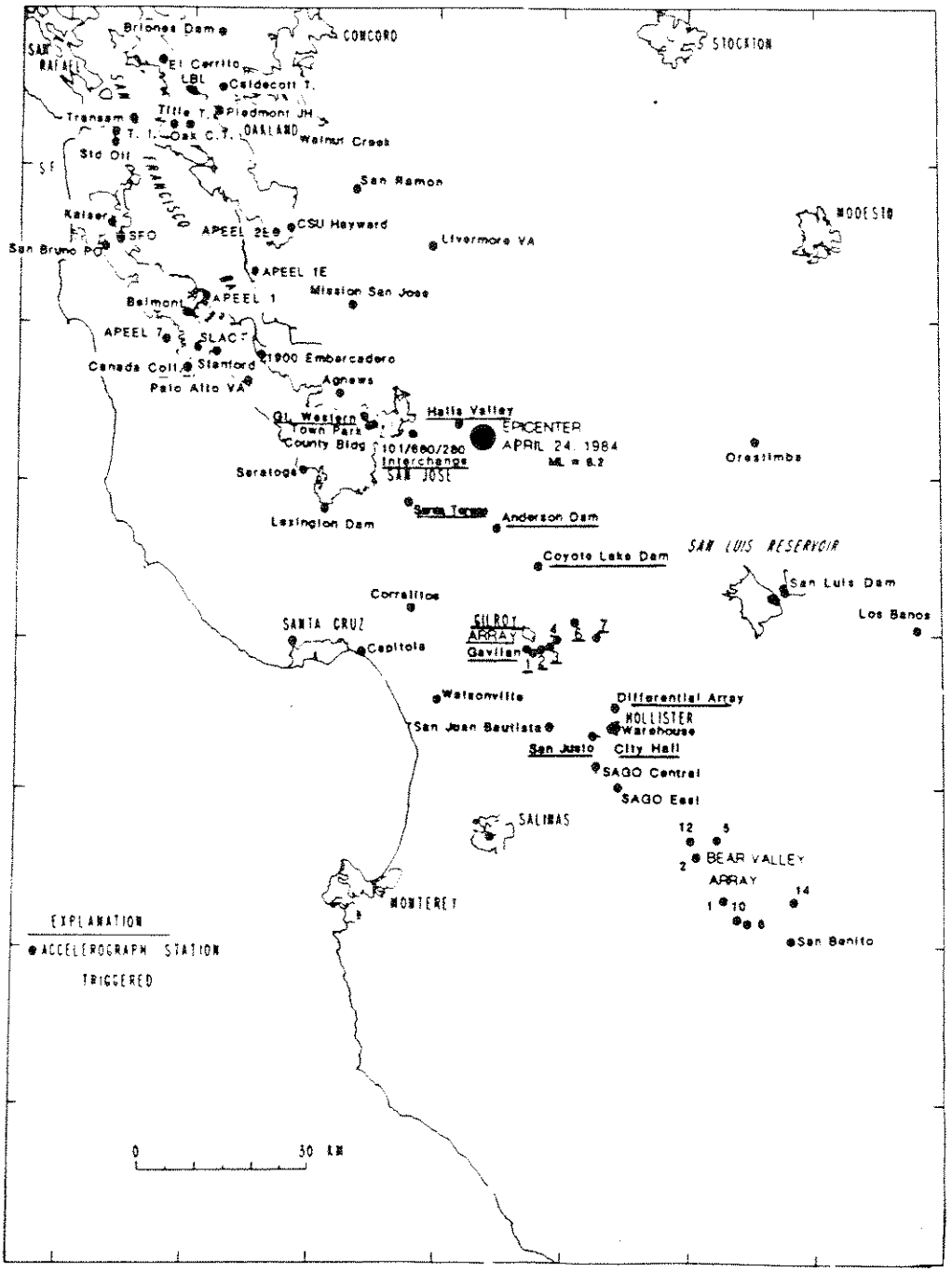

Fig. (1) Epicenter of 1984 Morgan Hill Earthquake [EERI (1985)]

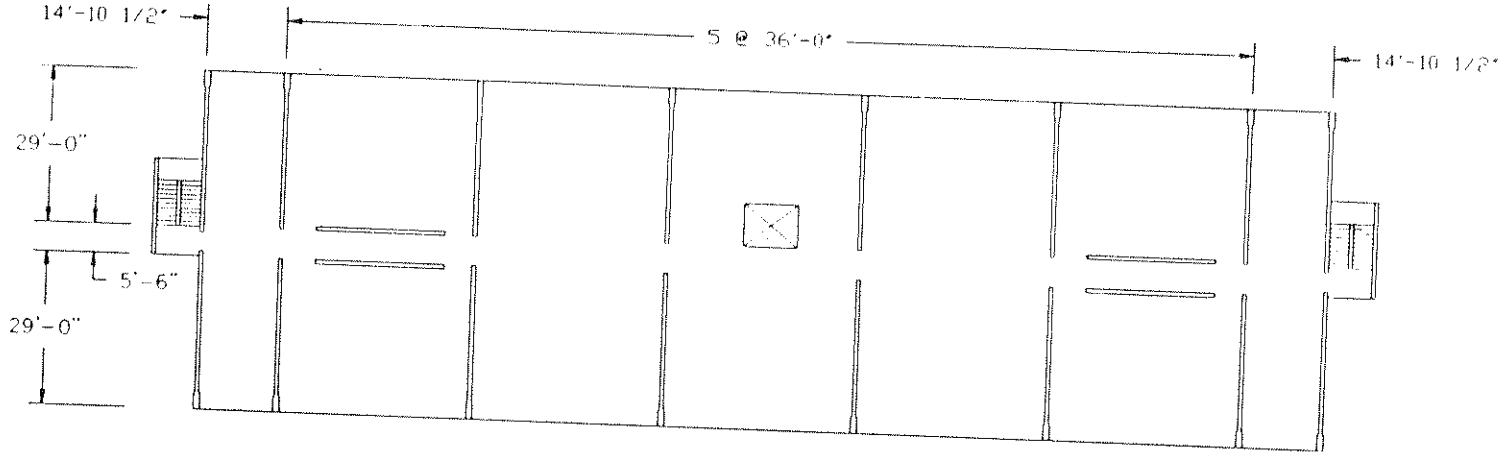

CSMIP BUILDING SN356 - FLOORS 6-10

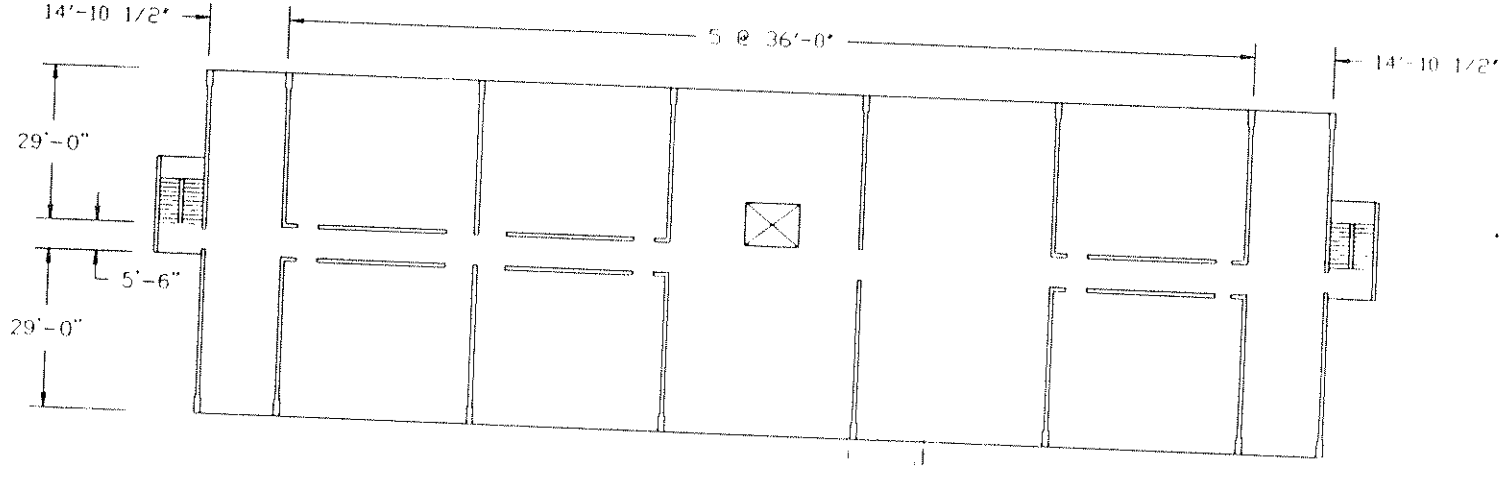

CSMIP BUILDING SN356 - FLOORS 2-5

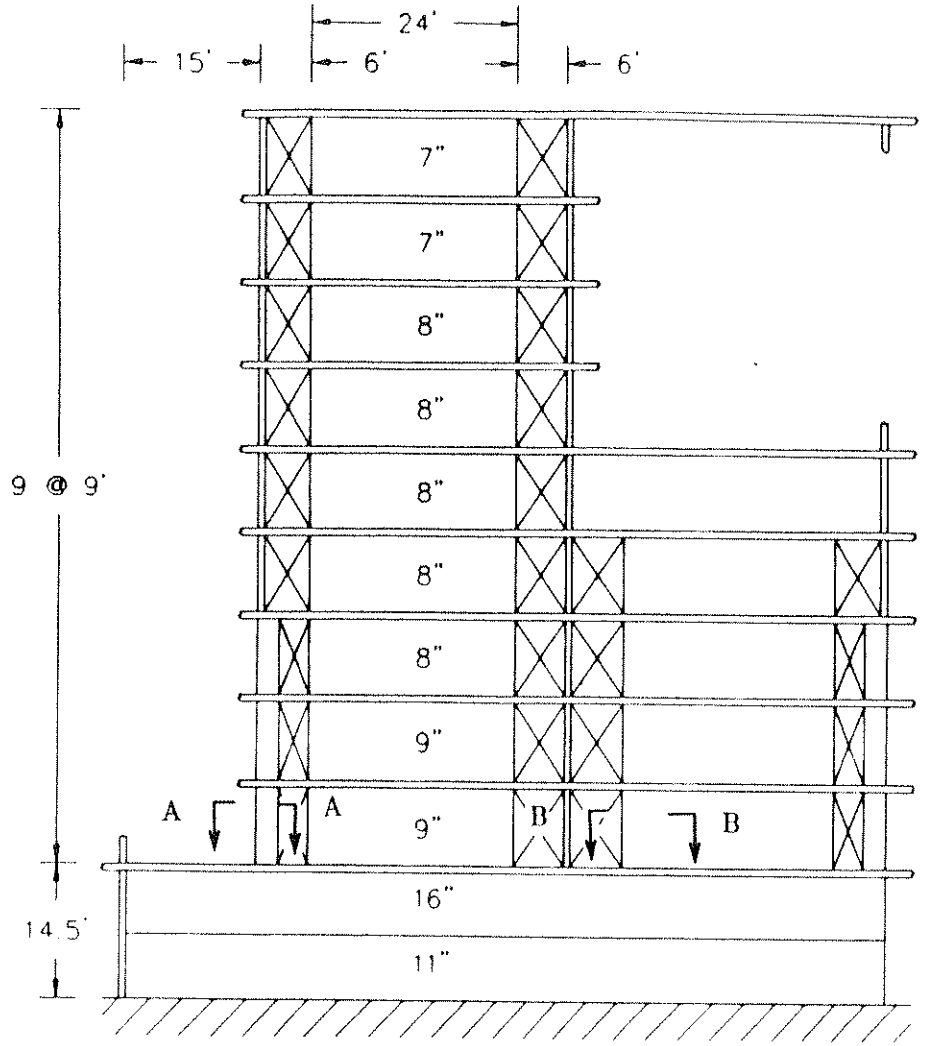

Fig. (3.b) Elevation View - Longitudinal Direction

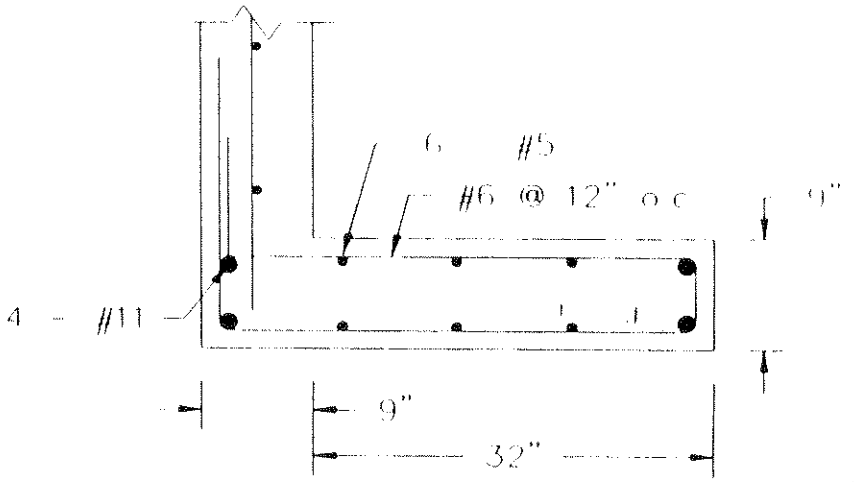

Section A - A

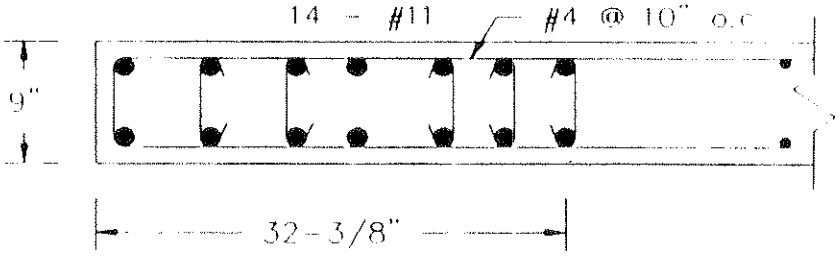

Section B - B

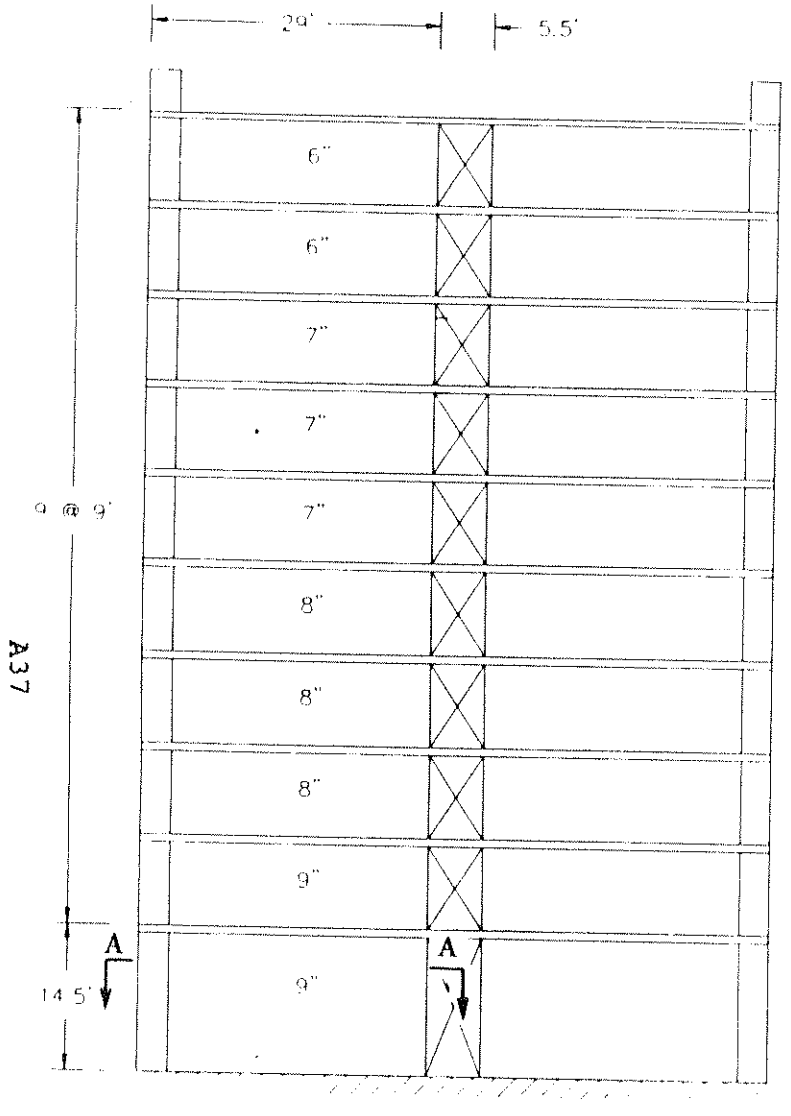

Fig. (3.a) Elevation View - Transverse Direction

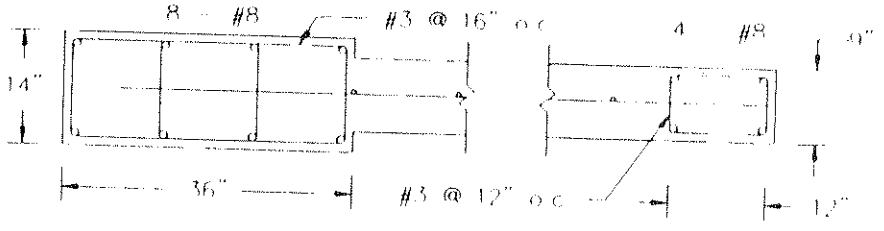

Section A - A

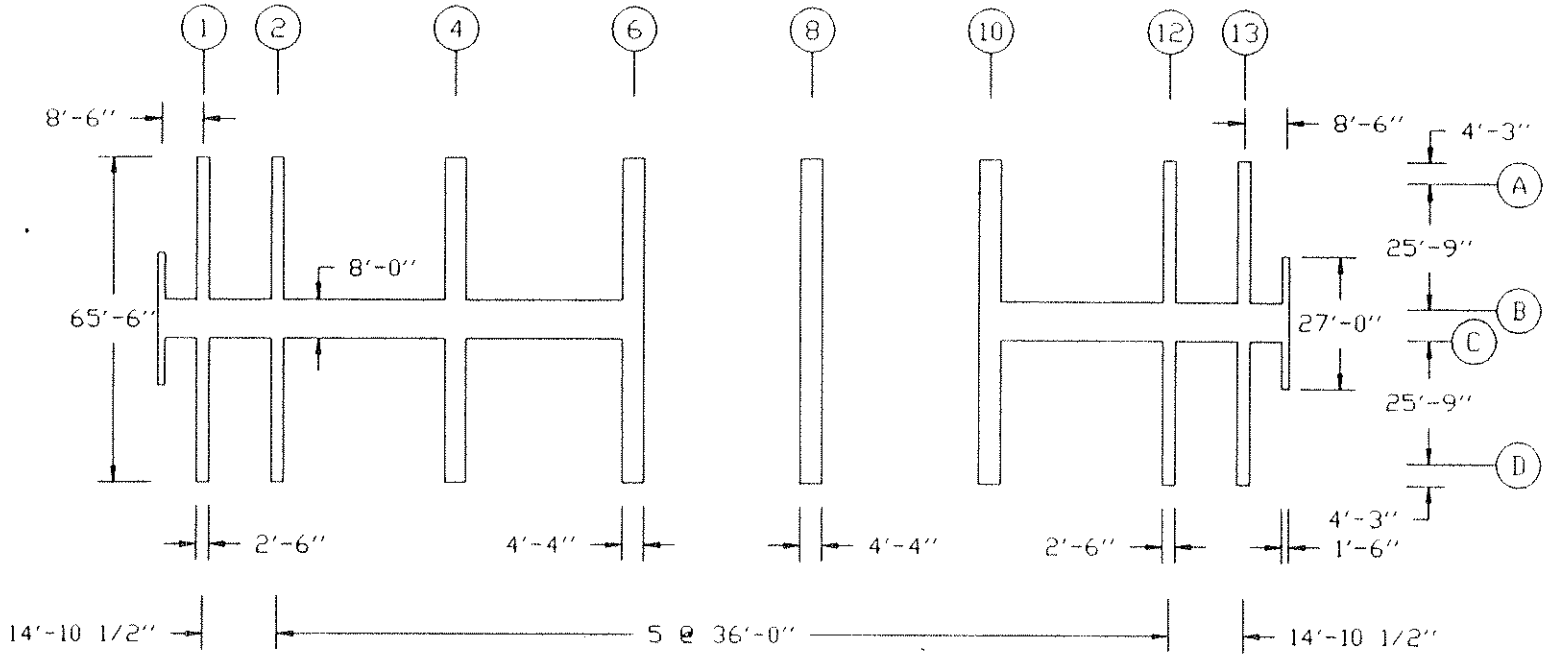

Fig. (4) Plan View - Foundation

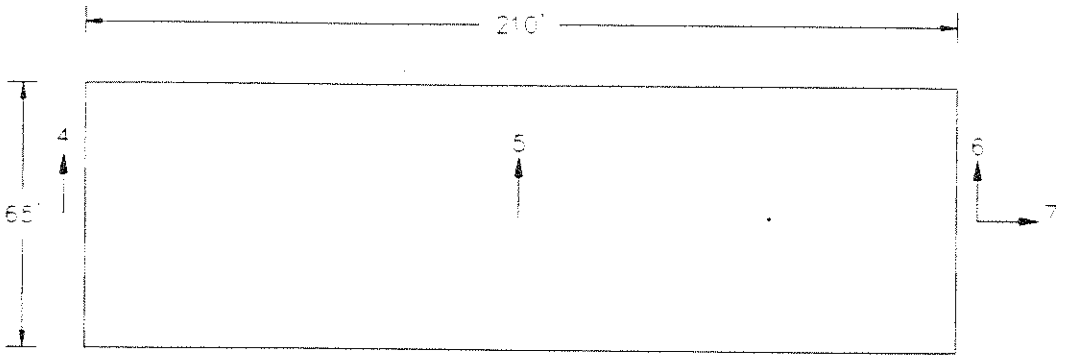

ROOF PLAN

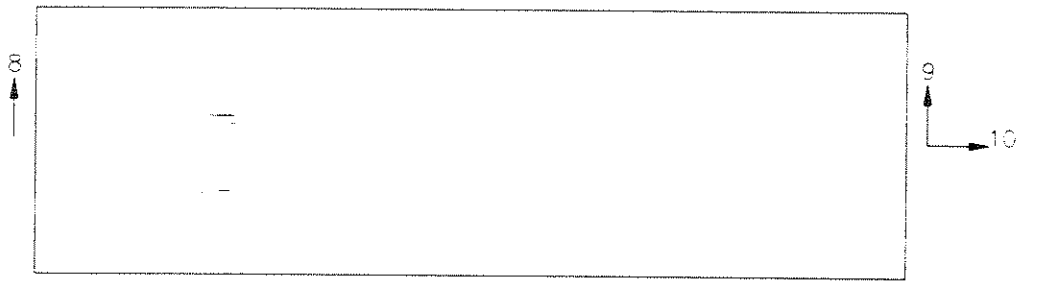

6th FLOOR PLAN

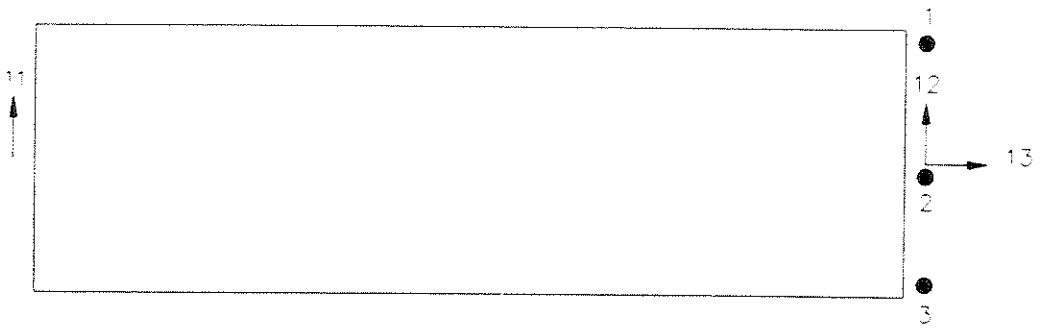

GROUND FLOOR PLAN

Fig. (5) Sensor Layout

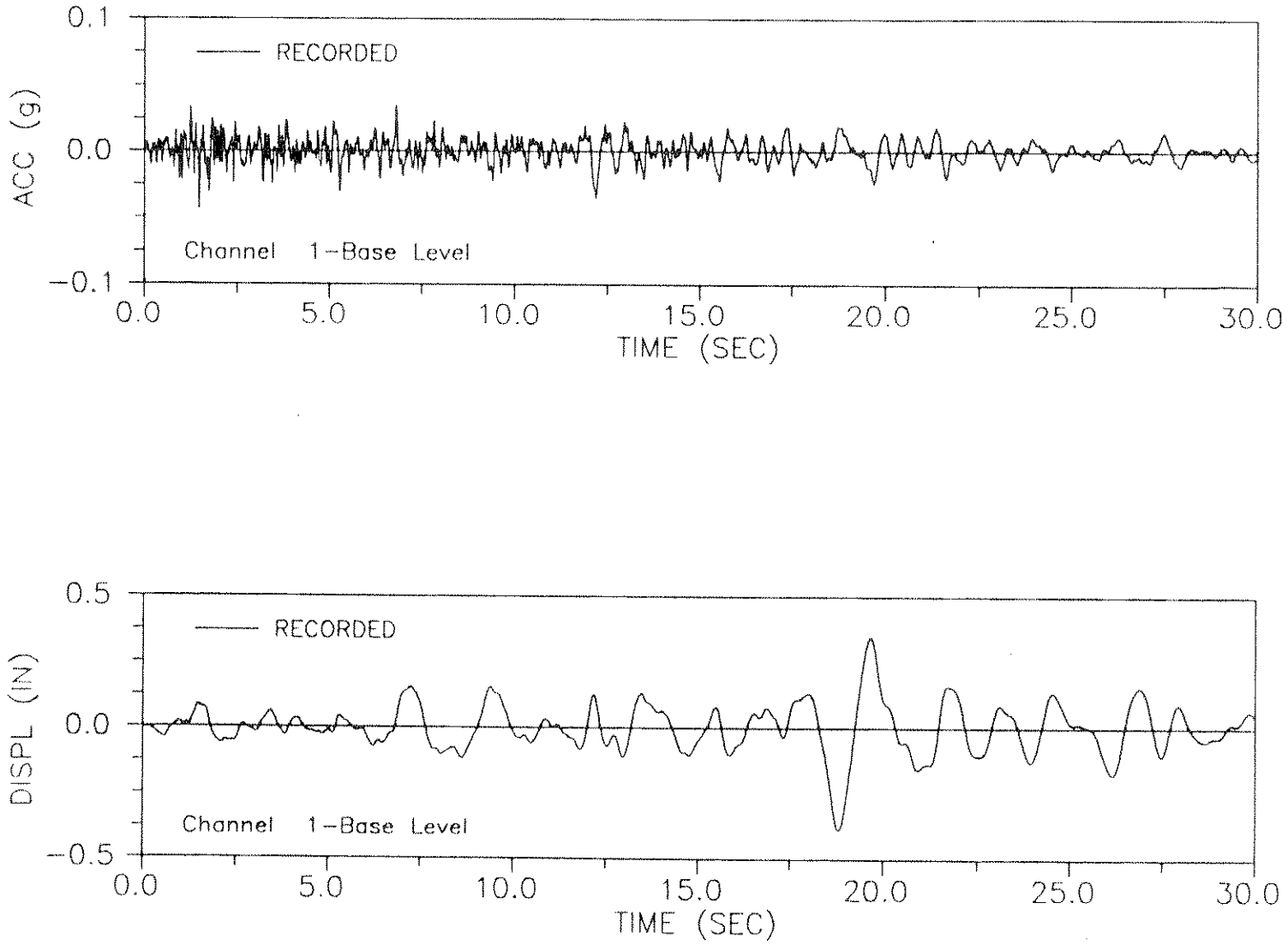

Fig. (6.a) Recorded Response - Channel 1

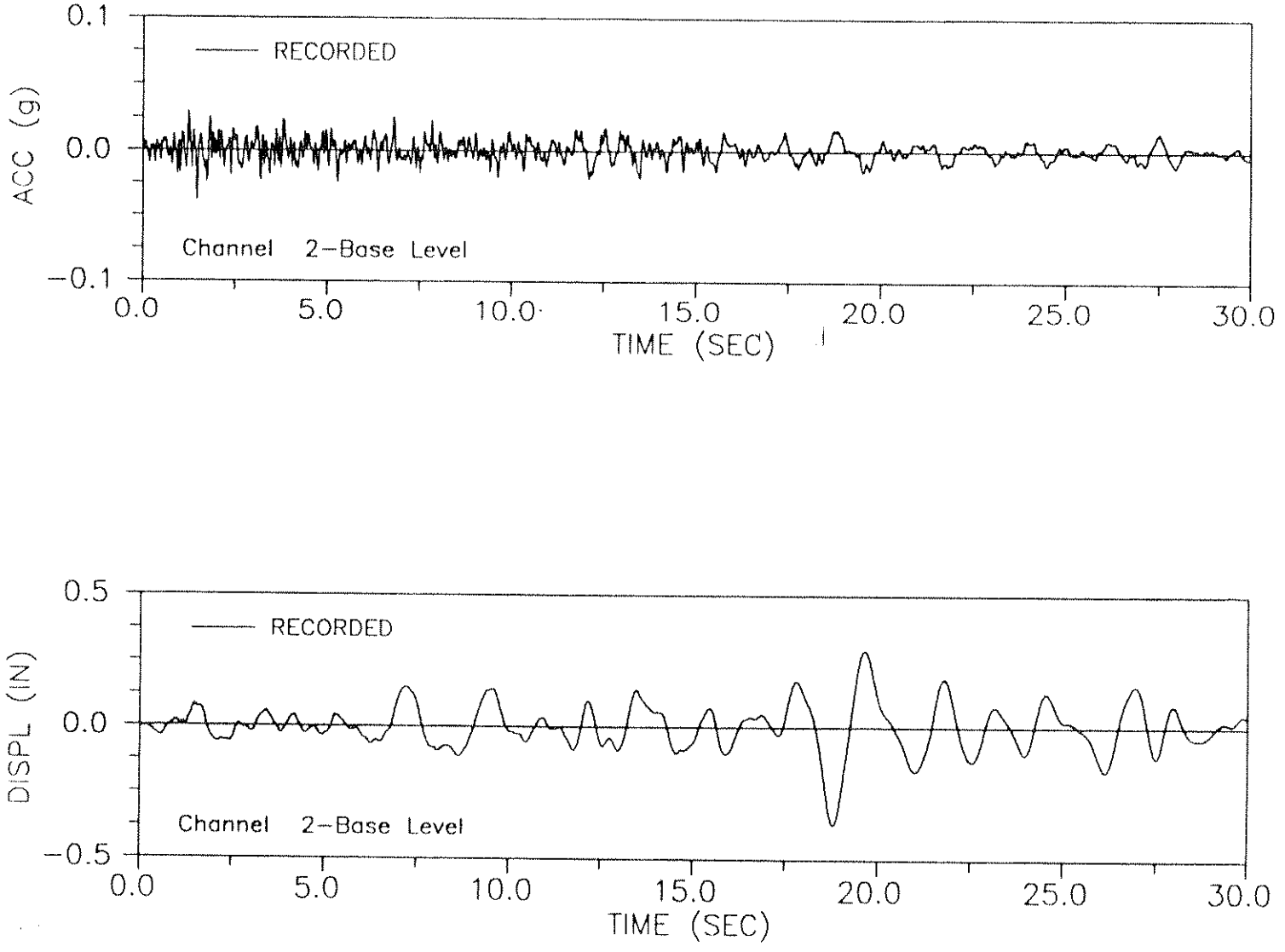

Fig. (6.b) Recorded Response - Channel 2

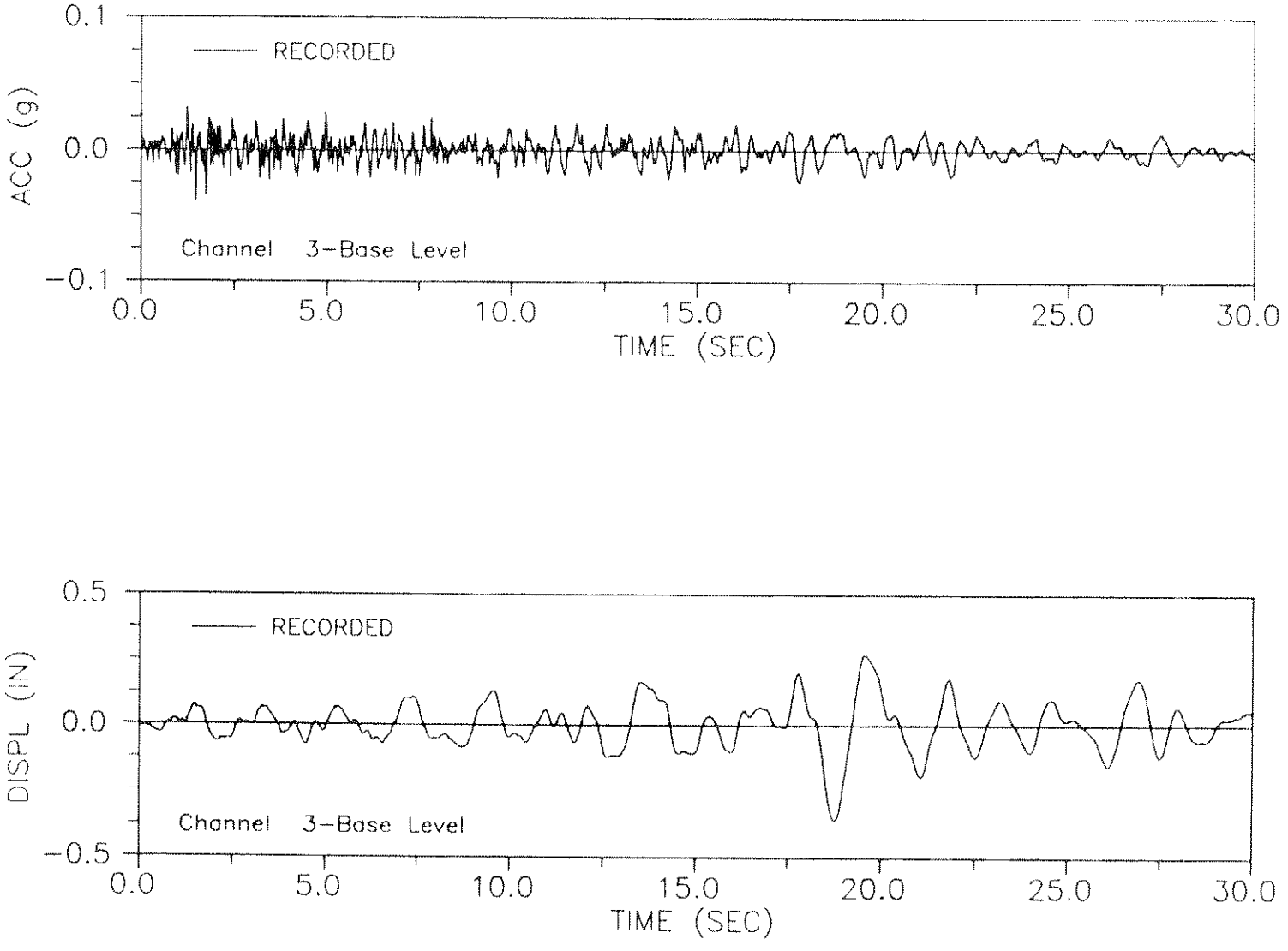

Fig. (6.c) Recorded Response - Channel 3

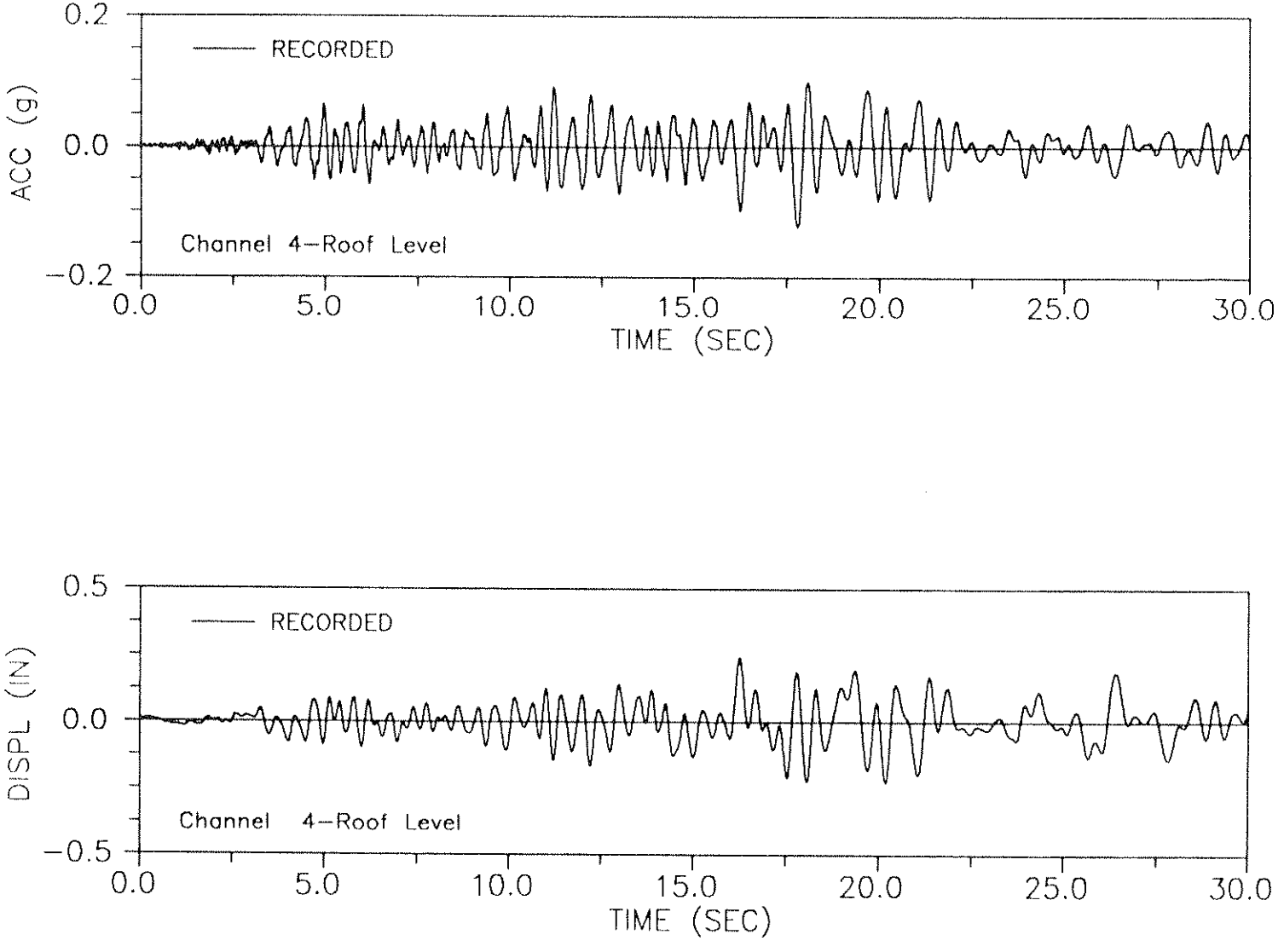

Fig. (6.d) Recorded Response - Channel 4

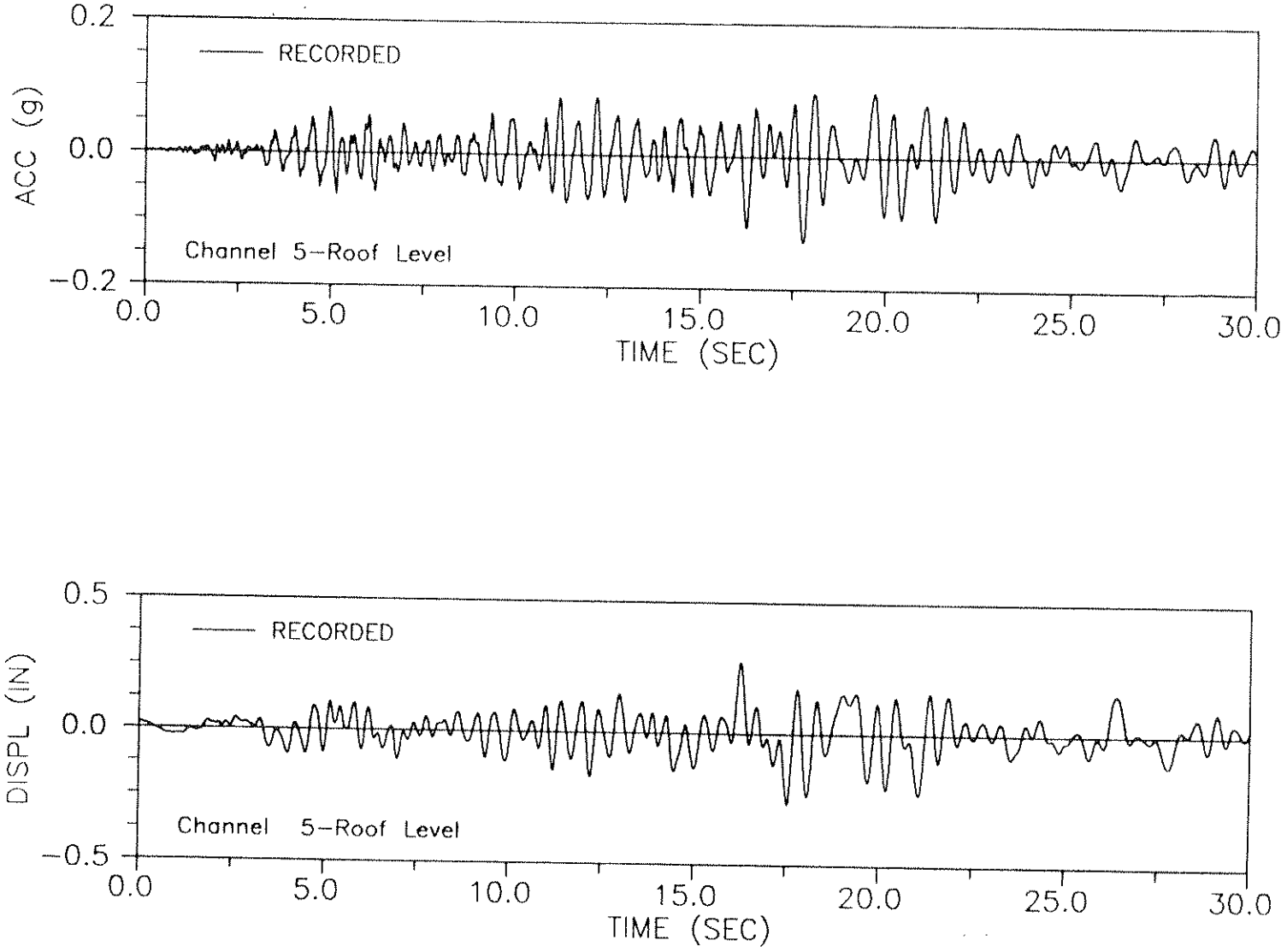

Fig. (6.e) Recorded Response - Channel 5

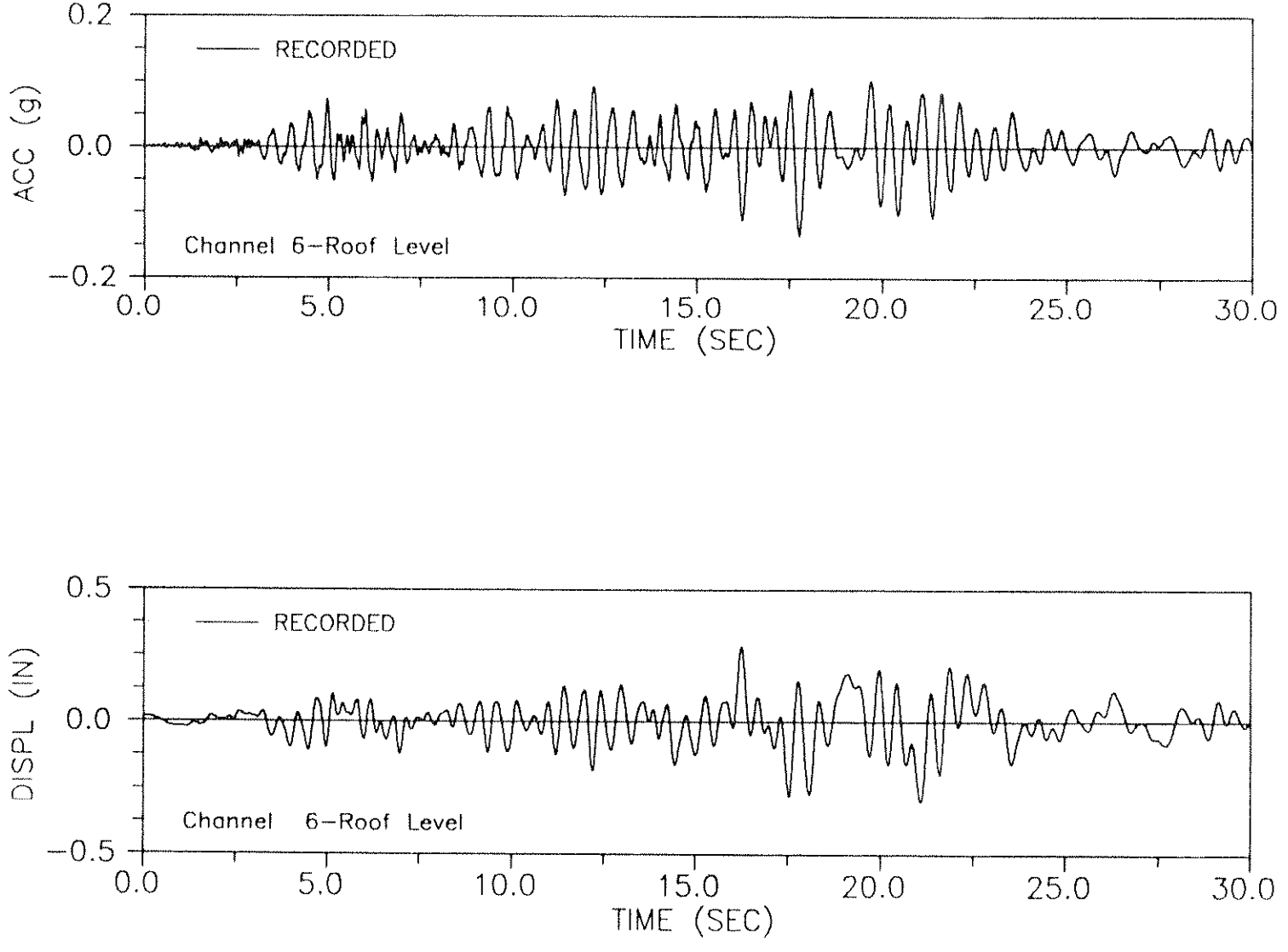

Fig. (6.f) Recorded Response - Channel 6

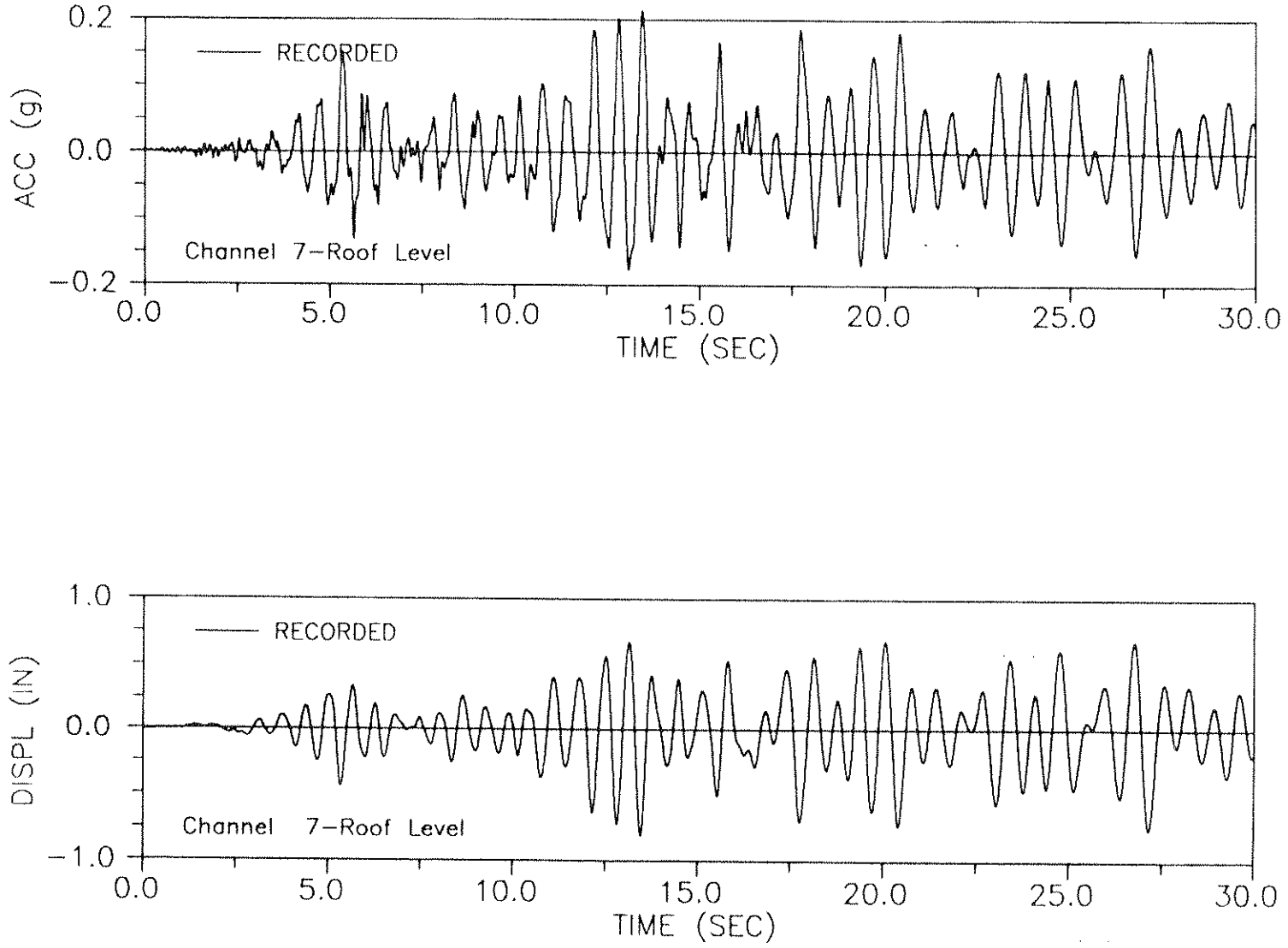

Fig. (6.g) Recorded Response - Channel 7

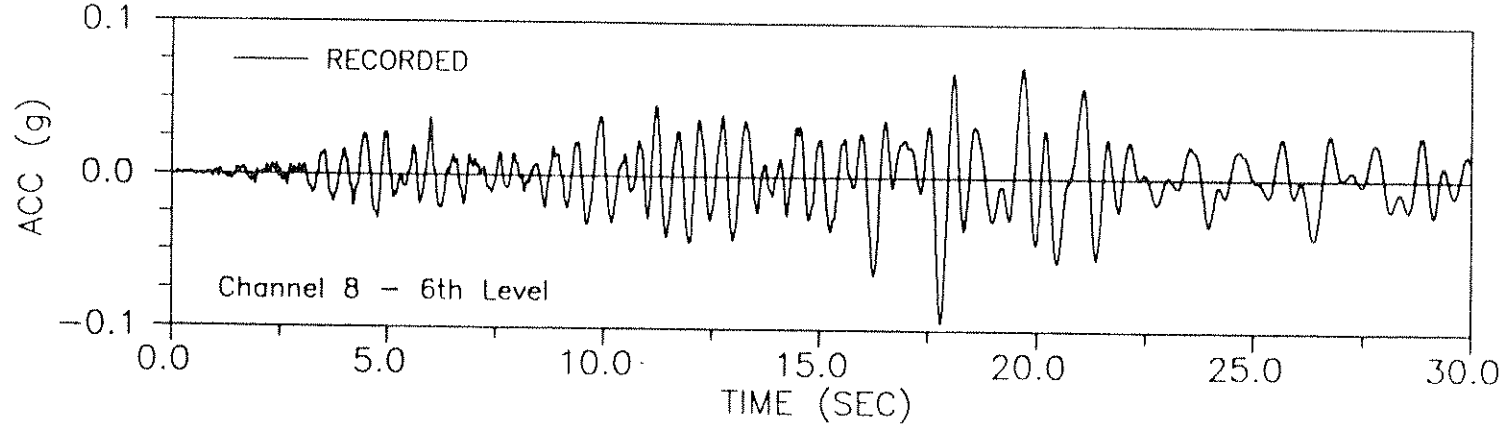

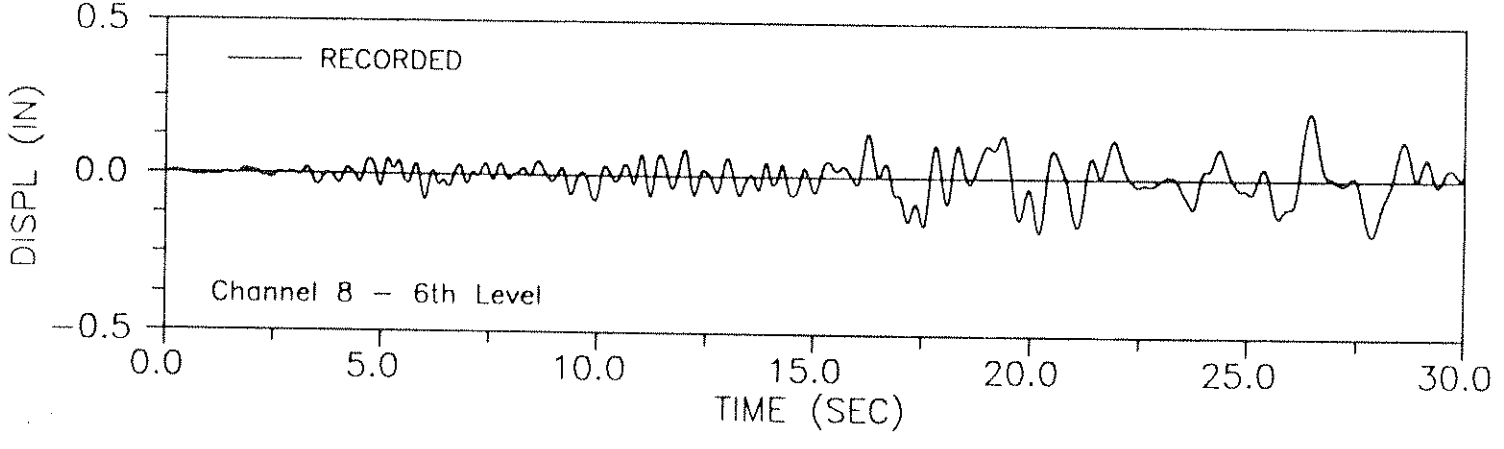

Fig. (6.h) Recorded Response - Channel 8

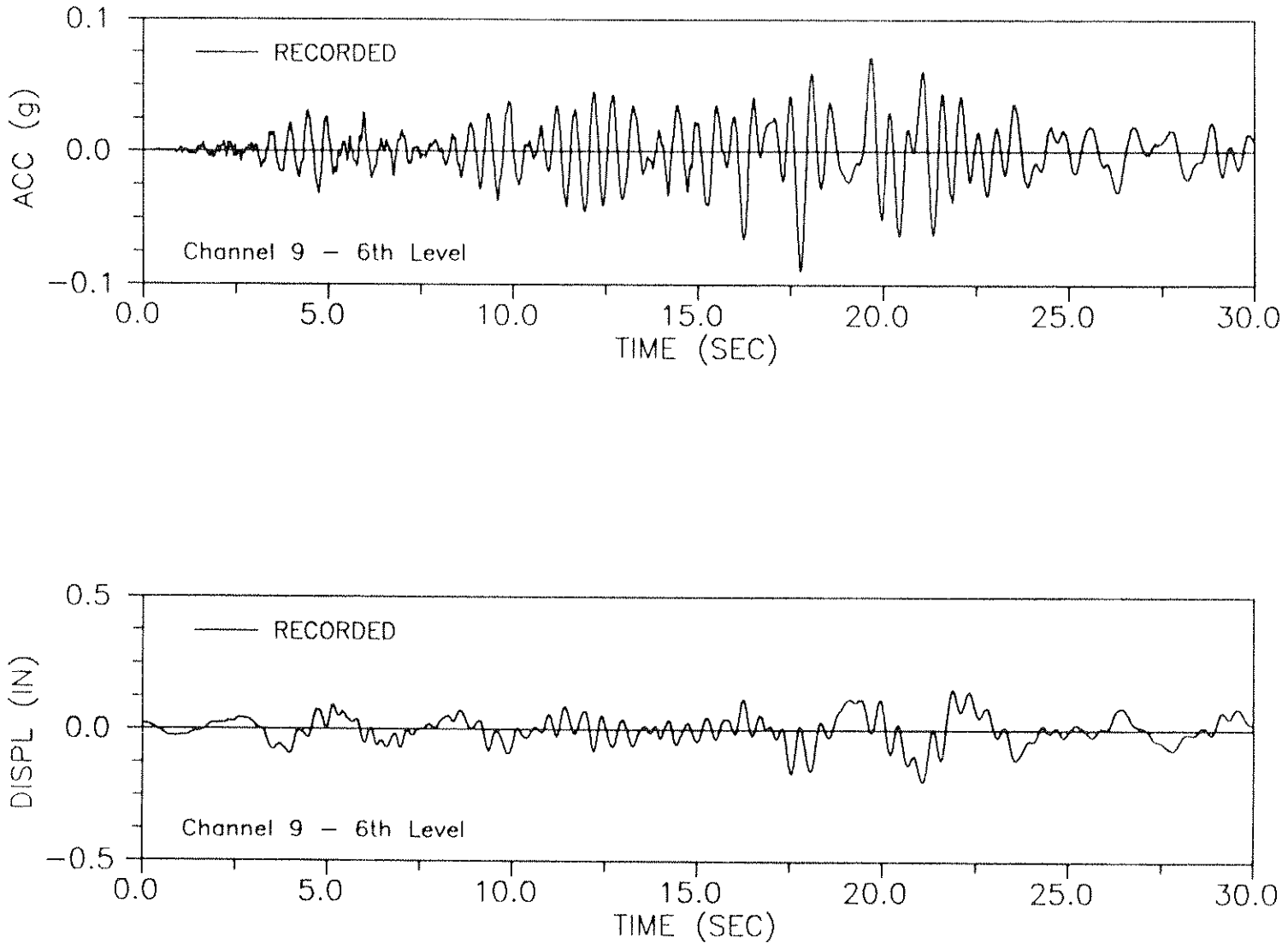

Fig. (6.i) Recorded Response - Channel 9

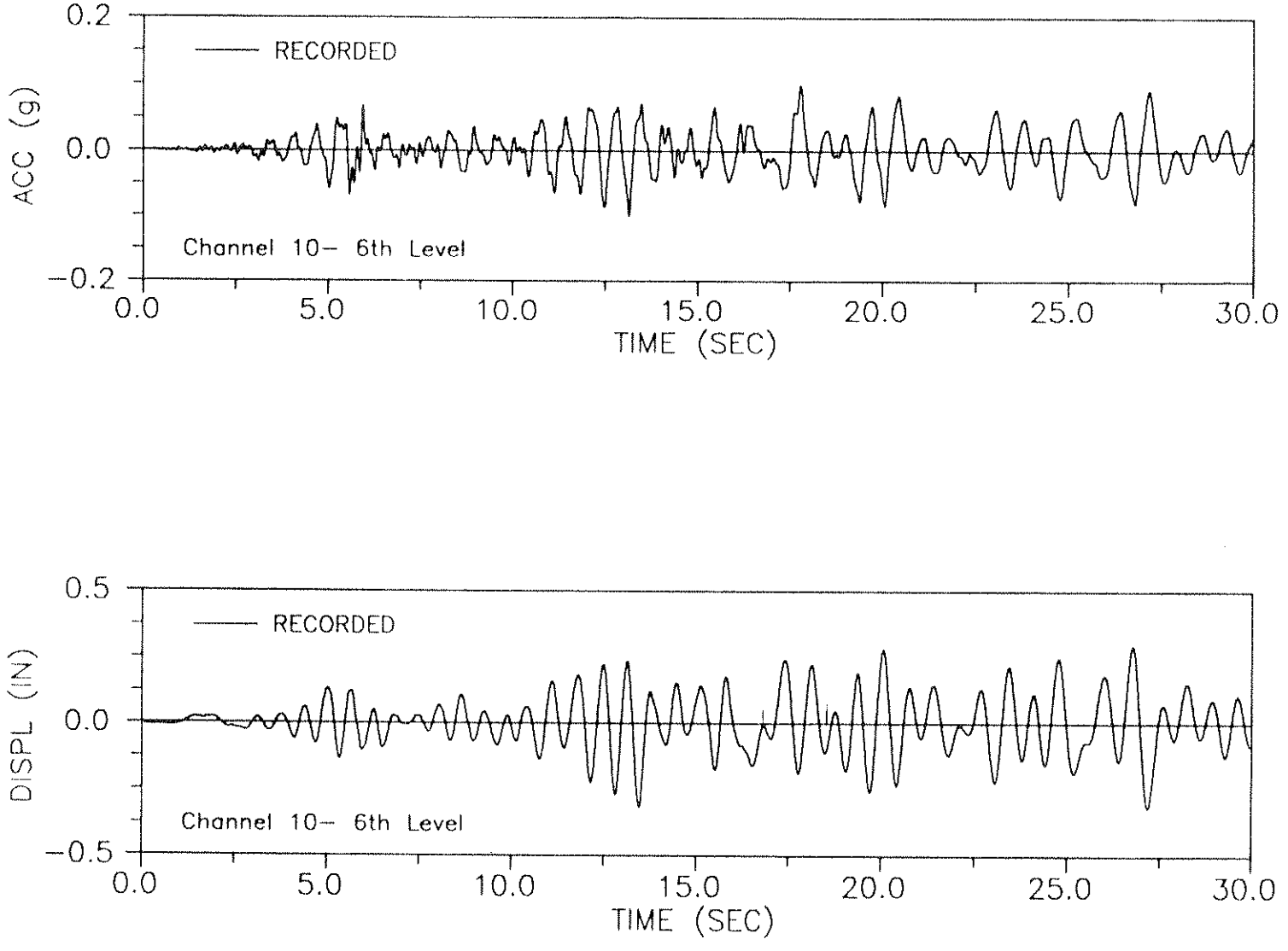

Fig. (6.j) Recorded Response - Channel 10

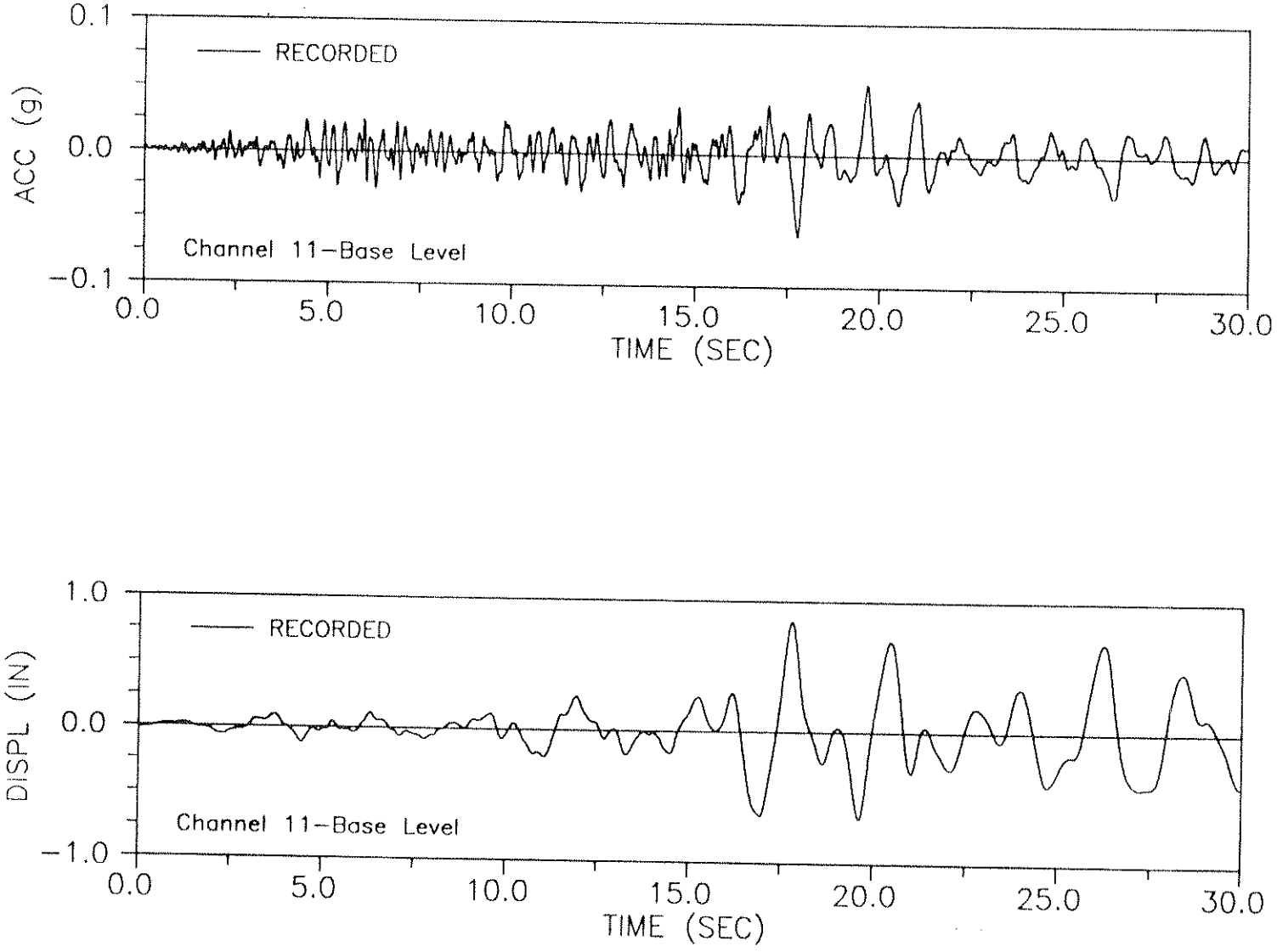

Fig. (6.k) Recorded Response - Channel 11

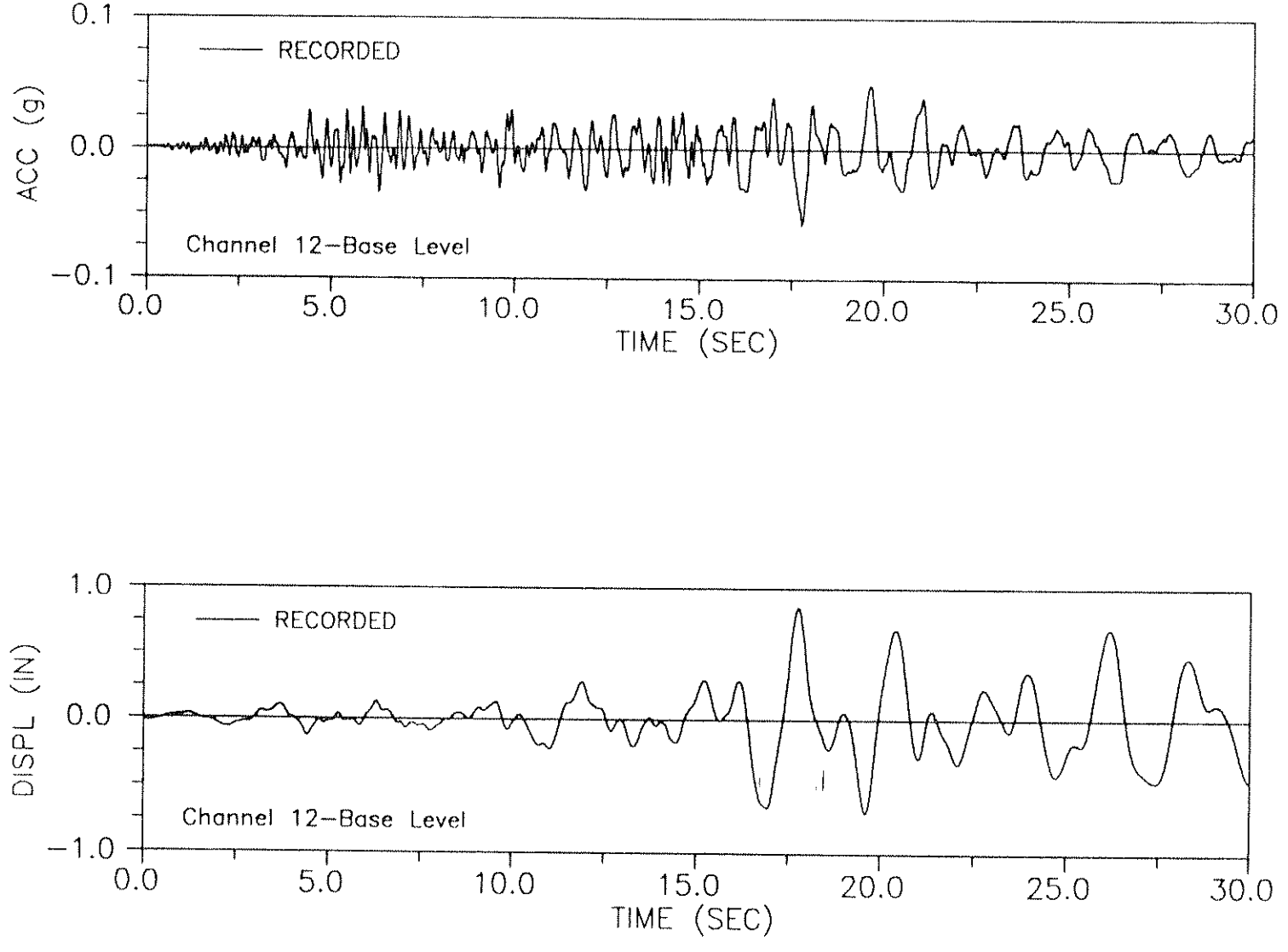

Fig. (6.1) Recorded Response - Channel 12

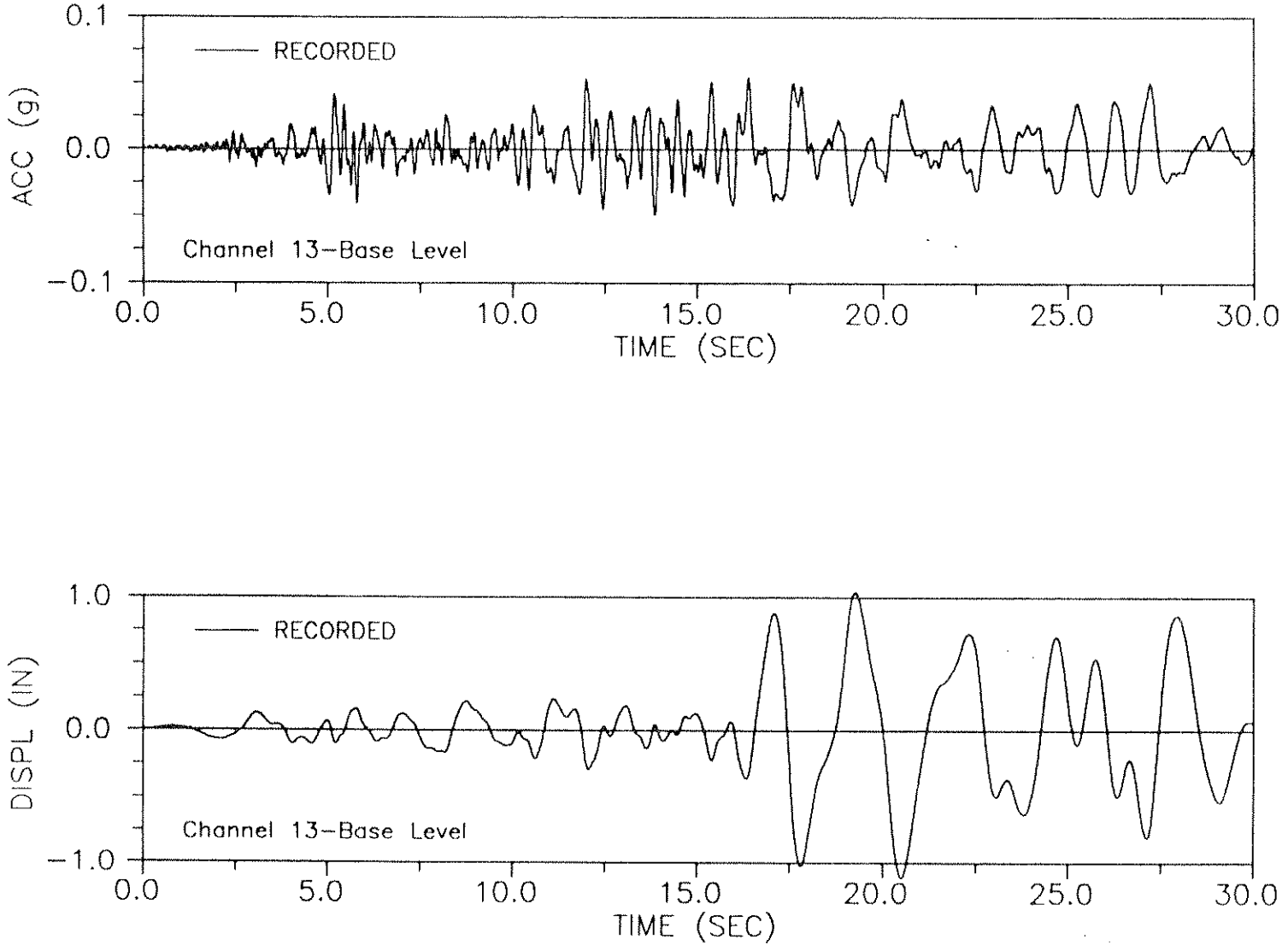

Fig. (6.m) Recorded Response - Channel 13

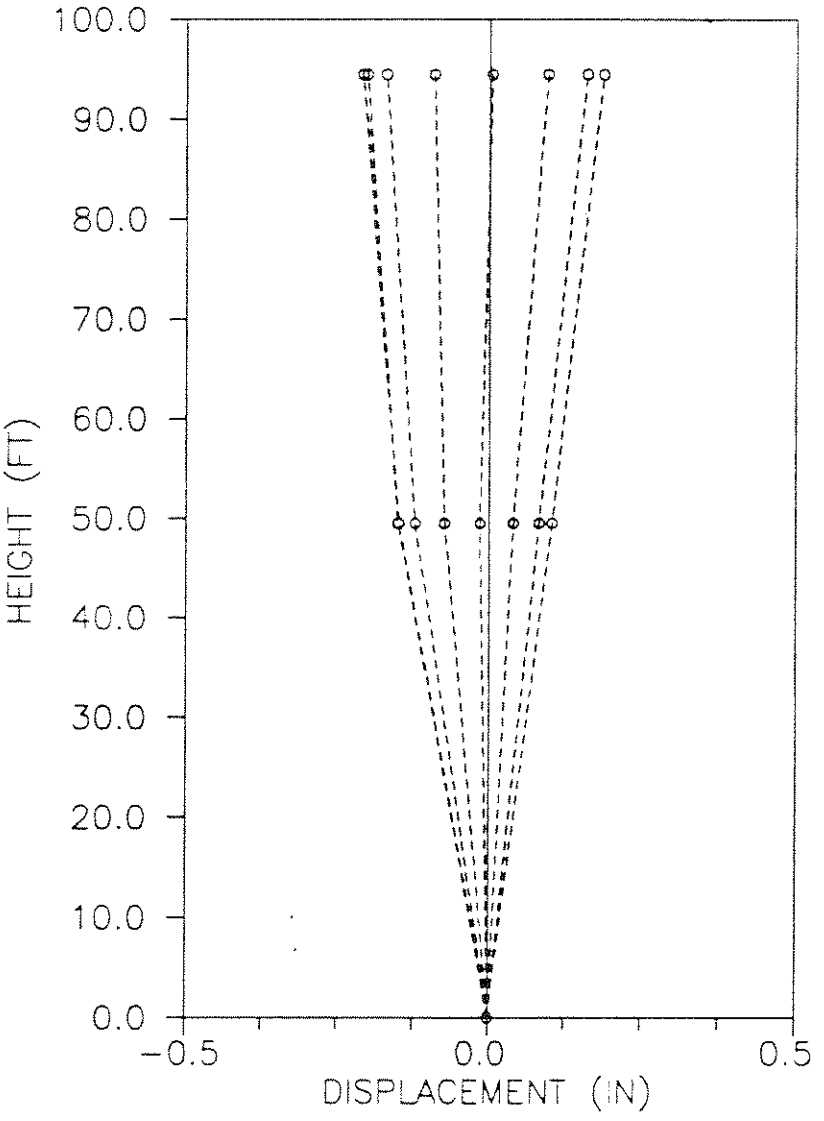

Fig. (7) Displacement Response at t = 17.5 sec to 17.8 sec- Transverse direction

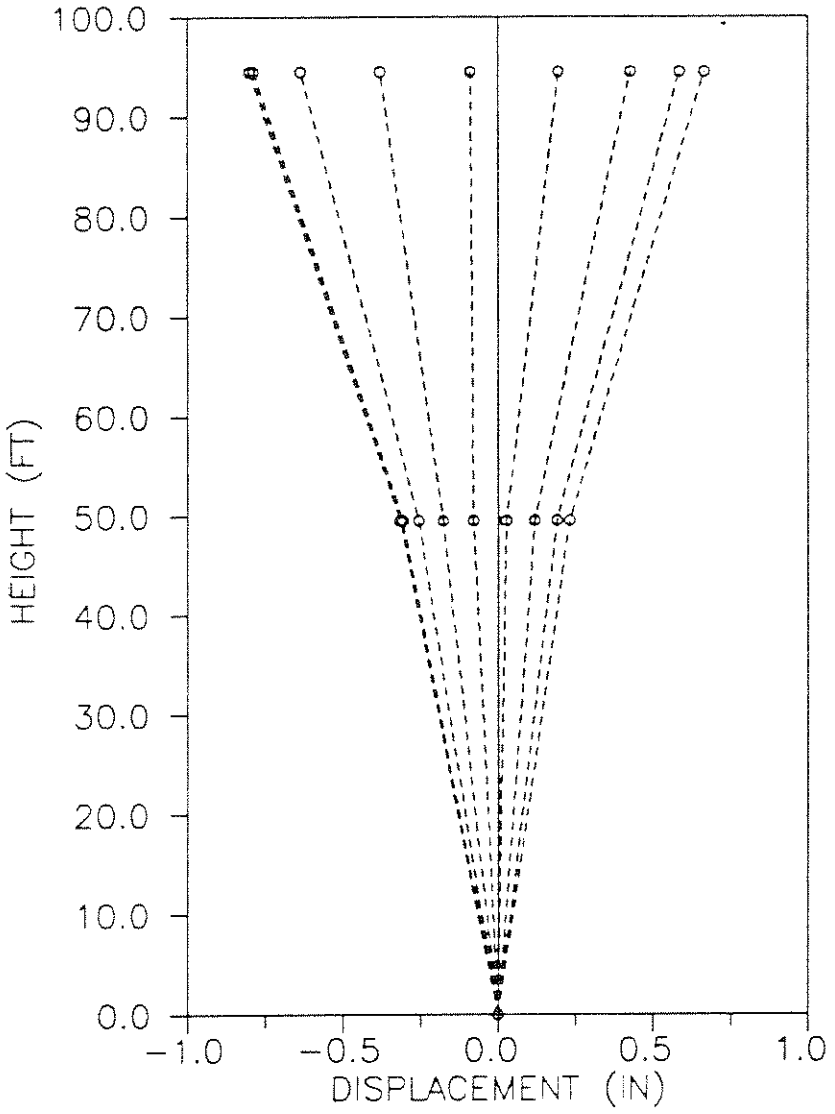

Fig. (8) Displacement response at t = 13.14 sec to 13.48 sec - Longitudinal direction

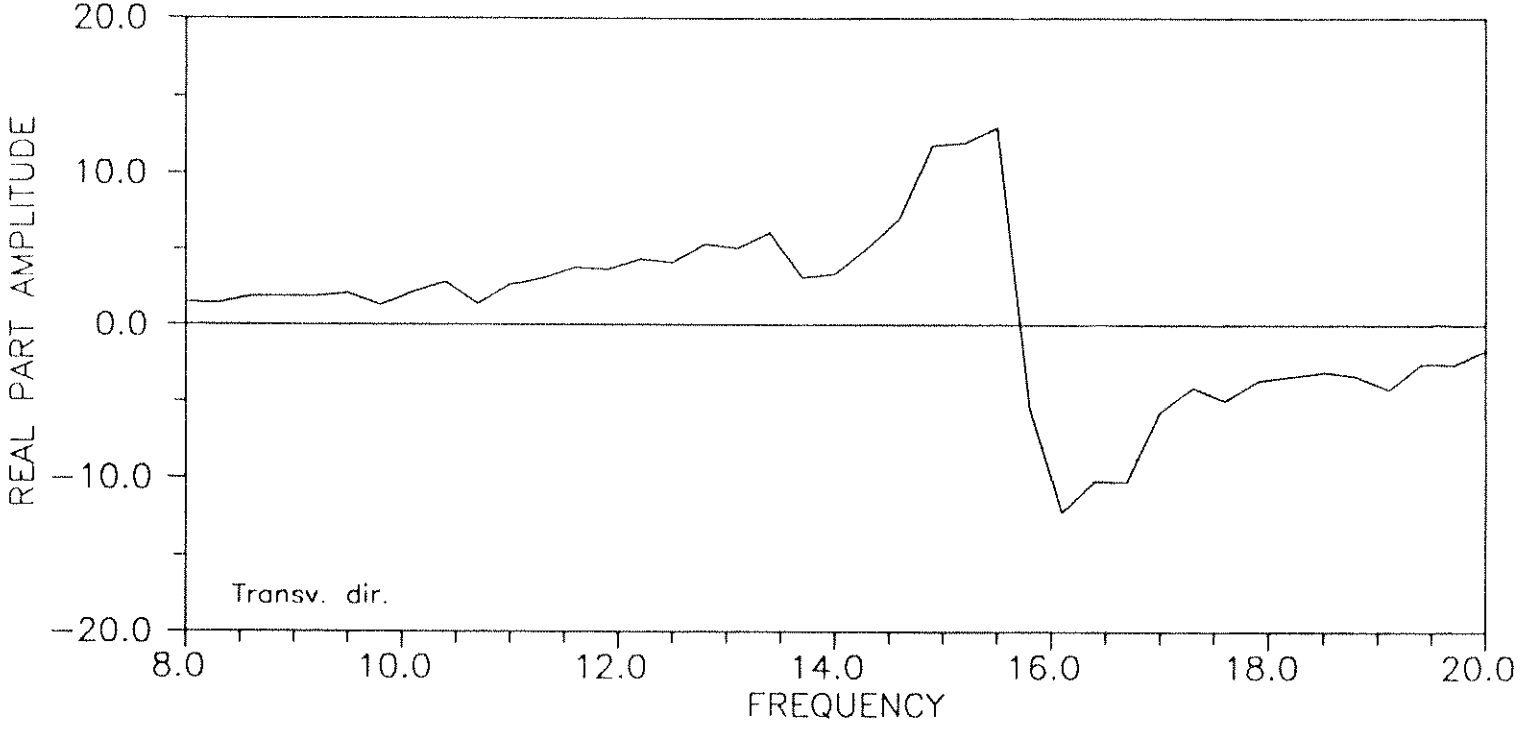

Fig. (9) The Real Part of a measured frequency response function - Transverse direction

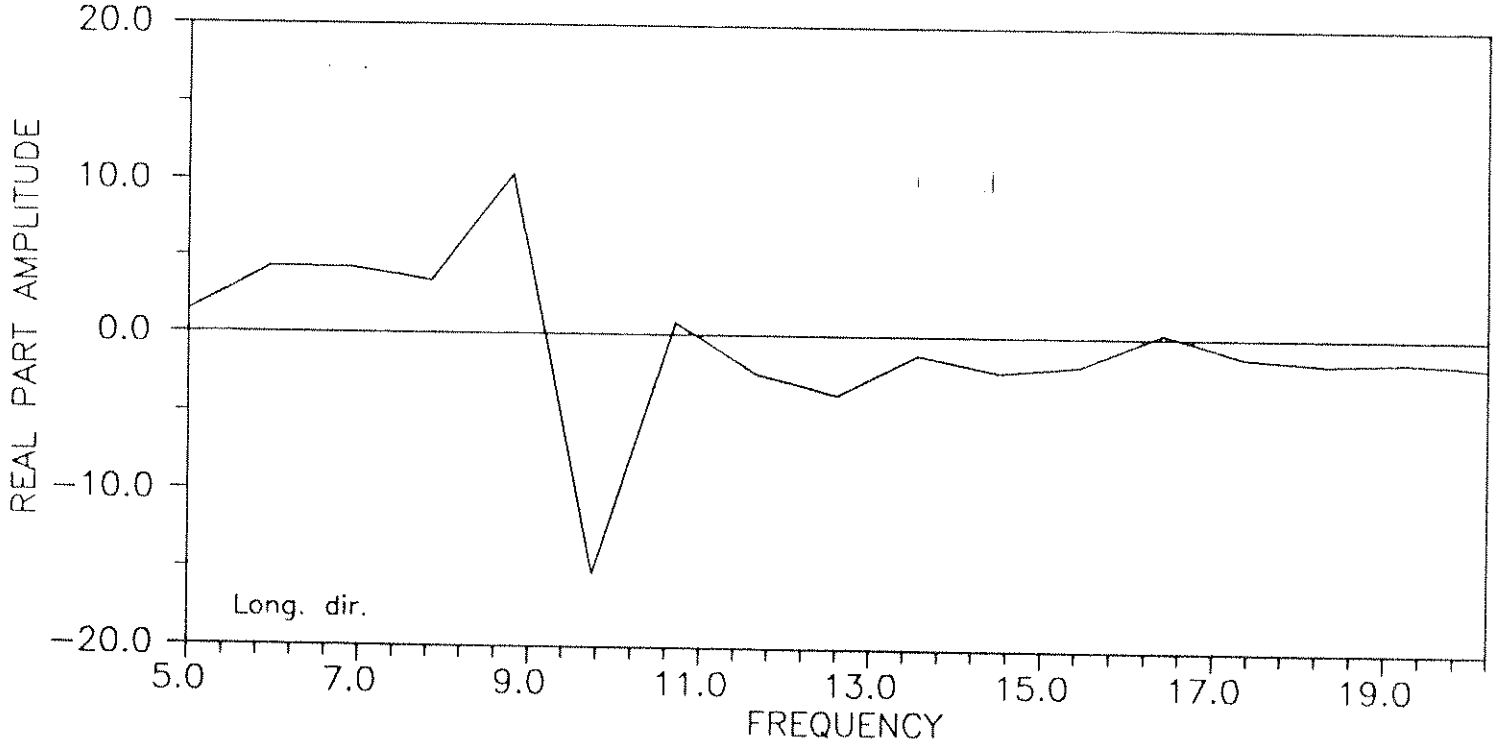

Fig. (10) The Real Part of a measured frequency response function - Longitudinal direction

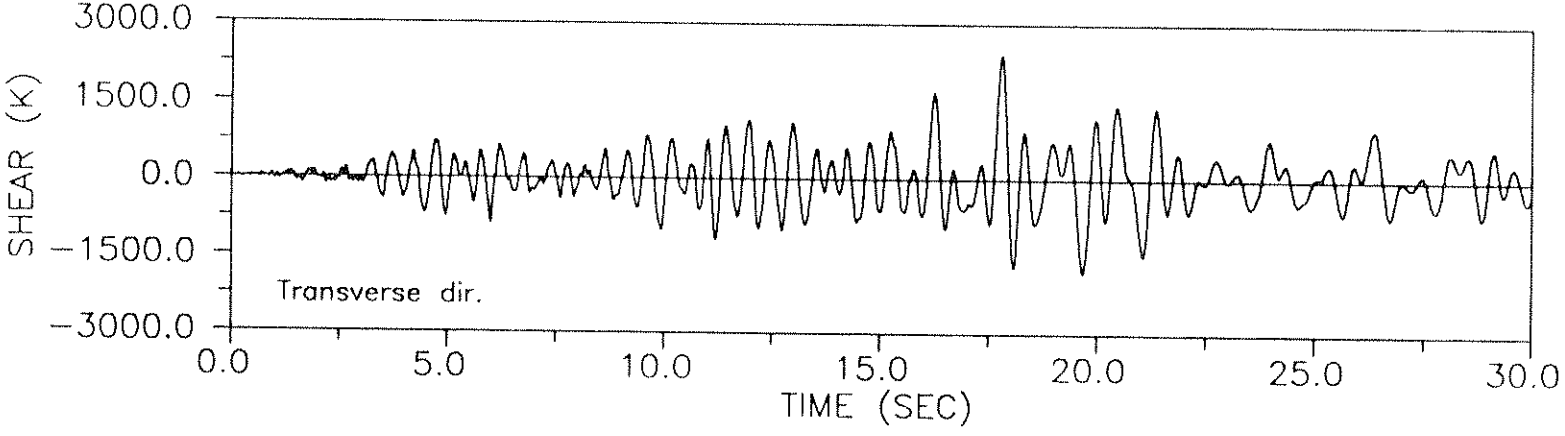

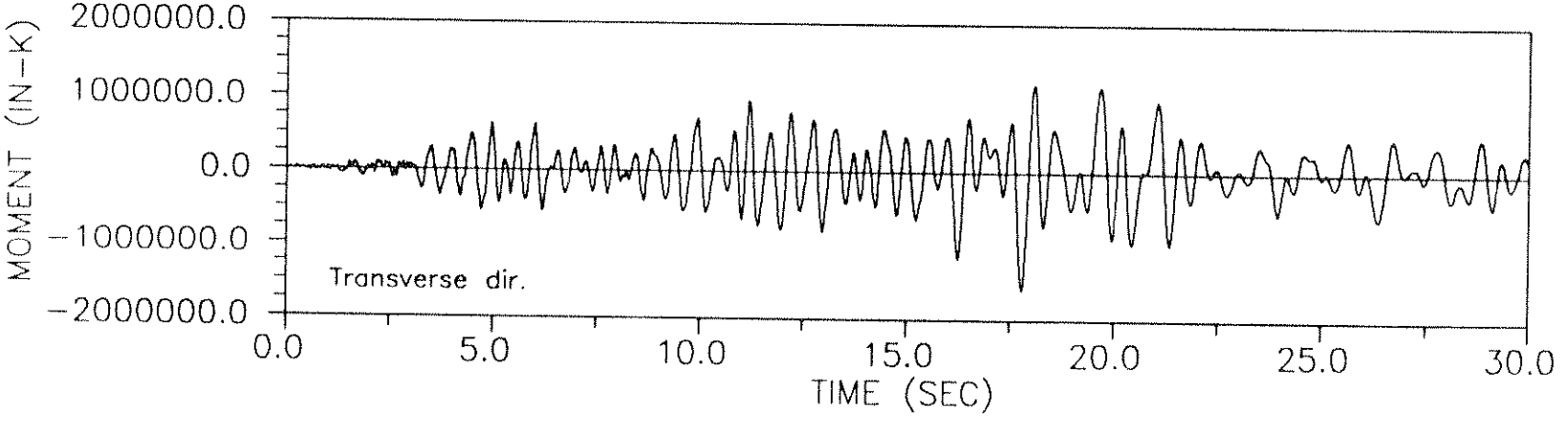

Fig. (11) Base-Shear and Base-Overturning Moment Response - Transverse direction

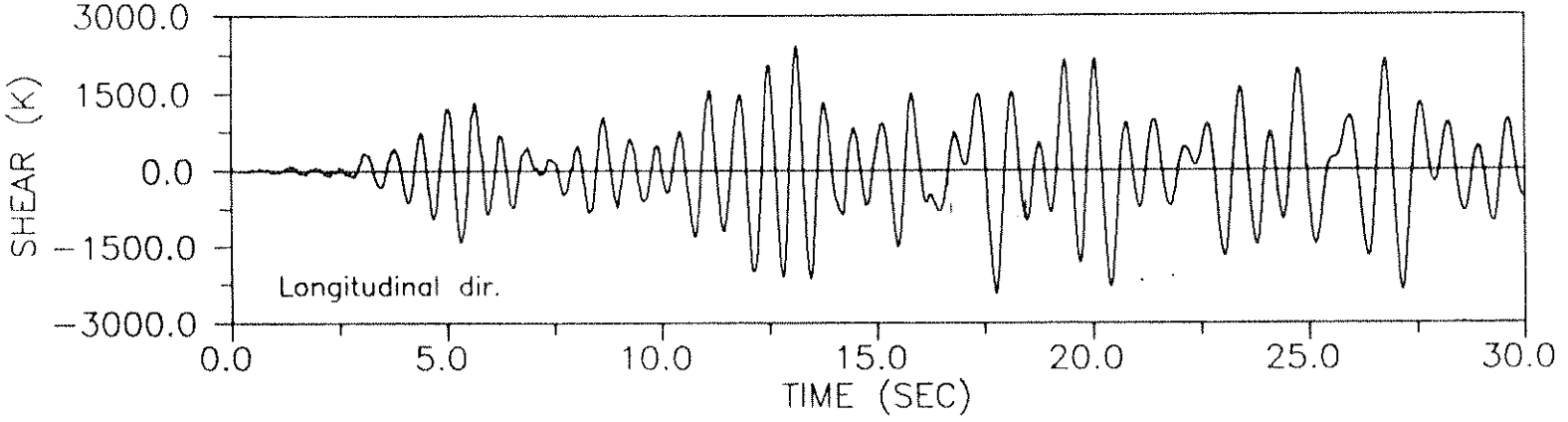

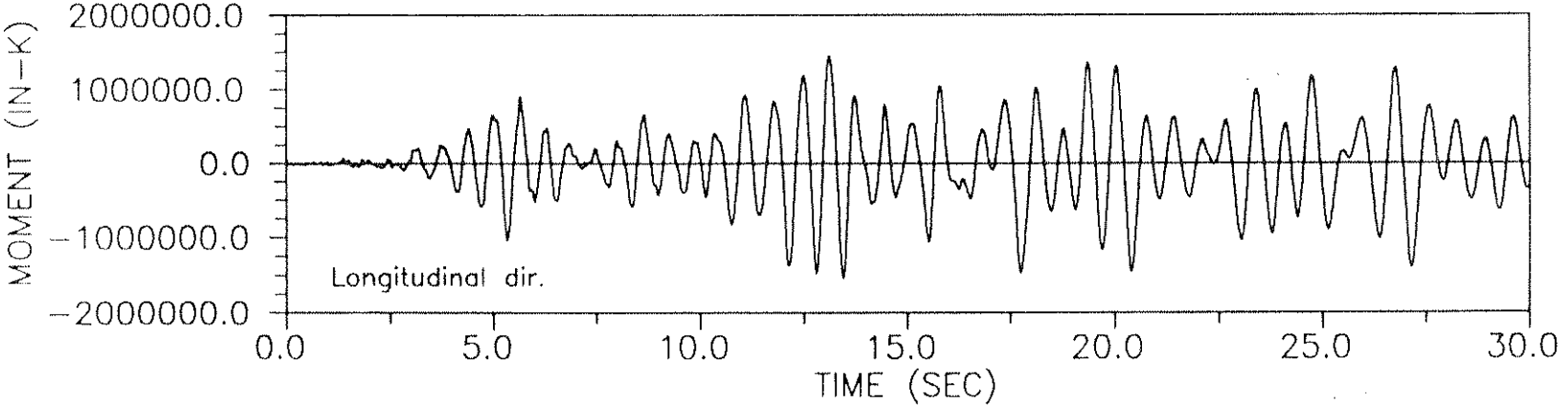

Fig. (12) Base-Shear and Base-Overturning Moment Response - Longitudinal direction

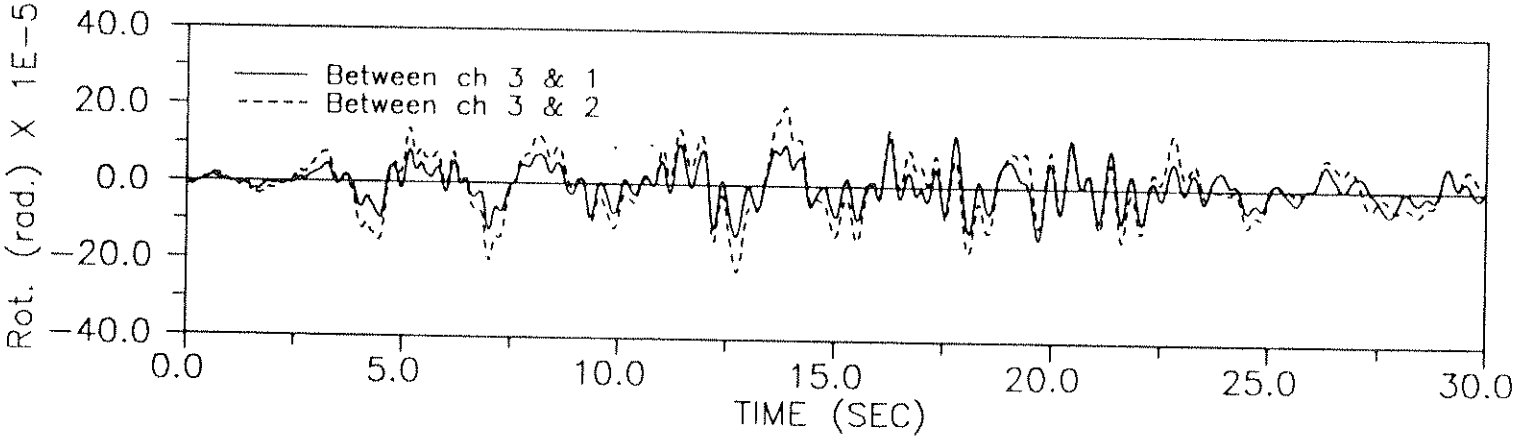

Fig. (13) Base-Rotation - Transverse direction

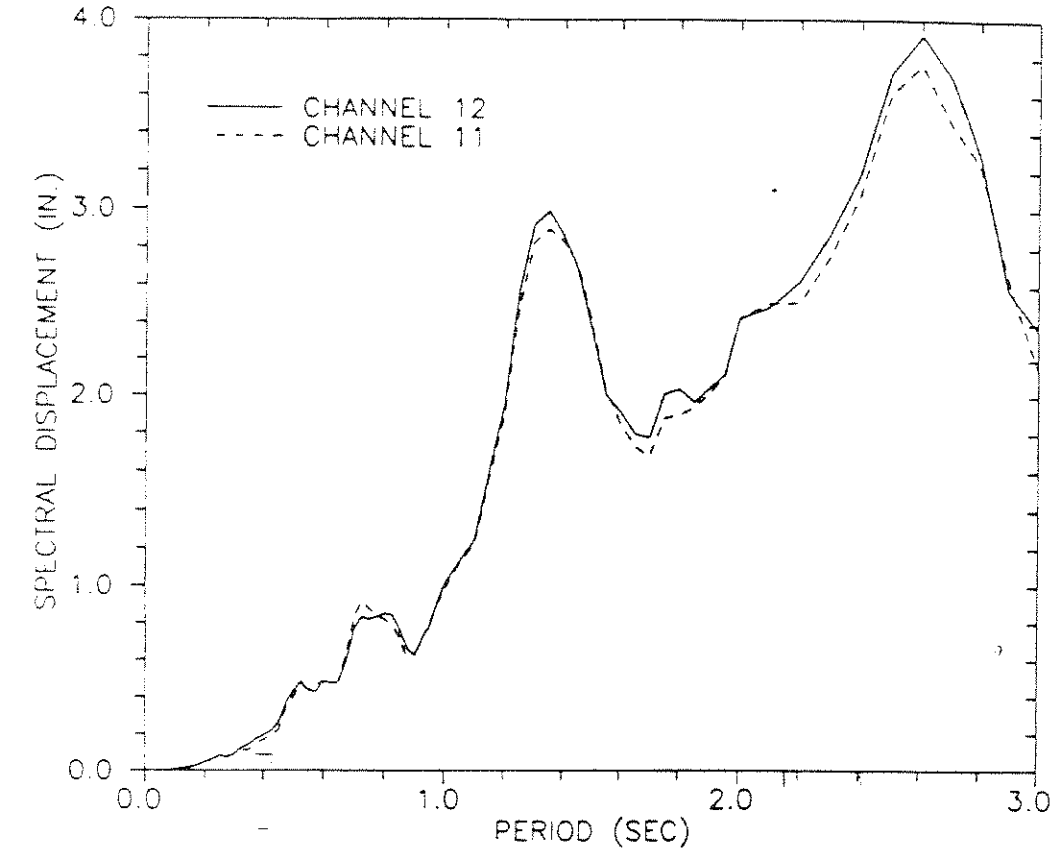

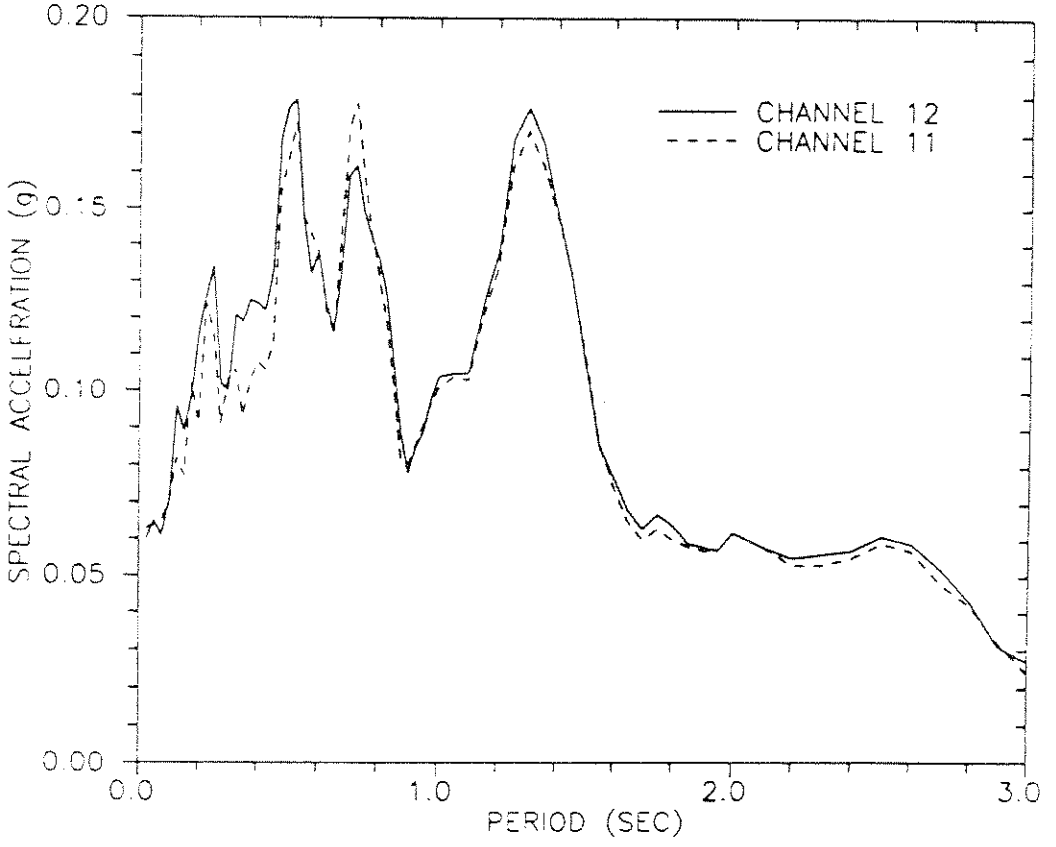

Fig. (14.a) Elastic Response Spectra - Transverse direction

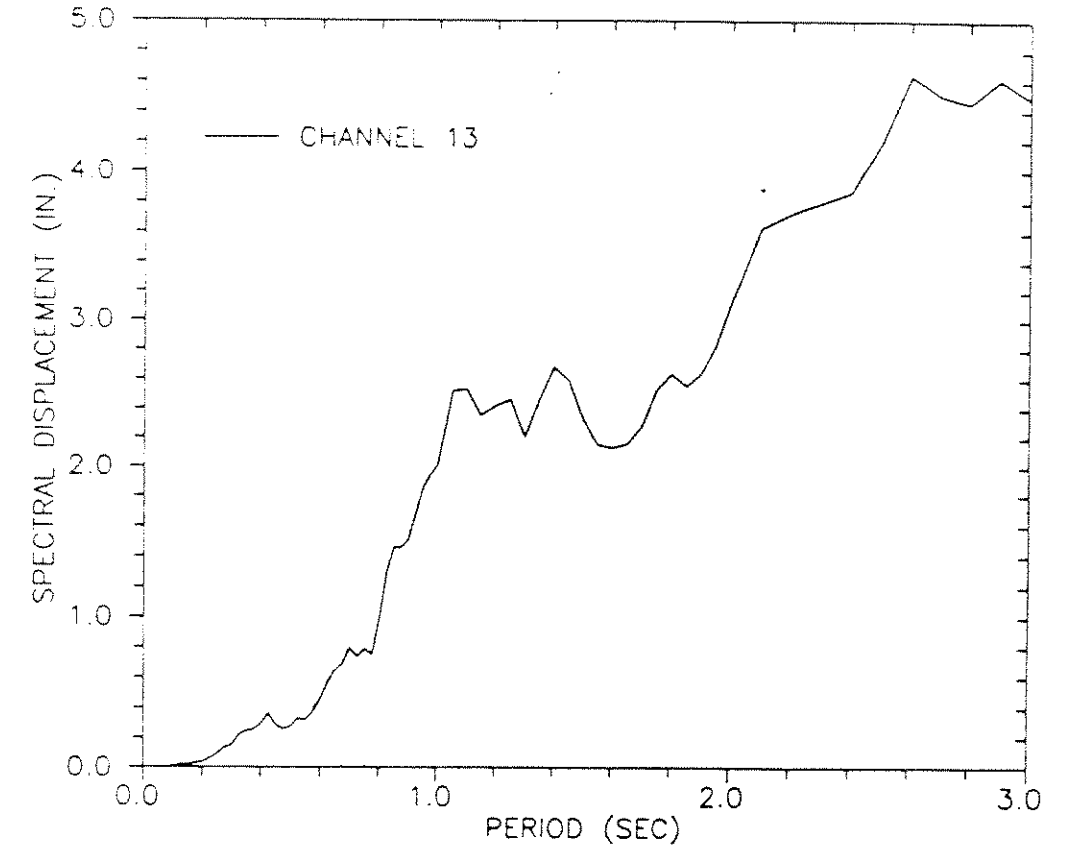

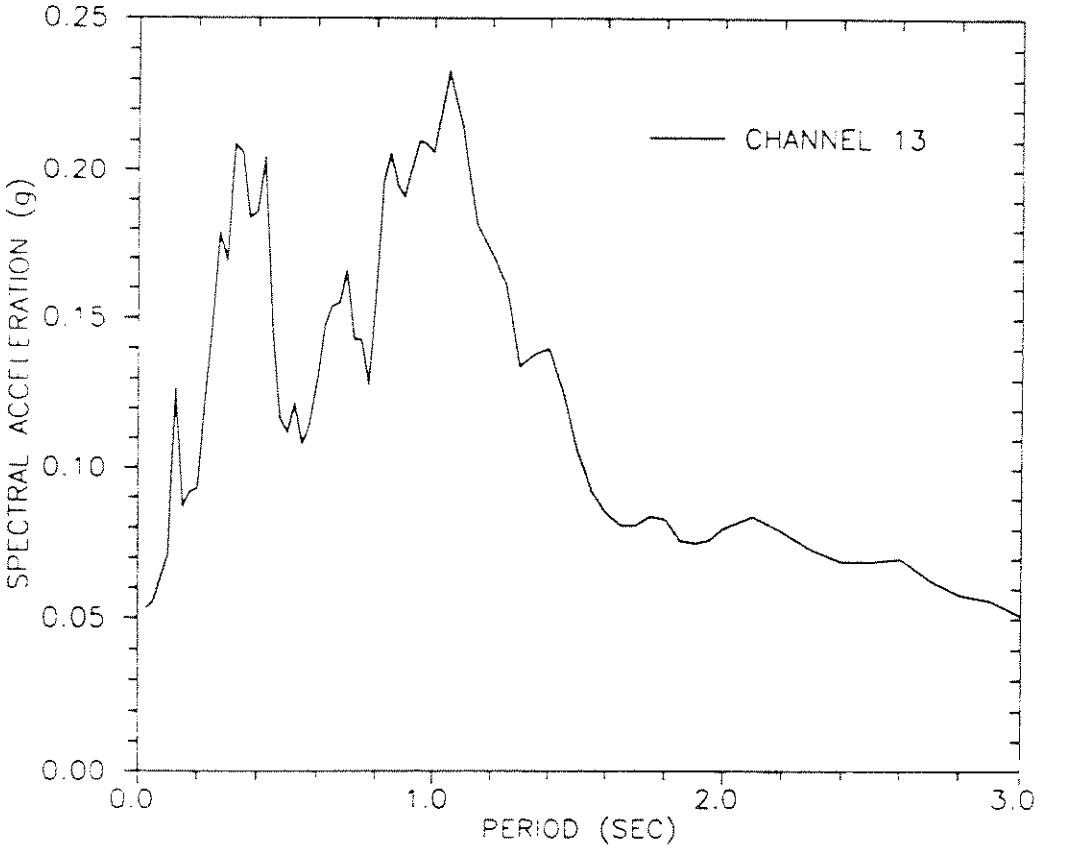

Fig. (14.b) Elastic Response Spectra - Longitudinal direction

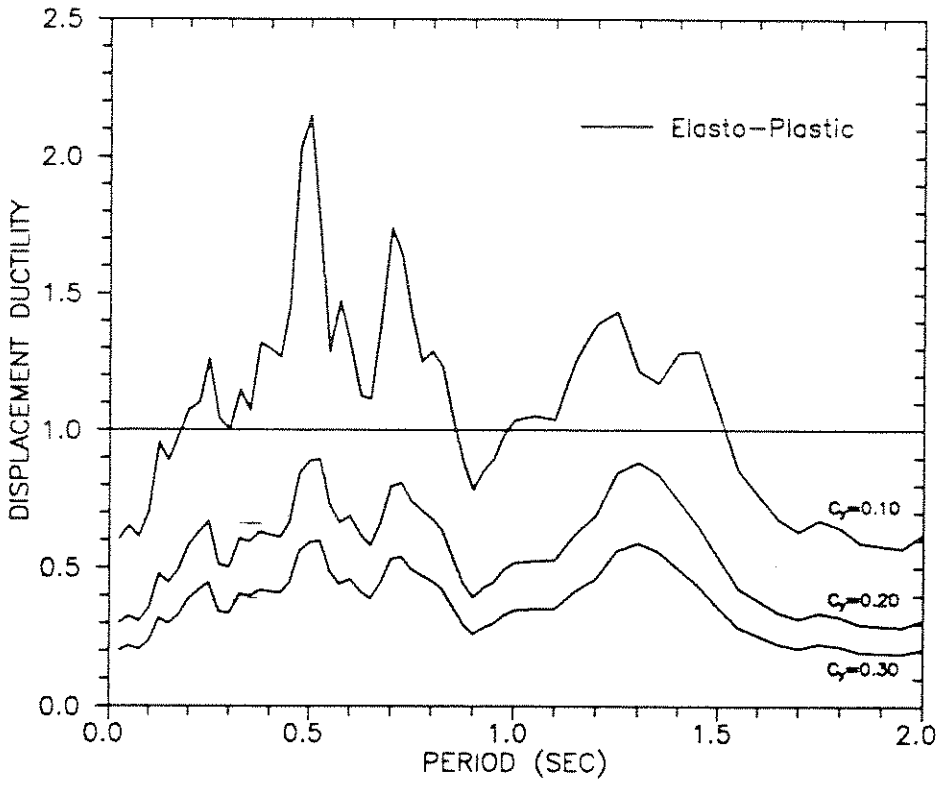

Fig. (15.a) Displacement Ductility Spectra - Transverse direction

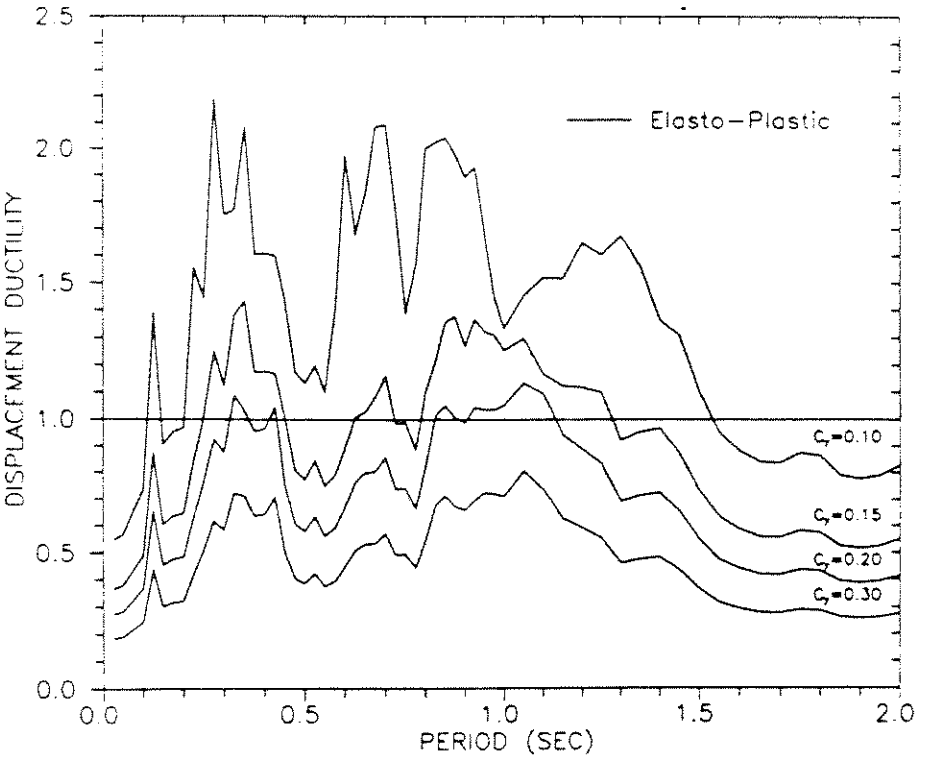

Fig. (15.b) Displacement Ductility Spectra - Longitudinal direction

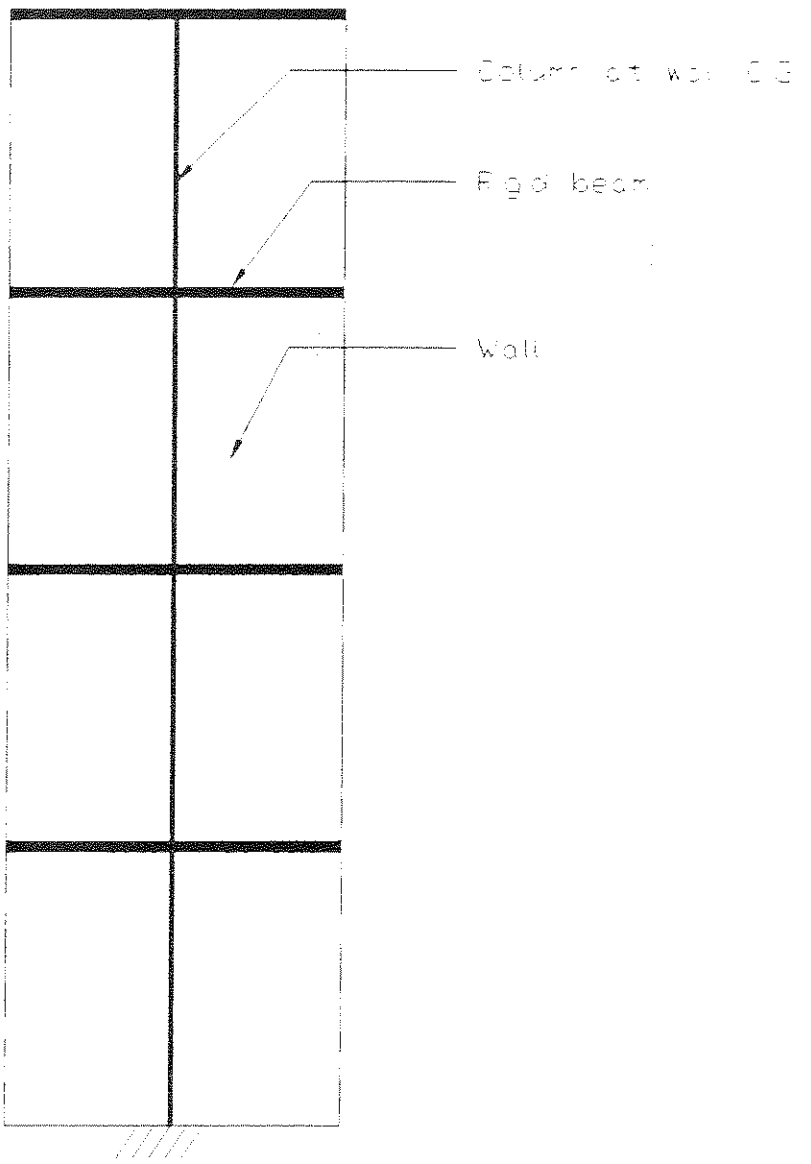

Fig. (16) Column Analogy

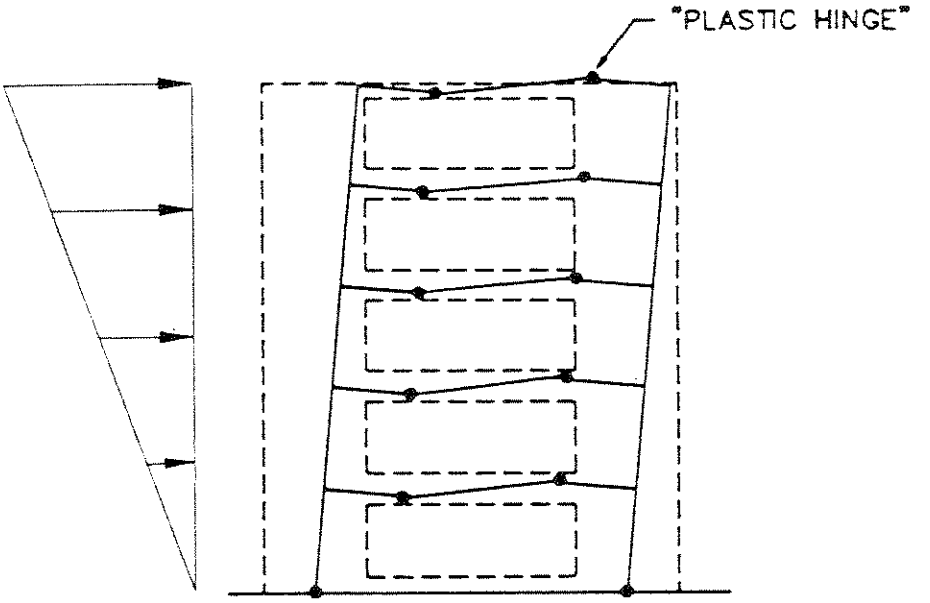

Fig. (17) Base Wall and Coupling Beam Yielding Mechanism

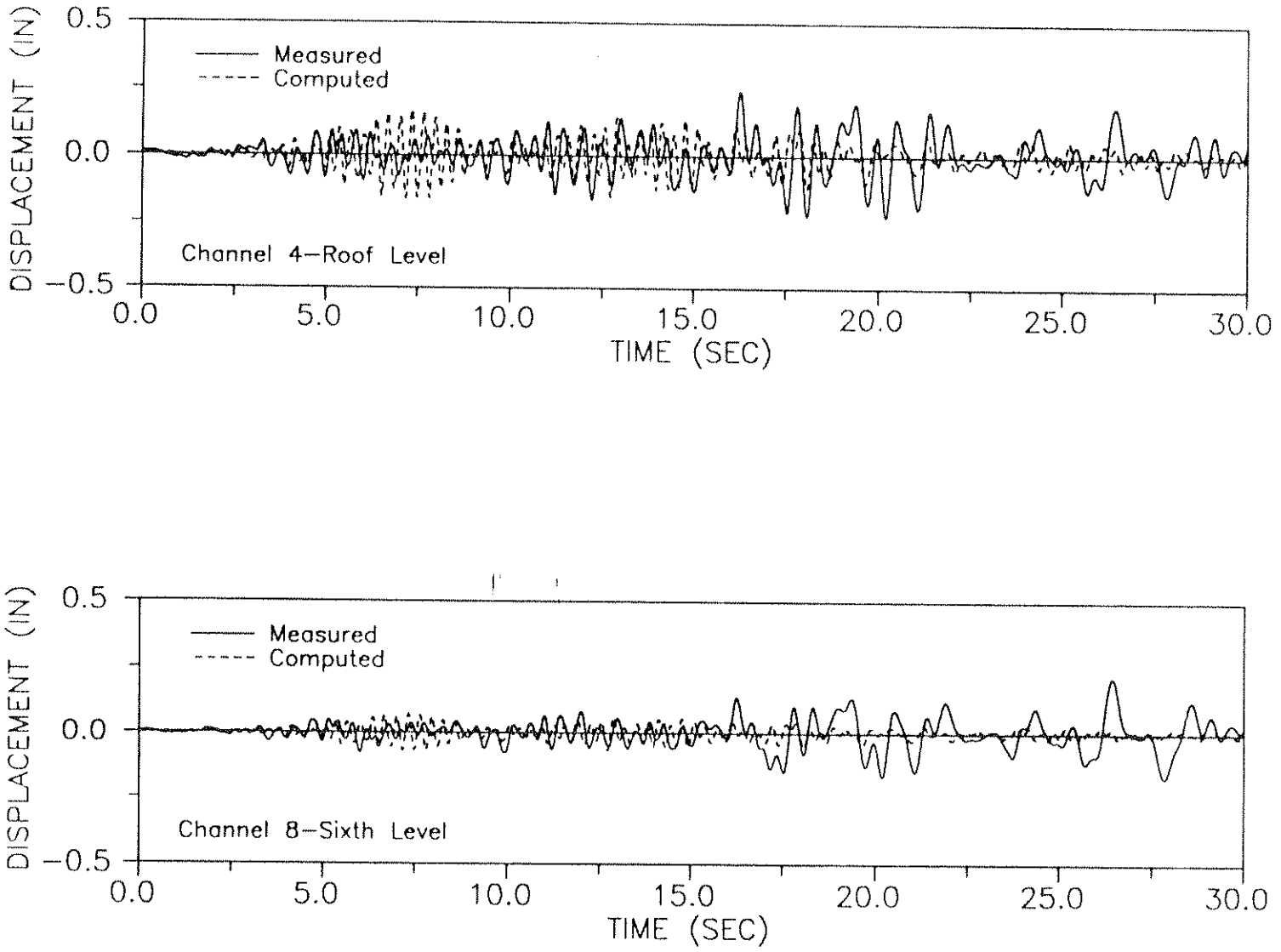

Fig. (18.a) Computed and Measured Displacement Response (Analysis - 1) - Transverse direction

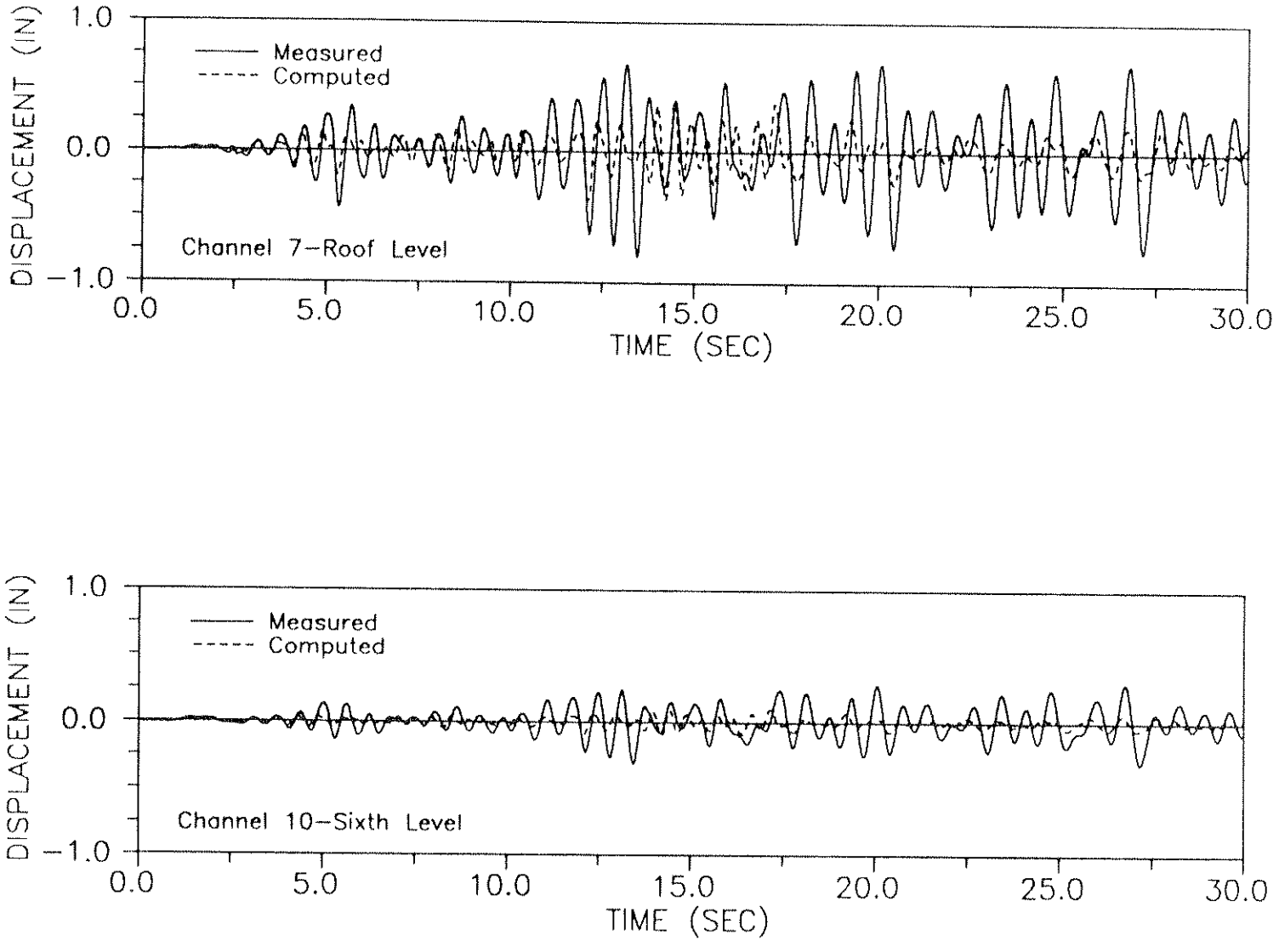

Fig. (18.b) Computed and Measured Displacement Response (Analysis - 1) - Longitudinal direction

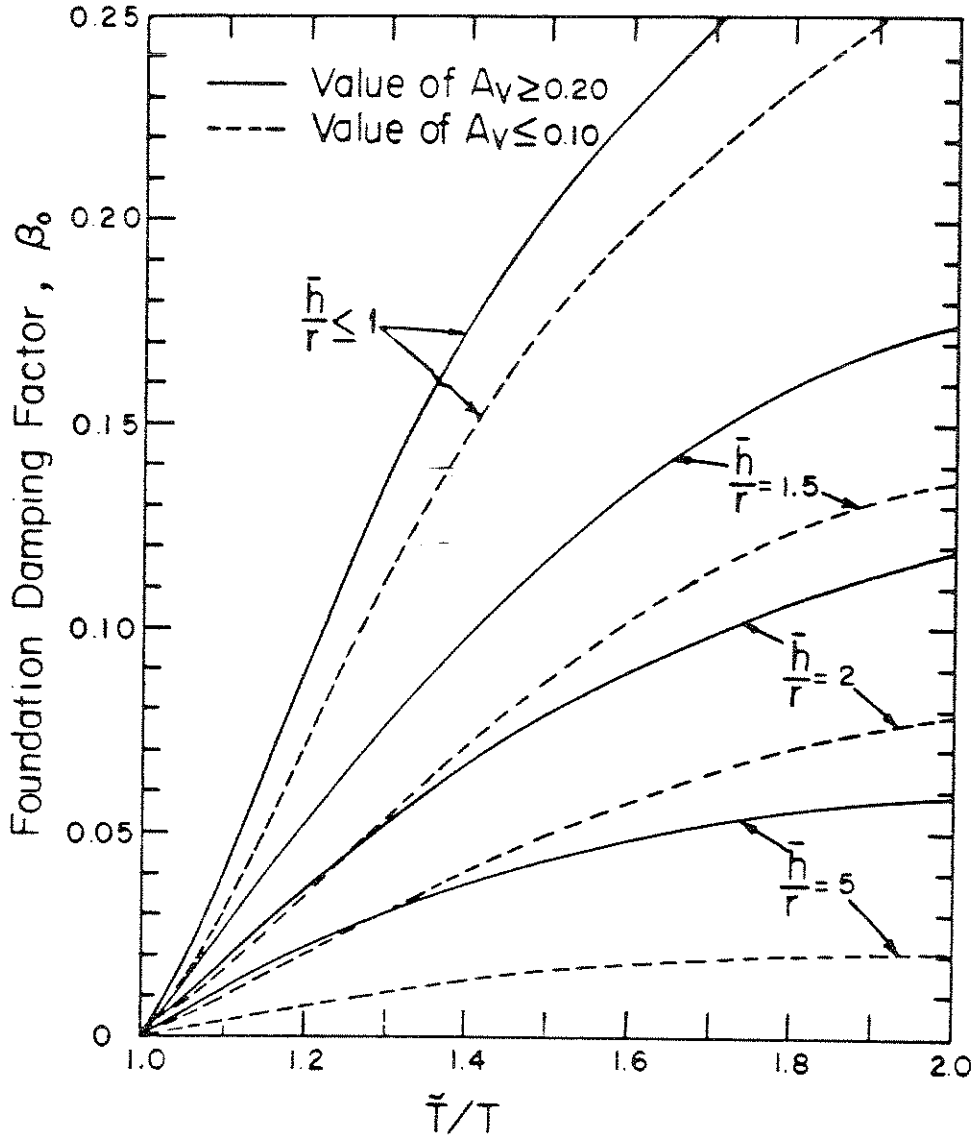

Fig. (19) Foundation Damping Factor, $\tilde{\beta}_0$

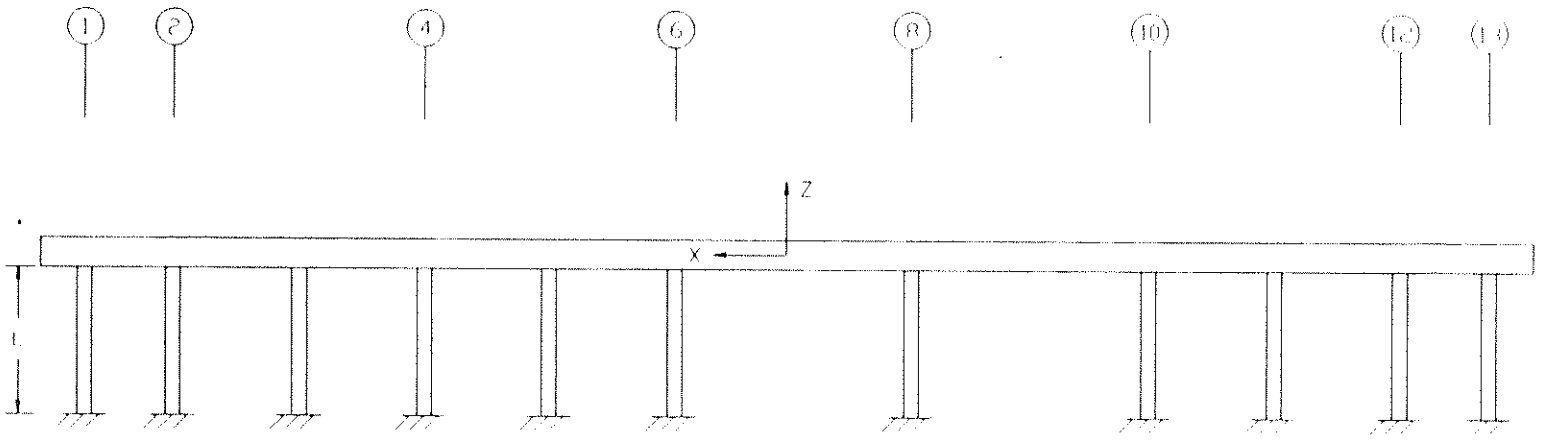

Fig. (20) Soil-Structure Interaction Model - Longitudinal direction

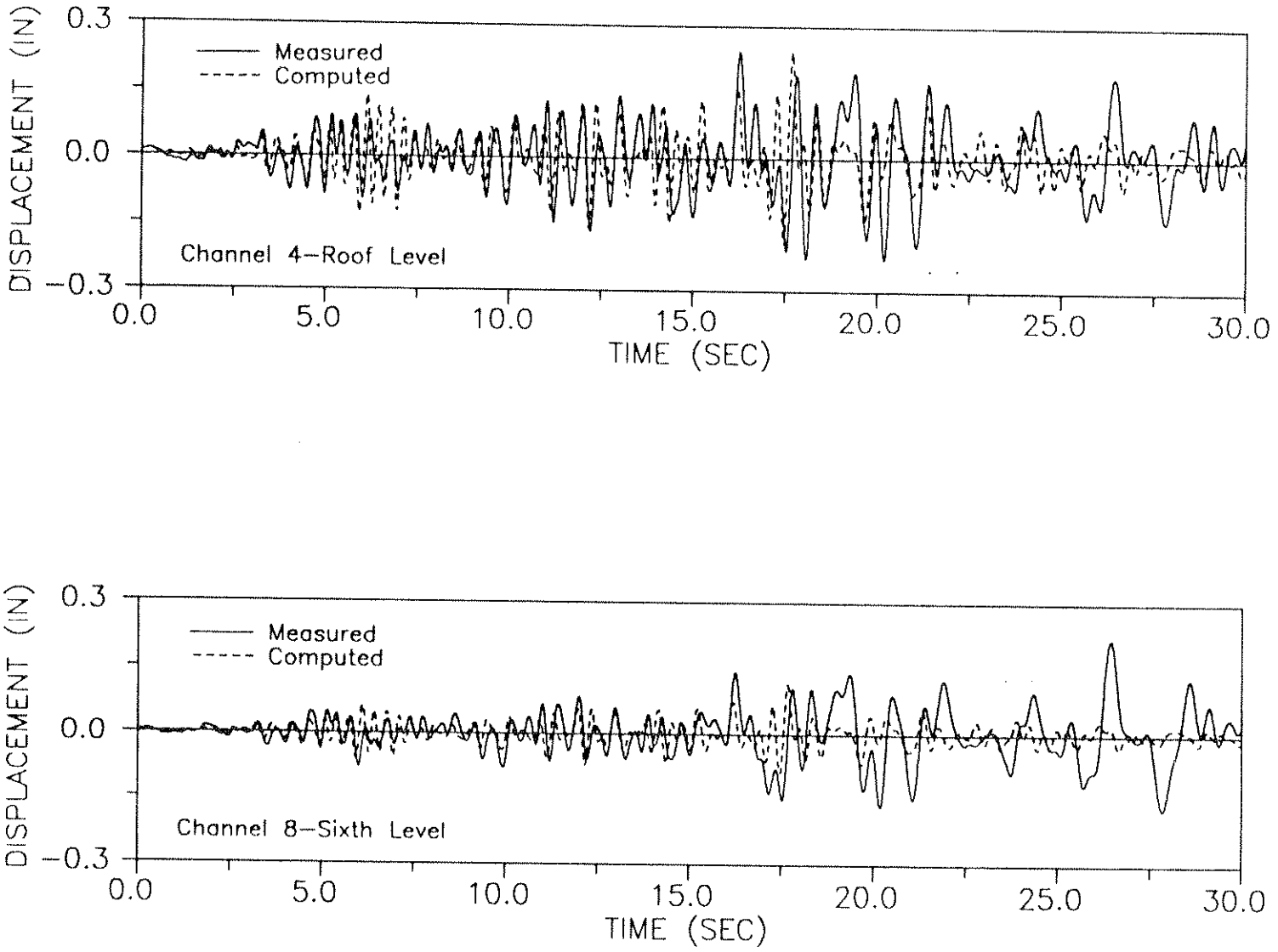

Fig. (21.a) Computed and Measured Displacement Response (Analysis - 2) - Transverse direction

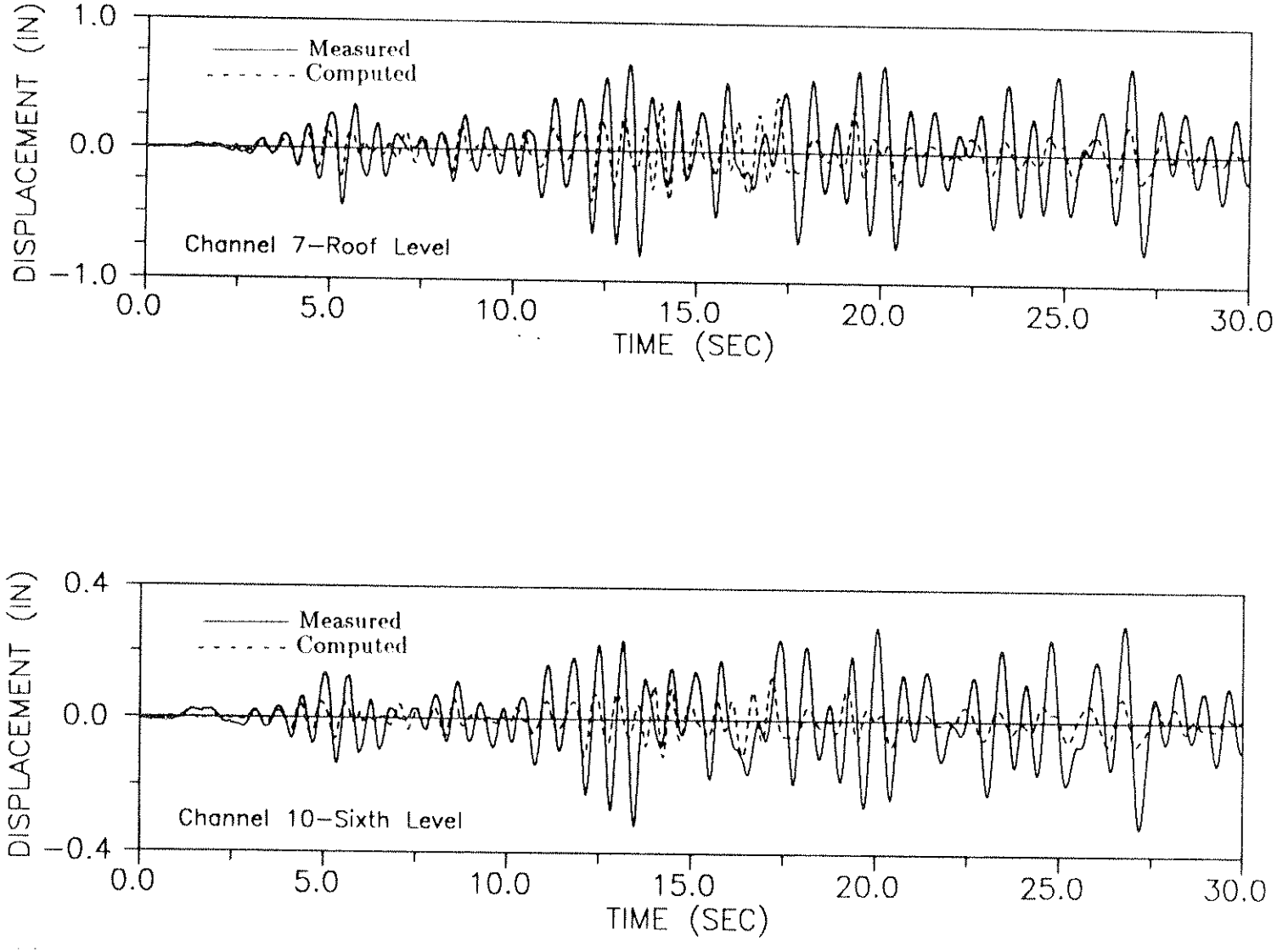

Fig. (21.b) Computed and Measured Displacement Response (Analysis - 2) - Longitudinal direction

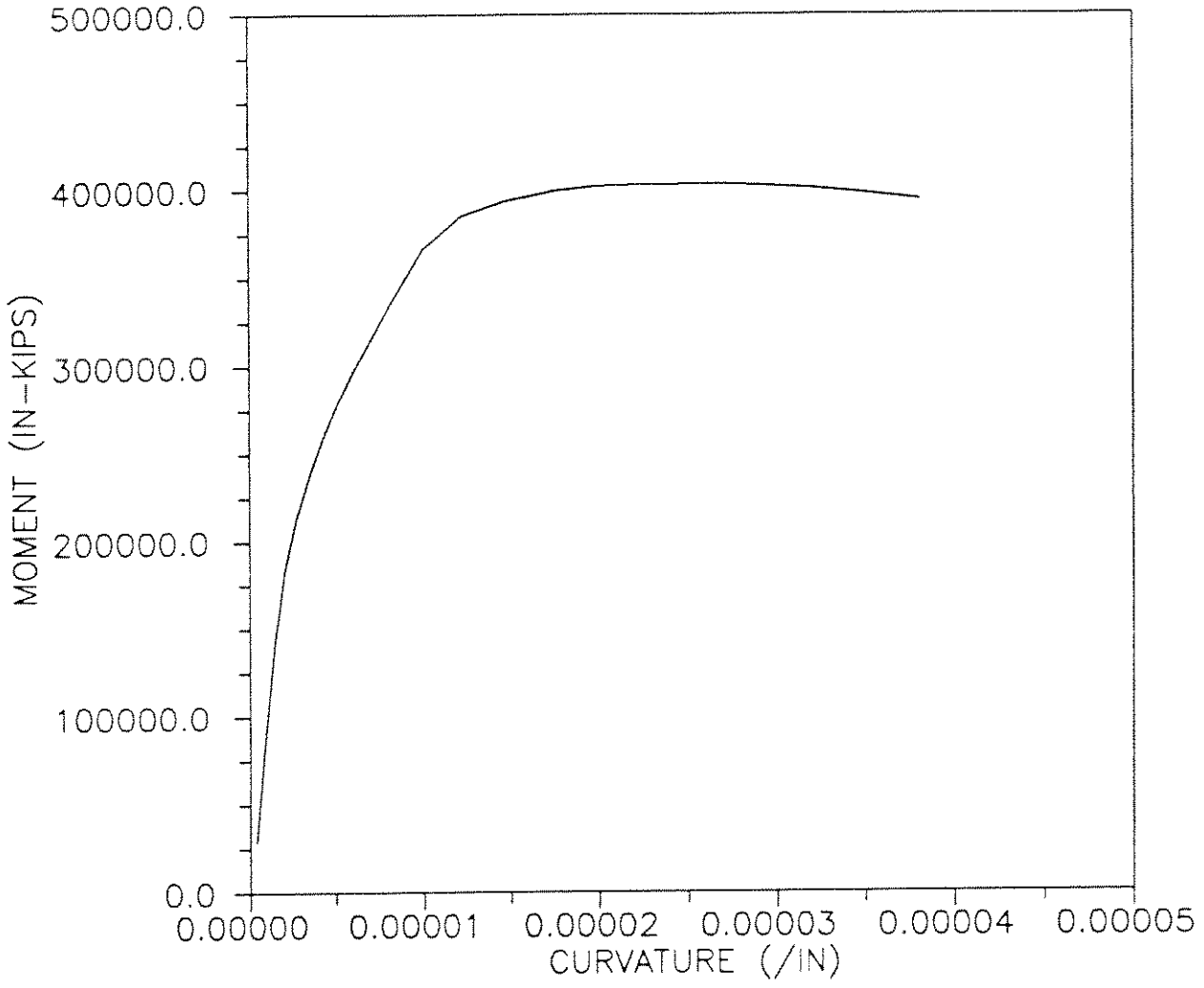

Fig. (22) Moment - Curvature Relationship - Transverse Direction

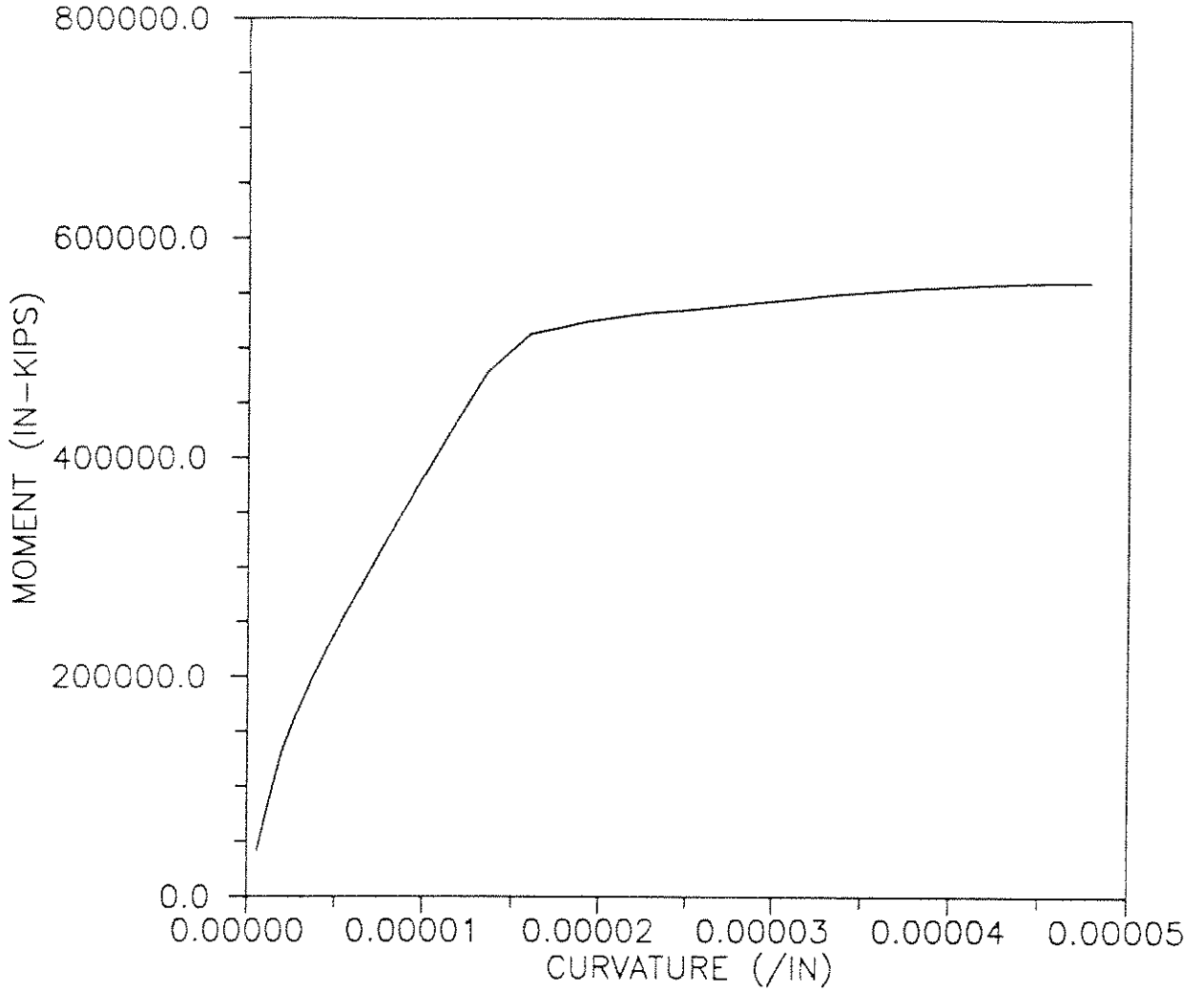

Fig. (23) Moment - Curvature Relationship - Longitudinal Direction

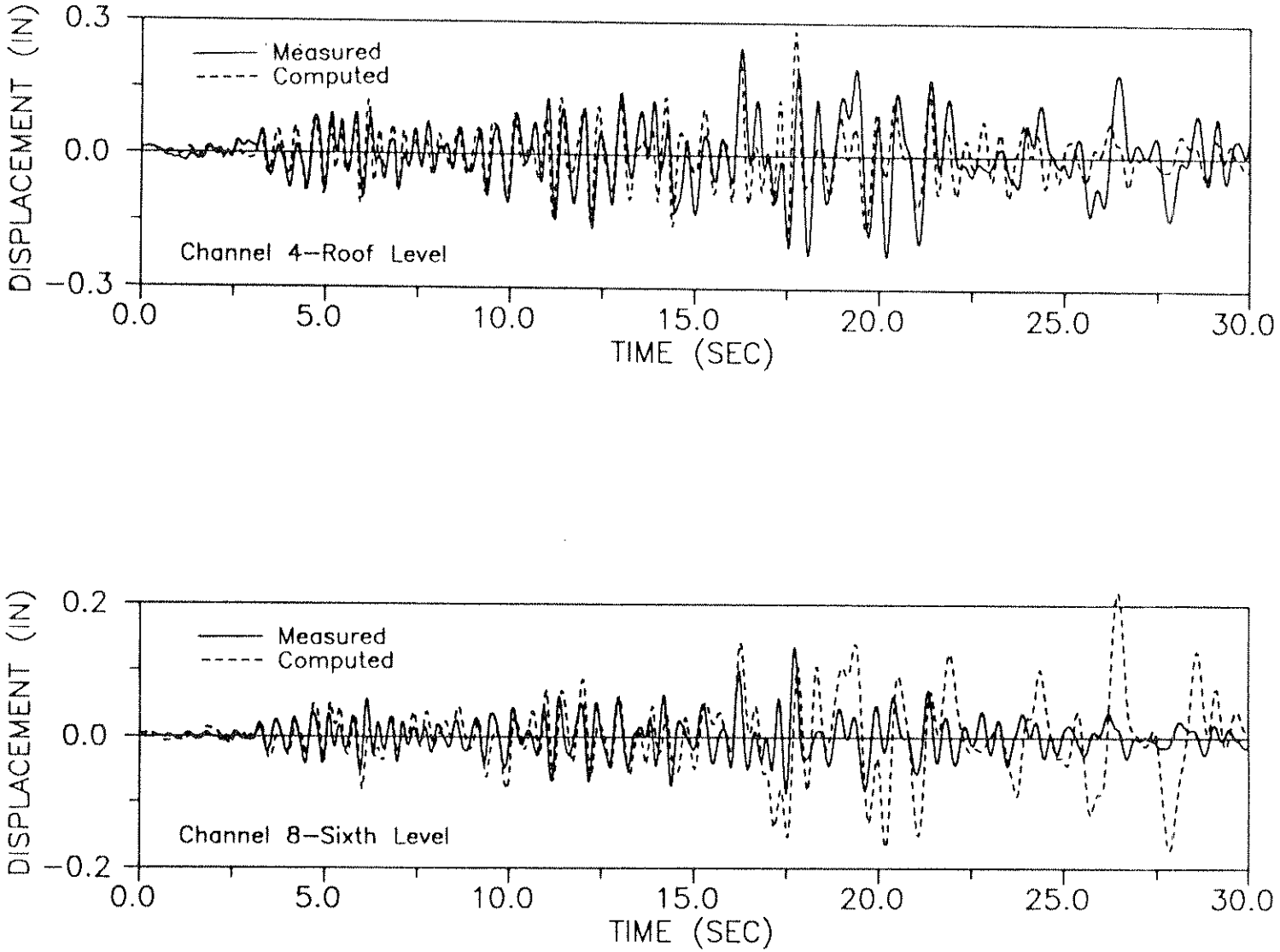

Fig. (24.a) Computed and Measured Displacement Response (Analysis - 3) - Transverse direction

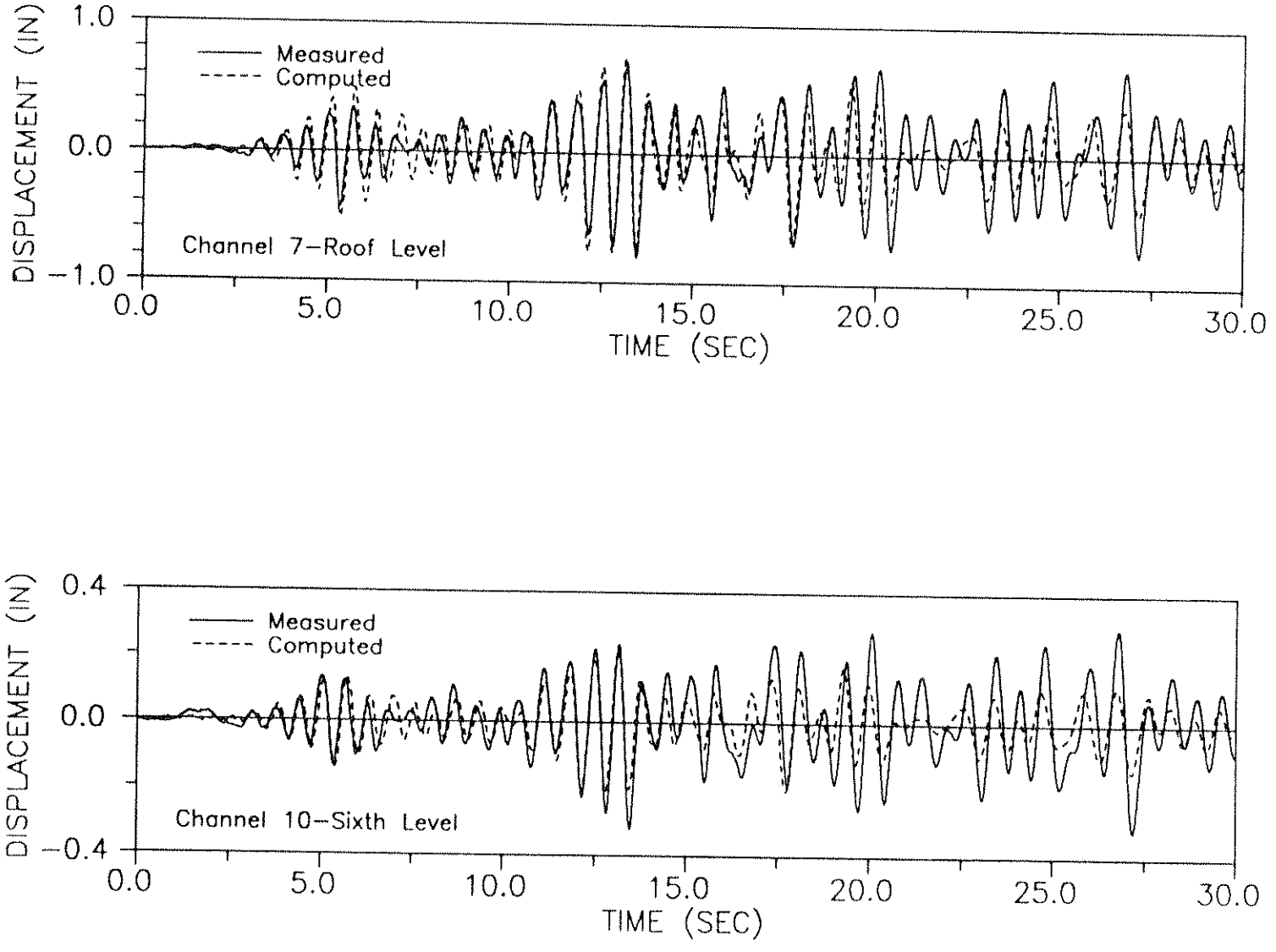

Fig. (24.b) Computed and Measured Displacement Response (Analysis - 3) - Longitudinal direction

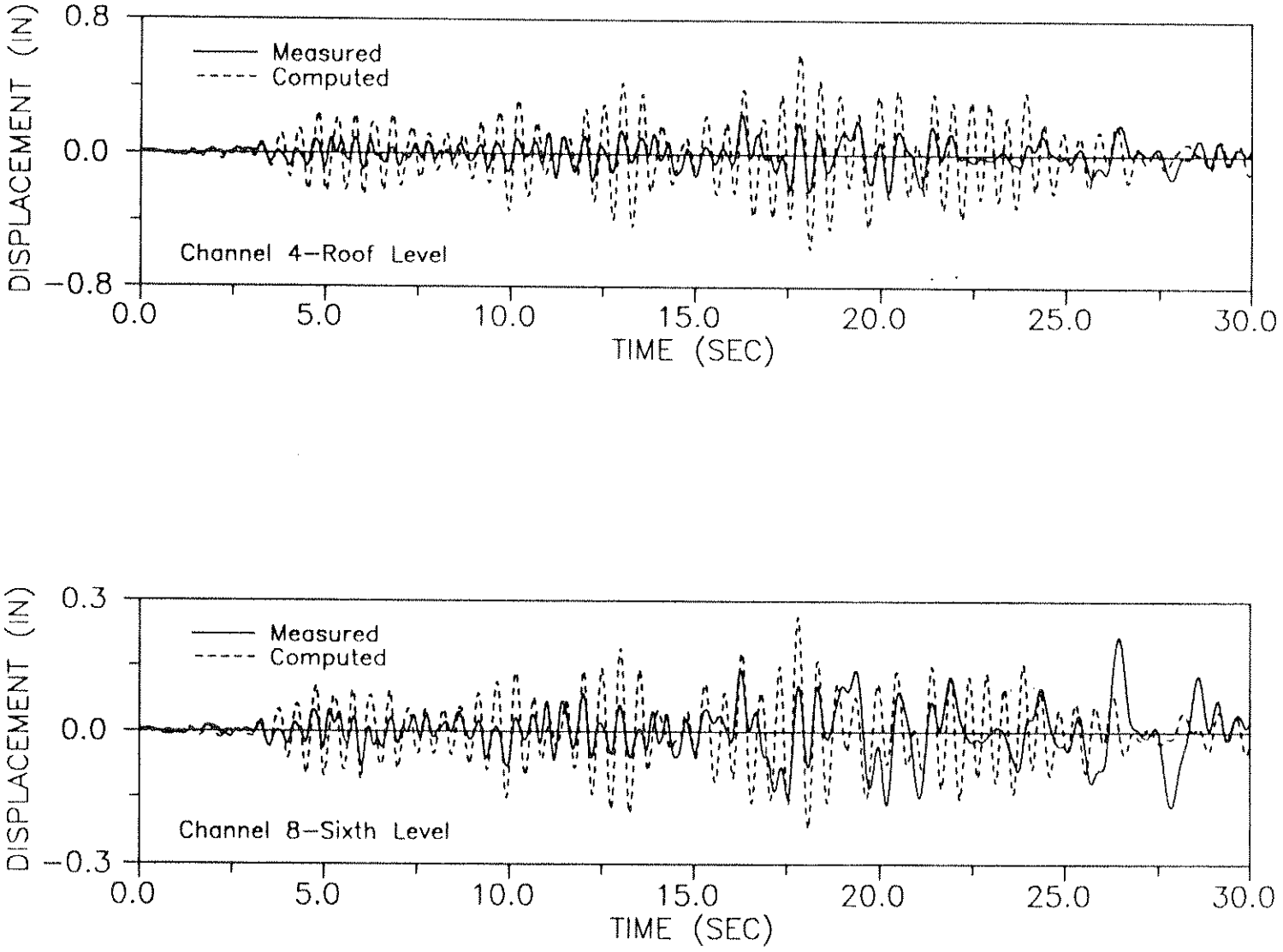

Fig. (25.a) Computed and Measured Displacement Response (Analysis - 4) - Transverse direction

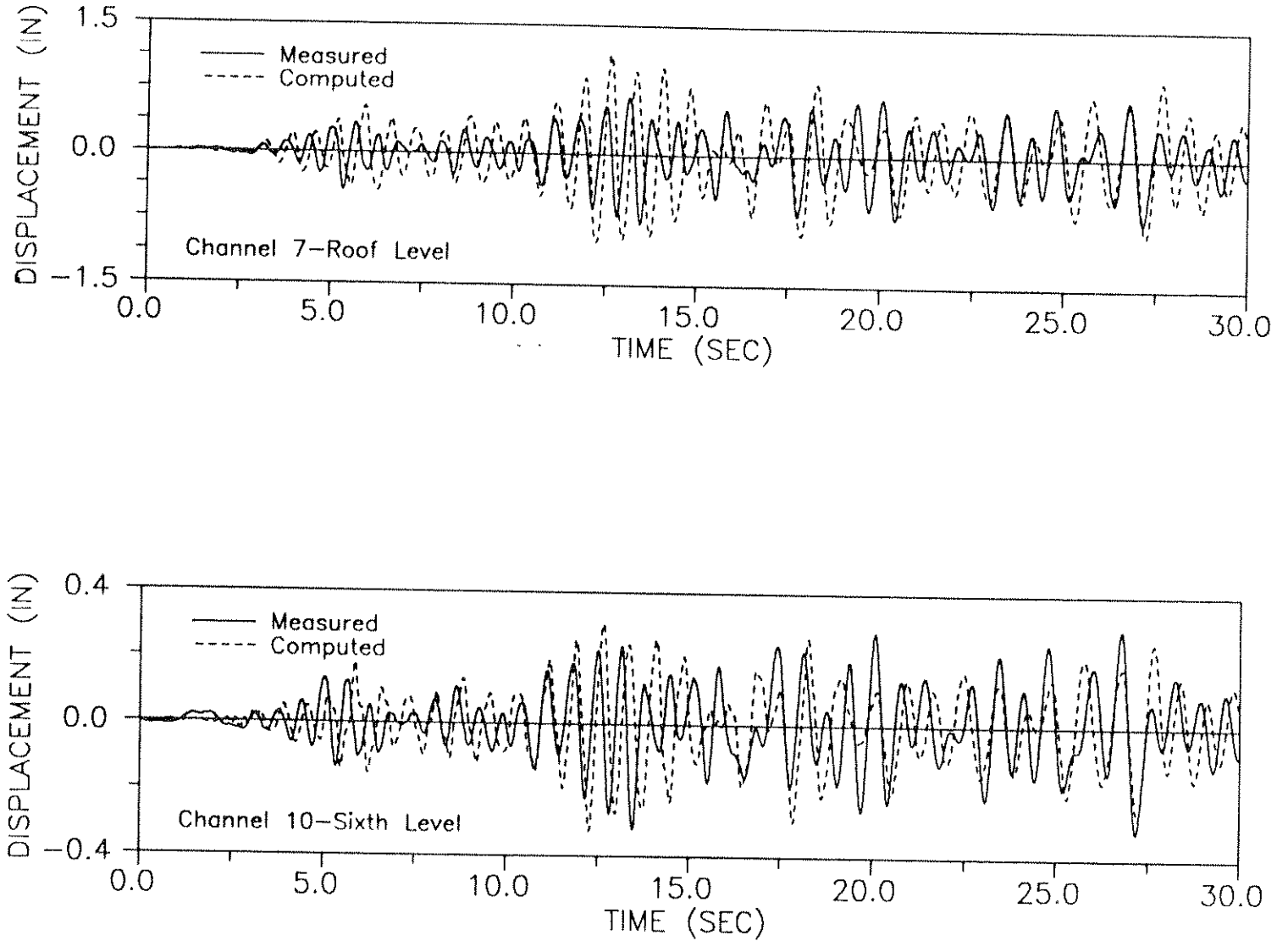

Fig. (25.b) Computed and Measured Displacement Response (Analysis - 4) - Longitudinal direction

APPENDIX
B

DETAILED EVALUATION OF CSMIP BUILDING SN-385

Prepared by

Jose Martinez-Cruzado and Jack P. Moehle

INDEX

LIST OF FIGURES

LIST OF TABLES

NOTATION

A = Total section area of considered frame

Ac = Area of concrete section resisting shear transfer

Ai = Section area of column i

Ao = Total area of the actual foundation

As = Total area of wall interface

Av = Ground Acceleration Coefficient

Avf = Area of shear-friction reinforcement

c = Perpendicular distance from neutral axis to the extreme fiber in tension

di = Perpendicular distance from the rocking axis in consideration to the column i

E = Modulus of elasticity

f'c = Specified compressive concrete strength

fpu = Specified tensile strength of prestressing tendons

fpy = Specified yield strength of prestressing tendons

fse = Effective stress in prestressed reinforcement after losses

fsi = Effective stress in prestressed reinforcement at initial

ft = Tensile concrete strength

Fy = Specified yield strength of reinforcement

G = Static shear modulus

g = Acceleration of gravity

H = Total height of the building

h = Effective height of the building. Equal to 70% of the total height

Icr = Moment of inertia of cracked section

Igr = Moment of inertia of gross section

Io = Moment of inertia of the actual foundation

K = Stiffness of the building fixed at the base

Ky = Traslational stiffness of the foundation

K_θ = Rocking stiffness of the foundation

L = Height of basement story

Lo = Overall length of the side of the foundation in the direction being analyzed

M = Moment resisted by the considered frame

P = Axial load

Q = First moment of area with respect to the centroid of area of the considered frame

r = Characteristic foundation length

ra = Radius of a disk that has the area Ao

rm = Radius of a disk that has the moment of inertia Io

T = Fundamental Period of vibration of the structure not considering soil-structure interaction

t = Total contact width of wall interface

V = Total shear resisted by the considered frame

Vn = Shear strength of the building

Vp = P-wave velocity through the soil

W = Total weight of the building

We = Effective gravity load of the building

x = Perpendicular distance from the arbitrary axis in the transverse direction to the longitudinal rocking axis

xi = Perpendicular distance from the arbitrary axis in the

transverse direction to the centroid of area of column i

y = Perpendicular distance from the arbitrary axis in the longitudinal direction to the transverse rocking axis

y_i = Perpendicular distance from the arbitrary axis in the longitudinal direction to the centroid of area of column i

α = Coefficient of friction

β = Effective damping factor

β_o = Foundation damping factor

σ = Tensile stress in concrete

σ_c = Tensile stress in concrete at point C

σ_d = Tensile stress in concrete at point D

μ = Poisson's ratio

τ_a = Actual shearing stress into wall interface

τ_n = Shearing strength of wall interface

∂ = Unit weight of the soil

ρ = Ratio of reinforcement

Introduction

The current earthquake resistant design philosophy establishes that in the presence of the most severe earthquake, neither the structural system nor any of its components should fail. In addition, the structure must protect life safety. However, the high cost of building contents stored in many buildings has caused structural designers to avoid not only collapse, but also damage to non-structural elements. This means that the maximum drift allowed in a structure must be controlled.

This situation represents a tremendous disadvantage for structural systems like moment resistant space frames, mainly for buildings of ten stories or more. On the other hand, it is an invitation to use a structural system based on structural walls which have high rigidity.

In this report the behavior of a ten-story building subjected to a moderately intense earthquake is studied. Its lateral force structural system is based on structural walls constructed with precast wall panels. The structure apparently did not incur either structural or non-structural damage. The structure is analyzed using the records of fourteen accelerographs that were installed in the structure. Measured responses are correlated with a dynamic analytical model using the computer program SUPER-ETABS [6]. Based on obtained results, design recommendations are presented.

Description of the Building

The structure studied is a ten-story residential building located in Burbank, California at 700 meter above mean sea level. The building is part of the California Strong Motion Instrumentation Program (CSMIP) and has been designated as CSMIP Building SN 385. It was designed and built in 1974 in accordance with the requirements of the Uniform Building Code (UBC-1973). The vertical load carrying system of the building consists of precast and poured in place concrete floor slabs tied together with prestressing strands and supported by precast concrete bearing walls. The lateral force resisting system consists primarily of precast concrete walls in both directions.

A typical plan view (from the 2nd to the 10th floor) of the precast concrete wall system is presented in Fig. 1A. The typical story height is 8'-8". Some walls have typical openings like the ones on axis D and J, with openings of 3'-4½" X 6'-10½". In addition, the elevator core has two typical openings of 3'-0" X 7'-0" and 3'-6" X 7'-0" at its north wall. The plan view of the ground floor is in Fig. 1B. This floor is 10'-0" tall and has some additional openings. The most important are at axes 3 and 4, where the south flexural walls that span from the 2nd to 10th floors are supported by two columns. The other openings are in the north wall of axis 3, having size of 6'-2½" X 6'-10½"; in the north wall of axis 5 with a size of 5'-6" X 6'-10½"; and finally, in axes 1 and 10 with an opening of 8'-4" X 6'-10½".

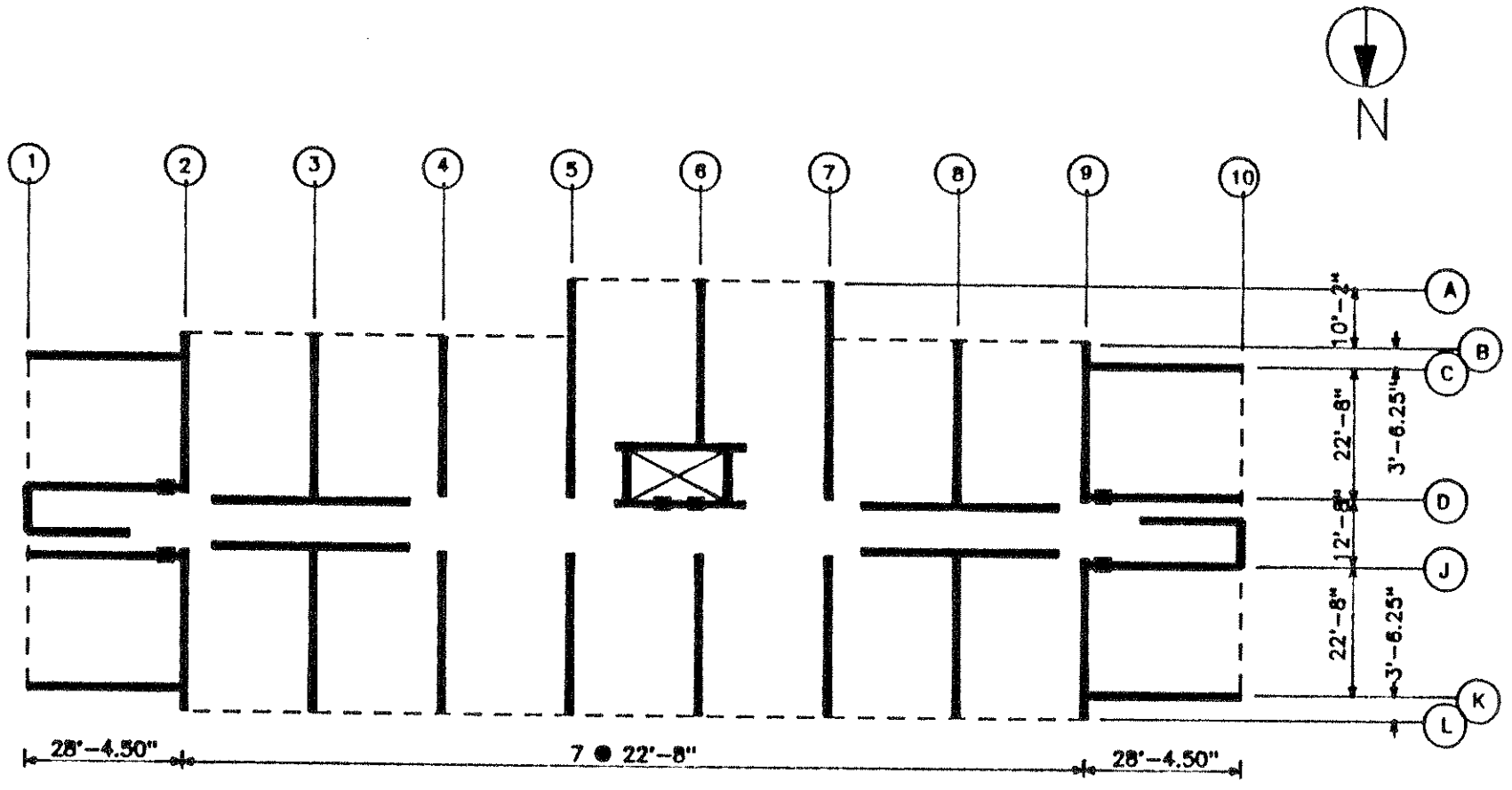

Figure 1A. Typical Plan View (2nd to 10th floor)

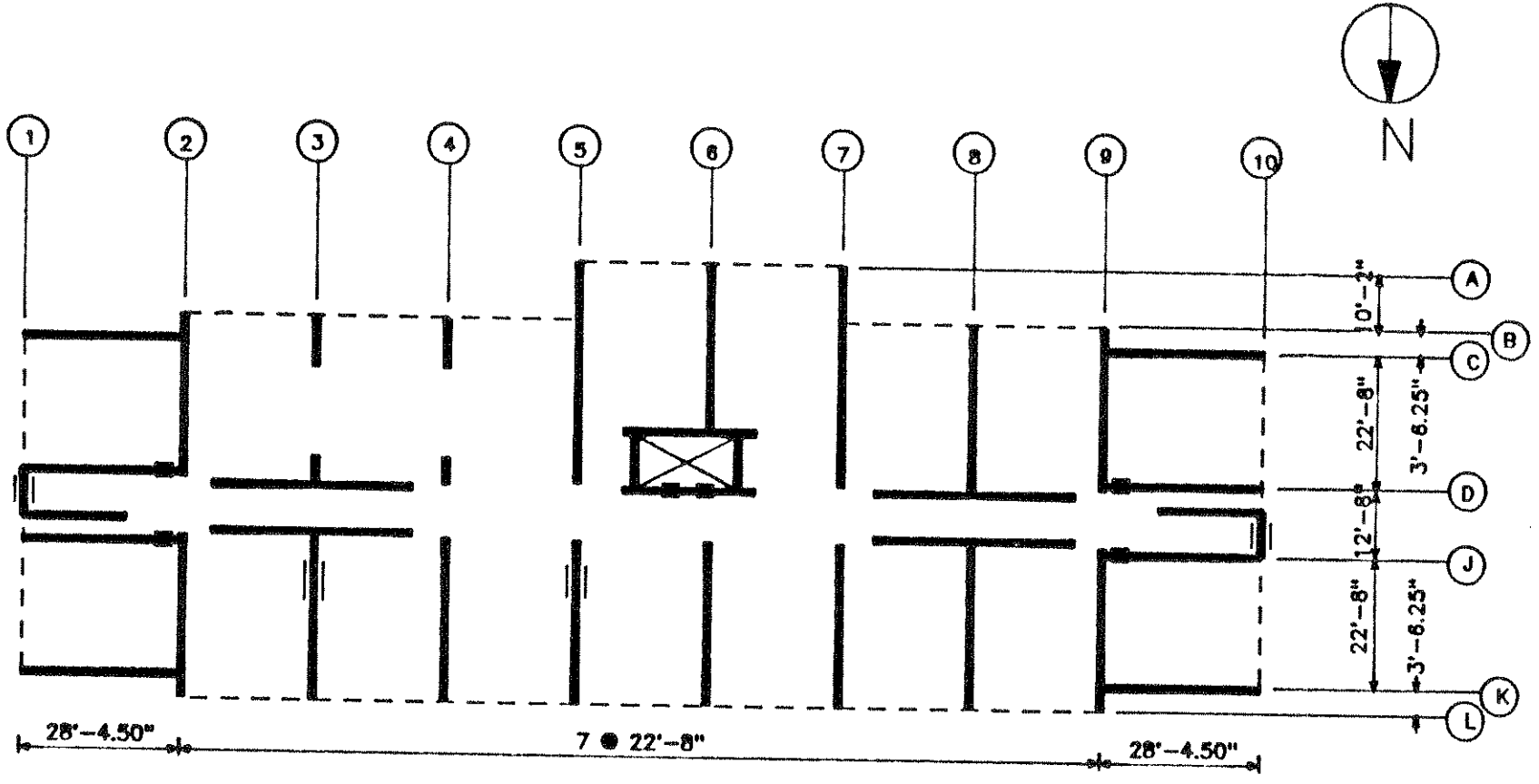

Figure 1B. Plan View of Ground Floor

Precast wall panels were built with normal weight concrete (NWC, 150 pcf) having a design concrete strength of 5 ksi. All reinforcing steel specified on the drawings was grade 60. Wire mesh ASTM A185-61T of size 4"X4"/#4X#4 was placed in each face of the panels with the exterior wire vertical and having 0.75" clearance from the exterior face. Rectangular spirals were formed around the two end mandrel cells at each end of each panel, and at each door jamb, using ½"ϕ wire with 4" pitch, conforming to ASTM A82. Wall panels are 8" thick. Mandrel cell sizes are 4½" X 8½" at the top of panel and 5" X 9" at the bottom. Mandrel cells were filled with normal weight concrete having a specified concrete strength of 4 ksi.

Precast slab panels are made of ligthweight concrete (LWC, 120 pcf), while cast-in-place floor panels are NWC, both having a design concrete strength of 5 ksi. The reinforcing steel is grade 60. Prestressing strands conform to ASTM A-416-59T. The drawings specify fpu = 270 ksi (ultimate), fpy = 216 ksi (yield), fsi = 189 ksi (initial) and fse = 162 ksi (effective). Design live loads are 20 psf on the roof, 50 psf in apartments, corridors and balconies, and 100 psf on stairs. The foundation consists of 202 NWC piles of two feet diameter and depth varying from 25 to 35 ft. The piles are embedded 4" in the 42" X 42" continuous pile caps made of reinforced concrete, as showed in Fig. 1C.

The soil is described as silty sand. It is the product of alluvial deposits. Neither soil properties nor a soil report was

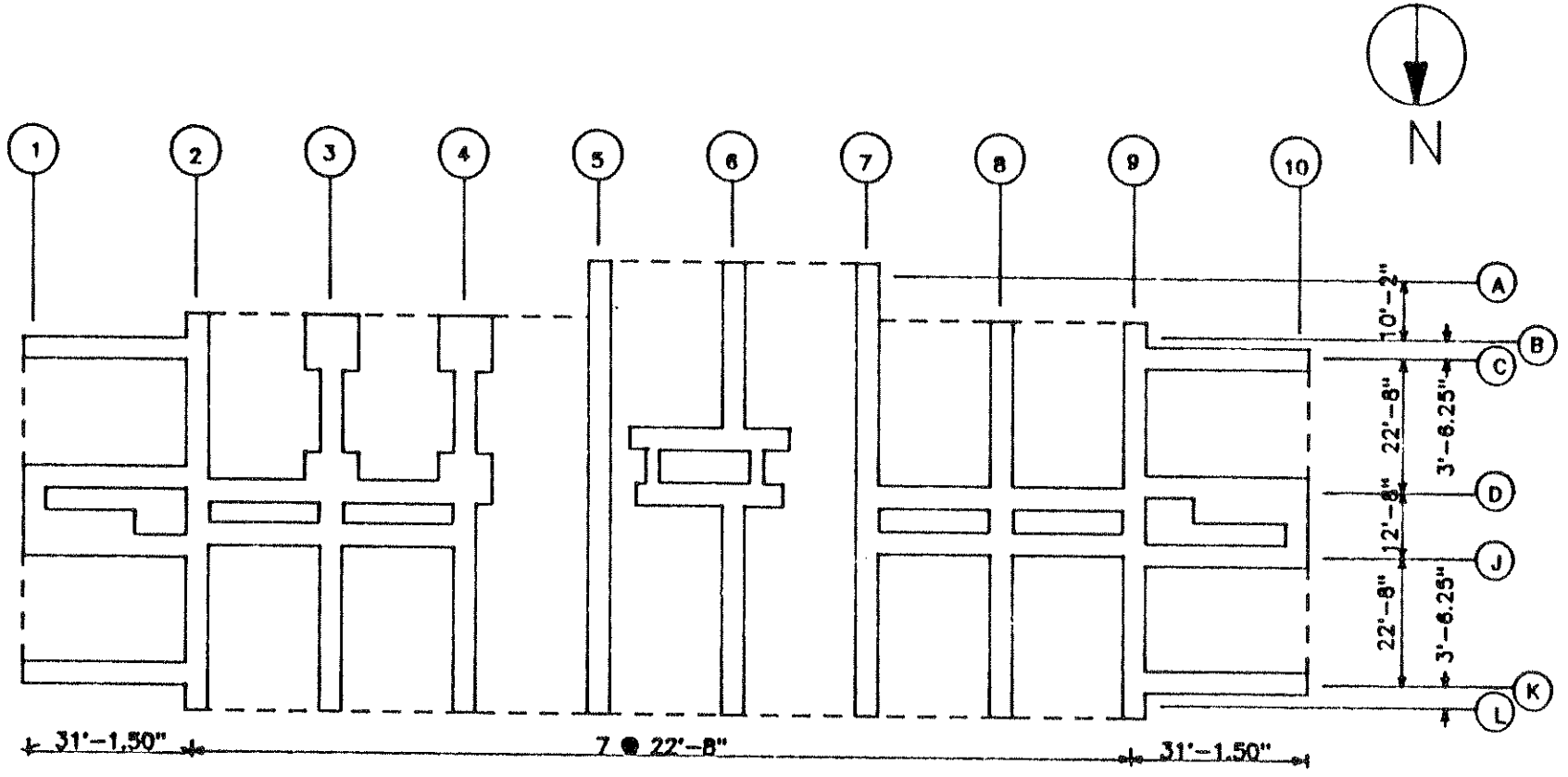

Figure 1C. Foundation Plan View

available.

Description of the Event

The structure was subjected to the Whittier-Narrows Earthquake on October 1st, 1987, at 7:42 PDT. The earthquake had an epicentral distance of 21 km. and a focal depth of 9 km. The local magnitude in Richter scale for the event was calculated as 6.1. The peak horizontal and vertical ground accelerations of 0.23g and 0.06g, respectively, were measured at the ground level of the building. The strong ground motion duration was four seconds, defined as the elapse time from the first to the last incursion of 0.05g in the ground acceleration record.

Building Records

Sixteen acceleration records were registered in the building from fourteen SMA-1 accelerographs. These were installed on the 1st, 4th and 8th floors, and on the roof level in such a way that response features such as traslational motions, torsional motion, and in-plane diaphragm deformation can be studied. Sketches of the position and direction of each channel are presented on Fig. 2.

Absolute displacement records were provided by the California Strong Motion Instrumentation Program (CSMIP). They were calculated from measured acceleration records using a bandpass filter with ramps at 0.250 - 0.500 and 23.00 - 25.00 Hz.

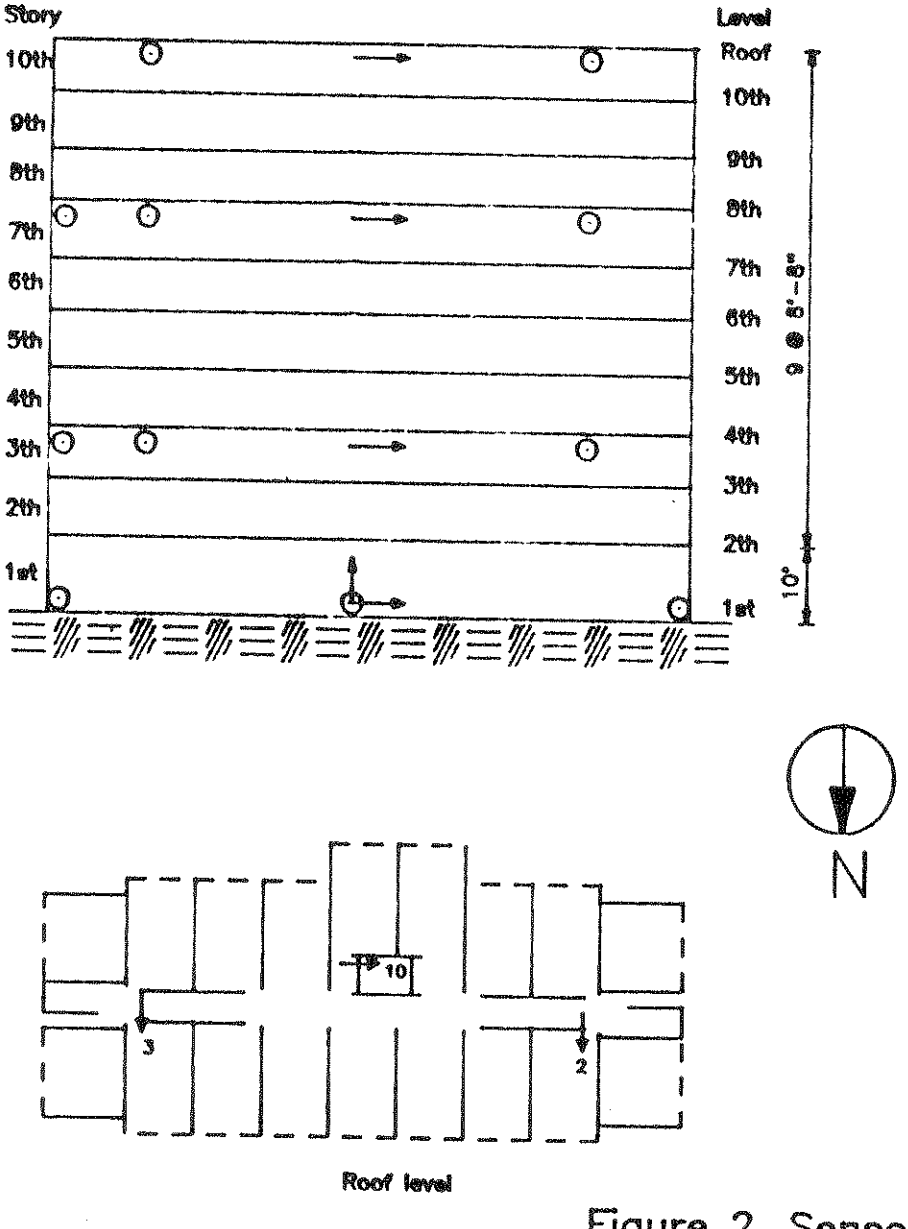

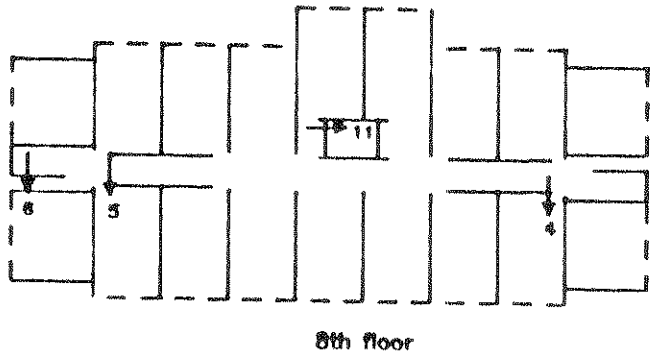

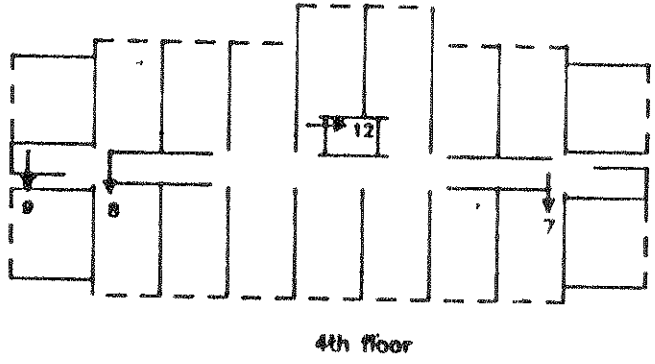

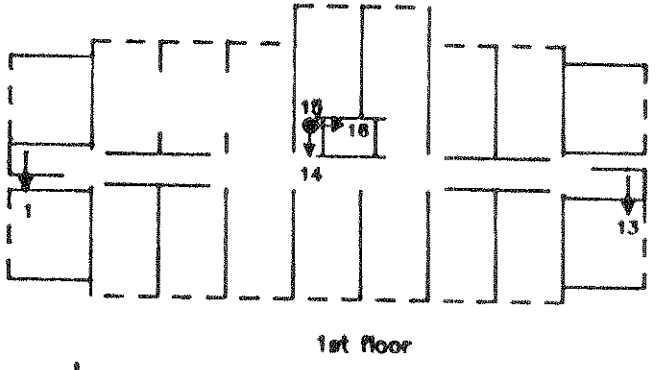

Figure 2. Sensor Layout

The absolute acceleration records and absolute displacement records for the sixteen channels are presented in Figs. 3 and 4, respectively.

Building Response

Acceleration and Displacement Response - The average measured absolute ground acceleration in the transverse direction was 0.18g and the peak measured absolute acceleration at the roof was 0.33g. This represents an amplification factor of 1.79. In the longitudinal direction, the peak ground acceleration was recorded as 0.21g and it was amplified to 0.53g at the roof, which represents an amplification factor of 2.53. The amplification factors for 4th and 8th floor were also computed, as shown in Table 1. They were considerably higher in the longitudinal direction. Furthermore, the acceleration records indicate a larger flexibility in the longitudinal direction. The distributions of absolute acceleration through the height of the building near the time of maximum base shear are presented in Fig. 5.

	Transverse		Longitudinal	
Floor	Mea. Absolute Acceleration	Amp. Factor	Mea. Absolute Acceleration	Amp. Factor
Ground	.18g	1.00	.21g	1.00
4th	.22g	1.21	.31g	1.50
8th	.20g	1.07	.27g	1.29
Roof	.33g	1.79	.53g	2.53

TABLE 1; Absolute Acceleration Amplification Factors.

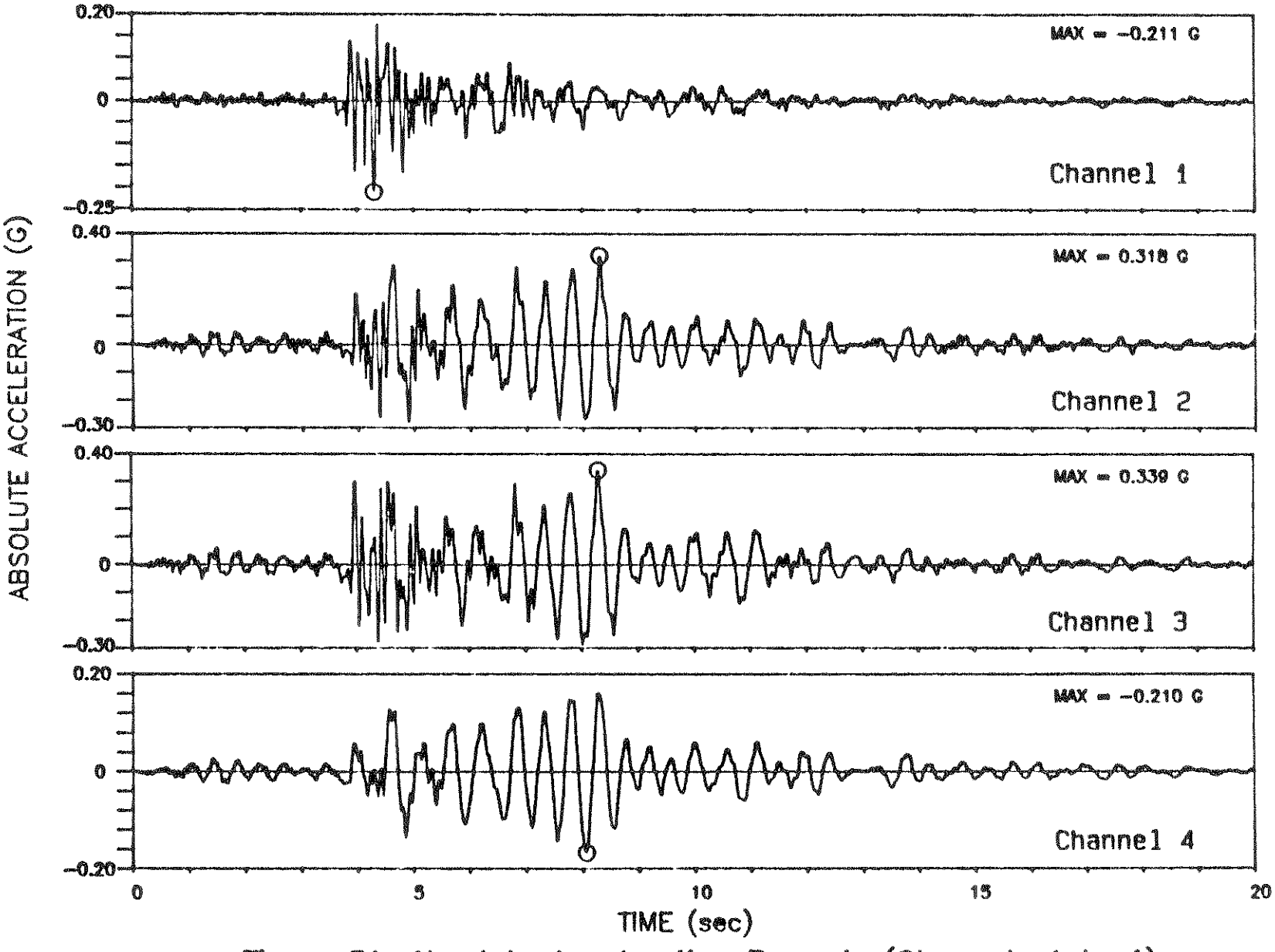

Figure 3A. Absolute Acceleration Records (Channels 1 to 4)

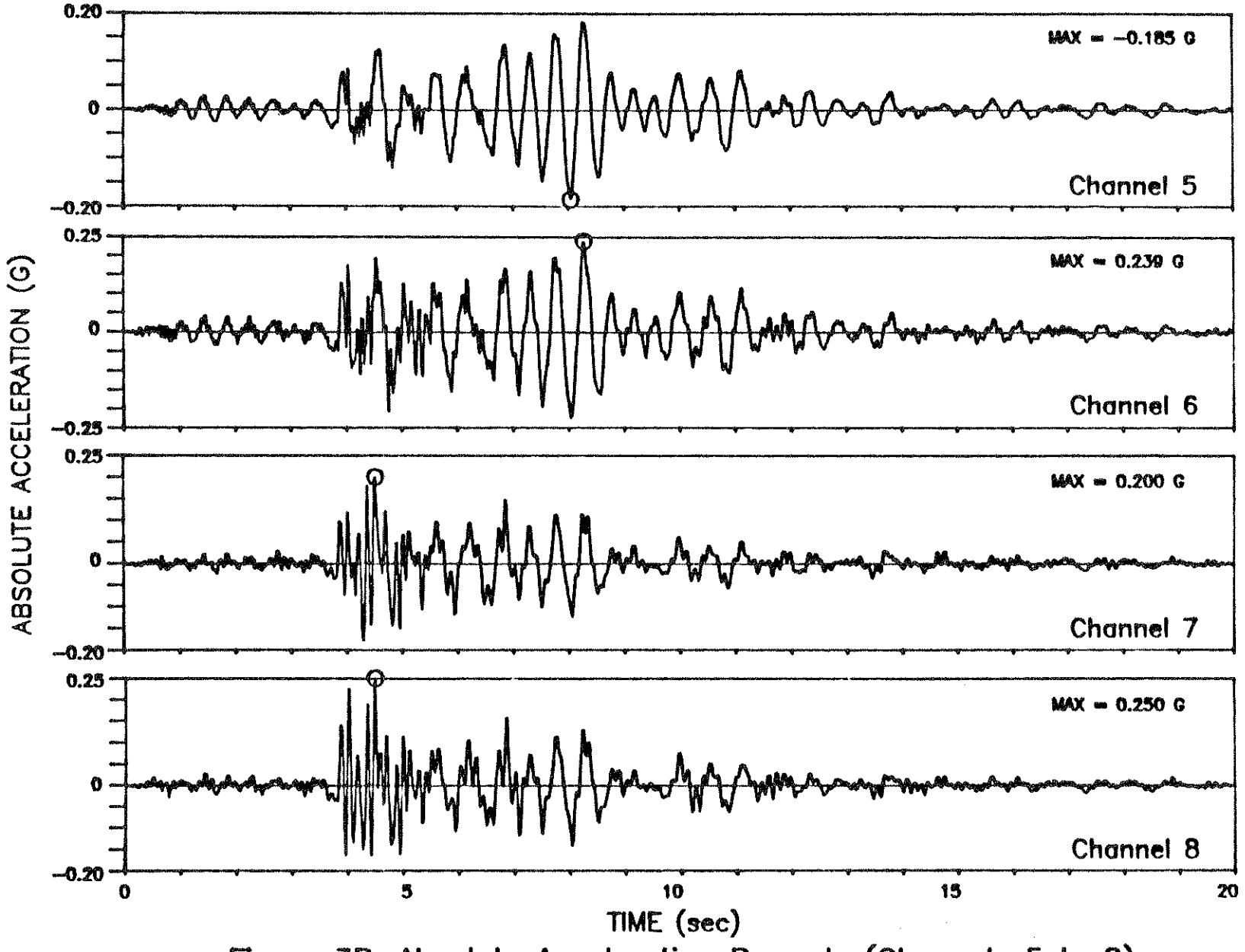

Figure 3B. Absolute Acceleration Records (Channels 5 to 8)

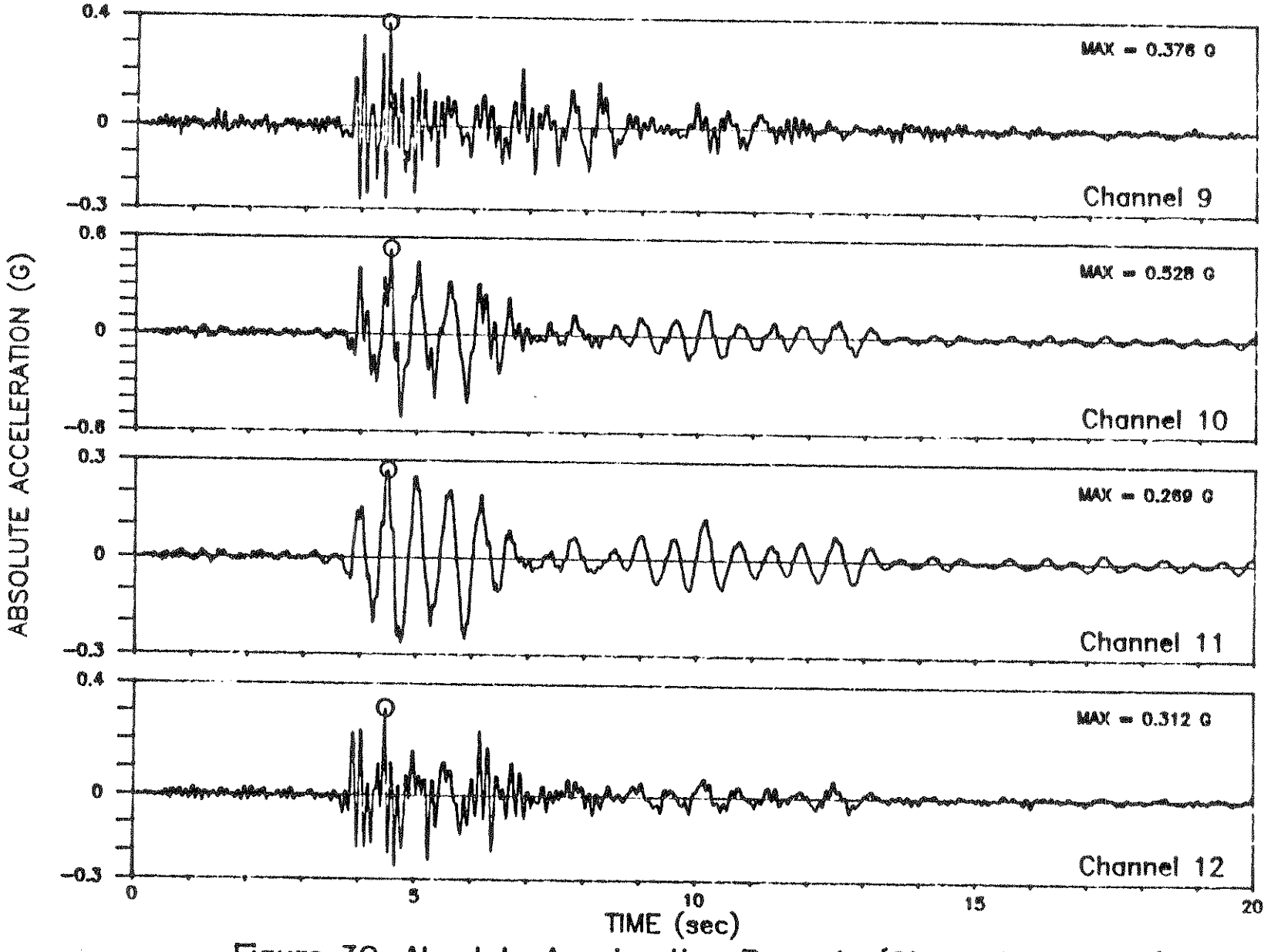

Figure 3C. Absolute Acceleration Records (Channels 9 to 12)

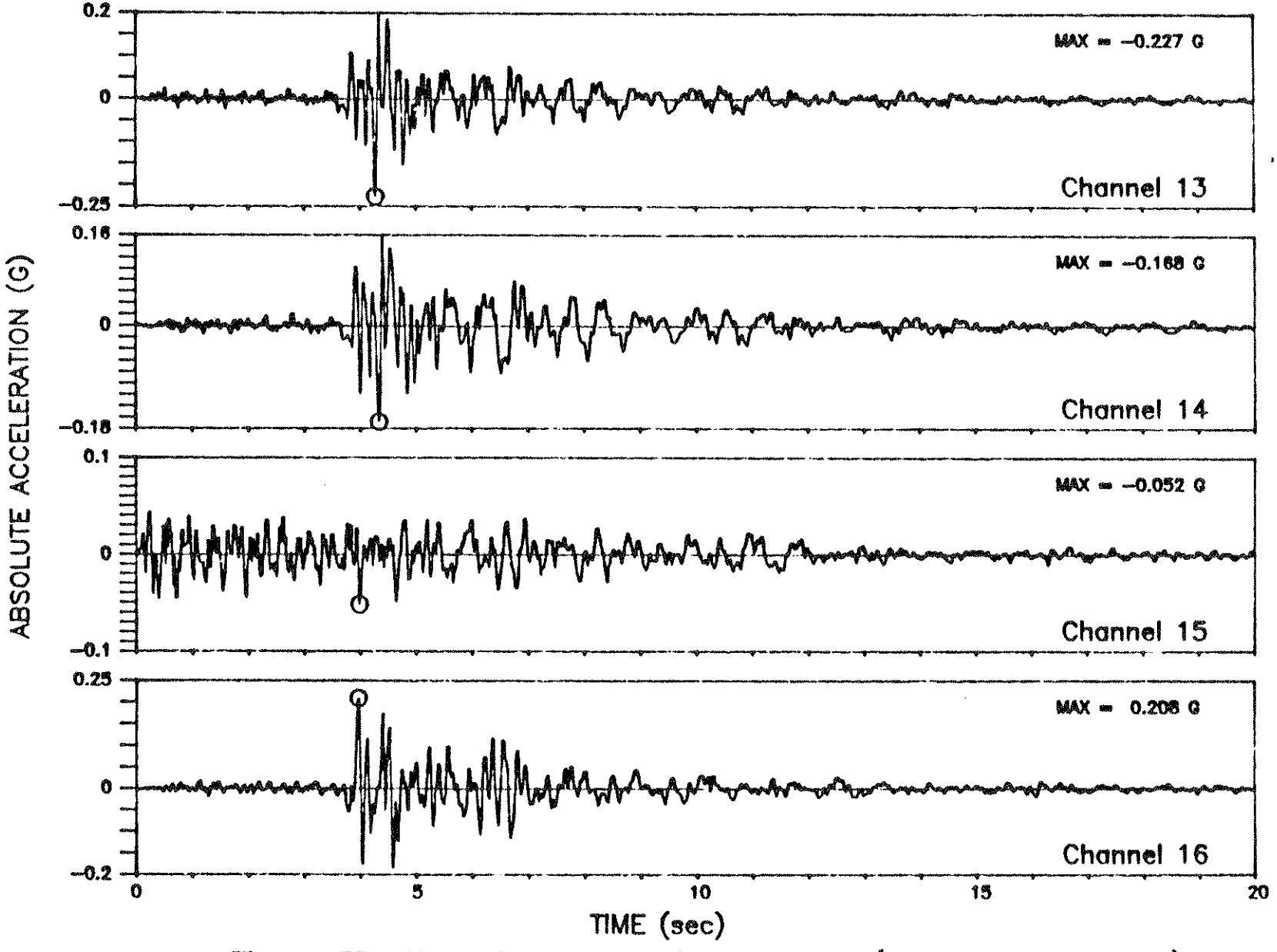

Figure 3D. Absolute Acceleration Records (Channels 13 to 16)

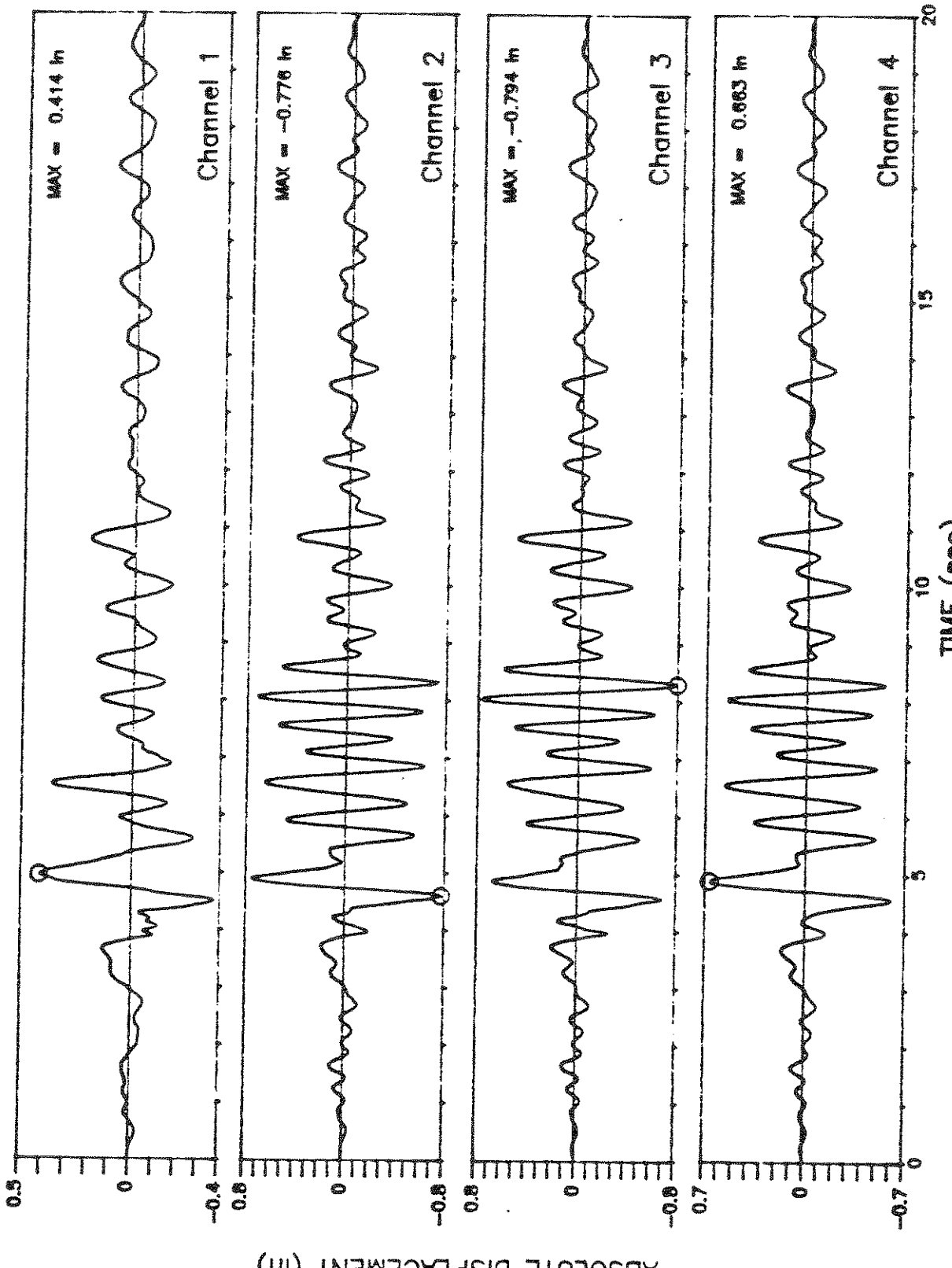

Figure 4A. Absolute Displacement Records (Channels 1 to 4)

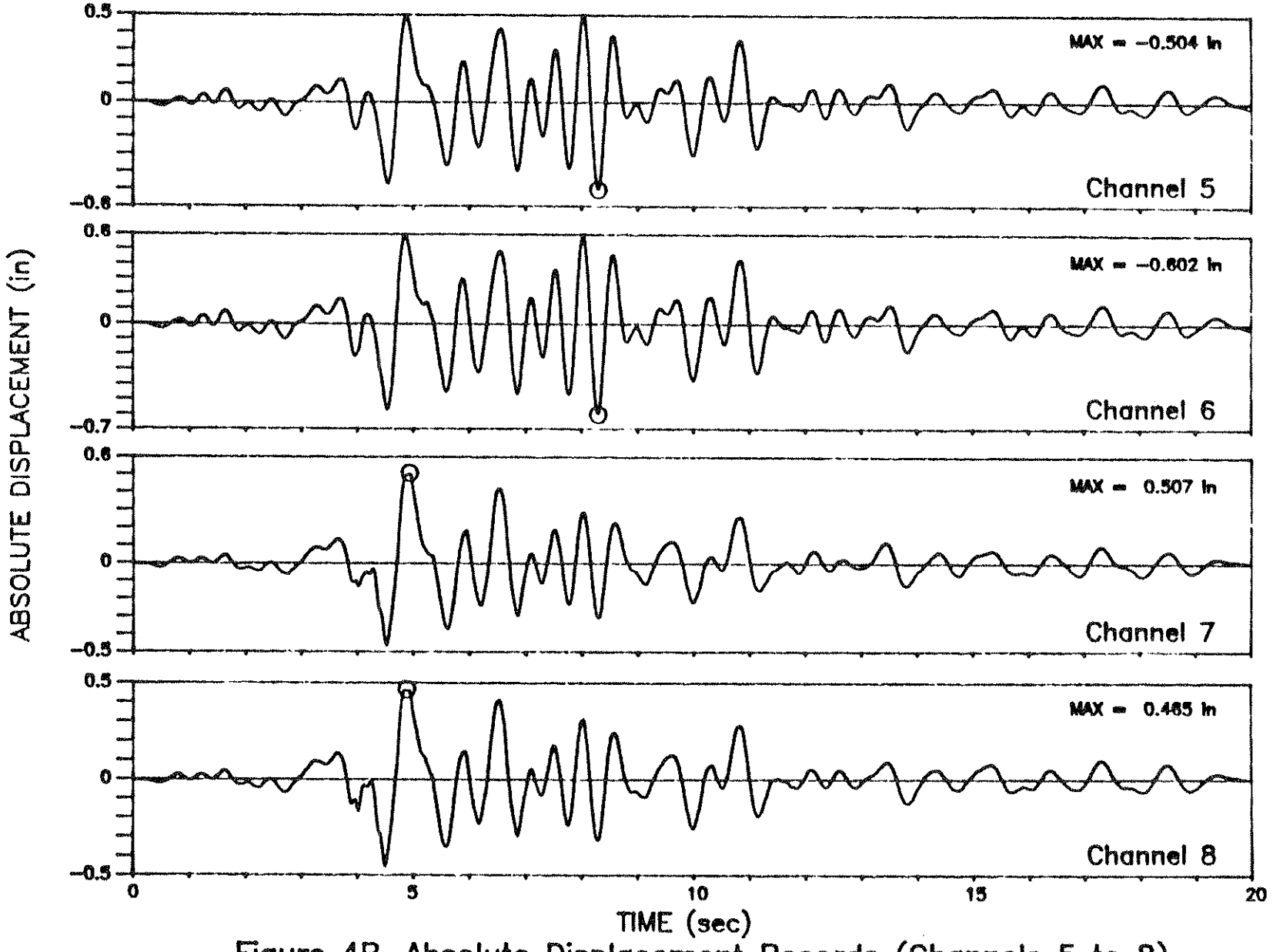

Figure 4B. Absolute Displacement Records (Channels 5 to 8)

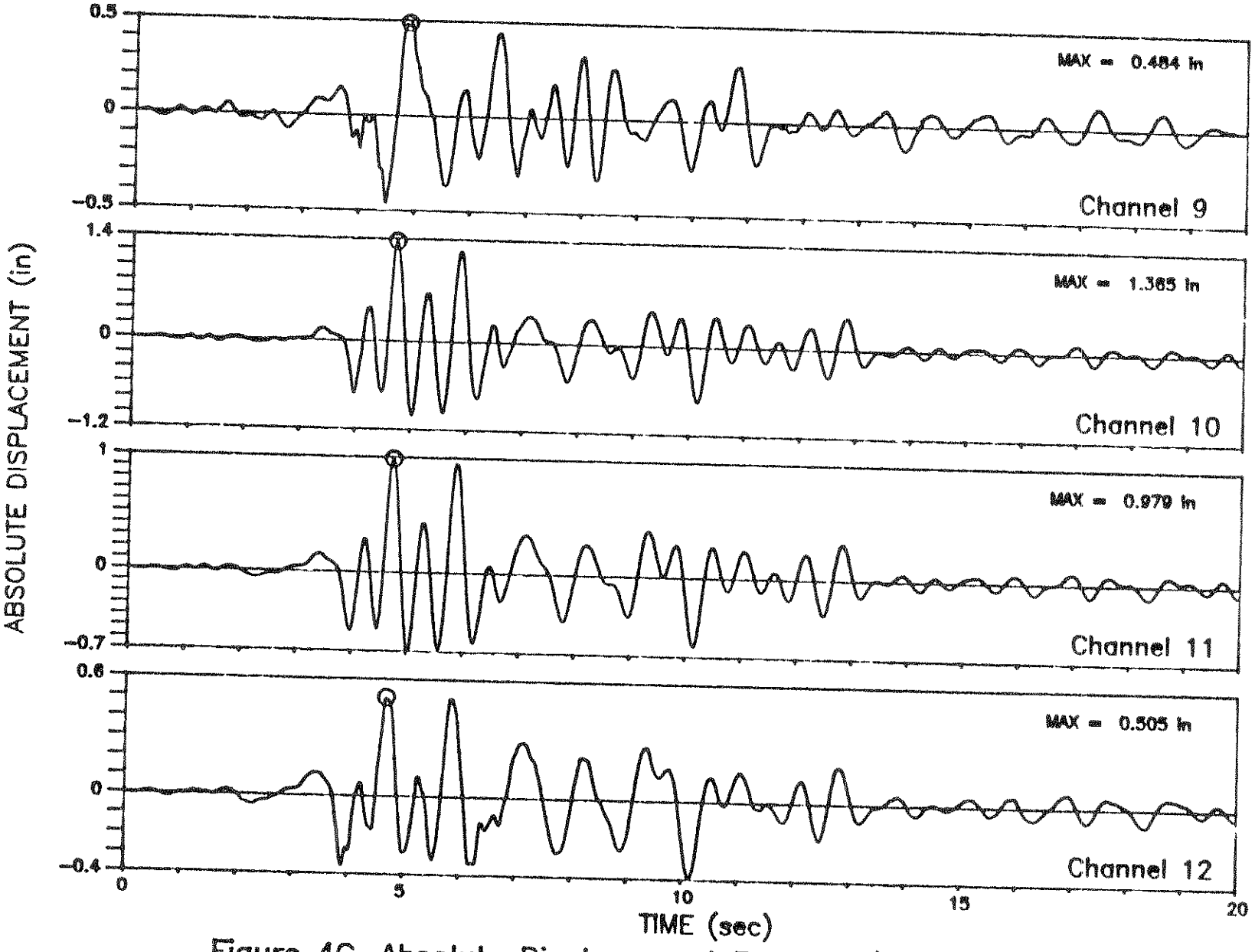

Figure 4C. Absolute Displacement Records (Channels 9 to 12)

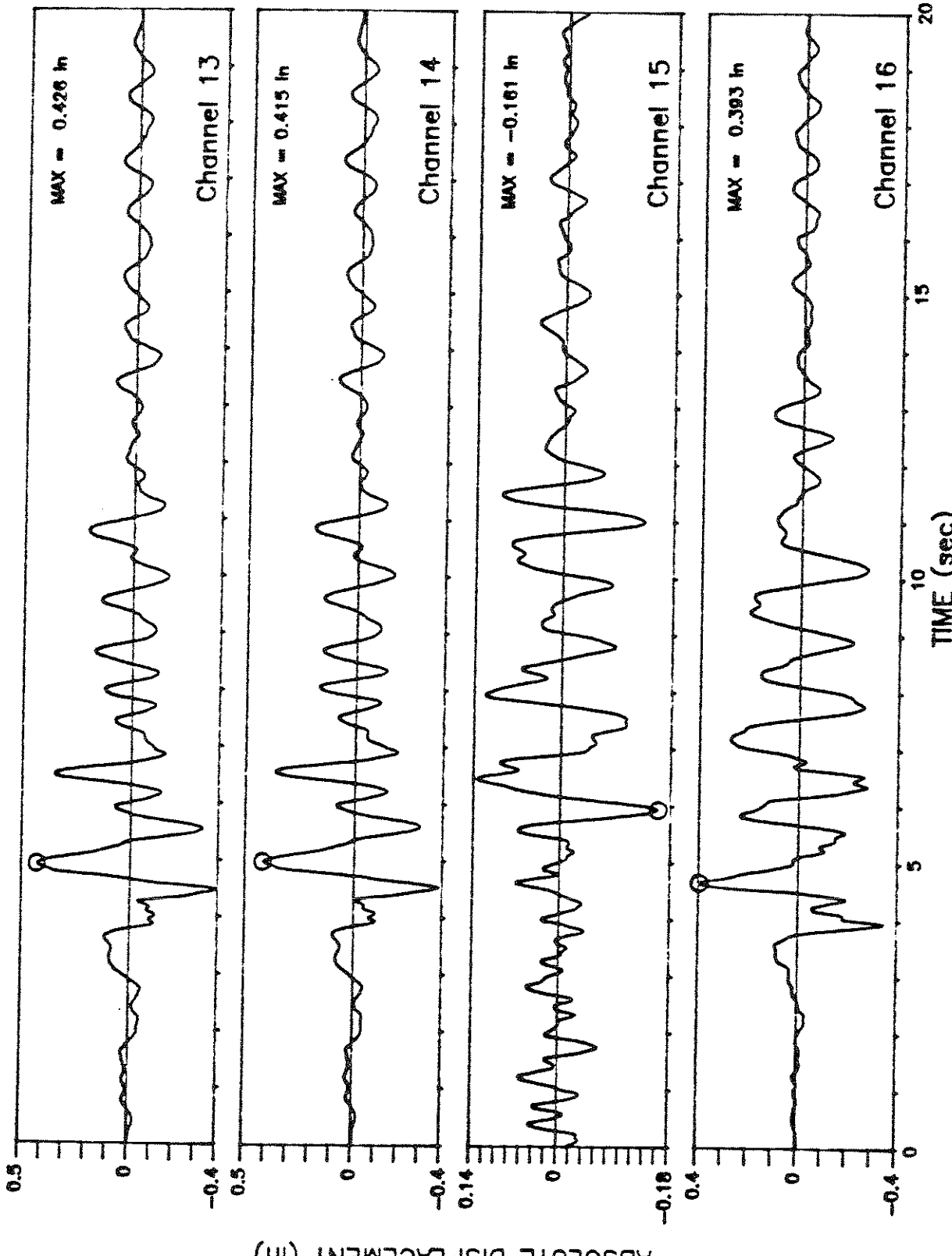

Figure 4D. Absolute Displacement Records (Channels 13 to 16)

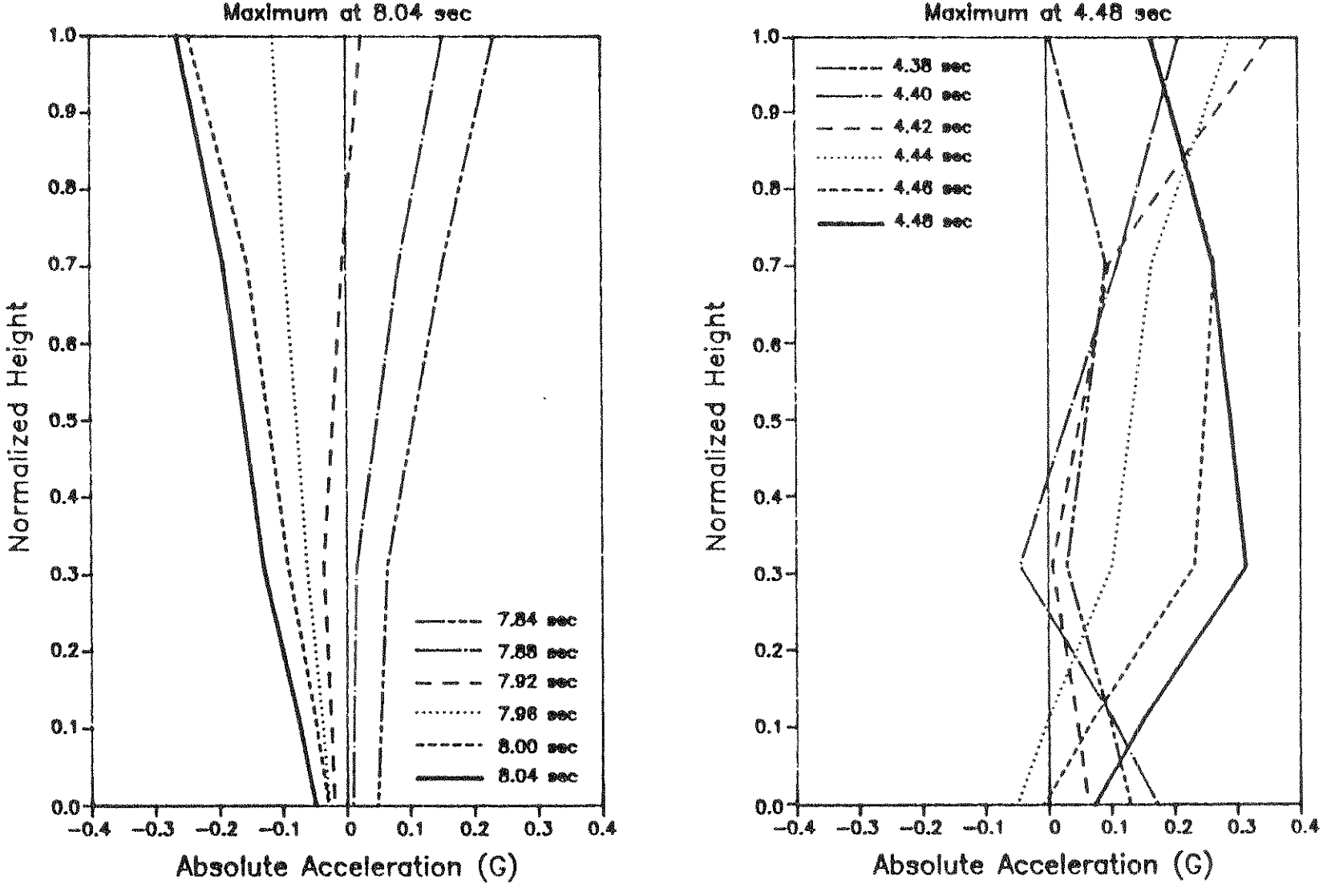

A) Transverse Direction

B) Longitudinal Direction

Figure 5. Distribution of Absolute Acceleration at Maximum Base Shear

A similar pattern was obtained from absolute displacement records. The measured absolute displacement at the ground was similar in both directions. However, the amplification factor in the longitudinal direction was 3.47, almost twice the value of 1.83 for the transverse direction. Displacement amplification factors were also computed for the 4th and 8th floors (Table 2).

	Transverse		Longitudinal	
Floor	Mea. Absolute Displacement, in.	Amp. Factor	Mea. Absolute Displacement, in.	Amp. Factor
Ground	0.42	1.00	0.39	1.00
4th	0.49	1.17	0.50	1.28
8th	0.58	1.38	0.98	2.49
Roof	0.76	1.83	1.37	3.47

TABLE 2; Absolute Displacement Amplification Factors.

Measured relative displacements for each channel were computed as the difference between the measured absolute displacements at that level and the measured absolute displacements at the base. The computed records are presented in Fig. 6. The maximum relative displacement was calculated on the roof in the longitudinal direction. Its magnitude was 1.06 in. (0.0010H), while for the transverse direction it was 0.63 in. (0.0006H). The relative displacement throughout the height of the building was normalized with respect to the roof relative displacement and is shown in Table 3. The relative displacement shape of the building, near the time of maximum relative displacement in each direction, is presented in Fig. 7.

Figure 8 presents the plan view of the roof near the time

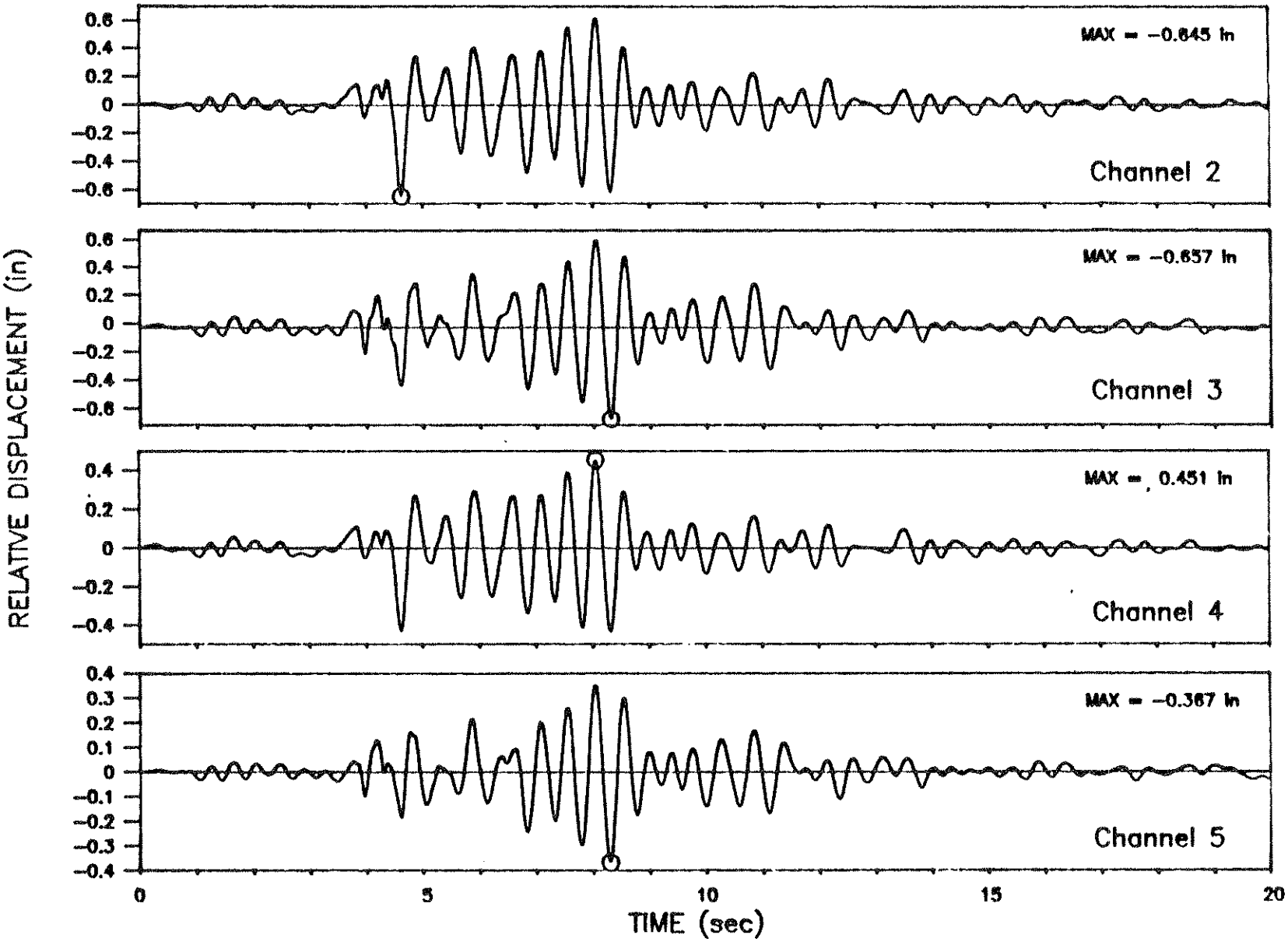

Figure 6A. Relative Displacement Records (Channels 2 to 5)

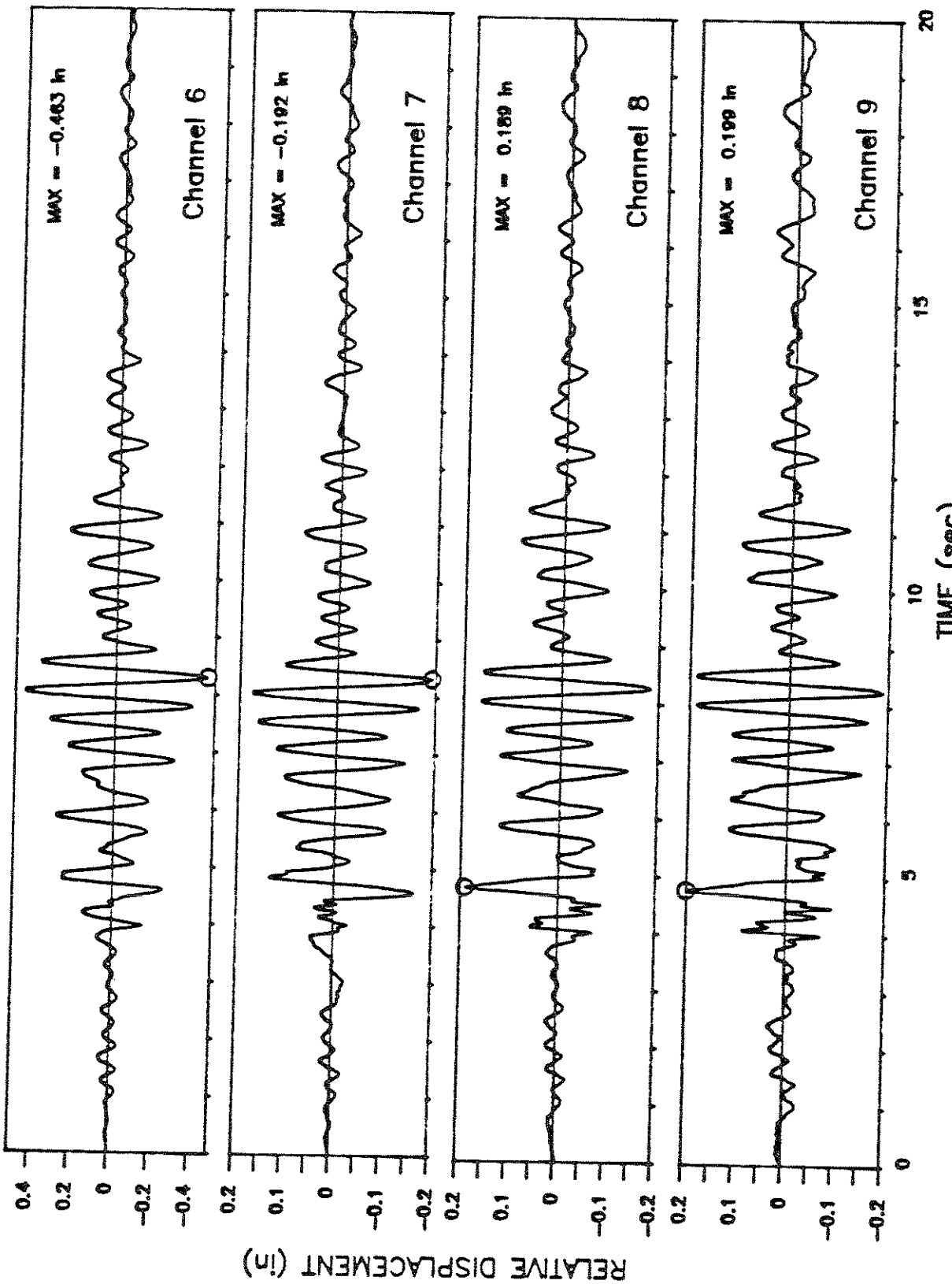

Figure 6B. Relative Displacement Records (Channels 6 to 9)

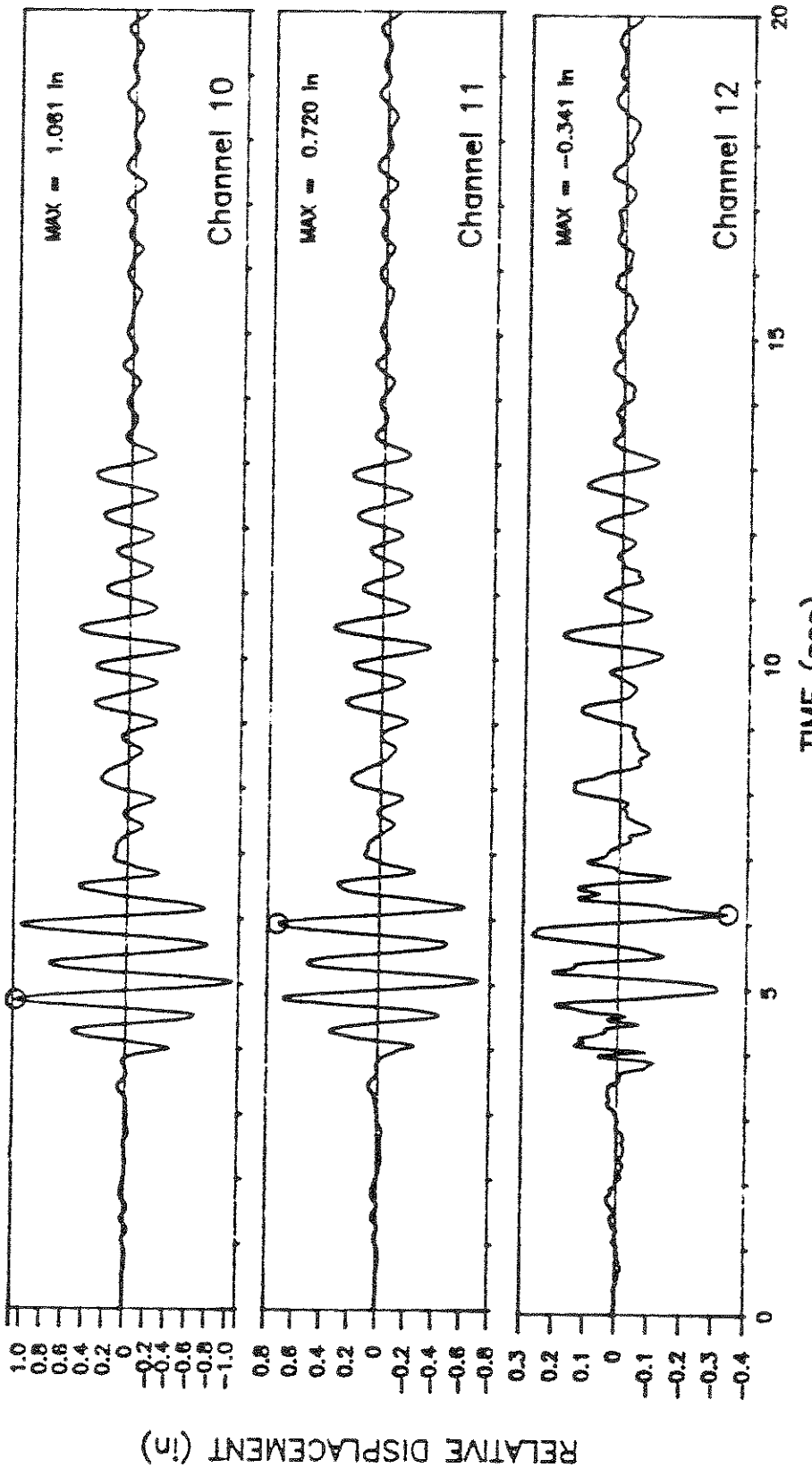

Figure 6C. Relative Displacement Records (Channels 10 to 12)

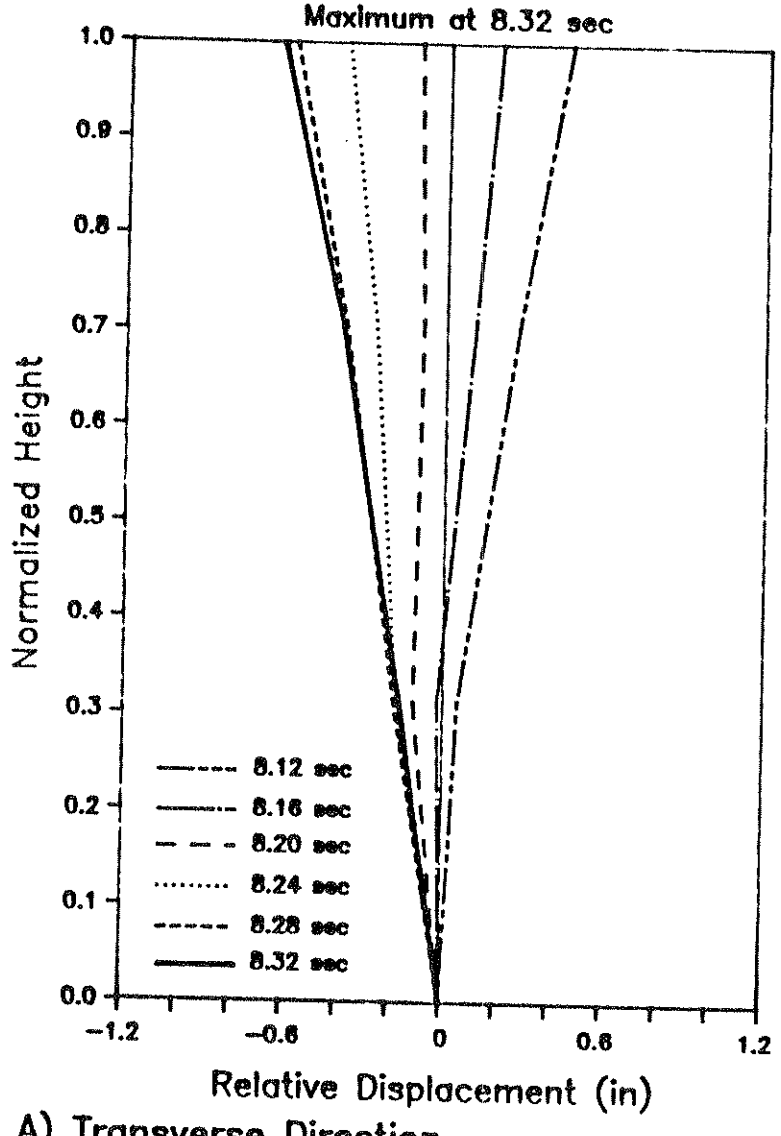

A) Transverse Direction

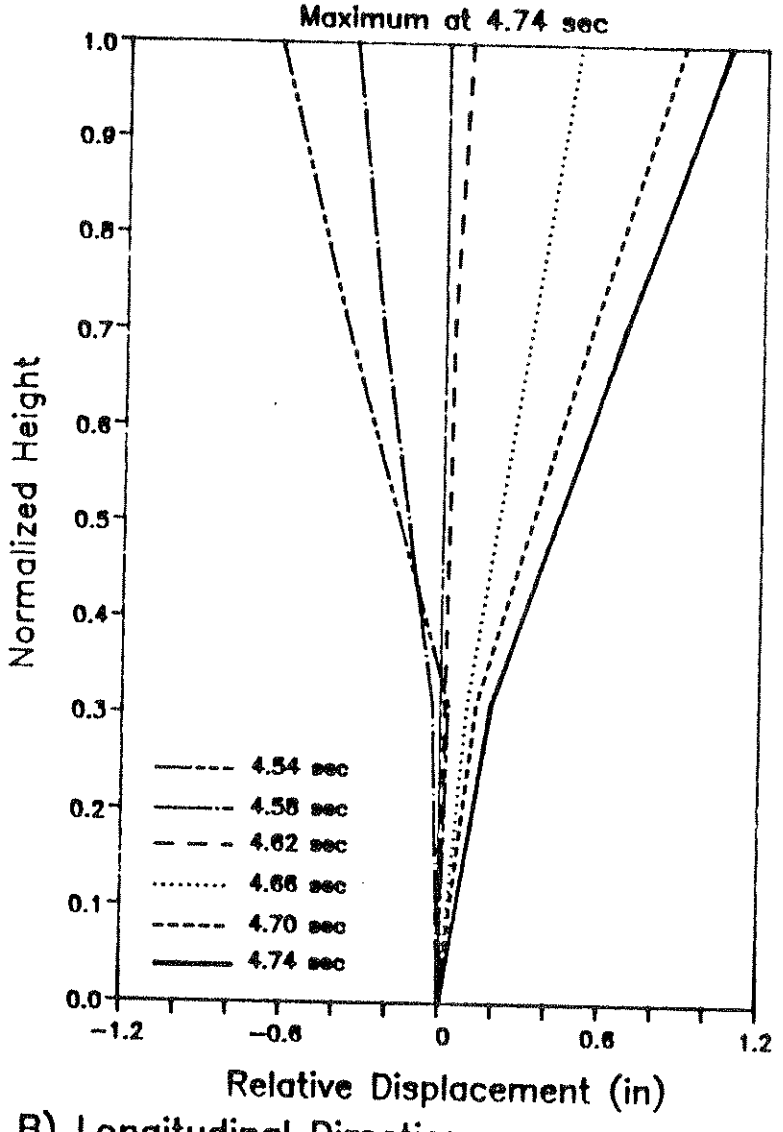

B) Longitudinal Direction

Figure 7. Relative Displacement Shape

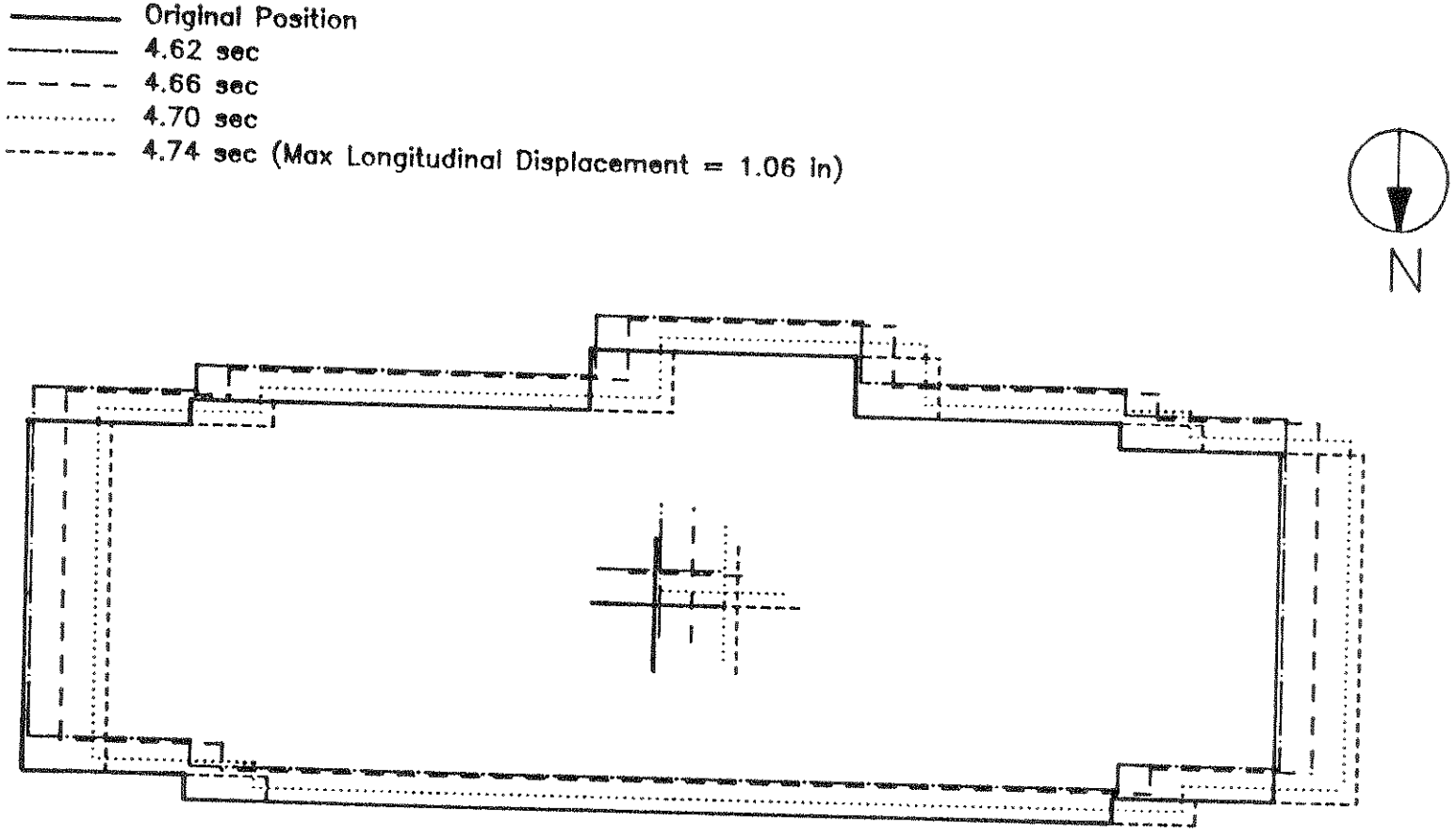

Note: Relative Displacement have been amplified 165 times.

Figure 8. Plan View of the Roof with Maximum Relative Displacement

of the maximum relative displacement in the longitudinal direction. The plotted displacements are amplified 165 times; otherwise, they would not be visible in the plot. Twisting is not pronounced.

	Transverse		Longitudinal	
Floor	Mea. Relative Displacement	Normalized Displacement	Mea. Relative Displacement	Normalized Displacement
Ground	0.00"	----	0.00"	----
4th	-0.17"(.05%)	0.26	0.18"(.05%)	0.17
8th	-0.40"(.05%)	0.62	0.68"(.09%)	0.64
Roof	-0.63"(.06%)	1.00	1.06"(.10%)	1.00

TABLE 3; Measured Relative Displacements. Values in parentheses are expressed as a percent of height to that level.

It should be pointed out that the maximum response in the longitudinal direction occurs between the fourth and fifth seconds of the record. The maximum response for the transverse direction occurs between the eigth and ninth seconds.

In-Plane Diaphragm Response - A study of floor diaphragm distorsion was carried out for the 4th and the 8th floors, where three acceleration records registered the transverse response of the structure (Fig. 2). It is noted that the walls along the plan length of the building are well-distributed (Fig. 1A). However, there are no walls at the transverse edges (axes 1 and 10 in Fig. 1A). With this uniform wall distribution, it is not likely that extensive in-plane diaphragm distorsion occurred between channels 7 & 8 on the 4th floor and channels 4 & 5 on

the 8th floor. In the absence of walls at the transverse edges, an additional displacement may have occurred at the lateral wings of the structure. It may be possible to detect this distorsion with the available instruments.

The displacements relative to the base at channels 9 and 6 were calculated extrapolating a straight line from channel 7 to channel 8 on the 4th floor, and from channel 4 to channel 5 on the 8th floor, respectively. This calculated displacement is compared with the corresponding measured relative displacement in Fig. 9. The broken line at 45 degrees represents the behavior of an in-plane rigid diaphragm. The measured relative displacements on the 4th floor keep an angle between 43 and 48 degrees. The angle has almost a constant value of 53 degrees on the 8th floor. The maximum measured relative displacement on the 8th floor was 0.46" vs a calculated of 0.36". It is a difference of 0.10" in 340" or 0.03%. It is concluded that although there may have been some diaphragm distorsion in the wings, it was not of significant magnitude.

Drift - The maximum average interstory drift and the allowable interstory drift under design loads according to UBC-1988 are presented in Table 4. The measured maximum interstory drift is .0012, which is less than one third the allowable by UBC-1988.

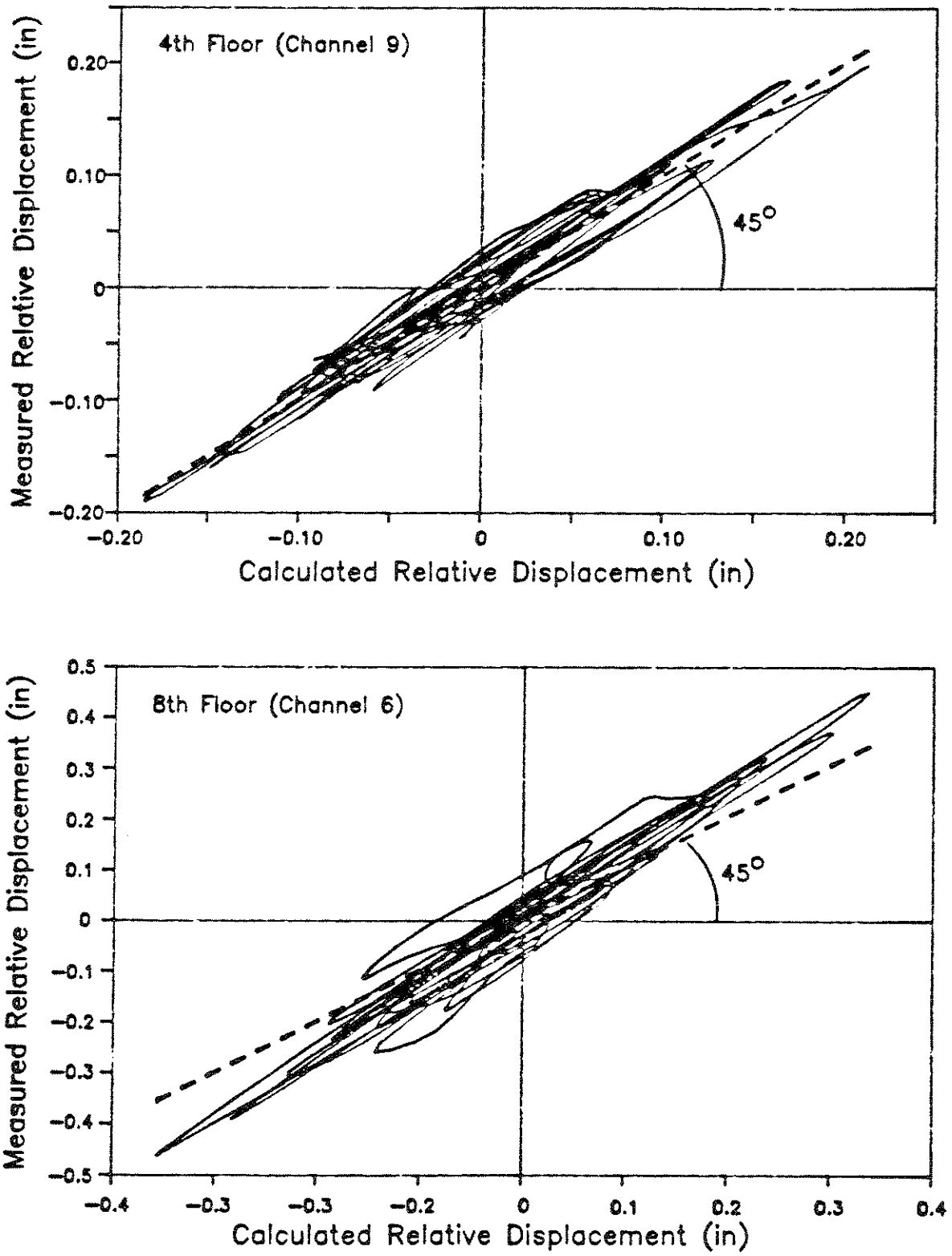

Figure 9. Measured vs Calculated Relative Displacement

	8th - Roof	4th - 8th	1st - 4th	UBC 1988
Transverse	.0008	.0006	.0006	.0040
Longitudinal	.0012	.0012	.0010	.0040

TABLE 4; Maximum Average Interstory Drift.

Force Responses - The inertia forces through the height of the building were computed using the following procedure:

1- Compute the mass of each floor level considering:

a) 150 pcf for NWC panels.

b) 120 pcf for LWC panels.

c) 20 psf sustained load over the floors.

d) A gravity acceleration of 386.4 in./sec^2.

The mass of each floor level includes the mass of the floor slab with its sustained load, and one half the sum of the mass of the walls in the story above and below the level in consideration. Total mass per floor and total building mass are tabulated in Table 5.

Level	Mass (K-sec^2/in.)
Roof	5.14
3th - 10th	5.89
2th	6.07
1st	1.57
Total	59.92

Table 5. Mass per Floor and Total Building Mass.

2- Compute the absolute acceleration of each story by

linear interpolation using the absolute acceleration at ground, 4th, 8th, and roof floor.

3- Compute inertia forces in the nth floor as the product of the lumped mass in the nth floor and the absolute acceleration of the same nth floor level.

The maximum inertia forces at different levels and their respective times of occurrence are presented in Table 6, and the distribution of inertia forces through the building near the time of maximum base shear in each direction is shown in Fig. 10A. The distribution of inertia forces through the building near the time of maximum base overturning moment is presented in Fig. 10B.

	Longitudinal			Transverse		
Max. at	4th	8th	Roof	4th	8th	Roof
Time (sec)	4.48	4.50	4.54	4.50	8.04	8.30
4th	710	219	- 475	518	-300	155
8th	595	612	289	104	-442	421
Roof	327	522	1,048	-351	-528	658

TABLE 6; Maximum Inertia Forces (Kips).

The shear force in each story was computed by summing all the inertia forces from the floor level in consideration to the roof. The maximum shear forces at different stories and the respective times of occurrence are tabulated in Table 7. The base shear history in each principal direction is presented in Fig. 11A. The shear distribution through the building near time of maximum base shear in each direction is shown in Fig. 11B.

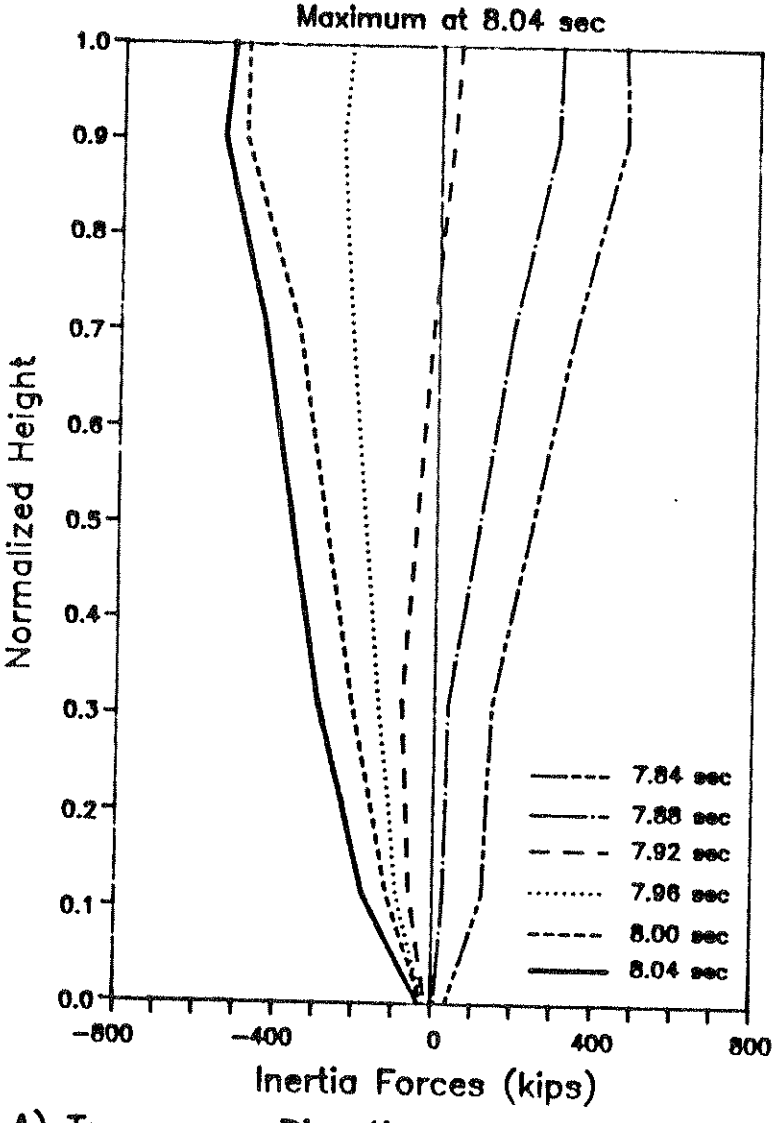

A) Transverse Direction

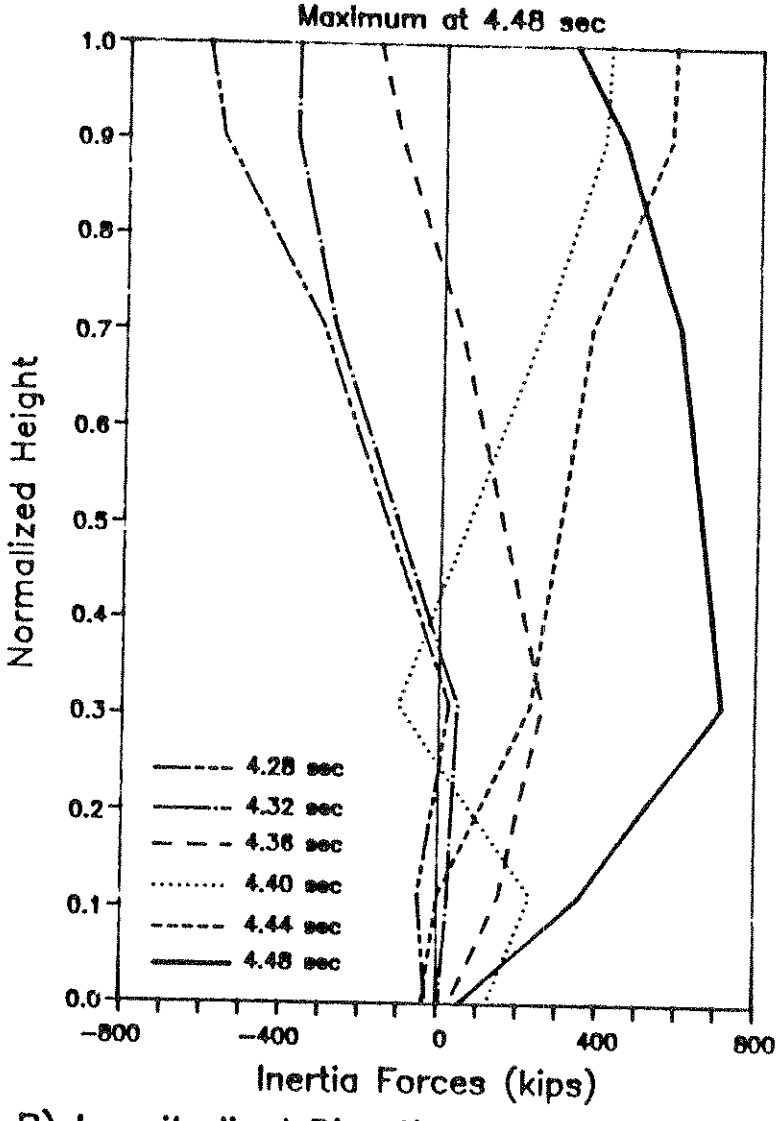

B) Longitudinal Direction

Figure 10A. Distribution of Inertia Forces at Maximum Base Shear

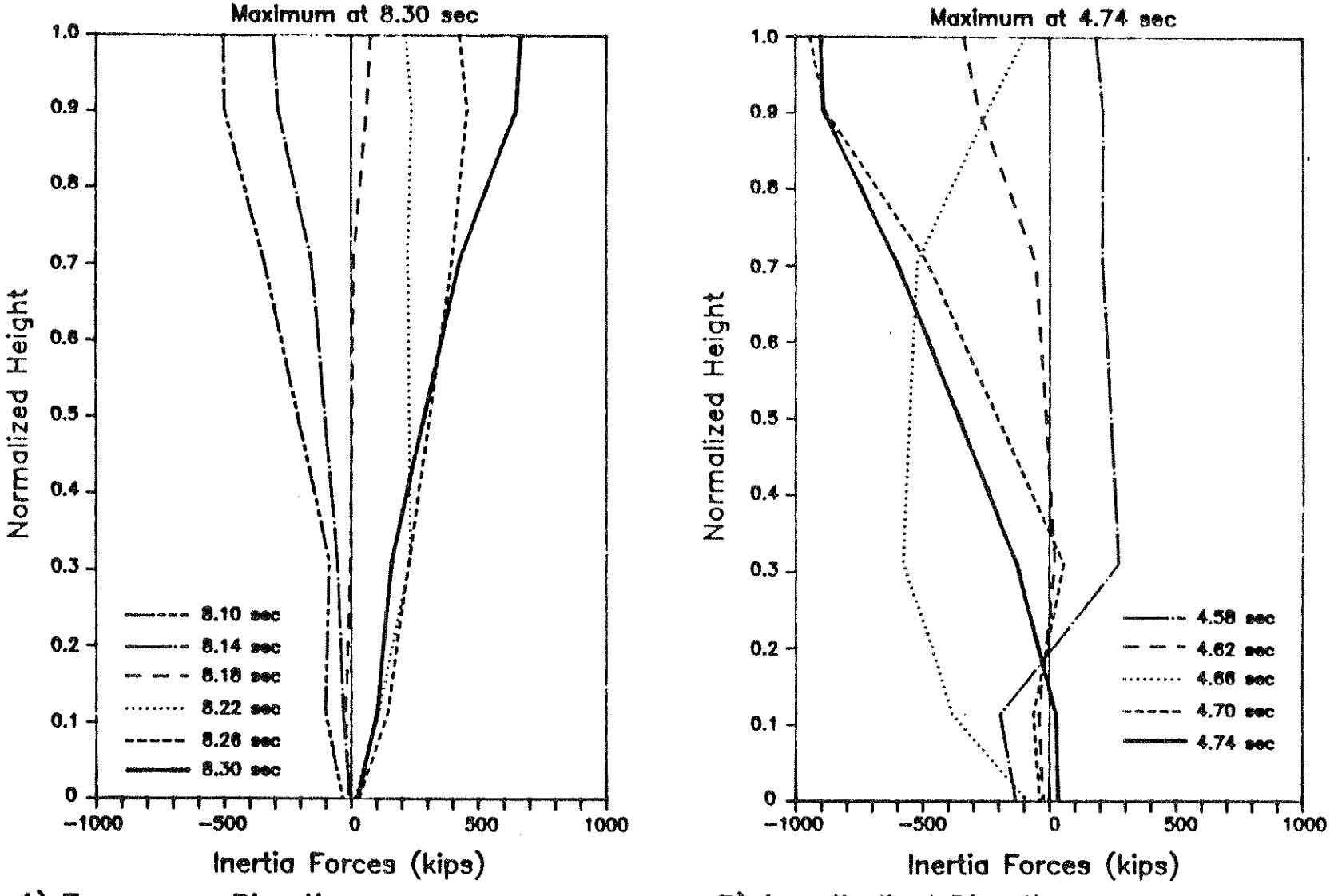

A) Transverse Direction

B) Longitudinal Direction

Figure 10B. Distribution of Inertia Forces at Max. Overturning Moment

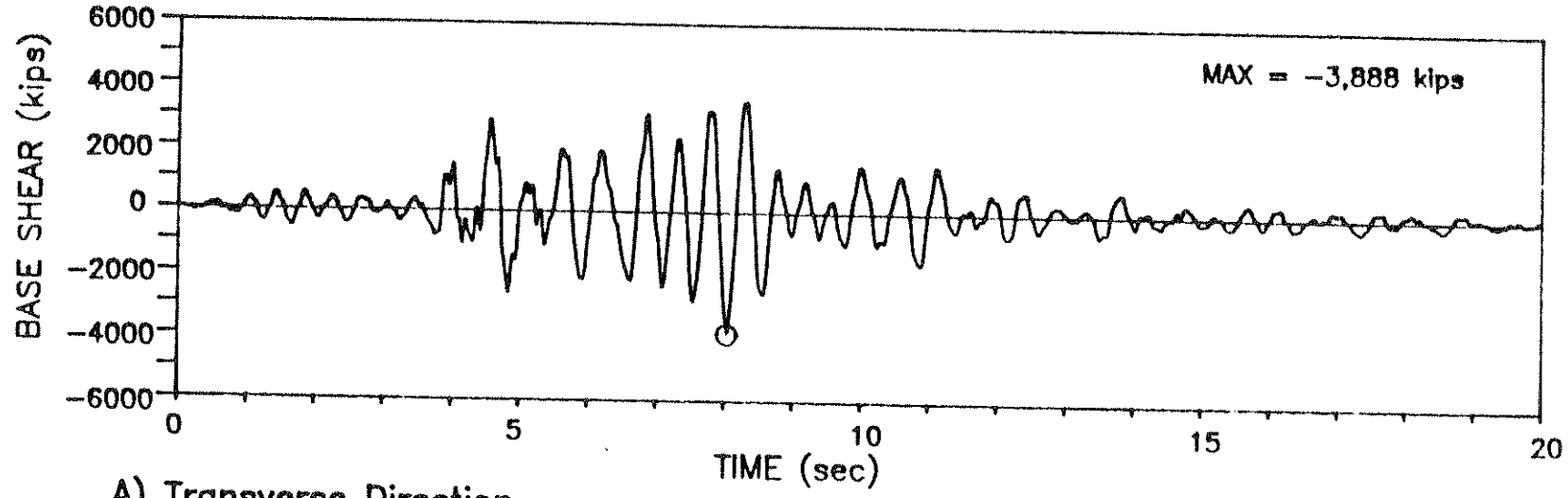

A) Transverse Direction

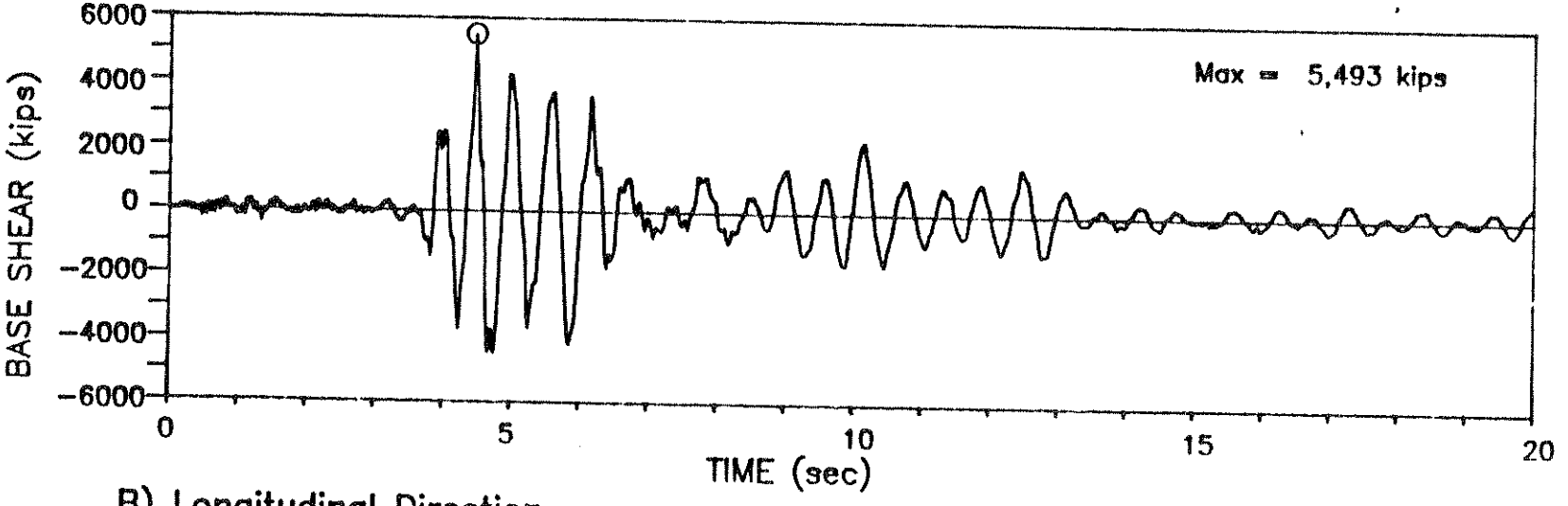

B) Longitudinal Direction

Figure 11A. Base Shear Histories

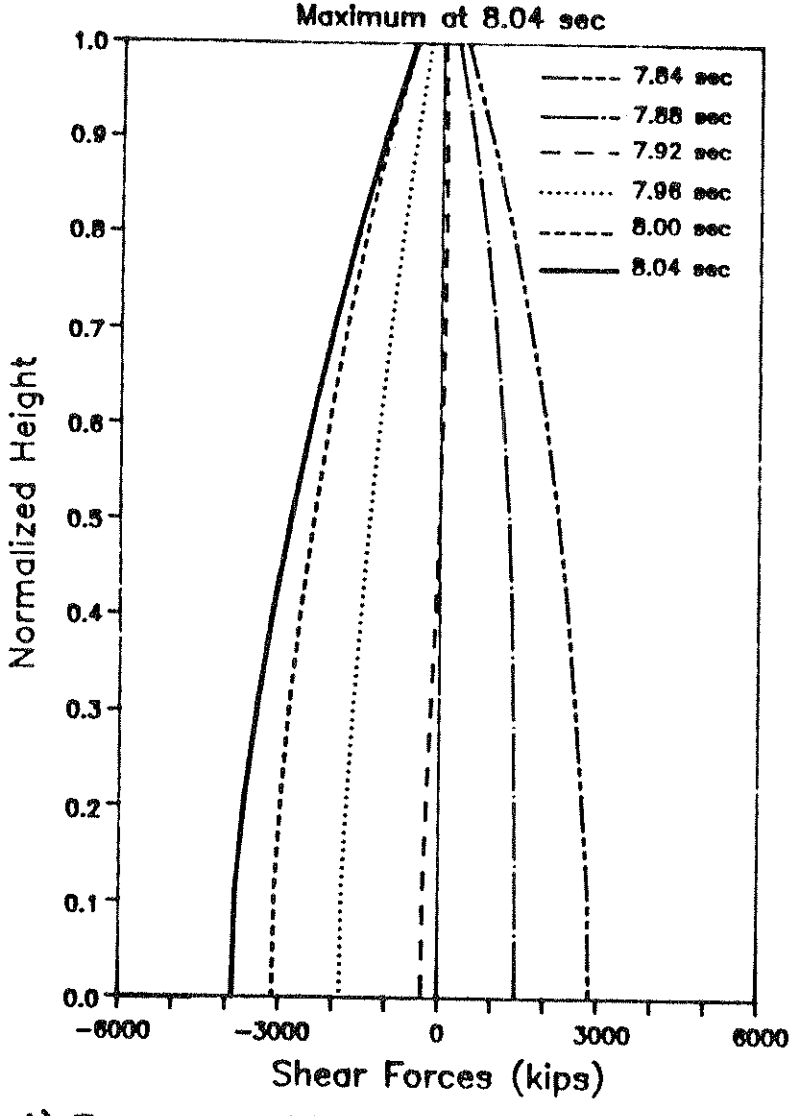

A) Transverse Direction

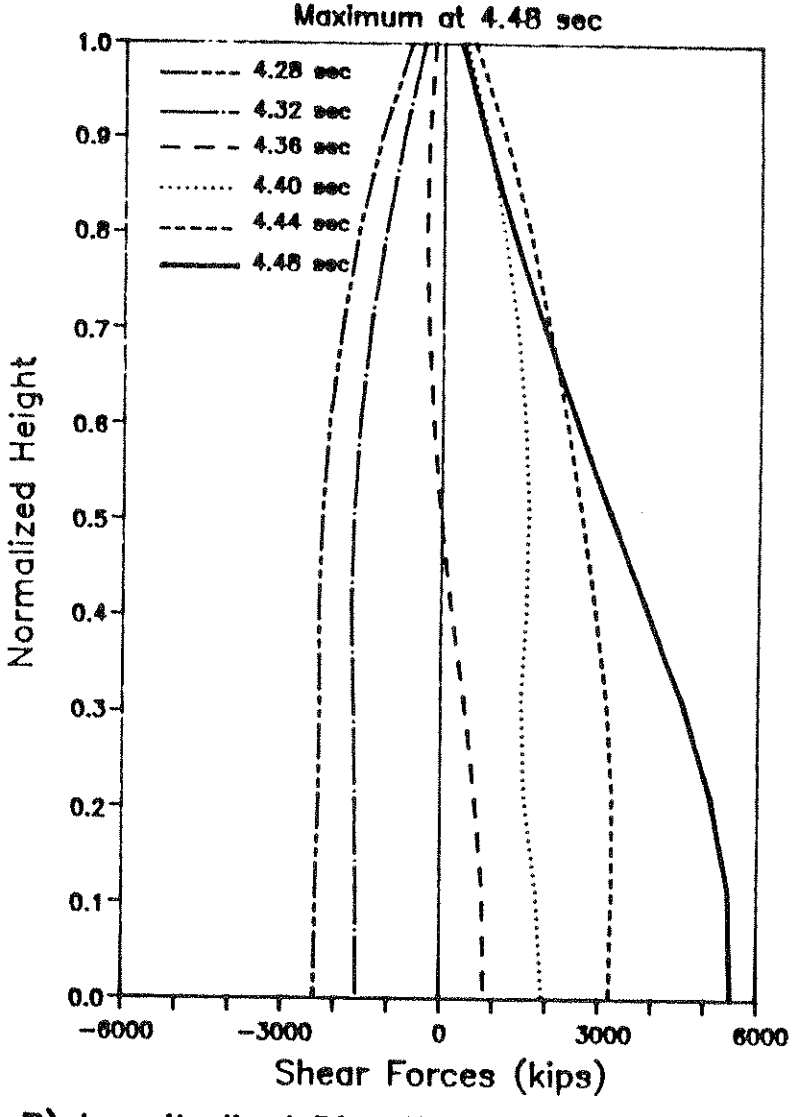

B) Longitudinal Direction

Figure 11B. Distribution of Shear at Maximum Base Shear

	Longitudinal			Transverse	
Max at	1st & 3th	7th	10th	1st & 3th	7th & 10th
Time (sec)	4.48	4.72	4.54	8.04	8.30
1st	5,490	-3,730	1,770	-3,890	3,520
3th	4,560	-3,850	2,070	-3,430	3,270
7th	1,890	-3,260	2,830	-2,020	2,250
10th	327	-1,020	1,050	- 530	660

TABLE 7; Maximum Experimental Shear at Different Stories (Kips).

The design base shear, according to UBC-1988, was calculated as 4,170 kips. This amount is only 75% of the maximum measured base shear in the longitudinal direction. However, the maximum measured base shear in the transverse direction was around 90% the design base shear.

The overturning moment at each floor level was computed by summing the products of the inertia force and its respective distance to the floor level in consideration. The maximum overturning moment at different levels and its respective time of occurrence are presented in Table 8. The base overturning moment history in each principal direction is presented in Fig. 12A. The overturning moment distribution through the building near the time of maximum base overturning moment is shown in Fig. 12B. The overturning moment distribution throughout the building near the time of maximum base shear is presented in Fig. 12C.

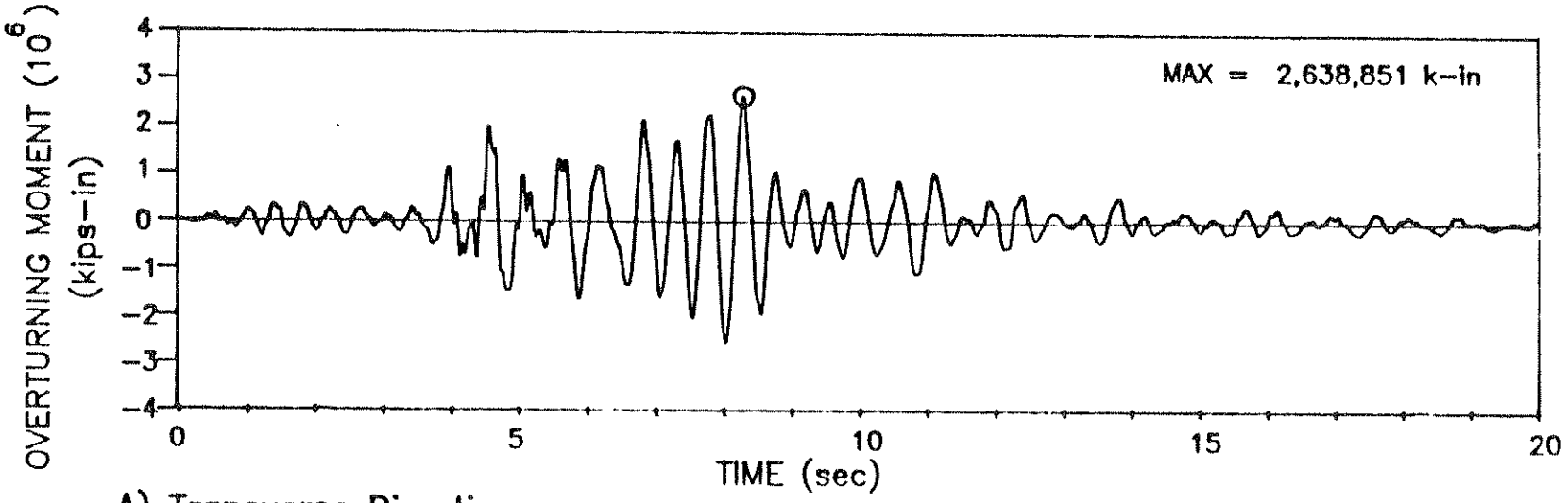

A) Transverse Direction

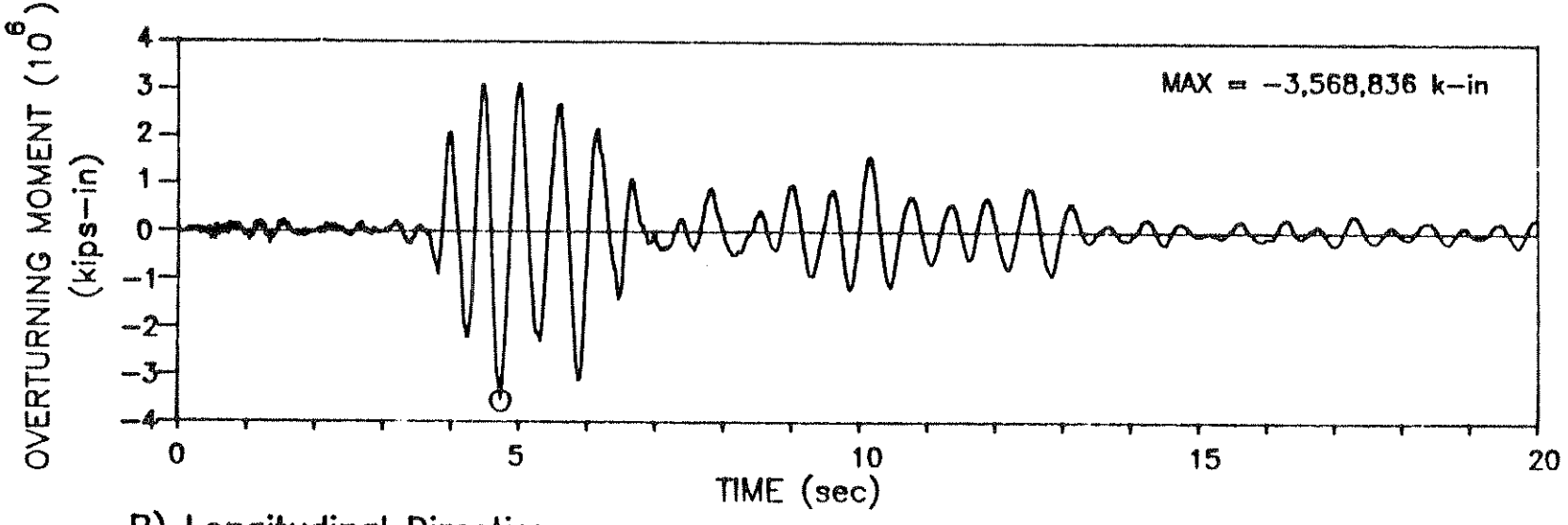

B) Longitudinal Direction

Figure 12A. Overturning Moment Histories

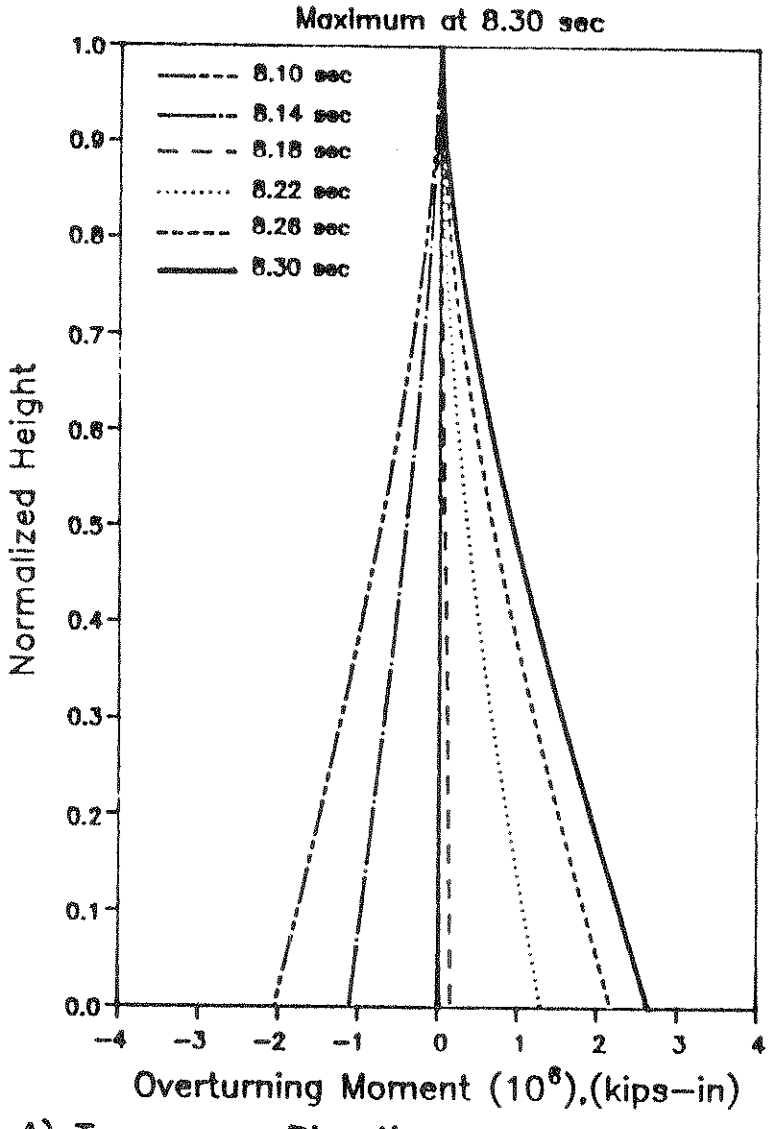

A) Transverse Direction

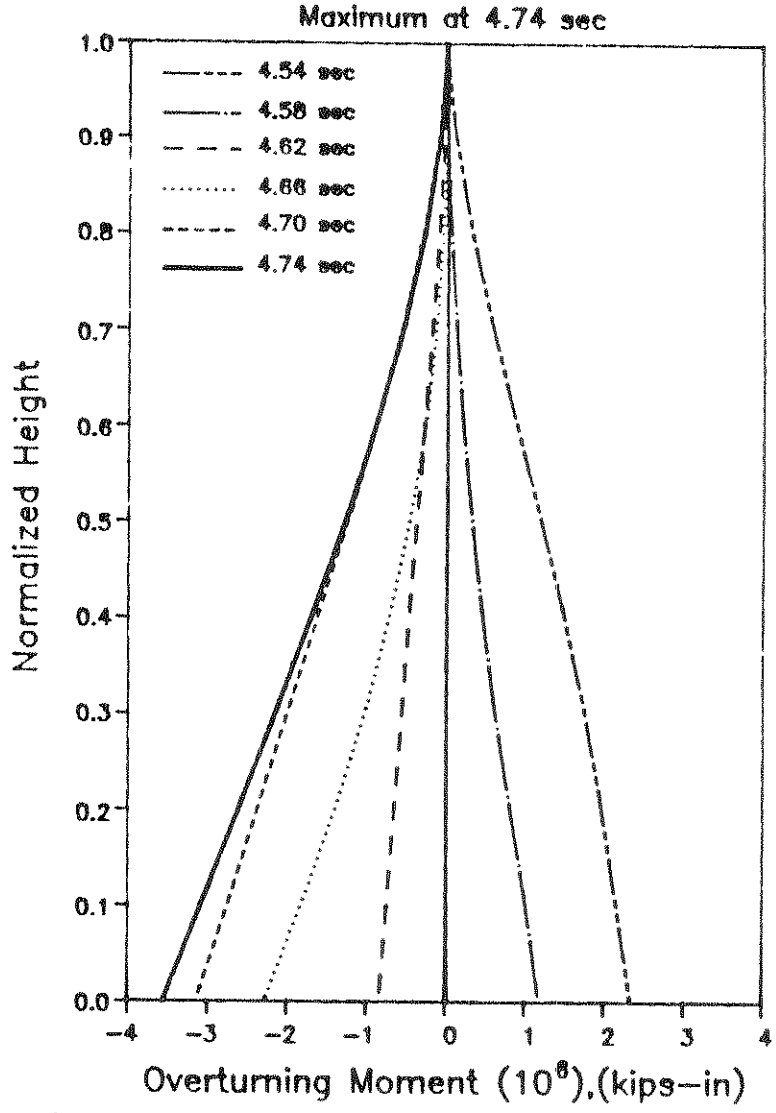

B) Longitudinal Direction

Figure 12B. Distribution of Overturning Moment at Max. Overturning Moment

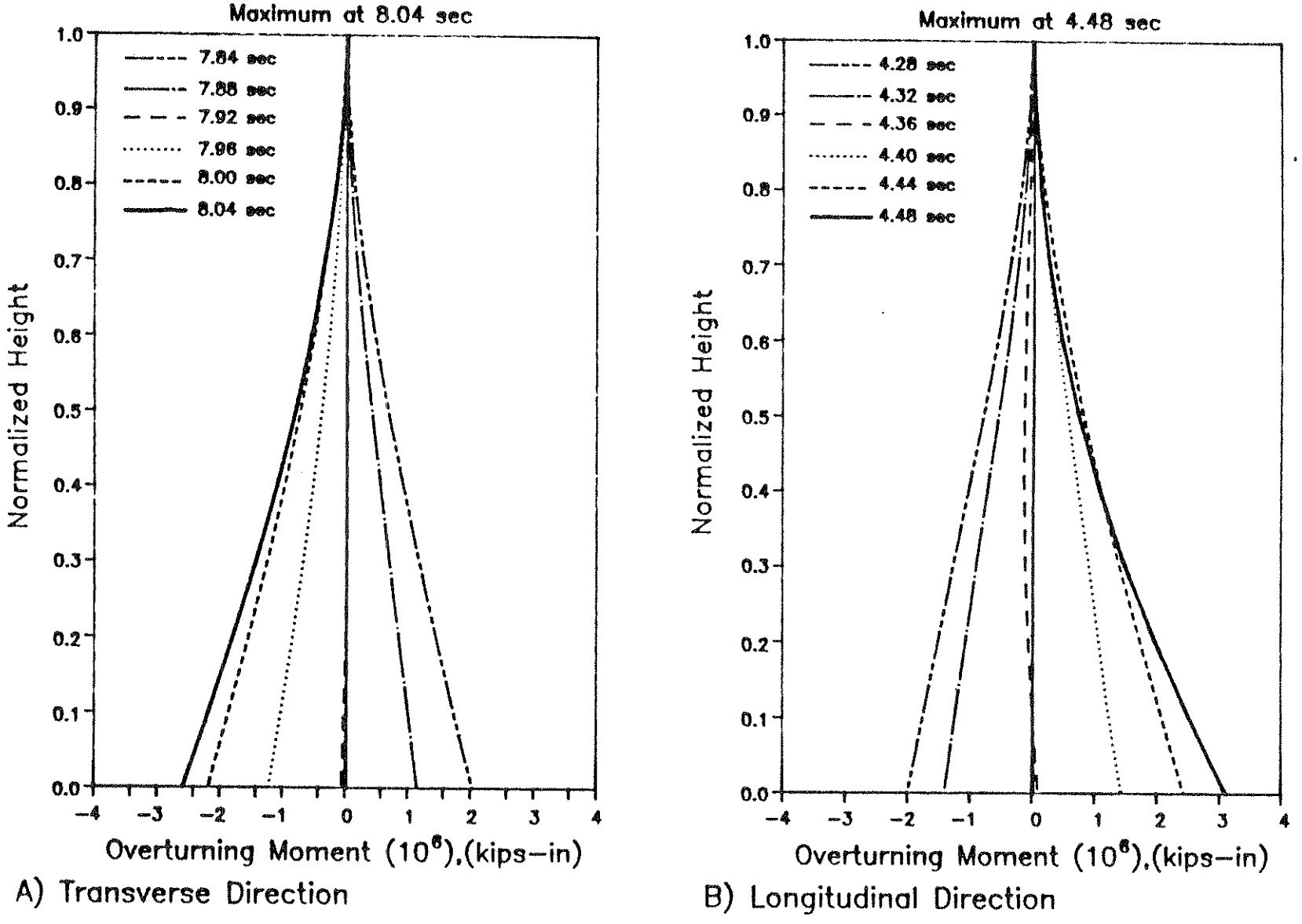

Figure 12C. Distribution of Overturning Moment at Maximum Base Shear

	Longitudinal		Transverse
Max. at	1st	4th & 8th	1st, 4th & 8th
Time (sec)	4.74	4.72	8.30
1st	-3,570,000	-3,370,000	2,640,000
4th	-2,120,000	-2,120,000	1,530,000
8th	- 550,000	- 600,000	390,000

TABLE 8; Maximum Overturning Moment at Different Levels (K-in).

The design base overturning moment was around 2,930,000 K-in which represents 80% of the maximum measured base overturning moment in the longitudinal direction, whereas the maximum measured base overturning moment in the transverse direction was close to 90% of the design base overturning moment.

Analytical Correlation

Building Strengths - In order to compute the collapse strength of the building subjected to monotonic load, it was assumed that all the walls in a story must reach their individual strength simultaneously. The first story is often the one that limits the load capacity. This is so because the design of first level extends over several floors (changes at every floor are avoided) and the first floor, being subjected to the largest loads, will therefore limit the strength. For this reason, the first story was assumed to be the most critical. Its flexural strength was calculated and then the strength of upper

stories was considered to be in proportion to the amount of provided steel area. With this assumed distribution of flexural strengths, conventional limit analysis showed the first story to have the smaller overstrength as was expected.

The flexural strength of the building was calculated first considering a perfect coupling in the interface of orthogonal walls, and second considering no coupling at all. Both assumption were selected so as to obtain bounds on the strength. This was necessary as connection details were not available. The slabs connecting the walls were assumed not to significantly couple the walls, and were thus ignored. The following general procedure was used:

1- The interaction diagrams for T-walls, U-walls and rectangular walls were computed considering the constitutive relations presented on Fig. 13, a maximum concrete compression strain of 0.004, and a straight line variation of strain across the section. The computer program BIAX [13] was used for the calculations.

2- The moment strength was obtained for each wall from its interaction diagram considering the tributary gravity axial load.

3- The curvature corresponding to the moment capacity was obtained for each wall from the moment vs curvature diagram for the tributary gravity axial load.

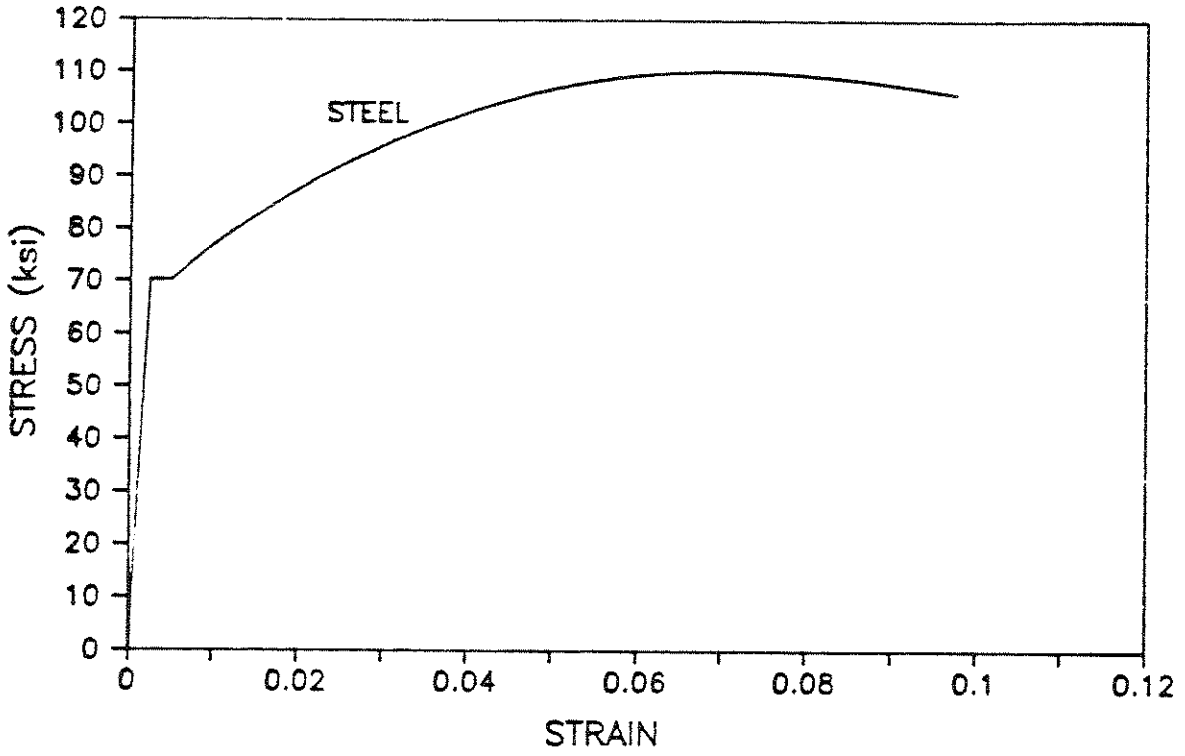

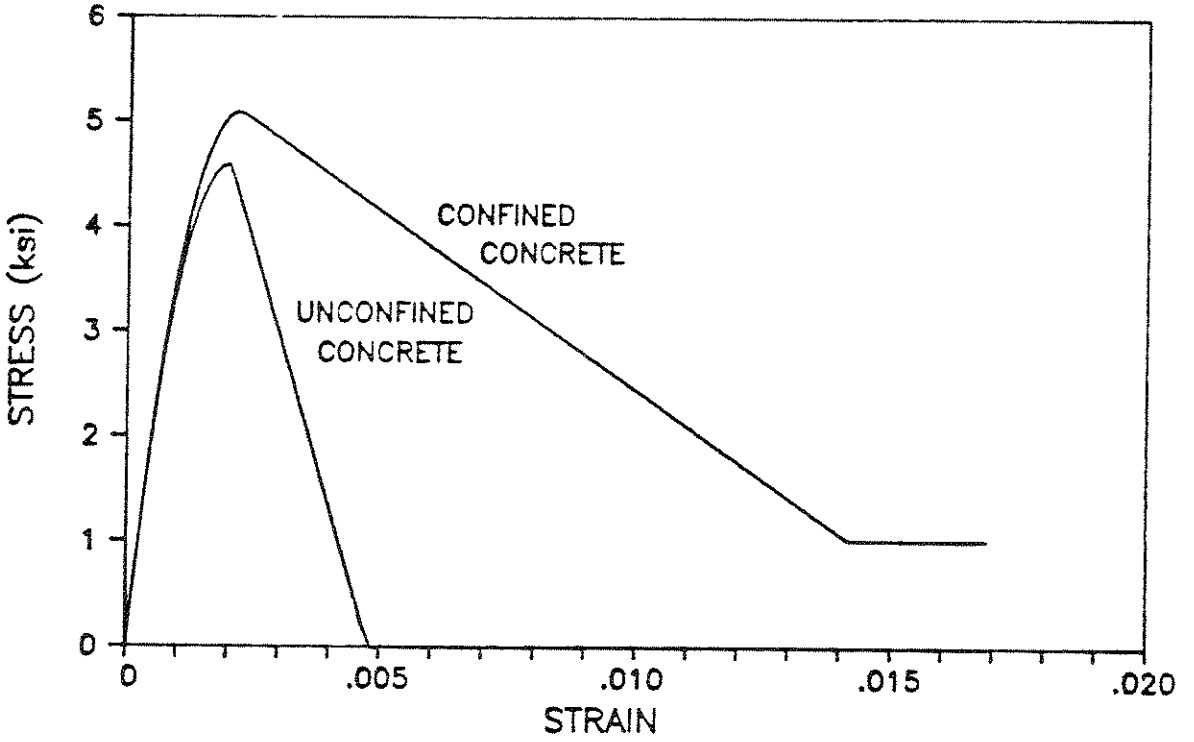

Figure 13. Constitutive Relations of Materials

4- The smallest curvature among all the walls in the same direction was applied to all the walls in the considered direction obtaining its corresponding moment capacity. This procedure was used because the lateral displacement of each wall was essentially the same as a result of the small torsional movements to which the building was subjected.

5- The overturning moment capacity was calculated adding up the moment capacity of each wall parallel to the direction in consideration.

6- The flexural strength was then calculated considering a linear distribution of lateral forces ranging from zero at the base to a maximum at the roof. Thus, that the overturning moment capacity was divided by two-third of the total height of the building.

Building base shear strength was also calculated considering wall shear strengths. The wall panels were reinforced with two grids of wire mesh 4"x4"/#4x#4 (Fy = 70 ksi and equivalent diameter of 0.2253" [1]). Two main assumptions were made to calculate the wall shear strengths: first, axial loads were ignored; and second, only the area of the concrete section of the structural walls parallel to the direction in consideration was considered effective. These assumptions are believed to be on the conservative side. The wall shear strength

was computed according to the ACI 318-83 [5] by

$$Vn = ((2*\sqrt{f'c}) + (\rho*Fy))*\Sigma Ac.$$

In this way the building base shear strength in each principal direction was calculated. The results are compared in Table 9 with the measured maximum base shear (the total weight of the building was calculated as 23,155 kips). From this comparison can be concluded that the structure remained

	Shear Strength	Flexural Strength Composite	Non-Composite	Max Experimental Base Shear
Transverse	0.62W	0.71W	0.32W	0.17W
Longitudinal	0.56W	0.59W	0.29W	0.24W

TABLE 9; Comparison of Base Strengths and Maximum Experimental Base Shear.

effectively in the elastic range throughout the ground motion, although the strength may have been approached in the longitudinal direction. Note that, using the UBC-1988 code with a soil factor equal to 1.5, the design base shear is 0.18W.

Dynamic Analytical Model - In order to model a structure, several assumptions must be made. In the present study a linear-elastic model was considered; a nonlinear model was not justified because significant nonlinear action was highly unlikely during this earthquake (Table 9). Because the structure is not perfectly symmetric a three-dimensional model was used. Three degrees of freedom per story were considered (two traslational and one rotational). Floor diaphragms were assumed

to be rigid in their own plane. Perfectly rigid coupling was assumed in the connection of intersecting orthogonal walls, providing a composite wall behavior. Walls were assumed to be fixed at the foundation level. Soil flexibility was considered in some analyses as will be described later in this report.

Flexural walls were modeled using columns, beams and panel elements. For instance, a simple flexural wall is modeled placing two columns lines, one at each edge of the flexural wall. These columns have zero stiffness. Beams, with infinite flexural rigidity, are placed connecting the column lines at each story in such a way that the rotation of the wall can be traced. Finally, panel elements having appropriate material and geometry properties are placed in each story within the column and beam frame. The modeling procedure is described more fully in reference [4].

Geometrical properties for walls with openings were calculated using the cross-section (in an horizontal plane) which considered the opening.

A light coupling beam was considered between walls along each of axes 4 to 8 only (Fig. 1A). Steel beams apparently had been provided at this locations to support the precast slab panels. Each steel beams is an inverted T-beam WT 6X20.

The modulus of elasticity used in the model was calculated according to the ACI [5] and corresponds to a compressive concrete strength of 4.6 ksi. This value is a weighted average of the concrete used for precast wall panels and the concrete

used for their mandrel cells.

An equivalent viscous damping of 5% of critical was considered throughout the analysis.

Correlation of the Fundamental Periods of Vibration - In Tables 10 and 12 the results of the correlation between experimental and analytical fundamental periods of vibration are presented. The explanation of Tables 10 and 12 is the objective of this section. Therefore, reference to them will be made several times.

Direction	Measured	Analytical					
		Coupled Walls				Uncoupled Walls	
		Igr	Icr	Icr w/ ATC	Icr SSI ETABS	Igr	Icr
	I	II	III	IV	V	VI	VII
Transverse	0.51	0.32	0.44	0.51	0.50	0.43	0.66
Longitudinal	0.57	0.35	0.54	0.56	0.58	0.49	0.70
Rotational	0.56	0.28	0.38	----	0.47	0.38	0.52

TABLE 10; Correlation of Measured and Analytical Periods.

A) Measured Values - The measured periods of vibration (column I of Table 10) were calculated from the plots of the measured roof relative displacement histories. For this purpose, an interval of time in the history was divided by the number of cycles registered in the same specified interval of time. In the longitudinal direction only channel 10 was used, in the transverse direction an average between channels 2 & 3 was considered and, from the difference of channels 2 & 3 the rotational period was calculated (Fig. 2). The average values thus measured are reported in Table 10.

B) Gross-Section Model - The computer program SUPER-ETABS was executed considering gross-section member properties

throughout the structure. The analysis gives a lower bound to the fundamental period of vibration. The results (column II of Table 10) were from 60% to 100% of the measured values. In Fig. 14 the computed relative roof displacement histories for the gross-section model are compared with the measured histories. The computed fundamental period of vibration as well as the amplitude of displacements are well below the measured values as a consequence of the unrealistically high stiffness of the model.

Important causes of the discrepancy between measured and computed responses are summarized in the following three points:

1) The building was subjected to a base shear as high as 83% of its capacity in the longitudinal direction and 53% in the transverse direction (considering no coupling at all in orthogonal walls). Lateral loading of this magnitude is likely to result in cracking in the structural walls. However, cracking was not reported. In addition, cracking due to shrinkage and temperature effects is known to significantly impact the stiffness of the walls.
2) Some discrepancy could be attributed to the soil-structure interaction, which can increase the fundamental period of vibration by approximately 10%.
3) The uncoupling of composite walls. Cracking in the vertical interface between orthogonal wall panels, produced by shrinkage or by the same earthquake,

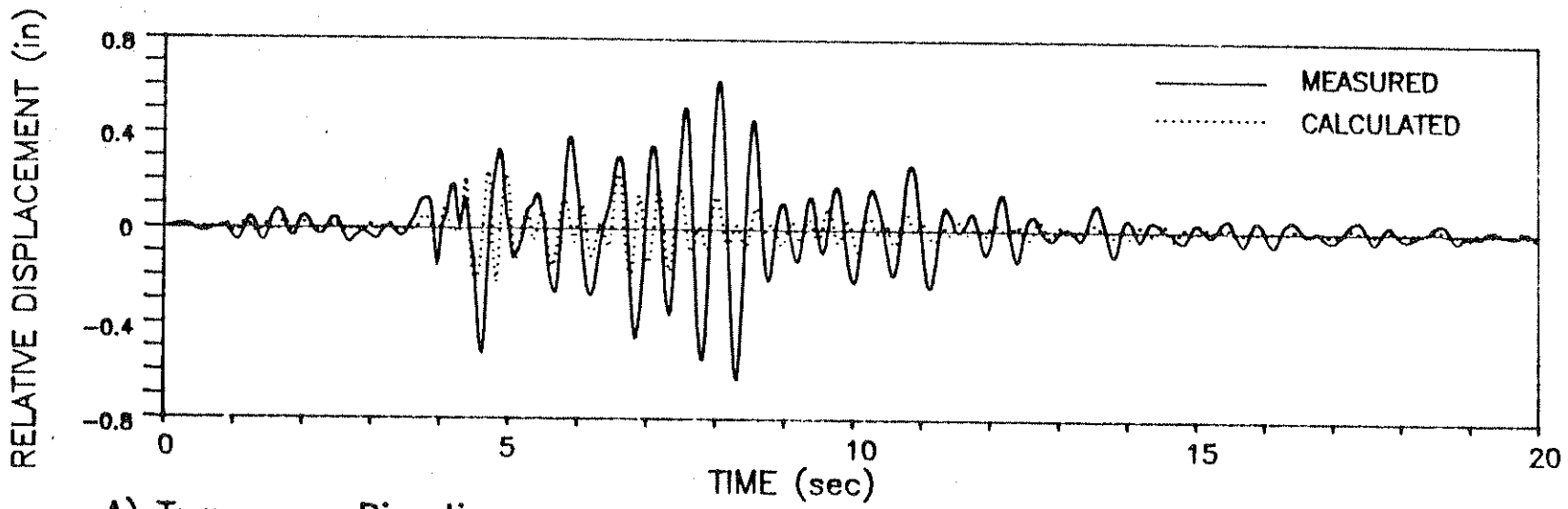

A) Transverse Direction

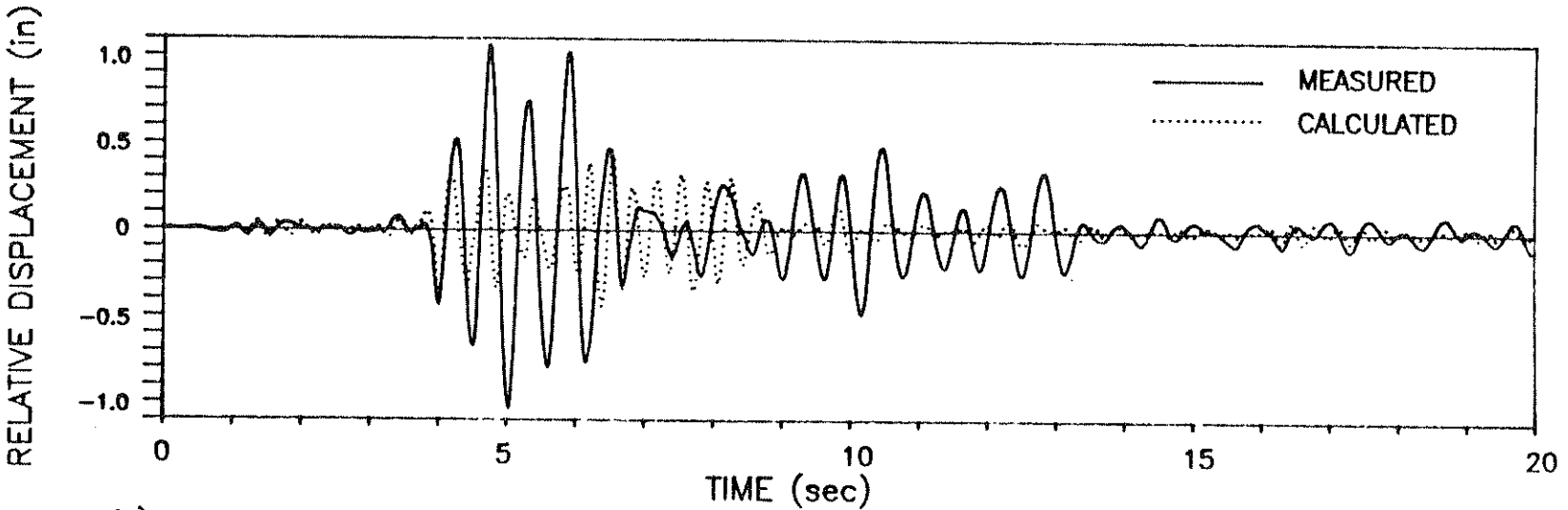

B) Longitudinal Direction

Figure 14. Measured & Computed Roof Responses, Gross-Section Model

could allow some sliding in the wall connections increasing the flexibility of the structure.

C) Cracked-Section Model - In the absence of a well-defined technique to calculate the degree of cracking in a structure, an effective moment of inertia corresponding to a 80% of ultimate moment capacity was assigned to each flexural panel in the first three levels of the building (The stiffness was taken as the tangent to the calculated moment curvature relation of a wall, and corresponds nearly to the fully-cracked stiffness). Such reduction in stiffness might be reasonable because the maximum measured base shear was 83% of the flexural strength of the building considering no coupling at all between orthogonal walls. Walls above the third story were considered to maintain the gross section stiffness. The calculated periods of vibration for this cracked-section model were obtained from the computer program SUPER-ETABS [6] and are presented in the column III of the Table 10. The measured and calculated roof relative displacement histories for this case are shown in the Fig. 15. As can be noted, the degree of correlation has been greatly improved even though the calculated periods are still too short. The degree of correlation in the longitudinal direction is considerably better than that for the transverse direction. This difference in correlation can be explained in some degree by the fact that soil-structure interaction has a greater influence in the transverse direction than in the longitudinal direction, and it has not been included in the correlations.

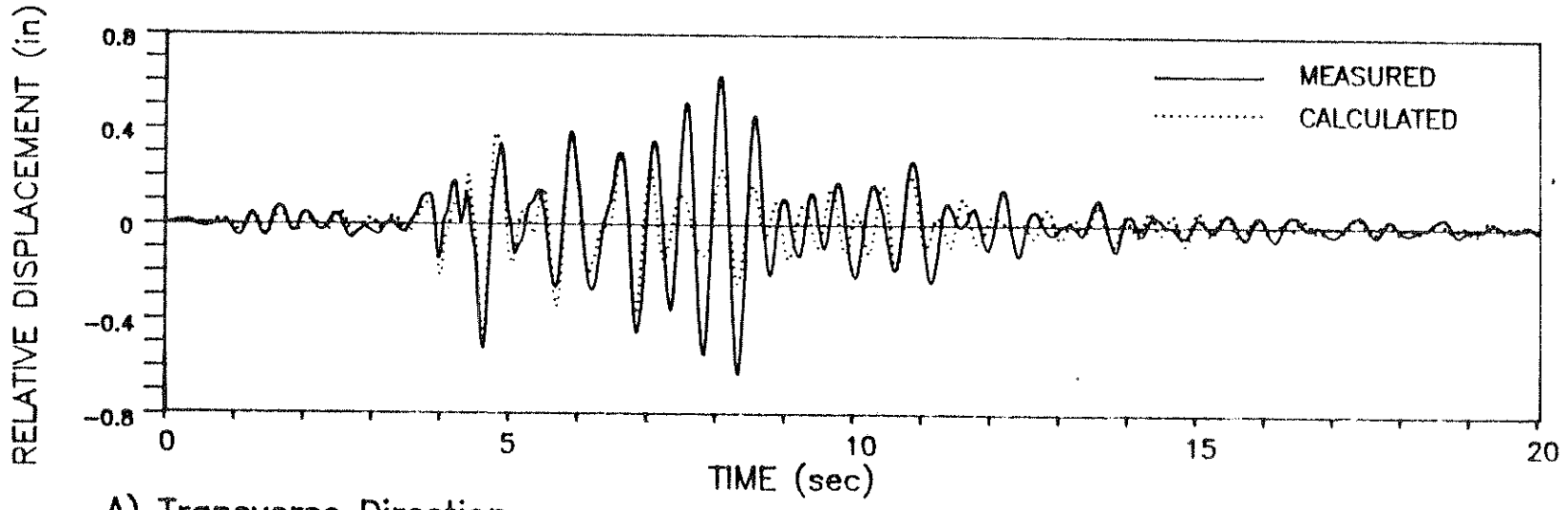

A) Transverse Direction

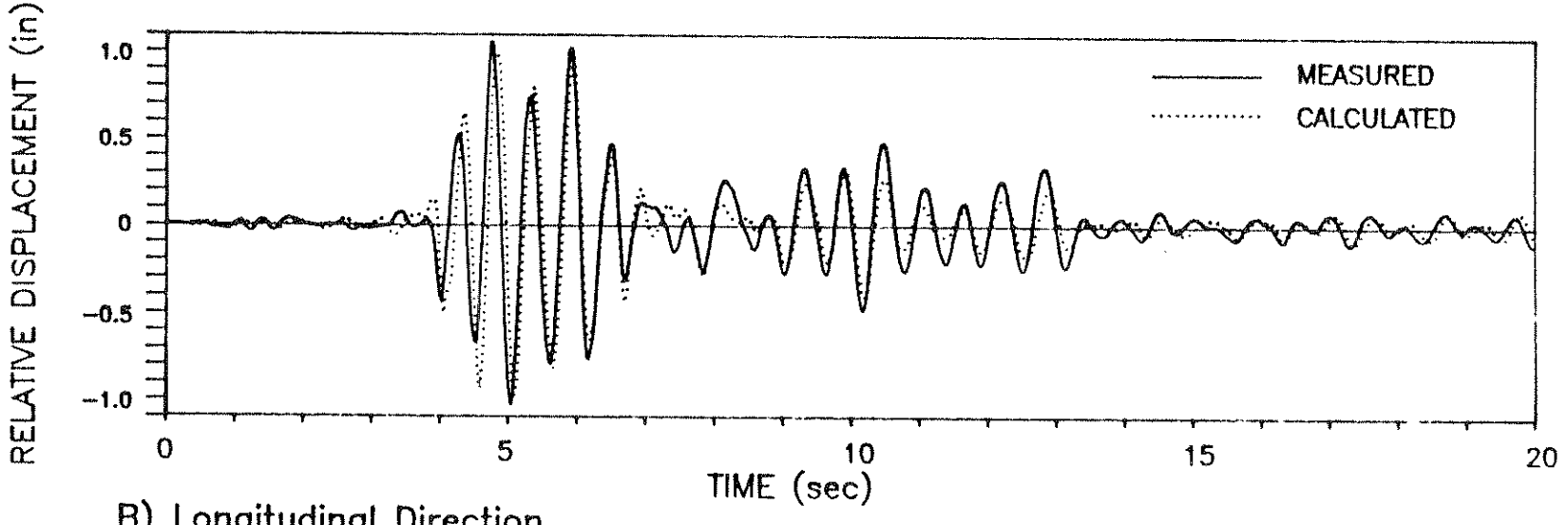

B) Longitudinal Direction

Figure 15. Measured & Computed Roof Responses, Cracked–Section Model

D) Cracked-Section Model with Soil-Structure Interaction - The soil-structure interaction represents the difference in response of the structure in part by considering the free field ground motion and the ground motion modified by the same structure. The ground acceleration recorded at the base of the building being studied here is already influenced by the soil-structure interaction, which includes a translational and rocking component in each direction. In addition, soil-structure interaction is reflected in a lengthening of the fundamental period of vibration due to the flexibility of the foundation, and a change on the effective viscous damping due to radiation and material damping in the soil.

For this particular building no soil report was available, resulting in a tremendous amount of uncertanty in the soil properties. Therefore, it was considered inappropriate to attempt to be precise in modeling the foundation. Rather, the relatively simple approach was adapted whereby the foundation was considered as a general mat, with resulting soil-structure interaction properties calculated according to the procedure suggested by ATC [3].

The soil properties required are the unit weight, the Poisson's ratio, and the static shear modulus.

The unit weight was obtained considering values for loose and dense angular-grained silty sands in dry and saturated conditions. A value of 115 pcf was used based on recommendations by Das [9].

A value of 0.40 for Poisson's ratio is generally suggested for practical purpose [3]. However, ATC [3] suggests 0.33 for clean sands and gravel, Das [7] suggests a range from 0.35 to 0.40 for sands (dry, moist & partially saturated), and Zeevaert [8] suggests 0.25 for sands, compact silts, alluvial soils, compact and well-graded sediments and compact alluvial sediments. Based on the former suggestions a value of 0.35 was selected.

The static shear modulus is the soil property most difficult to correctly estimate without a soil study because of to the wide range of values that can be assumed. Some empirical formulas have been developed [2, 3, 7]. However, any of them require field measures of parameters, such as the shearing strain of the soil and the void ratio, or the selection of coefficients with a wide and highly variable range of values. The situation was handled in this study by using elasticity and waves theories. If the P-wave velocity through the soil is known, the modulus of elasticity can be calculated by

$$E = \frac{Vp^2 \delta (1-2\mu)(1+\mu)}{g(1-\mu)}$$

and the static shear modulus is calculated by

$$G = \frac{E}{2(1+\mu)}.$$

Once the static shear modulus is known, the traslational stiffness of the foundation as well as the rocking stiffness can be calculated by

$$Ky = \frac{8Gra}{2-\mu}$$

$$K_\theta = \frac{8Grm^3}{3(1-\mu)}$$

where ra and rm are defined as

$$ra = \sqrt{(Ao/\pi)}$$

$$rm = (4Io/\pi)^{0.25}$$

and, the stiffness of the building when it is fixed at the base is calculated by

$$K = \frac{4\pi^2 We.}{gT^2}$$

The period increment factor (PIF) due to the soil-structure interaction can be calculated by

$$PIF = \sqrt{(1+(K/Ky)(1+(Kyh^2/K_\theta)))}$$

The period increment factor for the gross-section and cracked-section models in both directions is plotted vs the P-wave velocity in Fig. 16. The range for the P-wave velocity can vary from 600 fps to 4,000 fps. This range was suggested by Das [7] for dry sands at shallow depths. Lacking specific guidance, a P-wave velocity of 2,000 fps was selected for this study. This value leads to a static shear modulus of 3,300 ksf.

The period of vibration modified by the soil-structure interaction was obtained by multiplying the calculated fixed-base periods by the corresponding period increment factors. The modified periods for the cracked-section model are shown in column IV of Table 10. The periods including soil-structure interaction are very close to the measured values.

The effective damping factor was calculated following the

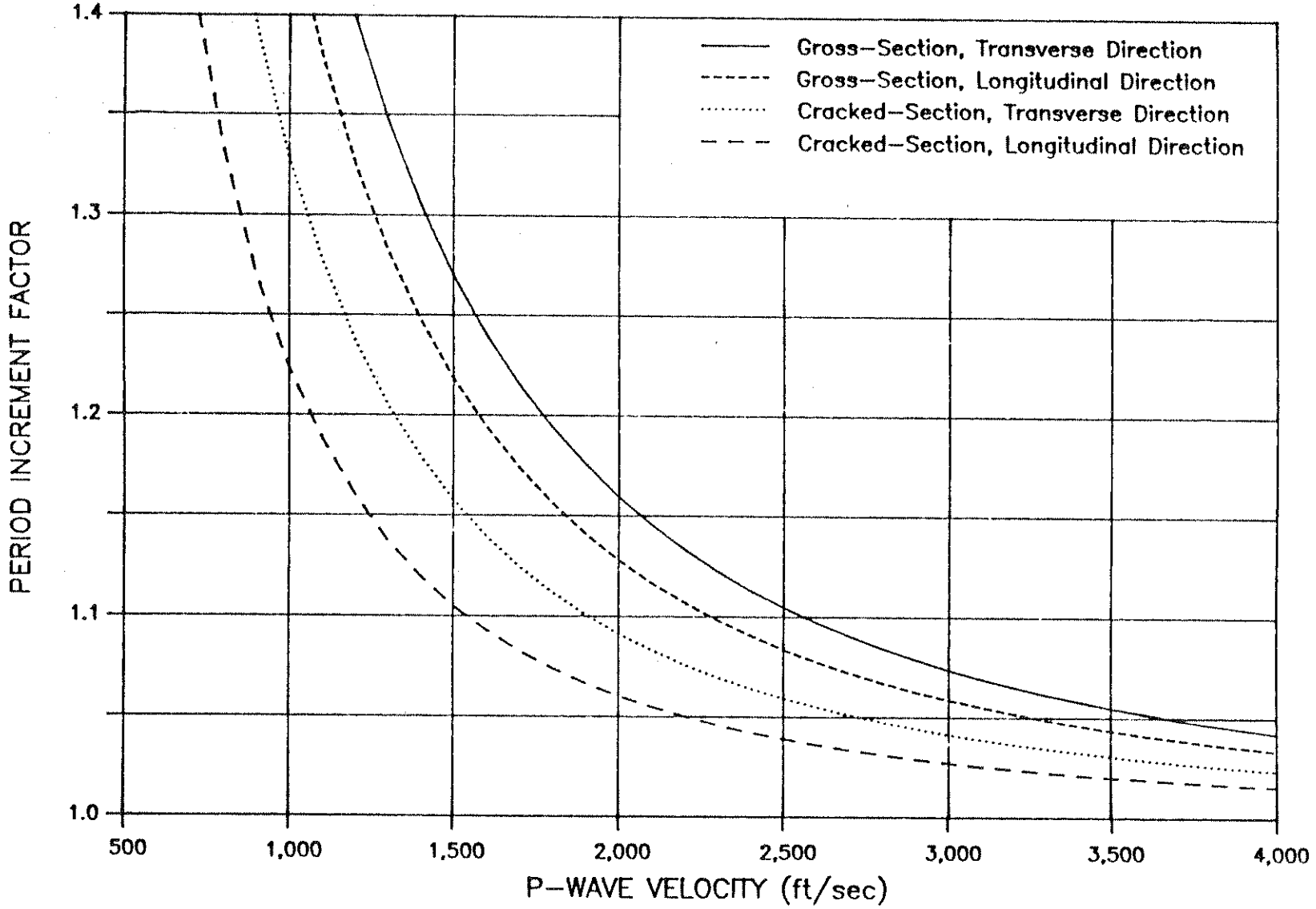

Figure 16. Period Increment Factor vs P–Wave Velocity

procedure suggested by ATC [3]. Thus,

$$\beta = \beta_o + \frac{0.05}{PIF^3}$$

where β_o is obtained from Fig. 17. To use Fig. 17, two parameters, Av and r, must be obtained. Av represents the ground acceleration coefficient. The characteristic foundation length (r) is determined by the following formulas:

For $h/L_o \leq 0.5$ $\quad r = r_a$

For $h/L_o \geq 1$ $\quad r = r_m$.

For intermediate values of h/L_o, the value of r is determined by linear interpolation. In this manner the effective damping factor increased from 5.0% to 7.1% in the transverse direction and, from 5.0% to 6.4% in the longitudinal direction.

In order to model the soil-structure interaction in the computer program SUPER-ETABS [6], an additional story, having columns and beams, was built as a basement. At the top of this new story all the frames were connected using beams with a very large (relatively) flexural stiffness simulating a mat foundation. No wall panel elements were used in this story. Thus, the required translational and rocking stiffness depends only on the column properties and on a lateral spring placed at ground level in each direction.

The appropiate rocking stiffnesses in each direction were obtained simultaneously using the following procedure:

1) The columns of the basement were divided in two groups, A and B, according to their section area. Only six columns constitute the B group which were selected close to

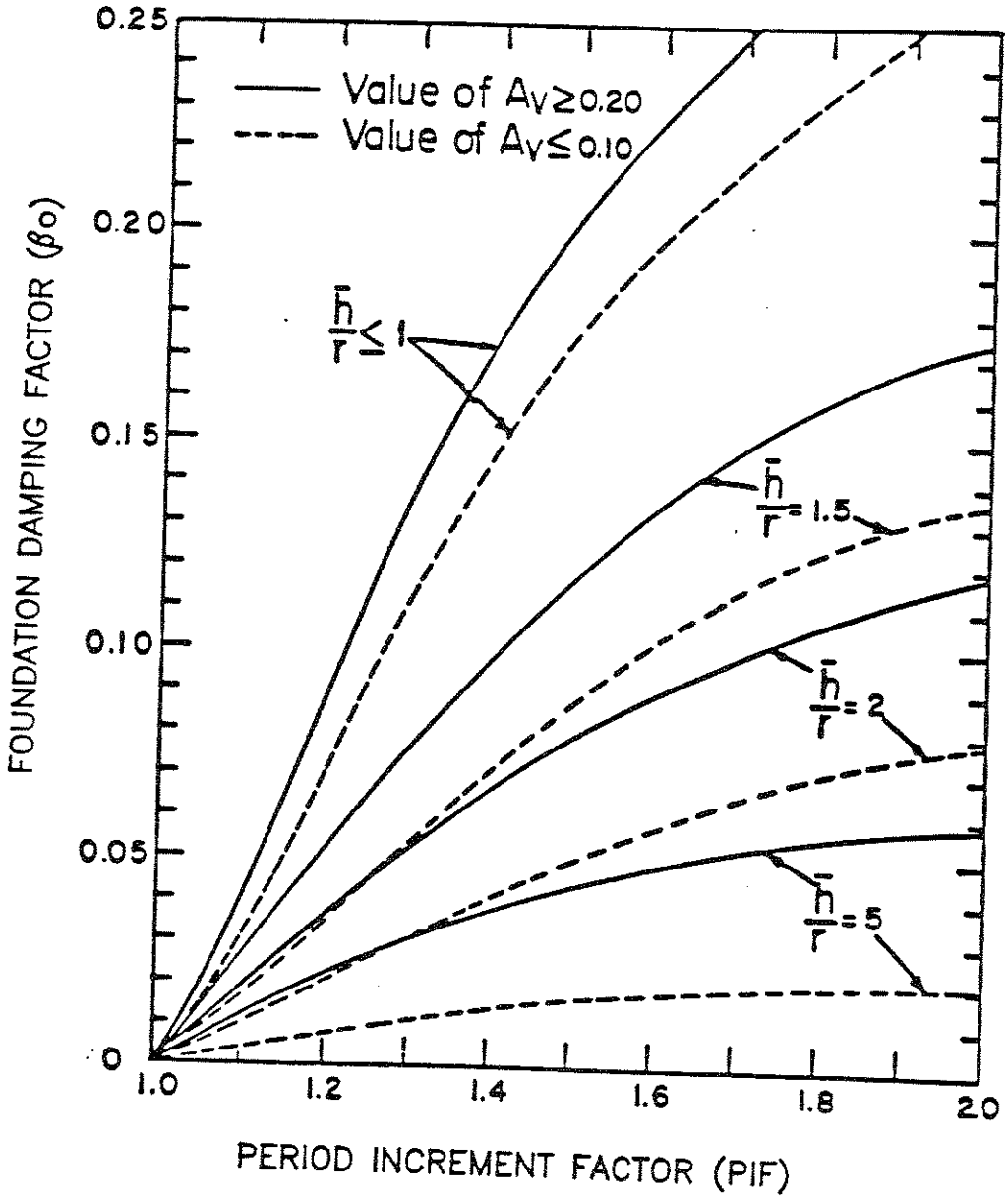

Figure 17. Foundation Damping Factor

the longitudinal rocking axis in such a way that any change in their area would have very little effect in the longitudinal rocking stiffness of the foundation.

2) The rocking axis were calculated assuming a rigid diaphragm perpendicular to its own plane. Thus,

$$x = \frac{\Sigma\, Aixi}{\Sigma\, Ai} \qquad y = \frac{\Sigma\, Aiyi}{\Sigma\, Ai}$$

where the summation is for all the columns.

3) The rocking stiffness is calculated using:

$$K_\theta = (E/L)\ \Sigma\, Aidi^2 .$$

Following the procedure described, a computer program was written in which values for section area of the columns of each group were assigned and, the rocking stiffness was computed for both directions. The value of the modulus of elasticity (E) and the height of the basement story (L) were fixed arbitrarly. The section area of the columns of group A and B was adjusted so that the desired rocking stiffnesses were obtained.

The translational stiffness was obtained assigning the same moment of inertia for all columns in both directions and adjusting the lateral springs.

The periods of vibration obtained from the computer program SUPER-ETABS [6] are presented in column V of Table 10. The values are close to those calculated using the ATC procedure (Table 10). The calculated roof relative displacement history is compared with the measured one in the Fig 18. A high degree of correlation is obtained. Periods and response amplitudes closely coincide in both directions.

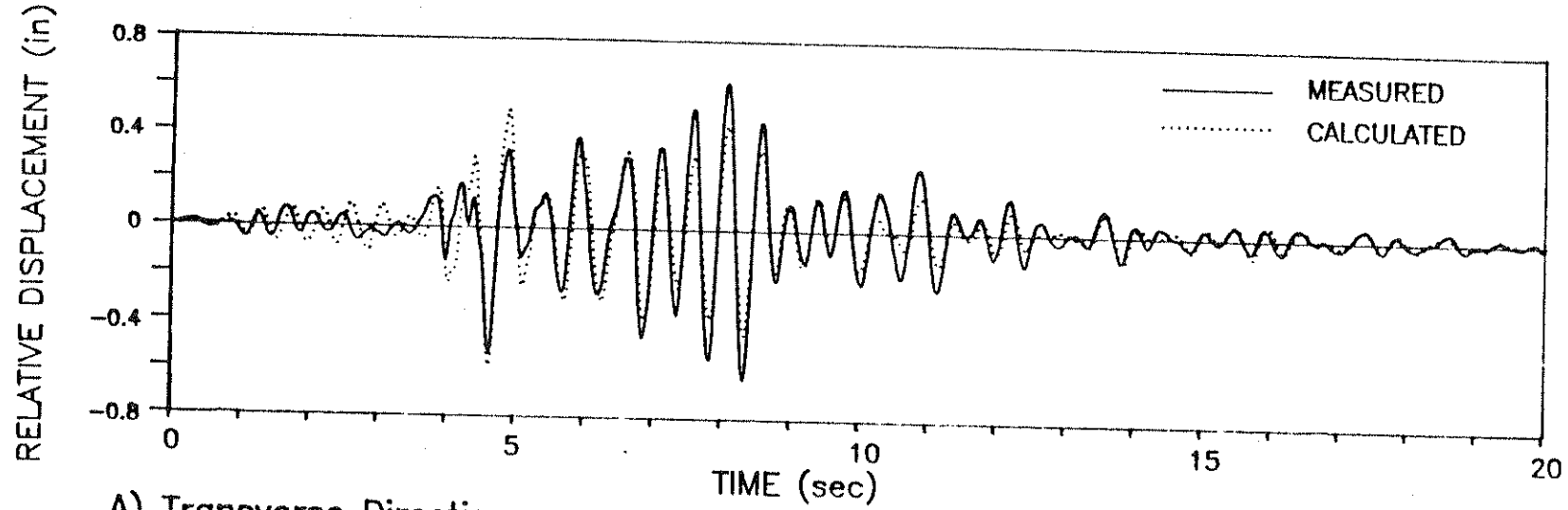

A) Transverse Direction

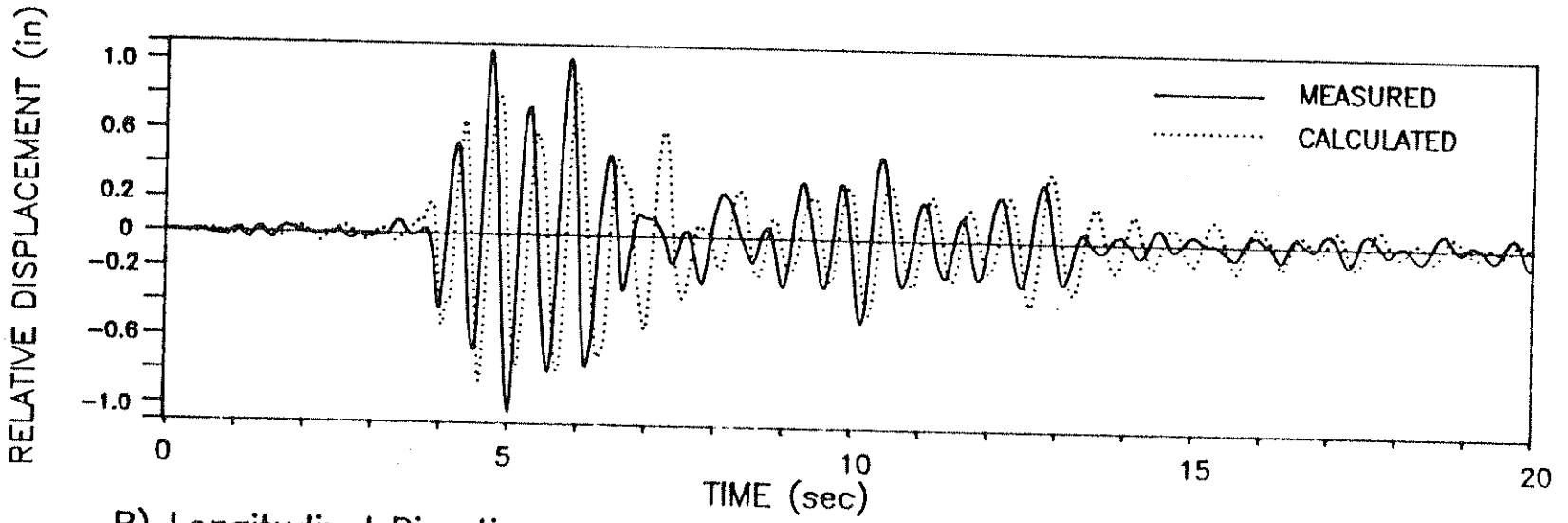

B) Longitudinal Direction

Figure 18. Measured & Computed Roof Responses, Soil–Structure Interaction Model

It is important to point out that the input acceleration records used in the computer program are those obtained on the ground floor level, and that these records thus are already influenced by the soil-structure interaction. It is a source of error that may or may not contribute to discrepancies between measured and computed responses in Fig. 18. However, the error is not studied here.

E) Uncoupled Walls Model - Another possible source of analytical error, mentioned previously, is the uncoupling of orthogonal walls. The effect was studied for the U and T-shaped walls. The U-shaped walls are located at the east and west ends of the building (Fig. 1). In the study, a lateral load, corresponding to the maximum calculated base shear to which the structure was subjected, was applied in the longitudinal direction of the building (Fig. 19). Its magnitude was 5,493 kips. The studied U-shaped wall was assumed to resist 14% of the total shear. The shearing stress at the interface of the composite wall was calculated as $\tau a = 0.15$ ksi using the expression

$$\tau a = \frac{V\ Q}{I g t}.$$

Because no connection details of the orthogonal walls were available, a minimun horizontal steel area (#4 @ 12 in.) was assumed in order to calculate the shearing strength. The shearing strength was calculated according to ACI 318-83 [5] by

$$\tau n = \frac{Avf Fyα}{As}.$$

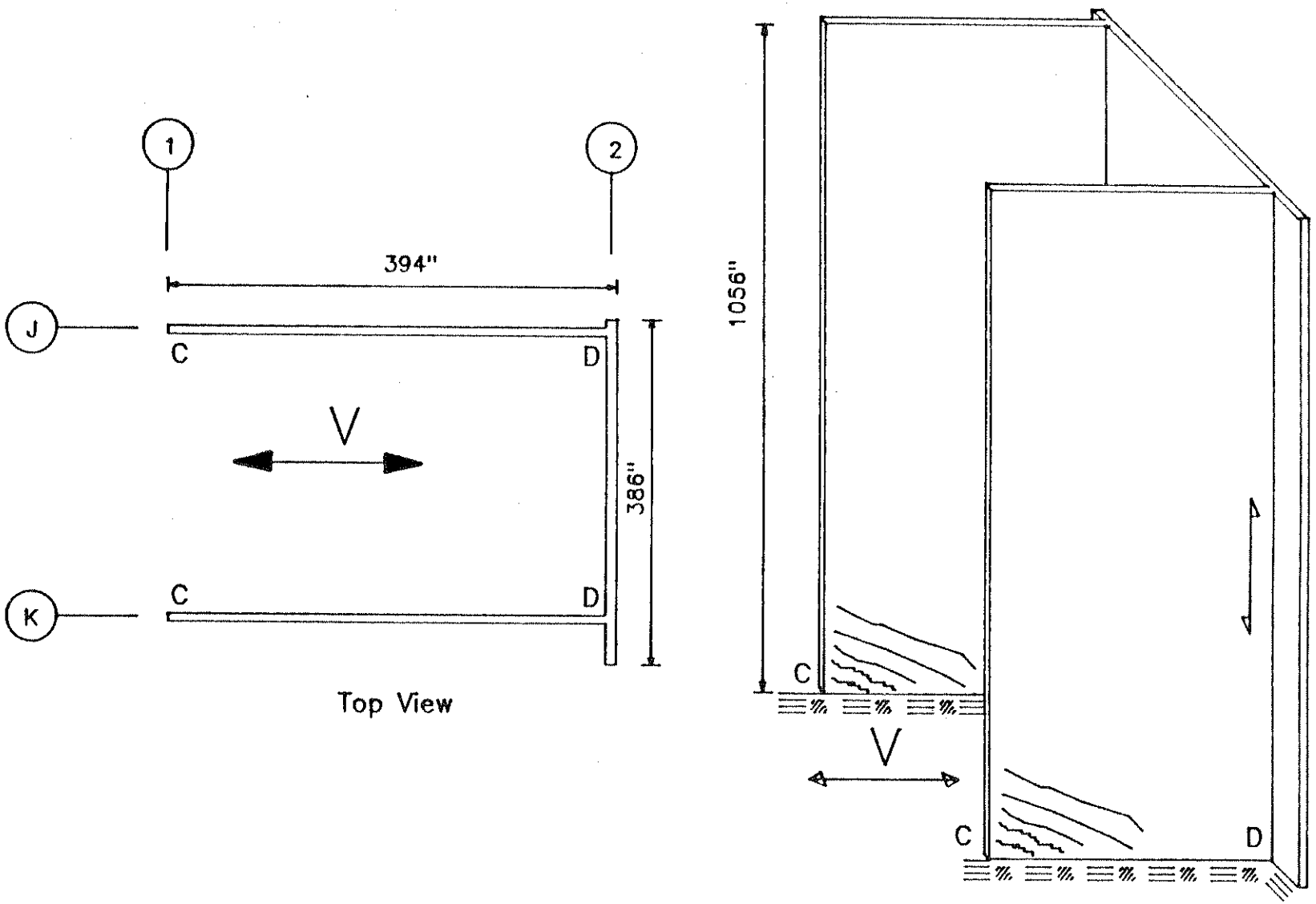

Figure 19. Shearing Stress vs Tensile Stress in U-Shape Composite Walls

The calculated strength was 0.08 ksi, which means that, unless the horizontal steel area was twice that assumed, a considerable amount of cracking and some sliding along the interface might occur because the capacity is calculated to have been exceeded. The steel area required to avoid failure of the interface when the building is at its calculated strength is calculated according to the preceding two equations to be 0.88 in^2/ft.

The tensile stress at points C and D (Fig. 19) were calculated as σac = 0.75 ksi and σad = 0.31 ksi. The tensile stresses were calculated combining axial and flexural stresses according to the expression

$$\sigma a = \frac{P}{A} \pm \frac{Mc}{Ig}.$$

These results indicate that some cracks should be formed at point C because its tensile stress exceeded the likely tensile strength of the concrete ($f_t \approx$ 0.50 ksi). However, no new cracks due to the earthquake loading are expected at point D (cracks due to shrinkage and temperature effects are not considered here). Cracks in any of those two points (C and D) were not reported.

An analogous study was carried out for a T-shaped wall. For

	U-Shaped Wall	T-Shaped Wall
Maximum Shearing Stress	0.15	0.11
Minimum Shearing Strength	0.08	0.08
Required Shearing Strength	0.33(0.88in²/ft)	0.38(1.03in²/ft)
Tensile Stress at C	0.75	0.33
Tensile Stress at D	0.31	-0.08

TABLE 11; Sliding Shear Stress vs Tensile Stress for U and T Shaped Walls (Ksi).

this particular case a steel area of 1.03 in^2/ft was required to avoid sliding in the interface. Such amount of steel area is unlikely to be available in the connections. The results are summarized in Table 11.

To obtain a bound of the extent to which wall uncoupling could affect the building response, the fundamental period of vibration was calculated considering no coupling at all. Both, gross-section and cracked-section models, were considered with cross sectional properties as defined previously. (It is noted that the model considering gross-section properties with completely uncoupled walls is considered grossly unrealistic because cracking along the vertical wall interfaces with no flexural cracking is highly unlikely). Soil-structure interaction was not considered in either case. The results are presented in columns VI and VII of Table 10, respectively. The results from the gross-section model show that the building can undergo total uncoupling of the composite walls but still have periods less than the measured values.

The effects of soil-structure interaction on the

gross-section period can be estimated based on results obtained previously. Comparing columns III and IV in Table 10, soil-structure interaction is observed to result in 16 percent and 4 percent increases in period in the transverse and longitudinal directions, respectively. Applying these same percentages to the results in column VI of Table 10, periods of 0.50 sec and 0.51 sec are obtained. These results are in mild contrast with the measured periods (column I of Table 10).

The cracked-section model produces fixed-base periods significantly longer than measured values. If soil-structure interaction is considered, the discrepancy increases.

F) ATC and Half-Gross-Section Models - Three additional analytical models were considered. In the first of these, the gross-section model was considered with the soil-structure interaction (and composite walls). This case, although believed to be unrealistic, is important because it represents a model commonly used in design practice. The calculated periods are presented in columns III and IV of Table 12. Although the results represent an improvement over the original case where the soil-structure interaction was not considered (column II of Table 12), the calculated periods are still well below the measured values. The difference in measured and calculated results is apparent also in the comparison of measured and computed roof relative displacement histories presented in Fig. 20.

In order to obtain improved correlation with minimum

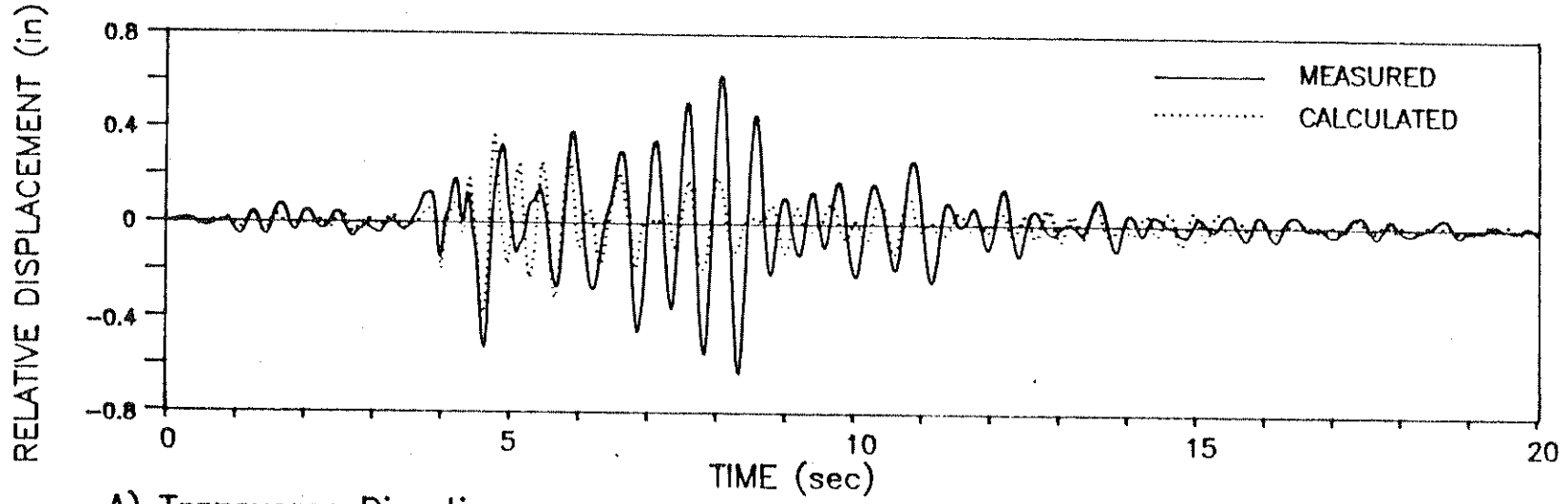

A) Transverse Direction

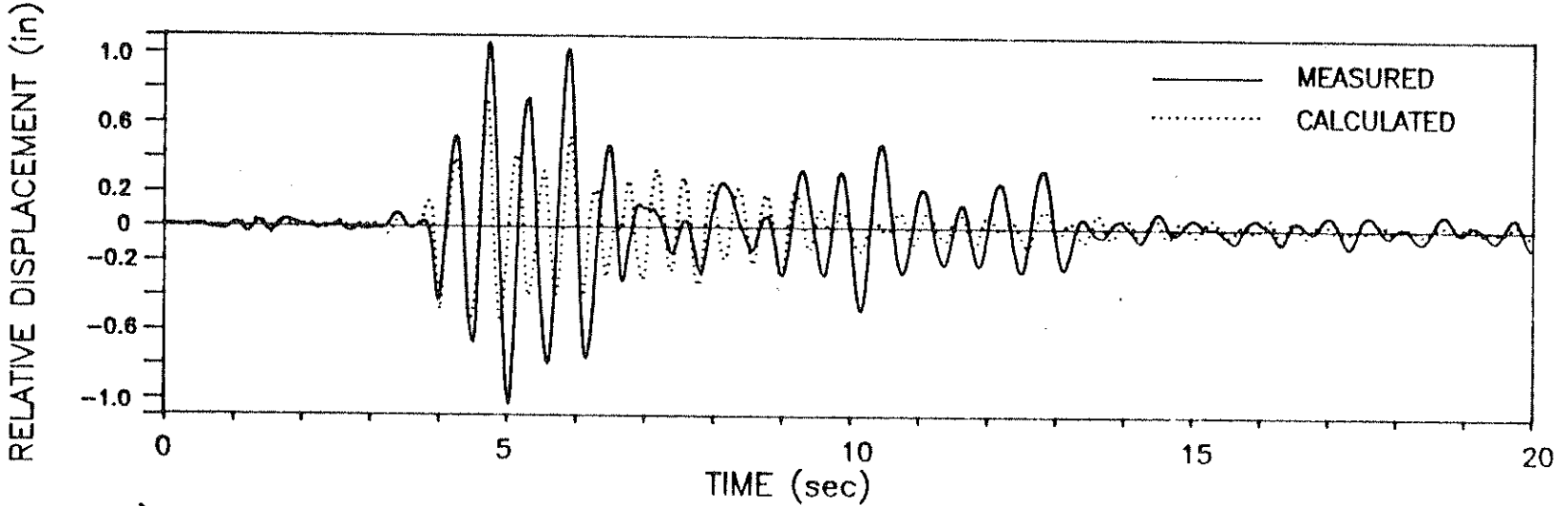

B) Longitudinal Direction

Figure 20. Measured & Computed Roof Responses, Gross-Section Model with Soil-Structure Interaction

	Measured	Analytical (Coupled Walls)					
			Igr w/ SSI			Igr/2 w/ SSI	
			ATC	ETABS		ATC	ETABS
	I	II	III	IV	V	VI	VII
Transverse	0.51	0.32	0.37	0.38	0.45	0.49	0.50
Longitudinal	0.57	0.35	0.40	0.41	0.50	0.53	0.55
Rotational	0.56	0.28	----	0.35	0.40	----	0.45

TABLE 12; Measured and Analytical Periods for ATC and Half-Gross Section Models.

effort, a simplified model is suggested in which an effective moment of inertia equal to half the gross-section moment of inertia is used. (The reduction factor at one-half is typical of that which is appropriate for moderately cracked reinforced concrete flexural members with low axial load stresses.) Complete wall coupling of orthogonal walls is assumed. The fundamental periods calculated ignoring soil-structure interaction are presented in column V of Table 12. The results are much better than those obtained assuming gross-section properties even with the consideration of soil-structure interaction. The computed roof relative displacement histories are compared with the measured histories in Fig. 21. The correlation obtained is very similar to the correlation obtained with the cracked-section model (Fig. 15).

When soil-structure interaction is also considered a very good correlation is obtained as can be noticed in Fig 22. The periods calculated for this case are shown in columns VI and VII of Table 12. It is noted that, using the proposed simplified

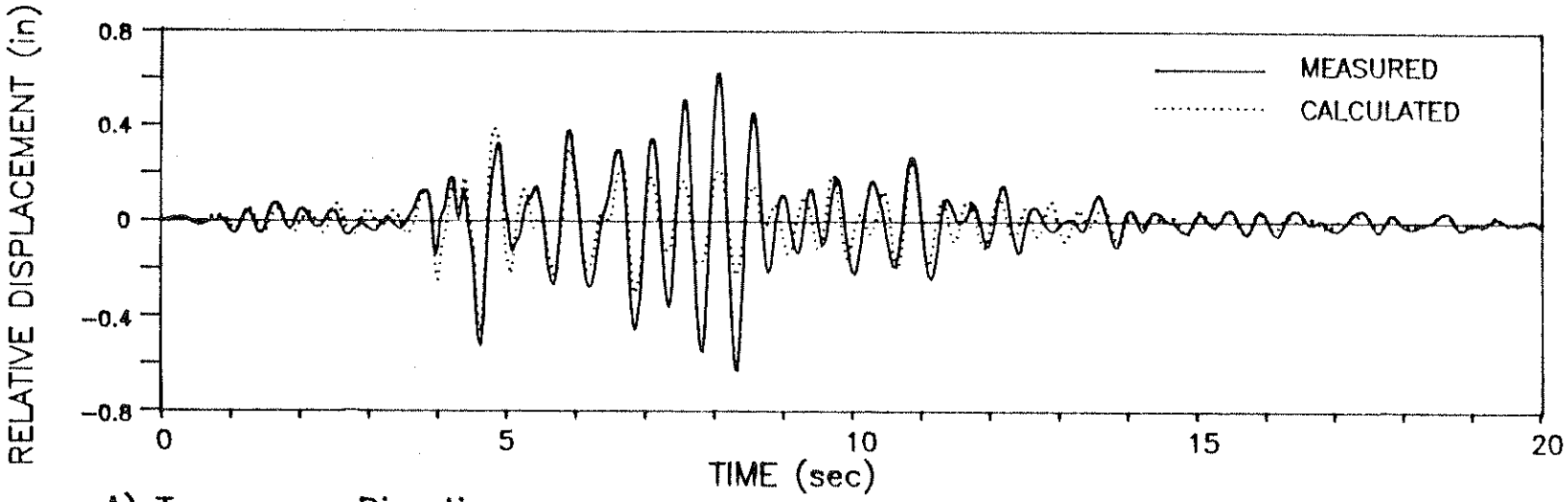

A) Transverse Direction

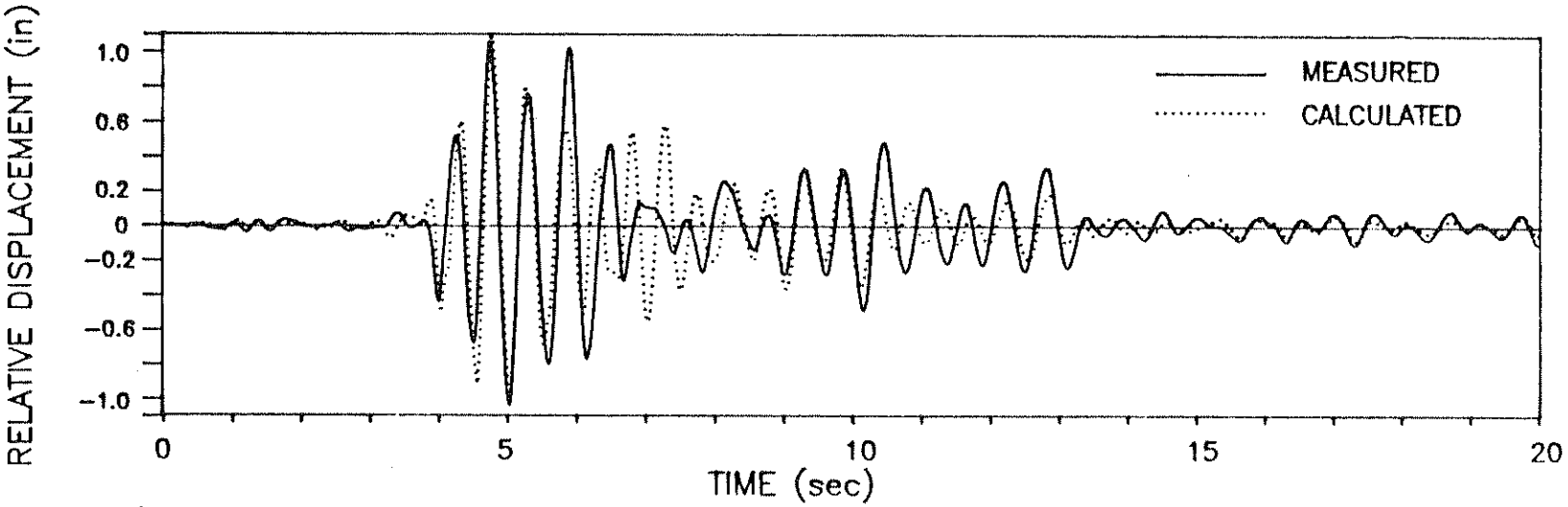

B) Longitudinal Direction

Figure 21. Measured & Computed Roof Responses, Half-Gross-Section Model

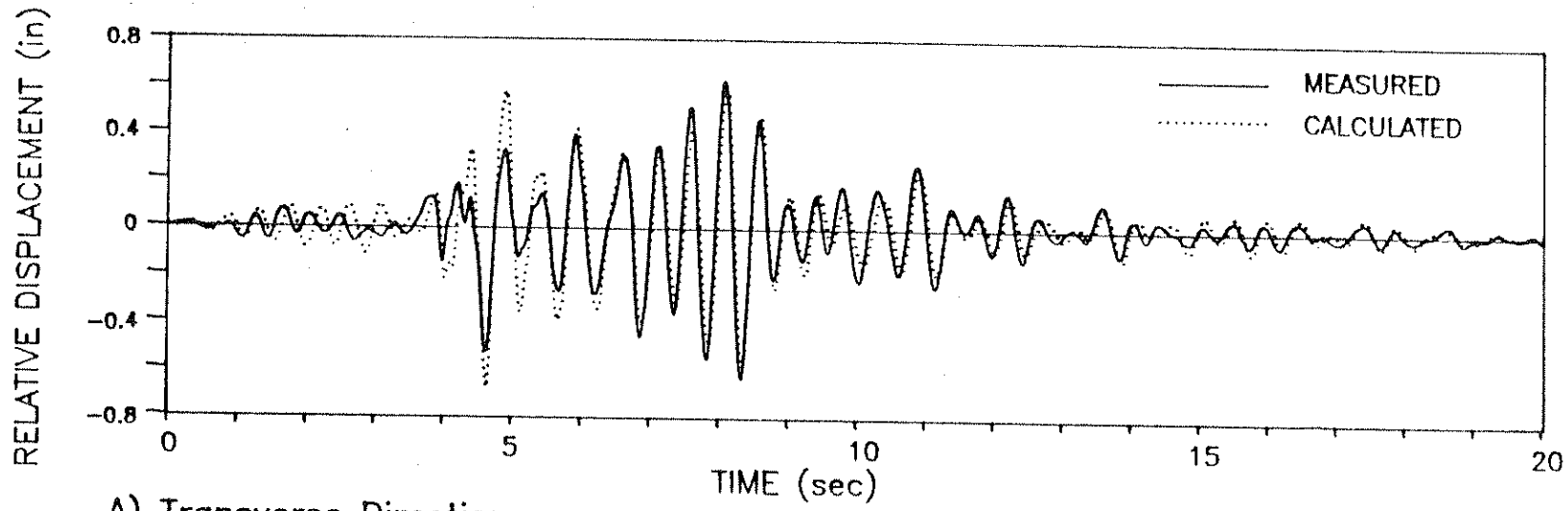

A) Transverse Direction

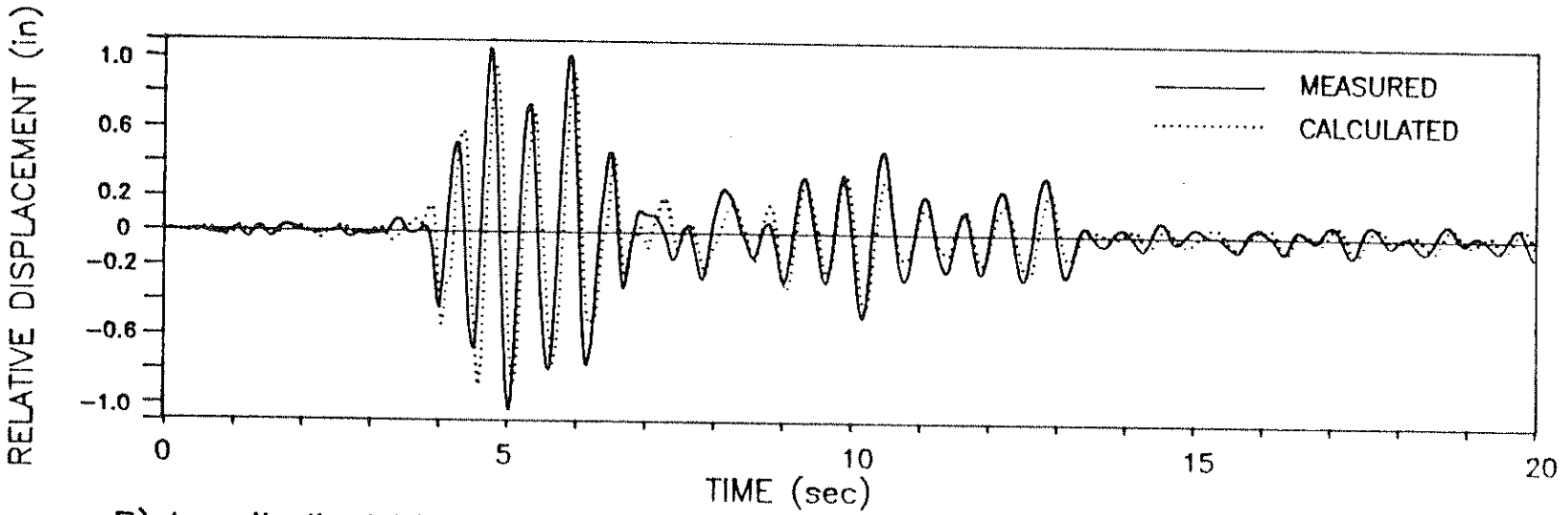

B) Longitudinal Direction

Figure 22. Measured & Computed Roof Responses, Half-Gross-Section Model with Soil-Structure Interaction

model, a tremendous amount of computation is avoided in comparison with that required to calculate cracked section properties.

Summary, Conclusions and Recommendations

The behavior of a 10-story RC bearing wall building subjected to a moderately intense earthquake was evaluated. The building response was studied using sixteen acceleration records that were registered on the 1st, 4th, 8th and roof levels. Base shear and base overturning moment histories were developed. Maximum responses and their distribution through the height of the building were examined. The in-plane diaphragm response was analyzed. Shear and flexural strengths of the building were calculated in both main directions. A linear-elastic dynamic analytical model was developed using the computer program SUPER-ETABS. Gross-section models and cracked-section models with and without soil-structure interaction were studied to compare the calculated roof relative displacement histories with the measured response histories. Simplified reduced stiffness models were also compared with the measured response.

Based on the obtained results and the observed building behavior, the following conclusions are made:

1) The strength of the building was sufficient to keep the response in the effectively elastic range, although some cracking due to lateral loads is likely.

2) The maximum relative displacement was 1.06 in. in the 88

ft tall building, resulting in a maximum average drift of 0.0012, less than one-third the allowable by UBC-1988 (0.0040). Thus, the high lateral stiffness of the building is likely to avoid damage to non-structural components.

3) The floor diaphragms behaved effectively rigidly in their own plane.

4) Fundamental periods obtained with a gross-section model represent a lower bound of actual values, and are not realistic when the structure is subjected to a moderately intense earthquake. The improved correlation obtained considering soil-structure interaction with a gross-section model is not sufficient; apparently soil-structure interaction is not the main source of the period discrepancy.

5) The correlation is improved considerably when cracked-section stiffness are used in the analytical model. The correlation was further improved by considering soil-structure interaction in addition to cracking. The cracks may be due to construction and long term effects on the concrete, or due to lateral load inducing tensile stresses as identified in this report. Such cracks may not be visible following the earthquake.

6) For members subjected to low axial stresses, such as the walls at the building under consideration, the cracked-section stiffness can be approximated as half the gross-section stiffness. This approximation reduces significantely the required members properties computation. Good correlation was obtained using this assumed member stiffness.

Acknowledgements

The author thanks Jack P. Moehle, Associate Professor of the University of California at Berkeley, for his valuable advices through the research. Professor Gregory Fenves provided valuable advice on modelling soil-structure interaction effects. Rubén Boroschek, Carlos Schuler, Xiaoxuan Qi, Juan Chávez, Juan C. De La Llera and Luis Bozzo provided valuable discussion. The patience and encouragement of my wife María is also appreciated.

Information on the building, and building response, and funds to carry out this study, were provided by the California Strong Ground Motion Instrumentation Program (CSMIP). The efforts of individuals working in this program, in particular A. Shakal, C. Ventura, and M. Huang, are appreciated. Views expressed in this report are those of the author and do not necessarily represent those of CSMIP or individuals acknowledged here.

Bibliography

1. ASTM STANDARDS in Building Codes. Specifications Methods of Test Definitions. Third edition. July, 1965.

2. Seed, H. B. and Idriss, I. M., Soil Moduli and Damping Factors for Dynamic Response Analyses., Earthquake Engineering Research Center. University of California. Report No. EERC 70-10. Berkeley, California. December, 1970.

3. Applied Technology Council, Tentative Provisions for the Development of Seismic Regulations for Buildings. ATC 3-06. U. S. Goverment Printing Office, Washington. 1978.

4. Wilson, E. L., Hollings, J. P. and Dovey, H. H., ETABS, Three Dimensional Analysis of Building Systems. Earthquake Engineering Research Center. University of California. Report No. EERC 75-13. Berkeley, California. March, 1979.

5. ACI Committee 318. Building Code Requirements for Reinforced Concrete (ACI 318-83). 1st printing. American Concrete Institute, Detroit, Michigan. 1983.

6. Maison, B. F. and Neuss, C. F., SUPER-ETABS, An Enhanced Version of the ETABS Program. J. G. Bouwkamp, Inc.. Berkeley, California. January, 1983.

7. Das, B. M., Fundamentals of Soil Dynamics. 1st edition. Elsevier Science Publishing Co., Inc.. New York, New York. 1983.

8. Zeevaert, L., Foundation Engineering for Difficult Subsoil Conditions. 2nd edition. Van Nostrand Reinhold Co., Inc.. New York - Cincinnati - Toronto - London - Melbourne. 1983.

9. Das, B. M., Principles of Foundation Engineering. 1st edition. Brooks/Cole Engineering Division, Monterey, California. 1984.

10. Uniform Building Code (U.B.C.). 1988.

11. Mahin, S. A., Boroschek, R. and Zeris, C., Engineering Interpretation of the Responses of Three Instrumented Buildings in San José. Report presented to the California Strong Motion Instrumentation Program (CSMIP). May, 1989.

12. Moehle, J. P., Implications of Strong Motion Data for Design of Reinforced Concrete Bearing Wall Buildings. Report presented to the California Strong Motion Instrumentation Program (CSMIP). May, 1989.

13. Wallace, J. W. and Moehle, J. P., BIAX: A Computer Program for the Analysis of Reinforced Concrete Sections. Department of Civil Engineering. University of California at Berkeley. Report No. UCB/SEMM-89/12. Berkeley, California. July, 1989.